Ph.D. Program in Civil, Chemical and Environmental Engineering

Curriculum in Structural and Geotechnical Engineering, Mechanics and Materials

Department of Civil, Chemical and Environmental Engineering

Polytechnic School, University of Genoa, Italy.

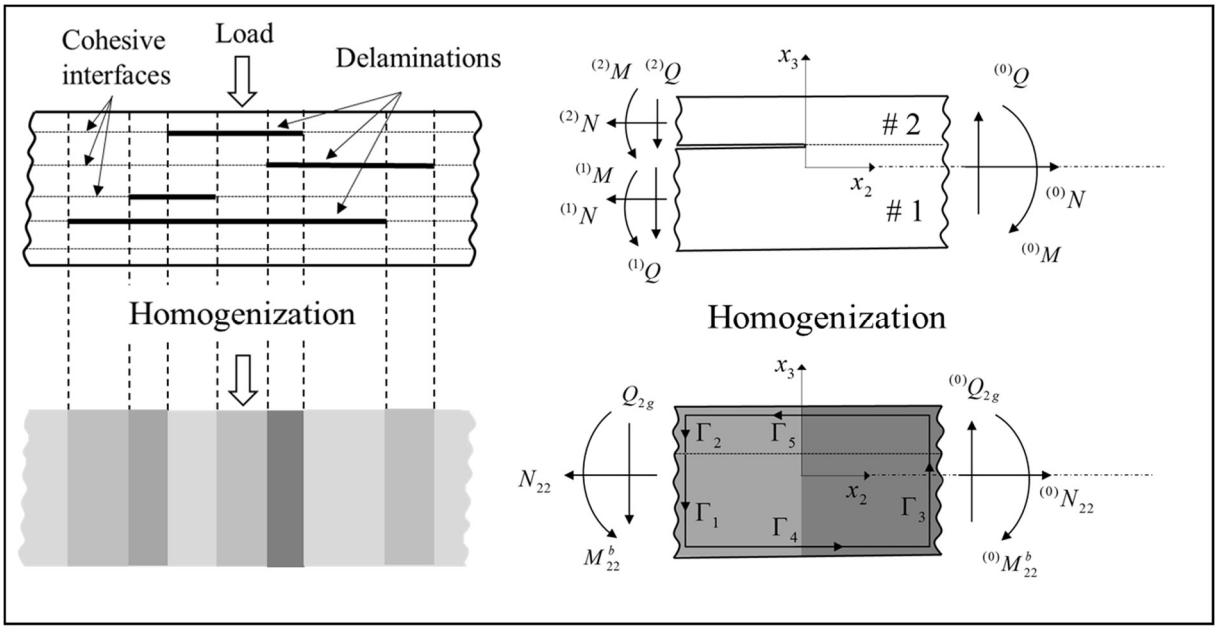

Multiscale Modeling of Delamination Fracture in Multilayered Structures

Hossein Darban

MULTISCALE MODELING OF DELAMINATION FRACTURE IN MULTILAYERED STRUCTURES

BY

HOSSEIN DARBAN

Dissertation discussed in partial fulfillment of
the requirements for the Degree of

DOCTOR OF PHILOSOPHY

Civil, Chemical and Environmental Engineering
Curriculum in Structural and Geotechnical Engineering, Mechanics and Materials
Department of Civil, Chemical and Environmental Engineering, University of Genoa, Italy

January, 2018

Adviser:
Prof. Roberta Massabò – Department of Civil, Chemical and Environmental Engineering, University of Genoa

External Reviewers:
Prof. Marco Gherlone – Department of Mechanical and Aerospace Engineering, Polytechnic University of Turin
Prof. Kwek-Tze Tan – Department of Mechanical Engineering, University of Akron

Examination Committee:
Prof. Antonio Brencich – Department of Civil, Chemical and Environmental Engineering, University of Genoa
Prof. Ivo Caliò – Department of Civil and Architecture Engineering, University of Catania
Prof. Marco Paggi – IMT School for Advanced Studies Lucca
Prof. Riccardo Zandonini – Department of Civil, Environmental and Mechanical Engineering, University of Trento

Ph.D. program in Civil, Chemical and Environmental Engineering
Curriculum in Structural and Geotechnical Engineering, Mechanics and Materials
Cycle XXX

Acknowledgements

The financial support provided by U.S. Office of Naval Research, ONR, grant no. N00014-14-1-0229 and N00014-14-1-0254, program manager Dr. Y.D.S. Rajapakse, is gratefully acknowledged.

Acknowledgements

Firstly, I would like to express my sincere gratitude to my dear advisor, professor Roberta Massabò, for the continuous support of my Ph.D. study and related research, for her patience, motivation, and immense knowledge. Her guidance helped me in all the time of research and writing of this thesis. Without her support, the completion of this work would be impossible.

I would like to thank professor Marco Gherlone from Polytechnic University of Turin, and professor Kwek-Tze Tan from The University of Akron, for reviewing this thesis.

I would also like to thank The University of Genoa and Italy for giving me this opportunity to do my Ph.D. studies.

And all my previous teachers, especially Mr. Haddad and professor Faramarz Djavanroodi from Imperial College London, and those who had a contribution to my education and culture.

And my beloved family…

ABSTRACT

In the recent years, there has been increased interest in using multilayered structures in the construction of mechanical devices and vehicles, such as turbines, wind-blades, aircrafts or ships. These structures are often subjected to severe mechanical loads and a wide range of operational temperatures. Under such loading conditions, the stresses in multilayered structures may exceed the elastic limit, and delaminations and debonds may form and propagate as a consequence of the high interfacial tractions caused by the inhomogeneous material structure. To design layered systems and define their load-bearing capacity and life, accurate understanding of their mechanical behavior in the elastic and post-elastic regimes is needed.

In this thesis, we focus on developing methods for multiscale modeling of elastic and delamination response of multilayered structures. We firstly formulate a matrix technique based on the transfer matrix method formulated in (Thomson, J. Applied Physics, 1950), and on the 2D/3D thermo-elasticity models in (Tungikar and Rao, Composite Structures, 1994) (Pelassa and Massabò, Meccanica, 2015), which use a classical displacement approach to solve the thermo-elasticity equations in rectangular simply supported plates with an arbitrary number of layers and thermally and/or mechanically perfect/imperfect interfaces subjected to stationary thermo-mechanical loading. Novel explicit expressions are derived for temperature, displacements and stresses. The expressions allow to easily generate exact solutions for plates with perfectly bonded or imperfectly bonded layers, and can be used for parametric analyses, to investigate the influence of the inhomogeneous material structure and interfacial imperfections on local fields or to verify the accuracy of approximate theories and numerical models. In this work the closed-form solutions are used to verify the capabilities of approximate multiscale structural models.

We formulate a homogenized fracture model for mode II dominant delamination problems in bi-material wide plates subjected to transverse loads. The formulation is based on the multiscale structural theory formulated in (Massabò and Campi, Composite Structures, 2014) for laminated plates with an arbitrary number of layers and mixed-mode cohesive or traction-free interfaces, which uses a fixed number of unknown variables independent of the number of layers and delaminations for the efficient closed-form solution of numerous thermo-mechanical problems. A delaminated bi-material wide plate is modeled by introducing a cohesive interface along the delamination line, which is governed by a piecewise linear interfacial traction law to approximate Linear Elastic Fracture Mechanics. The model is applied to an edge cracked bi-material wide plate subjected to arbitrary generalized end forces, for which accurate solutions are available in the literature for verification. The energy release rate of the model system is derived in closed-form through an application of the J-integral and using the local fields calculated through the multiscale model. The derived expression for the energy release rate does not account for the contribution of the crack tip root-rotations, which are relative rotations of the arms at the delamination tip cross section, used in the literature to account for the near tip deformations. The contribution can be calculated a posteriori using the equations and tables given in (Li, Wang and Thouless, J. of the Mechanics and Physics of Solids, 2004) (Andrews and Massabò, Engineering Fracture Mechanics, 2007) as function of the crack tip force and moment resultants predicted by the multiscale model. Except for the root-rotations contribution, the derived expression of the energy release rate coincides with those obtained in the literature, for bi-material and homogeneous plates. The energy release rate is also derived through an application of the J-integral

along a path surrounding the delamination surfaces to show the accuracy of the homogenized model to capture the relative crack displacements. The fracture model is used to analyze delamination growth and investigate the structural response of End-Notched Flexural (ENF) specimens; comparisons between the results of the homogenized model and those of the accurate two-dimensional elasticity solutions and a discrete-layer interface model demonstrate that the model is able to accurately predict the fracture parameters and capture the macro-structural response, including snap-back instabilities. This is done through a homogenized description of the problem and using the same number of variables as that needed for modeling a single intact homogenous layer. The main drawback of the approach is that it underestimates the compliance of the specimen due to neglecting shear deformations in the delaminated portion of the specimen.

To try and overcome this limitation of the homogenized model, we extend the refined zigzag theory developed in (Tessler, Di Sciuva and Gherlone, J. of Composite Materials, 2009) for fully bonded plates, to account for the presence of imperfect interfaces. The theory accounts more accurately for the contribution of the shear deformations in the displacement field of partially or fully debonded plates and resolves some difficulties of the previous multiscale model in modeling clamped boundaries, where fictitious boundary layers occur due to neglecting shear deformations. The model is formulated for plates deforming in cylindrical bending, the interfaces are assumed to be rigid against relative opening displacements and their mechanical behaviour is described through a linear elastic interfacial constitutive law. Applications to simply supported and cantilevered wide plates prove the accuracy of the model in predicting displacement and stress fields in plates with continuous imperfect and fully debonded interfaces. Preliminary applications of the model to delamination problems are also presented. It is shown that when the model is applied to solve plates with finite length imperfect interfaces, the accuracy of the results depends on the difference between the interfacial stiffnesses of the interfaces ahead and behind the crack tip. This limitation strongly affects applications to Linear Elastic Fracture Mechanics problems and is expected to have effects in cohesive crack modeling.

TABLE OF CONTENTS

1 INTRODUCTION 1

1.1 MULTILAYERED MATERIALS AND STRUCTURES 1

1.2 PROBLEM DEFINITION AND METHODOLOGY 1

1.3 MOTIVATIONS 2

1.3.1 Elastic regime of laminated composites 2

1.3.2 Post-elastic regime of laminated composites 3

1.4 OBJECTIVES 4

1.5 THESIS OUTLINE 5

2 STATE OF THE ART 7

2.1 INTRODUCTION 7

2.2 THERMO-ELASTICITY MODELS FOR MULTILAYERED STRUCTURES 7

2.2.1 Perfectly bonded multilayered composites 7

2.2.2 Imperfectly bonded multilayered composites 8

2.2.3 Matrix formulations in thermo-elasticity: the transfer matrix method 10

2.3 STRUCTURAL THEORIES FOR MULTILAYERED COMPOSITES 11

2.3.1 Equivalent single layer theories 12

2.3.2 Zigzag theories: perfectly bonded layers 12

2.3.3 Zigzag theories: imperfectly bonded layers 15

2.3.4 Homogenized structural theory ([25]) 16

3 A MATRIX TECHNIQUE FOR THERMO-ELASTIC ANALYSIS OF MULTILAYERED STRUCTURES 27

3.1 INTRODUCTION 27

3.2 CLOSED-FORM 2D THERMO-ELASTICITY SOLUTIONS FOR MULTILAYERED WIDE PLATES WITH IMPERFECT INTERFACES AND IMPERFECT THERMAL CONTACT 27

3.2.1 Heat conduction and thermo-elastic problems 30

3.2.2 Solution of the heat conduction problem through the transfer matrix method 32

3.2.3 Solution of the thermo-elastic problem through the transfer matrix method 35

3.2.4 Application to simply supported plates and sandwiches subjected to mechanical loading 41

3.2.5 Application to simply supported plates subjected to thermal loading 55

3.3 CLOSED-FORM 3D THERMO-ELASTICITY SOLUTIONS FOR MULTILAYERED PLATES WITH IMPERFECT INTERFACES AND IMPERFECT THERMAL CONTACT 63

3.3.1 Problem formulation 65

3.3.2 Solution of the heat conduction problem through the transfer matrix method 67
3.3.3 Solution of the thermo-elastic problem through the transfer matrix method 68
3.3.4 Application to simply supported plates subjected to mechanical loading 78
3.3.5 Application to simply supported plates subjected to thermal loading 83
3.4 CONCLUSIONS 93
4 A HOMOGENIZED APPROACH FOR DELAMINATION FRACTURE OF LAMINATED WIDE PLATES AND BEAMS 95
4.1 INTRODUCTION 95
4.2 HOMOGENIZED STRUCTURAL THEORY FOR BI-MATERIAL WIDE PLATES AND BEAMS 95
4.2.1 Model assumptions 95
4.2.2 Multiscale treatment and homogenization 98
4.2.3 Homogenized field equations 101
4.3 DERIVATION OF LOCAL FIELDS 106
4.4 ENERGY RELEASE RATE 113
4.4.1 J-integral along the external boundaries of the element 114
4.4.2 Energy release rate in a homogeneous layer 118
4.4.3 Energy release rate in terms of local measures 119
4.4.4 Energy release rate through total potential energy 121
4.5 MODEL APPLICATIONS AND DISCUSSION 122
4.5.1 Energy release rate in a homogeneous ENF specimen with equal thickness layers 124
4.5.2 Homogeneous ENF specimen with unequal thickness layers 125
4.5.3 Bi-material ENF specimen with equal thickness layers 125
4.5.4 Numerical results and discussion 126
4.5.5 Macro-structural behavior of a homogeneous ENF specimen 130
4.5.6 Displacements, stresses and interfacial tractions in a homogeneous ENF specimen 132
4.6 CONCLUSIONS 135
5 A HOMOGENIZED STRUCTURAL THEORY BASED ON THE REFINED ZIGZAG THEORY FOR WIDE PLATES AND BEAMS WITH IMPERFECT INTERFACES AND DELAMINATIONS 137
5.1 INTRODUCTION 137
5.2 MODEL ASSUMPTIONS 137
5.3 HOMOGENIZED STRUCTURAL THEORY 139
5.3.1 Derivation of the zigzag functions 140
5.3.2 Homogenized field equations 146

5.4 MODEL VERIFICATION AND APPLICATIONS 151
5.5 PRELIMINARY APPLICATIONS TO DELAMINATION PROBLEMS 159
5.6 CONCLUSIONS 165
6 CONCLUSIONS 167
6.1 FUTURE DEVELOPMENTS 169
APPENDIX A: DERIVATION OF THE UNKNOWN CONSTANTS OF THE HEAT CONDUCTION PROBLEM IN CHAPTER 3 170
APPENDIX B: UNKNOWN CONSTANTS OF THE PARTICULAR SOLUTION OF LAYER *K* IN CHAPTER 3 172
APPENDIX C: MATRIX $^{(k)}\boldsymbol{E}$ IN CHAPTER 3 173
APPENDIX D: DERIVATION OF DISPLACEMENTS AND STRESSES IN CHAPTER 3 176
APPENDIX E: MATRIX $^{(k)}\boldsymbol{E}(x_3)$ IN CHAPTER 3 178
APPENDIX F: CONSTANTS $^{(1)}\boldsymbol{M}_l(x_3^0)$, $^{(k)}\Omega_{rl}$ AND $^{(k)}\boldsymbol{S}_t$ IN CHAPTER 3 183
APPENDIX G: COEFFICIENTS AND TERMS IN THE EQUILIBRIUM EQUATIONS AND BOUNDARY CONDITIONS IN CHAPTER 4 184
APPENDIX H: PERTURBATION ANALYSIS IN CHAPTER 4 185
REFERENCES 189

List of Figures

Figure 1-1: Schematic illustration of a homogenized approach for modeling delamination fracture in laminates subjected to transverse loading. The shaded parts indicate regions characterized by different global properties accounting for the presence of one or more delaminations.

Figure 2-1: Schematic illustration of defects in the bonding region between two composite layers and their relative displacements after loading.

Figure 2-2: Interfacial temperature jump due to the interfacial thermal resistance.

Figure 2-3: Murakami zigzag functions in a three-layer system.

Figure 2-4: Schematic illustration of the displacement field of Di Sciuva's theory for a three-layer system: global model enriched by zigzag functions.

Figure 2-5: Schematic illustration of the displacement field of the refined zigzag theory for a three-layer system: global model enriched by zigzag contribution.

Figure 2-6: (a) Laminated composite plate with multiple delaminations and cohesive interfaces. (b) Exemplary piecewise linear cohesive traction law.

Figure 3-1: Simply supported multilayered plate subjected to thermo-mechanical loadings. Surface tractions correspond to the case $p = \pi/L$, $(m = 1)$.

Figure 3-2: Schematic of the Transfer Matrix Method.

Figure 3-3: (a) Longitudinal at $x_2 = 0$ and (b) transverse at $x_2 = L/2$ displacements through thickness in a simply supported three-layer plate $(0,90,0)$ under plane-strain conditions, $L/h = 4$, normal surface tractions $f_3 = f_u \sin(\pi x_2/L)$ acting on upper surface. Elastic constants: $E_L/E_T = 17$, $G_{LT}/E_T = 0.7$, $G_{TT}/E_T = 0.6$, $\nu_{LT} = 0.28$ and $\nu_{TT} = 0.4$.

Figure 3-4: (a) Bending at $x_2 = L/2$, (b) transverse shear at $x_2 = 0$ and (c) transverse normal at $x_2 = L/2$ stresses through thickness in a simply supported three-layer plate $(0,90,0)$ under plane-strain conditions, $L/h = 4$, normal surface tractions $f_3 = f_u \sin(\pi x_2/L)$ acting on upper surface. Elastic constants: $E_L/E_T = 17$, $G_{LT}/E_T = 0.7$, $G_{TT}/E_T = 0.6$, $\nu_{LT} = 0.28$ and $\nu_{TT} = 0.4$.

Figure 3-5: (a) Longitudinal at $x_2 = 0$ and (b) transverse at $x_2 = L/2$ displacements through thickness in a simply supported five-layer plate $(0,90,0,90,0)$ under plane-strain conditions, $L/h = 4$, normal surface tractions $f_3 = f_u \sin(\pi x_2/L)$ acting on upper surface. Elastic constants: $E_L/E_T = 17$, $G_{LT}/E_T = 0.7$, $G_{TT}/E_T = 0.6$, $\nu_{LT} = 0.28$ and $\nu_{TT} = 0.4$.

Figure 3-6: (a) Bending at $x_2 = L/2$, (b) transverse shear at $x_2 = 0$ and (c) transverse normal at $x_2 = L/2$ stresses through thickness in a simply supported five-layer plate $(0,90,0,90,0)$ under plane-strain conditions, $L/h = 4$, normal surface tractions $f_3 = f_u \sin(\pi x_2/L)$ acting on upper surface. Elastic constants: $E_L/E_T = 17$, $G_{LT}/E_T = 0.7$, $G_{TT}/E_T = 0.6$, $\nu_{LT} = 0.28$ and $\nu_{TT} = 0.4$.

Figure 3-7: (a) longitudinal at $x_2 = 0$, (b) transverse at $x_2 = L/2$ displacements, (c) bending at $x_2 = L/2$, (d) transverse shear at $x_2 = 0$ and (e) transverse normal at $x_2 = L/2$ stresses through thickness in a simply supported symmetric sandwich plate under plane-strain conditions, $L/h = 4$, normal surface tractions

$f_3 = f_u \sin(\pi x_2/L)$ acting on upper surface. Thickness of face sheets and core $0.1h$ and $0.8h$. Elastic constants: $E_2^f/E_3^f = 17$, $G_{23}^f/E_3^f = 0.7$, $\nu_{23}^f = \nu_{21}^f = 0.28$, and $\nu_{31}^f = 0.4$, $E_2^c/E_3^f = 0.016$, $E_3^c/E_3^f = 0.026$, $G_{23}^c/E_3^f = 0.006$ and $\nu_{23}^c = \nu_{21}^c = \nu_{31}^c = 0.32$.

Figure 3-8: (a) Through-thickness temperature distribution at $x_2 = L/2$ in a three-layer plate $(0,90,0)$, $L/h = 4$, applied temperature $T = -T_0 \sin(\pi x_2/L)$ on upper surface, and (b) normalized temperature in the upper layer at the interface at $x_2 = L/2$ on increasing RK_L/h ($RK_L/h = 0$ perfect contact; $h/(RK_L) = 0$ impermeable interface). The thermal conductivities of the layers, $K_T/K_L = 0.16$.

Figure 3-9: (a) Longitudinal at $x_2 = 0$ and (b) transverse at $x_2 = L/2$ displacements through thickness in a simply supported three-layer plate $(0,90,0)$ under plane-strain conditions, $L/h = 4$, applied temperature $T = -T_0 \sin(\pi x_2/L)$ on upper surface. Thermo-elastic constants: $E_L/E_T = 17$, $G_{LT}/E_T = 0.7$, $G_{TT}/E_T = 0.6$, $\nu_{LT} = 0.28$, $\nu_{TT} = 0.4$, $\alpha_T/\alpha_L = 1125$ and $K_T/K_L = 0.16$. Imperfect thermal contact, $RK_L/h = 10$.

Figure 3-10: (a) Bending at $x_2 = L/2$, (b) transverse shear at $x_2 = 0$ and (c) transverse normal at $x_2 = L/2$ stresses through thickness in a simply supported three-layer plate $(0,90,0)$ under plane-strain conditions, $L/h = 4$, applied temperature $T = -T_0 \sin(\pi x_2/L)$ on upper surface. Thermo-elastic constants: $E_L/E_T = 17$, $G_{LT}/E_T = 0.7$, $G_{TT}/E_T = 0.6$, $\nu_{LT} = 0.28$, $\nu_{TT} = 0.4$, $\alpha_T/\alpha_L = 1125$ and $K_T/K_L = 0.16$. Imperfect thermal contact, $RK_L/h = 10$.

Figure 3-11: Simply supported multilayered plate with thermally and/or mechanically imperfect interfaces.

Figure 3-12: Through thickness variation of (a) displacements in x_1 direction at $(x_1 = 0, x_2 = a/2)$, (b) displacements in x_2 direction at $(x_1 = b/2, x_2 = 0)$, (c) transverse displacements at $(x_1 = b/2, x_2 = a/2)$, (d) bending stresses in x_1 direction at $(x_1 = b/2, x_2 = a/2)$ and (e) bending stresses in x_2 direction at $(x_1 = b/2, x_2 = a/2)$ in a simply supported three-layer square plate $(0,90,0)$, $a/h = b/h = 4$, normal surface tractions $f_3 = f_u \sin(\pi x_1/b)\sin(\pi x_2/a)$ acting on upper surface. Elastic constants: $E_L/E_T = 25$, $G_{LT}/E_T = 0.5$, $G_{TT}/E_T = 0.2$ and $\nu_{LT} = \nu_{TT} = 0.25$. L direction coincides with x_2 axis in the outer layers. Identical interfaces with $K_{S1} = K_{S2} = K_S$.

Figure 3-13: Through thickness variation of (a) in-plane shear stresses at $(x_1 = 0, x_2 = 0)$, (b) transverse shear stresses σ_{13} at $(x_1 = 0, x_2 = a/2)$, (c) transverse shear stresses σ_{23} at $(x_1 = b/2, x_2 = 0)$ and (d) transverse normal stresses at $(x_1 = b/2, x_2 = a/2)$ in a simply supported three-layer square plate $(0,90,0)$, $a/h = b/h = 4$, normal surface tractions $f_3 = f_u \sin(\pi x_1/b)\sin(\pi x_2/a)$ acting on upper surface. Elastic constants: $E_L/E_T = 25$, $G_{LT}/E_T = 0.5$, $G_{TT}/E_T = 0.2$ and $\nu_{LT} = \nu_{TT} = 0.25$. L direction coincides with x_2 axis in the outer layers. Identical interfaces with $K_{S1} = K_{S2} = K_S$.

Figure 3-14: (a) Through-thickness temperature distribution at $(x_1 = b/2, x_2 = a/2)$ in a three-layer plate $(0,90,0)$, $a/h = b/h = 8$, applied temperature $T_0 \sin(\pi x_1/b)\sin(\pi x_2/a)$ on upper and $-T_0 \sin(\pi x_1/b)\sin(\pi x_2/a)$ on lower surfaces, and (b) normalized temperature in the upper layer at the interface at $(x_1 = b/2, x_2 = a/2)$ on increasing RK_L/h ($RK_L/h = 0$ perfect contact; $h/(RK_L) = 0$ impermeable interface). The thermal conductivities of the layers are $K_L/K_T = 38$. L direction coincides with x_2 axis in the outer layers.

Figure 3-15: Through thickness variation of (a) displacements in x_1 direction at $(x_1 = 0, x_2 = a/2)$, (b) displacements in x_2 direction at $(x_1 = b/2, x_2 = 0)$, (c) transverse displacements at $(x_1 = b/2, x_2 = a/2)$, (d) bending stresses in x_1 direction at $(x_1 = b/2, x_2 = a/2)$ and (e) bending stresses in x_2 direction at $(x_1 = b/2, x_2 = a/2)$ in a simply supported three-layer plate $(0,90,0)$, $a/h = b/h = 8$, applied temperature $T_0 \sin(\pi x_1/b)\sin(\pi x_2/a)$ on upper and $-T_0 \sin(\pi x_1/b)\sin(\pi x_2/a)$ on lower surfaces. Thermo-elastic constants: $E_L/E_T = 25$, $G_{LT}/E_T = 0.5$, $G_{TT}/E_T = 0.2$, $\nu_{LT} = \nu_{TT} = 0.25$, $\alpha_T/\alpha_L = 62$ and $K_L/K_T = 38$. L direction coincides with x_2 axis in the outer layers. Interfaces are mechanically perfect.

Figure 3-16: Through thickness variation of (a) in-plane shear stresses at $(x_1 = 0, x_2 = 0)$, (b) transverse shear stresses σ_{13} at $(x_1 = 0, x_2 = a/2)$, (c) transverse shear stresses σ_{23} at $(x_1 = b/2, x_2 = 0)$ and (d) transverse normal stresses at $(x_1 = b/2, x_2 = a/2)$ in a simply supported three-layer plate $(0,90,0)$, $a/h = b/h = 8$, applied temperature $T_0 \sin(\pi x_1/b)\sin(\pi x_2/a)$ on upper and $-T_0 \sin(\pi x_1/b)\sin(\pi x_2/a)$ on lower surfaces. Thermo-elastic constants: $E_L/E_T = 25$, $G_{LT}/E_T = 0.5$, $G_{TT}/E_T = 0.2$, $\nu_{LT} = \nu_{TT} = 0.25$, $\alpha_T/\alpha_L = 62$ and $K_L/K_T = 38$. L direction coincides with x_2 axis in the outer layers. Interfaces are mechanically perfect.

Figure 4-1: A bi-material element extracted from a wide plate subjected to transverse loads, and (b) its homogenized description obtained through the multiscale structural theory.

Figure 4-2: (a) Interfacial traction law used to approximate linear elastic fracture mechanics. (b) The interfacial traction law used in the solution of the problem through the multiscale model. (c) Schematic description of the assumed two length scales displacement field: global displacement and local perturbations.

Figure 4-3: (a) a bi-material cracked element subjected to end forces. The element is extracted from a loaded plate, e.g. Figure 4-1(a). (b) The homogenized representation of the cracked element, showing the path Γ used for the calculation of the J-integral.

Figure 4-4: Local coordinates and rotations of the layers in the homogenized element.

Figure 4-5: (a) the edge-cracked element under mode II dominant assumption, which is created by superposing intact (b), and cracked (c) problems.

Figure 4-6: (a) The ENF specimen under mode II dominant conditions and (b) the homogenized description of the problem.

Figure 4-7: Relative percent error between the energy release rates of the homogenized model and 2D solution [95] in homogeneous ENF specimen with ${}^{(2)}h = {}^{(1)}h = h$. Material: $E_T/E_L = 0.071$, $G_{LT}/E_L = 0.033$, $\nu_{LT} = 0.32$ and $\nu_{TT} = 0.45$ (L and T indicate in-plane principal material directions with L = x_2). "From sub-resultants Eq. (4-60)", "From crack surface displacements Eq. (4-63)" and "from compliance Eq. (4-65)" refer to relative percent errors of energy release rates in Eqs. (4-60), (4-63) and (4-65), and Eq. (4-70).

Figure 4-8: Relative percent error between the energy release rates of the homogenized model and 2D solution [95] in homogeneous ENF specimen with ${}^{(1)}h = 4h/3$ *and* ${}^{(2)}h = 2h/3$. Material: $E_T/E_L = 0.071$, $G_{LT}/E_L = 0.033$, $\nu_{LT} = 0.32$ and $\nu_{TT} = 0.45$ (L and T indicate in-plane principal material directions with L = x_2). "From sub-resultants Eq. (4-60)" and "From crack surface displacements Eq. (4-63)" refer to relative percent errors of energy release rates in Eqs. (4-60) and (4-63), and Eq. (4-72).

Figure 4-9: Relative percent error between the energy release rates of the homogenized model and 2D solution [103] in bi-material ENF specimen made of two incompressible isotropic layers with ${}^{(1)}h = {}^{(2)}h = h$ and ${}^{(2)}E/{}^{(1)}E = 2/3$. "From sub-resultants Eq. (4-55)" and "From crack surface displacements Eq. (4-63)" refer to relative percent errors of energy release rates in Eqs. (4-55) and (4-63), and Eq. (4-74).

Figure 4-10: Dimensionless critical load versus load point displacement of homogeneous ENF specimen with ${}^{(2)}h = {}^{(1)}h = h$, $2L = 200h/3$ and $a_0 = 20h$. Material: $E_T/\overline{C}_{22} = 0.071$, $G_{LT}/\overline{C}_{22} = 0.033$ (L and T indicate in-plane principal material directions with L = x_2). Shear correction factor, $k_{44} = 5/6$.

Figure 4-11: Comparison of the bending stresses at the lower surface of the plate through the length, calculated by the homogenized model and the discrete layer interface model.

Figure 4-12: Distributions of bending stresses at the traction-free delamination tip in the cracked and intact regions.

Figure 4-13: Comparison between the interfacial tractions calculated a posteriori by the homogenized model and those obtained through discrete layer interface model. The dimensionless interfacial shear tractions tend to the constant value -3/8, which is the maximum transverse shear stress of the layers far from the traction-free delamination tip.

Figure 5-1: Multilayered wide plate/beam with imperfect interfaces and delaminations.

Figure 5-2: Schematic description of the assumed displacement field in a three layers laminate: global displacement and local perturbations.

Figure 5-3: (a) Layers joined by imperfect interfaces. (b) Representing imperfect interfaces as thin layers. (c) Values of the zigzag functions below and above the thin layer $\bar{k}$, perfectly bonded to layers k and k+1 .

Figure 5-4: Three-layered plate with linear elastic interfaces subjected to sinusoidal transverse loading.

Figure 5-5: Longitudinal at $x_2 = 0$ and transverse at $x_2 = L/2$ displacements through the thickness in a simply supported three-layer wide plate $(0,0,0)$, $L/h = 4$, transverse loading $F_3^{S^+} = F_3^{S^-} = f_0/2\left[\sin(\pi x_2/L)\right]$. Elastic constants: $E_L/E_T = 25$, $G_{LT}/E_T = 0.5$, $G_{TT}/E_T = 0.2$ and $\nu_{LT} = \nu_{TT} = 0.25$. Shear correction factor $k_{44} = 5/6$.

Figure 5-6: Bending at $x_2 = L/2$ and transverse shear at $x_2 = 0$ stresses through the thickness in a simply supported three-layer wide plate $(0,0,0)$, $L/h = 4$, transverse loading $F_3^{S^+} = F_3^{S^-} = f_0/2\left[\sin(\pi x_2/L)\right]$. Elastic constants: $E_L/E_T = 25$, $G_{LT}/E_T = 0.5$, $G_{TT}/E_T = 0.2$ and $\nu_{LT} = \nu_{TT} = 0.25$. Transverse shear stresses are calculated a posteriori from bending stresses. Shear correction factor $k_{44} = 5/6$.

Figure 5-7: Transverse displacements at $x_2 = L/2$ at the top of a simply supported two-layer wide plate $(0,0)$, $L/h = 4$; layers connected by a linear elastic interface at the mid-thickness, transverse loading $F_3^{S^+} = f_0 \sin(\pi x_2/L)$ on its upper surface, while the lower surface of the plate is traction-free [25]. The results are normalized to those of a fully debonded plate, $(v_3)_{2D,\lim}$, and shown on varying the interfacial stiffness (decreasing interfacial stiffness from left to right). Elastic constants: $E_L/E_T = 25$, $G_{LT}/E_T = 0.5$, $G_{TT}/E_T = 0.2$ and $\nu_{LT} = \nu_{TT} = 0.25$. Shear correction factor $k_{44} = 5/6$.

Figure 5-8: Longitudinal at $x_2 = 0$ and transverse at $x_2 = L/2$ displacements through the thickness in a simply supported three-layer wide plate $(0,90,0)$, $L/h = 4$, transverse loading $F_3^{S^+} = F_3^{S^-} = f_0/2[\sin(\pi x_2/L)]$. Elastic constants: $E_L/E_T = 25$, $G_{LT}/E_T = 0.5$, $G_{TT}/E_T = 0.2$ and $\nu_{LT} = \nu_{TT} = 0.25$. Shear correction factor $k_{44} = 1$.

Figure 5-9: Bending at $x_2 = L/2$ and transverse shear at $x_2 = 0$ stresses through the thickness in a simply supported three-layer wide plate $(0,90,0)$, $L/h = 4$, transverse loading $F_3^{S^+} = F_3^{S^-} = f_0/2[\sin(\pi x_2/L)]$. Elastic constants: $E_L/E_T = 25$, $G_{LT}/E_T = 0.5$, $G_{TT}/E_T = 0.2$ and $\nu_{LT} = \nu_{TT} = 0.25$. Transverse shear stresses are calculated a posteriori from bending stresses. Shear correction factor $k_{44} = 1$.

Figure 5-10: A cantilevered plate composed of two layers joined by a linear elastic interface at the mid-thickness and subjected to transverse load F at the free end [26].

Figure 5-11: Interfacial tractions along the length of a cantilever two-layer with plate $(0,0)$, $L/h = 10$, subjected to a concentrated transverse force F at the free end (Figure 5-6) [26]. Two identical layers connected by a linear elastic interface at the mid-thickness. The elastic constants: $E_L/E_T = 25$, $G_{LT}/E_T = 0.5$, $G_{TT}/E_T = 0.2$ and $\nu_{LT} = \nu_{TT} = 0.25$. Interfacial tractions predicted by the model used in Chapter 4 [25] are calculated a posteriori from the bending stresses.

Figure 5-12: ENF specimen with two layers of equal thickness, bonded by two linear elastic interfaces with different interfacial stiffness for $0 \le x_2 \le a$ and $a \le x_2 \le 2L$.

Figure 5-13: Deflection of the specimen in Figure 5-12 with $2L/h = 100$ and $a/h = 30$ made of $E_T/E_L = 0.071$, $G_{LT}/E_L = 0.033$, $\nu_{LT} = 0.32$ and $\nu_{TT} = 0.45$. (a) $K_S h/E_L = 10$ for $0 \le x_2 \le a$ and $K_S h/E_L = 10^4$ for $a \le x_2 \le 2L$ (fully bonded), and (b) $K_S h/E_L = 10^{-3}$ for $0 \le x_2 \le a$ and $K_S h/E_L = 10^4$ for $a \le x_2 \le 2L$. Correction factor $k_{44} = 5/6$.

Figure 5-14: (a) Interfacial tractions and (b) interfacial jumps from $x_2 = 0$ to $x_2 = L$ in the specimen in Figure 5-12 with $2L/h = 100$ and $a/h = 30$ made of $E_T/E_L = 0.071$, $G_{LT}/E_L = 0.033$, $\nu_{LT} = 0.32$ and $\nu_{TT} = 0.45$. $K_S h/E_L = 10$ for $0 \le x_2 \le a$ and $K_S h/E_L = 10^4$ for $a \le x_2 \le 2L$ (fully bonded). Correction factor $k_{44} = 5/6$.

Figure 5-15: (a) Interfacial tractions and (b) interfacial jumps from $x_2 = 0$ to $x_2 = L$ in the specimen in Figure 5-12 with $2L/h = 100$ and $a/h = 30$ made of $E_T/E_L = 0.071$, $G_{LT}/E_L = 0.033$, $\nu_{LT} = 0.32$ and $\nu_{TT} = 0.45$. $K_S h/E_L = 10^{-3}$ for $0 \le x_2 \le a$ and $K_S h/E_L = 10^4$ for $a \le x_2 \le 2L$ (fully bonded). Correction factor $k_{44} = 5/6$.

Figure 5-16: (a) Deflection of the specimen in Figure 5-12 with $2L/h = 100$ and $a/h = 30$ made of $E_T/E_L = 0.071$, $G_{LT}/E_L = 0.033$, $\nu_{LT} = 0.32$ and $\nu_{TT} = 0.45$. $K_S h/E_L = 10^{-4}$ for $0 \le x_2 \le a$ and $K_S h/E_L = 10^4$ for $a \le x_2 \le 2L$ (fully bonded). (b) Deflection of a perfectly bonded specimen in Figure 5-13 with $2L/h = 100$ and $a/h = 30$ made of $E_T/E_L = 0.071$, $G_{LT}/E_L = 0.033$, $\nu_{LT} = 0.32$ and $\nu_{TT} = 0.45$. The shear modulus in the portion of the specimen within $0 \le x_2 \le a$ is reduced to $0.01G_{LT}$. Correction factor $k_{44} = 5/6$.

List of Tables

Table 3-1: Dimensionless quantities (with ${}^{(1)}\alpha_2$, h and ${}^{(1)}C_{22}$ as fundamental units).

Table 3-2: Simply supported three-layer plate $(0,90,0)$ under plane-strain conditions: normal surface tractions $f_3 = f_u \sin(\pi x_2/L)$ acting on upper surface. Elastic constants: $E_L/E_T = 17$, $G_{LT}/E_T = 0.7$, $G_{TT}/E_T = 0.6$, $\nu_{LT} = 0.28$ and $\nu_{TT} = 0.4$. Subscripts l and u correspond to values below and above the interface.

Table 3-3: Simply supported five-layer plate $(0,90,0,90,0)$ under plane-strain conditions: normal surface tractions $f_3 = f_u \sin(\pi x_2/L)$ acting on upper surface. Elastic constants: $E_L/E_T = 17$, $G_{LT}/E_T = 0.7$, $G_{TT}/E_T = 0.6$, $\nu_{LT} = 0.28$ and $\nu_{TT} = 0.4$. Subscripts l and u correspond to values below and above the interface.

Table 3-4: Simply supported symmetric sandwich plate under plane-strain conditions with thickness of face sheets and core $0.1h$ and $0.8h$: normal surface tractions $f_3 = f_u \sin(\pi x_2/L)$ acting on upper surface. Elastic constants $E_2^f/E_3^f = 17$, $G_{23}^f/E_3^f = 0.7$, $\nu_{23}^f = \nu_{21}^f = 0.28$, and $\nu_{31}^f = 0.4$; $E_2^c/E_3^f = 0.016$, $E_3^c/E_3^f = 0.026$, $G_{23}^c/E_3^f = 0.006$ and $\nu_{23}^c = \nu_{21}^c = \nu_{31}^c = 0.32$. Subscripts l and u correspond to values below and above the interface.

Table 3-5: Simply supported three-layer plate $(0,90,0)$ under plane-strain conditions: applied temperature $T = -T_0 \sin(\pi x_2/L)$ on upper surface. Thermo-elastic constants: $E_L/E_T = 17$, $G_{LT}/E_T = 0.7$, $G_{TT}/E_T = 0.6$, $\nu_{LT} = 0.28$, $\nu_{TT} = 0.4$, $\alpha_T/\alpha_L = 1125$ and $K_T/K_L = 0.16$. Perfect thermal contact, $R = 0$. Subscripts l and u correspond to values below and above the interface.

Table 3-6: Simply supported three-layer $(0,90,0)$ plate under plane-strain conditions: applied temperature $T = -T_0 \sin(\pi x_2/L)$ on upper surface. Thermo-elastic constants: $E_L/E_T = 17$, $G_{LT}/E_T = 0.7$, $G_{TT}/E_T = 0.6$, $\nu_{LT} = 0.28$, $\nu_{TT} = 0.4$, $\alpha_T/\alpha_L = 1125$ and $K_T/K_L = 0.16$. Imperfect thermal contact, $RK_L/h = 10$. Subscripts l and u correspond to values below and above the interface.

Table 3-7: Simply supported three-layer plate $(0,90,0)$, $a/h = 4$: normal surface tractions $f_3 = f_u \sin(\pi x_1/b)\sin(\pi x_2/a)$ acting on upper surface. Elastic constants: $E_L/E_T = 25$, $G_{LT}/E_T = 0.5$, $G_{TT}/E_T = 0.2$ and $\nu_{LT} = \nu_{TT} = 0.25$. L direction coincides with x_2 axis in the outer layers. Subscripts l and u correspond to values below and above the interface. Identical interfaces with $K_{S1} = K_{S2} = K_S$.

Table 3-8: Simply supported three-layer plate $(0,90,0)$, $a/h = 4$: applied temperature $T = T_u \sin(\pi x_1/b)\sin(\pi x_2/a)$ on upper surface. Thermo-elastic constants: $E_L/E_T = 25$, $G_{LT}/E_T = 0.5$, $G_{TT}/E_T = 0.2$, $\nu_{LT} = \nu_{TT} = 0.25$, $\alpha_T/\alpha_L = 62$ and $K_L/K_T = 38$. L direction coincides with x_2 axis in the outer layers. Perfect thermal contact, $R = 0$. Subscripts l and u correspond to values below and above the interface; Identical interfaces with $K_{S1} = K_{S2} = K_S$.

Table 3-9: Simply supported three-layer plate $(0,90,0)$, $a/h = 4$: applied temperature $T = T_u \sin(\pi x_1/b)\sin(\pi x_2/a)$ on upper surface. Thermo-elastic constants: $E_L/E_T = 25$, $G_{LT}/E_T = 0.5$, $G_{TT}/E_T = 0.2$, $\nu_{LT} = \nu_{TT} = 0.25$, $\alpha_T/\alpha_L = 62$ and $K_L/K_T = 38$. L direction coincides with x_2 axis in the

outer layers. Imperfect thermal contact with $RK_L/h = 15$. Subscripts *l* and *u* correspond to values below and above the interface. Identical interfaces with $K_{S1} = K_{S2} = K_S$.

Table H-1: Orders of the coefficients when $\delta = \overline{B} \to 0$.

INTRODUCTION

1.1 MULTILAYERED MATERIALS AND STRUCTURES

A multilayered composite is a stack of several layers joined together to achieve superior properties, such as high strength-to-weight ratio, energy absorption and fatigue life. Laminated composite plates and shells and sandwich structures are exemplary structures which use multilayered composites. A laminate is made up of several laminae which are bounded together to meet certain design requirements. A sandwich structure is composed of two relatively thin but stiff skins attached to a core which is made of lightweight materials such as balsa, foam or honeycomb. The mechanical properties of laminated composite structures depend on their fabrication quality. The fabrication methods include autoclave molding, filament winding and resin transfer molding [1].

Nowadays, laminated composite and sandwich structures are largely used in different areas of technology and industry. Their applications as primary structures in mechanical devices and vehicles, such as turbines, wind-blades, aircrafts or ships, are increasing. The interest in the use of layered materials is due to the fact that their mechanical properties can be tailored, by proper selection of the materials and design of the layups, to meet the growing design requirements of modern mechanical devices.

More than 50% weight of the Boeing 787 and the A350 XWB is made of composite materials [2]. Sandwich structures, are being used in Helicopter blades, vertical tail planes, airplane fuselage and wings, for instance in the Airbus A380 [3], and in ships due to their optimal performance as insulation, lower manufacturing cost and lack of corrosion. Composite laminates are being used in the construction of bridge decks [4] and have structural applications in automotive vehicles [5]. Use of composite laminates and sandwiches in the blades of wind turbine significantly increases the power output and reduces the cost. These are only a few examples of applications of laminated composite structures, which continue to expand. Understanding the mechanical behaviour of layered materials and structures is an active research line and the scientific community is currently working on the development of physically based predictive mechanical models for the confident design of such structures.

1.2 PROBLEM DEFINITION AND METHODOLOGY

Current applications of laminated composite and sandwich structures require withstanding severe mechanical loadings and surviving aggressive environments, characterized for instance by very high or very low temperatures. Laminated structures used in the external parts of aircrafts or ships, face a wide range of operational temperature, aerodynamic loads and impacts. These structures often have complex geometries and boundary conditions, and are composed of many layers exhibiting different material properties. To design layered structures and define their load-bearing capacity and life, accurate understanding of their mechanical behavior in the elastic and post-elastic regimes is needed.

The focus of this thesis is on the elastic and delamination response of layered composite structures subjected to stationary thermo-mechanical loading. In the first part of the thesis, the 2D/3D thermo-elasticity models previously developed in [6, 7] are used along with matrix techniques to derive novel explicit expressions for temperature, displacements and stresses in multilayered plates with an arbitrary number of imperfectly bonded layers in imperfect thermal contact. In the second part, a model is formulated to study the delamination of layered structures in a homogenized fashion through multiscale structural theories.

1.3 MOTIVATIONS

1.3.1 Elastic regime of laminated composites

Wherever possible, two- and three-dimensional thermo-elasticity approaches are the first choice to study the elastic response of layered plates because they exactly predict the field variables and allow to perform parametric analyses. In many case, the exact elasticity solutions are not available, due for instance to the complex geometry, loading and boundary conditions. For such cases, numerical models and/or approximate structural theories are applied to describe the response of the layered structures. The thermo-elastic solutions are valuable because they can be used to assess the accuracy of these numerical and approximate models.

While the early thermo-elastic solutions were derived for laminates with perfectly bonded layers, simple geometries, boundary and loading conditions [6, 8], recent works include solutions for plates with thermally and mechanically imperfect interfaces and boundary conditions other than the simple support [7, 9]. All the aforementioned thermo-elasticity theories firstly derive a general solution for a generic layer of the structure and then impose continuity and boundary conditions to obtain the unknown constants. Therefore, the problem becomes more complex on increasing the number of layers and may require numerical solutions. This limits the applicability of the methods and reference is often made to a few classical examples, which have been presented in some original papers for fully bonded layers in perfect thermal contact, e.g. [8, 10]. These solutions are often used also to verify theories which are based on different assumptions and account, for instance, of interfacial imperfections. This may lead to misjudgments on their accuracy and range of validity (see [11] for a discussion on this problem).

Matrix techniques have been formulated to overcome the above-mentioned limitation, i.e. computationally expensive solutions for laminates with many layers, and derive thermo-elastic solutions for laminates with many layers [12-18]. However, the solutions are derived and presented only in matrix form, can be obtained through many matrix multiplications and no expanded explicit expressions are given for the field variables; the solution then remains quite complex. Moreover, none of the current matrix formulations in the literature consider the effect of thermally imperfect interfaces.

Thermo-elastic models for multilayered plates with thermally and mechanically imperfect interfaces can be found in the literature, for instance in [7, 19]; however, closed-form expressions for the field variables do not exist in the open literature neither for perfectly bonded nor for imperfectly bonded laminates. It would be then desirable to derive explicit and easy to use expressions which exactly predict the stress and displacement components in laminates with any number of layers and thermally and mechanically

imperfect interfaces. Such expressions could be readily applied to generate benchmark solutions for the verification of numerical models and approximate theories.

1.3.2 Post-elastic regime of laminated composites

The post-elastic response of layered materials is governed by the interaction of different failure mechanisms which include intraply damage and interply damage or delamination. The intraply damage mechanisms in laminates are in the form of matrix cracking and fiber fracture, result in a global reduction of the stiffness of the layers and can be studied through material degradation and continuum damage models. Delamination is inherently a localized event and is one of the dominant failure mechanisms of layered structures, because of their weak interlaminar properties. Debonding of the layers or delamination takes place in the internal parts of structures and often its presence is undetectable by visual inspection. Delaminations can occur at the stages of fabrication, due to manufacturing errors, storage or transportation, or during the service life, due for instance to impacts. In many practical applications, e.g., those which involve impact or blast loadings, multiple delaminations may form within the layered structures. Because of the high level of interlaminar stresses caused by the inhomogeneous material structure, delaminations may then propagate and cause stiffness degradation or final failure of the components. Studying the onset and propagation of delaminations requires an accurate prediction of the stress field in each layer of the laminated composites.

Progressive delamination failure in laminated composites can be accurately studied through discrete-layer cohesive-crack models (e.g., [20, 21]). In these models, the laminated composite plate is divided through the thickness into discrete layers connected by cohesive interfaces; the mechanical behavior of the interfaces are governed by the cohesive traction laws which relate the interfacial cohesive tractions to the interfacial relative displacement of the layers. The number of the discrete layers is taken to be equal or higher than the number of physical layers. Appropriate kinematic fields are then assumed for the layers and displacements of the layers at the interfaces are related to each other through the cohesive traction laws. The discrete-layer cohesive-crack models are able to accurately predict the interlaminar stresses, and to account for the presence of delaminations. However, the number of unknown variables in these theories depends on the number of layers and delaminations, and therefore, these models become computationally expensive for nonlinear analysis (progressive failure), and when the laminated structure has many layers and delaminations. Therefore, analytical solutions can be obtained only for simple cases and numerical approaches such as finite element method are required for most problems [22-24].

An alternative approach to discrete-layer cohesive-crack modeling has been presented in [25], aimed at modeling delamination fracture in laminated composites through a homogenized structural theory which uses a fixed number of unknown variables independent of the number of layers and delaminations while capturing the local fields due to the inhomogeneous material structure and the presence of delaminations. The homogenized structural theory then removes the through thickness discretization used in discrete approaches and increases the range of problems, for which analytical solutions can be obtained. The schematic illustration of the idea is shown in Figure 1-1.

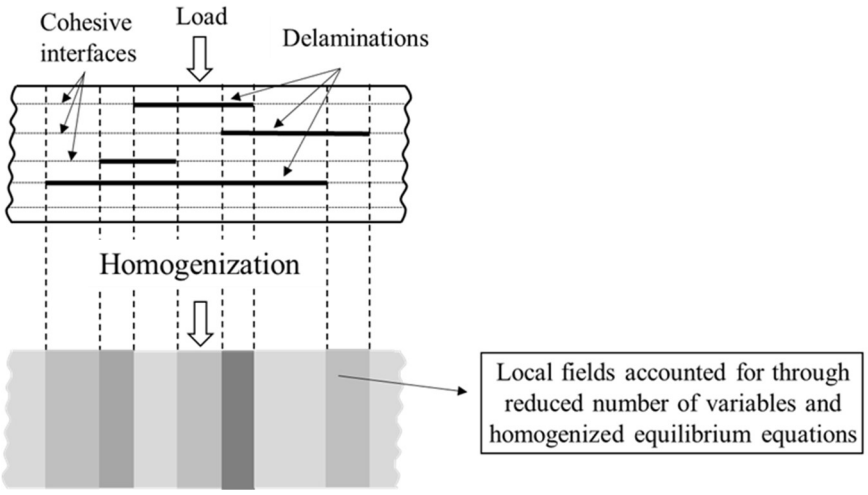

Figure 1-1: Schematic illustration of a homogenized approach for modeling delamination fracture in laminates subjected to transverse loading. The shaded parts indicate regions characterized by different global properties accounting for the presence of one or more delaminations.

The accuracy of the homogenized structural model in predicting the local and global fields in layered plates with continuous, imperfect and fully debonded interfaces and subjected to stationary thermo-mechanical loads has been verified in [7, 11, 25, 26]. In [26], the multiscale structural model has been applied to a delaminated cantilever plate, to preliminary assess the applicability of the model to study fracture problems. The homogenized structural model seems promising in modeling delamination fracture in laminates, and its limitations and advantages should be investigated.

1.4 OBJECTIVES

The general objective of this research is to formulate accurate and efficient physically based methods to model the elastic and delamination response of layered structures. In this regard, the work is divided into two parts. In the first part, a matrix method is formulated which is based on the thermo-elasticity models in [6, 7] and aims at efficiently obtaining exact solutions for stationary two- and three-dimensional problems. The objective of the second part is to formulate a homogenized fracture model, based on the multiscale structural theory in [25], and investigate its advantages and limitations through the application of the model to mode II dominant delamination problems in bi-material wide plates subjected to transverse loads.

The thesis yields:

- novel 2D/3D thermo-elasticity explicit expressions for temperature, displacements and stresses in simply supported multilayered plates with an arbitrary number of layers, arbitrary layups and interfacial thermal and mechanical imperfections, subjected to stationary thermo-mechanical loads;
- formulation and verification of a homogenized fracture model for studying mode II dominant delamination fracture in laminated composite wide plates, based on a multiscale structural approach which removes the through thickness discretization;

- formulation of a refined homogenized structural theory for wide plates with imperfect interfaces and delaminations, which is able to more accurately describe shear deformations, and preliminary application of the model to delamination problems.

1.5 THESIS OUTLINE

The thesis is divided into six chapters. In the first part of Chapter 2, a brief literature review is presented on some of the relevant two- and three-dimensional thermo-elasticity models for laminated and sandwich structures with thermally and mechanically perfect and imperfect interfaces. Thermo-elasticity models based on matrix formulations are also discussed. The second part of Chapter 2, focuses on the structural theories, and reviews some of the equivalent single layer and the zigzag theories. This chapter also covers zigzag theories formulated for layered structures with imperfect interfaces.

In Chapter 3, a matrix technique is formulated and novel 2D/3D thermo-elasticity explicit expressions are derived for the field variables of simply supported multilayered plates composed of imperfectly bonded orthotropic or isotropic layers in imperfect thermal contact and subjected to sinusoidally distributed transverse surface tractions and thermal gradients. The expressions are valid for an arbitrary layup and number of layers, and can be used to solve problems with load distributions other than sinusoidal using Fourier series and the principle of superposition. They are also applicable to the limiting cases of perfectly bonded layers in perfect thermal contact and fully debonded layers or impermeable interfaces. The expressions can be readily applied to generate benchmark solutions and used for the verification of numerical models and approximate theories, with no need to solve algebraic systems, as in the classical approaches, or to perform extensive matrix multiplications, as in other matrix formulations in the literature. The expressions are in dimensionless form to facilitate parametric analyses of the problem.

In Chapter 4, the multiscale structural theory formulated in [25] is particularized to a bi-material wide plate with a single delamination, and a homogenized fracture model is formulated to study mode II dominant problems. The homogenized fracture model is used to investigate a fracture mechanics model system for which accurate Linear Elastic Fracture Mechanics solutions are available for verification. The energy release rate is derived in closed-form through an application of the J-integral in the homogenized problem using the local fields calculated through the multiscale model. The expression of the energy release rate is shown to coincide with the classical solution of the problem, for both bi-material and homogeneous plates. The energy release rate of the model system is also derived through an application of the J-integral along a path surrounding the delamination surfaces to show the accuracy of the homogenized model to capture the relative crack displacements. The model is applied to study delamination growth and investigate the structural response of End Notched Flexural (ENF) specimens. The advantages and limitations of the homogenized approach are discussed.

In Chapter 5, a refined homogenized structural theory is formulated, based on the refined zigzag theory [27] and the homogenized structural theory [25], for wide plates with imperfect interfaces. The theory allows to accurately model all boundary conditions including clamped supports, and has enough kinematic flexibility to adequately describe the shear deformations through the thickness of wide plates with continuous imperfect interfaces. The new model is applied to study simply supported and cantilevered

plates with continuous linear elastic interfaces. For simply supported plates, expressions derived in Chapter 3 are used to generate benchmark solutions and verify the predictive capabilities of the model. The model has difficulties in analyzing wide plates with finite length imperfect interfaces due to the absence of the continuity condition on the slope of the transverse displacement at the cross sections, where two regions characterized by different interfacial stiffness are joined. This limitation affects applications of the model to delamination problems.

In Chapter 6, concluding remarks and suggestions for future research are presented.

STATE OF THE ART

2.1 INTRODUCTION

In the first part of this chapter, Sect. 2.2, some of the relevant available thermo-elastic solutions for perfectly and imperfectly bonded laminated composites are briefly introduced. The concepts of the mechanically and thermally imperfect interfaces, which are used in the literature to account for the interfacial imperfections, are described. The thermo-elasticity models based on the matrix formulations are reviewed in Sect. 2.2.3. The limitations of the current models, which motivated the work presented in Chapter. 3, are also discussed.

The second part of this chapter, Sect. 2.3, focuses on a class of reduced order models for mechanical analysis of laminated composites, known in the engineering community as the structural theories, and briefly introduces some of the equivalent single layer (or smeared laminate) and the zigzag theories; the zigzag theories belong to the more general approaches known as multiscale or global-local approaches [28]. In Sect. 2.3.3, the extension of the zigzag theories to plates with imperfect interfaces is discussed, and the idea of modeling the progressive delamination failure in laminated composite structures through the homogenized structural theories is introduced. The homogenized structural theory, which will be used in Chapter 4 to formulate a homogenized fracture model, is presented in Sect. 2.3.4.

2.2 THERMO-ELASTICITY MODELS FOR MULTILAYERED STRUCTURES

Multilayered structures are frequently used as load-bearing components, also for applications which necessitate withstanding severe thermo-mechanical loadings. Since these structures often have complex geometries, boundary and loading conditions, numerical models and approximate structural theories are typically applied to determine their response in the elastic and post-elastic regimes. Two- and three-dimensional thermo-elasticity solutions are valuable because they exactly predict the field variables and can be used to assess the accuracy of numerical and approximate models and to perform parametric analyses (e.g., [6, 8, 10, 19, 29-35]).

2.2.1 Perfectly bonded multilayered composites

In an early paper [29], Pagano used the Airy's stress function method to obtain an exact solution in the framework of the linear theory of elasticity for simply supported cross-ply laminates composed of perfectly bonded orthotropic/isotropic layers. The solution was given for plates subjected to sinusoidal transverse loads and deforming in cylindrical bending. The theory was extended to include uniformly distributed and concentrated loads described by means of Fourier series in [31] and to treat stationary sinusoidally distributed thermal loads, under the simplifying assumption of linear thickness-wise temperature distribution, in [36]. Thanks to these exact solutions, the limitations of classical laminated plate theory for the analysis of laminates with low span-to-thickness ratios were first revealed and the solutions are still

used nowadays to assess the range of validity of approximate theories and numerical models. Pagano's solution was completed in [37], using the displacement method, for cases where the characteristic equation of the problem has complex conjugate roots, as it occurs in sandwich plates with honeycomb cores having transverse stiffness much higher than the in-plane stiffnesses. An exact stationary thermo-elasticity solution for simply supported plates in plane strain and subjected to arbitrary thermo-mechanical loading was obtained in [34] using the method of displacement potentials and assuming perfect thermal contact at the layer interfaces.

In a later study by Pagano [8], three-dimensional elasticity solutions were obtained for rectangular simply supported bidirectional laminated and sandwich plates composed of perfectly bonded orthotropic/isotropic layers. The characteristic equation of this problem was restated in the form of a cubic equation whose discriminant controls the nature of the solution. Pagano obtained closed form solutions for the cases of negative and zero discriminants (e.g. isotropic layers) and later solutions for the case of a positive discriminant were presented in [38]. These exact solutions allowed to verify the faster convergence to the exact solution of classical plate theory on increasing the number of layers [30]. In parallel with Pagano's work, Srinivas et al. [33, 39] obtained elasticity solutions for simply supported perfectly bonded cross-ply laminates under arbitrary loading by expressing the displacement and stress components in terms of infinite series. The thermo-elastic problem was studied in [6, 10, 32] for plates with perfect thermal contact between the layers, by assuming a prescribed temperature distribution with a through-the-thickness linear variation in [10], and through the exact solution of the heat conduction problem in [6, 32]. Solutions for plates with boundary conditions other than the simple supports were obtained in the form of infinite series in [40, 41] and through the extended Kantorovich method in [9].

An exact elasticity solution for plane-strain simply supported laminated cylindrical shells with perfectly bonded orthotropic layers and subjected to transverse loading was derived in [42] using the Airy's stress function method. In [43], 3D elasticity solutions were derived for simply supported circular cylindrical shells made of perfectly bonded orthotropic layers, subjected to transverse loading. The solutions were derived by expressing the displacement and stress components in terms of infinite series.

2.2.2 Imperfectly bonded multilayered composites

The thermo-elasticity models mentioned above assume the layers to be perfectly bonded and in perfect thermal contact, which imply continuity of displacements, tractions, temperature and heat flux at the layer interfaces. This assumption does not describe systems with damaged interfaces or delaminations between the layers or systems where the plies are connected by very thin adhesive layers which are not described as regular layers in the formulation, to reduce the computational cost. Flaws and delaminations may develop during the manufacturing processes and/or in service due to, for instance, fatigue loads, impacts or environmental effects, such as temperature or humidity. They modify the continuity conditions at the layer interfaces and result in stiffness degradation and reduction of the load-carrying capacity of the plates [44]. Two models are introduced here, which allow to study the effect of imperfect bonding of two adjacent layers.

Mechanically imperfect interface model

From a mechanical point of view, an imperfect interface or a very thin interlayer can be represented as a zero-thickness surface across which the interfacial tractions are continuous, while the displacements are discontinuous (see Figure 2-1). The interfacial tractions can then be related to the relative displacements of the layers at the interfaces using interfacial traction laws able to describe different interfacial mechanisms. Linear interfacial traction laws have been frequently used in the literature; they assume that the interfacial tractions are proportional to the corresponding relative sliding and opening displacements and the proportionality factors are the interfacial tangential and normal stiffnesses. These laws well describe the response of thin adhesive elastic layers and the initial branch of more general interfacial traction laws, such as those which are typically used to model cohesive delamination fracture. In addition, these laws can be used to describe the limiting cases of perfectly bonded and fully debonded layers [7].

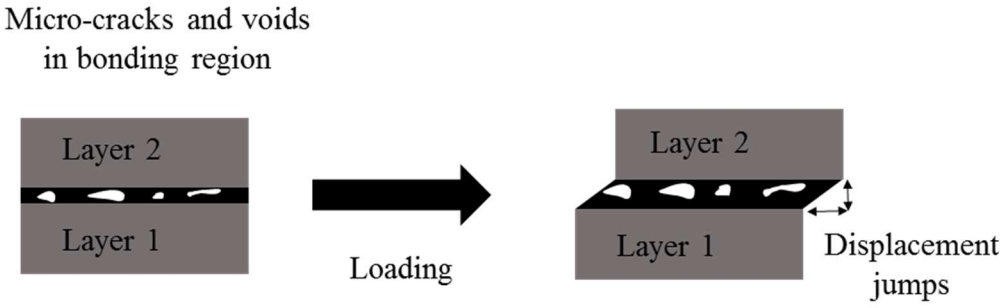

Figure 2-1: Schematic illustration of defects in the bonding region between two composite layers and their relative displacements after loading.

To the authors knowledge, Williams et al. [19] were the first to employ the concept of linear interfacial traction law in conjunction with Pagano's model [29] in order to obtain exact elasticity solutions for the cylindrical bending of laminates with imperfect interfaces subjected to mechanical loading. The extension is straightforward since the general solutions for stresses and displacements in each layer are unchanged, while the interfacial continuity conditions must account for the assumed interfacial traction laws. The same idea was applied in [11] to verify structural models based on a zigzag homogenization used to improve classical structural theories; in [12, 45] it was used along with the state-space approach, for the bending and free vibrations of simply supported cross-ply laminates and cylindrical panels with imperfect interfaces; in [46] it was applied to study plates subjected to arbitrary boundary conditions.

Thermally imperfect interface model

From a thermal point of view, heat transfer through the layers of a plate with interfacial imperfections is a rather complex process. Micro-cracks, voids and delaminations reduce the areas of actual physical contact between adjacent layers and create regions separated by air gaps which prevent the heat flow across the interface. Heat transfer across the imperfect interfaces takes place through conduction at the contact spots and conduction and/or radiation through the air gaps (see Figure 2-2). These mechanisms control and reduce the interfacial thermal conductance, which also depends on other factors, such as the applied pressure and the mean temperature. The consequence of this behavior is a jump in the temperatures of the layers at the interface [47]. Hence for laminates with interfacial imperfections, the assumption of perfect thermal contact between the layers, which implies a continuous temperature at the interface, is not valid.

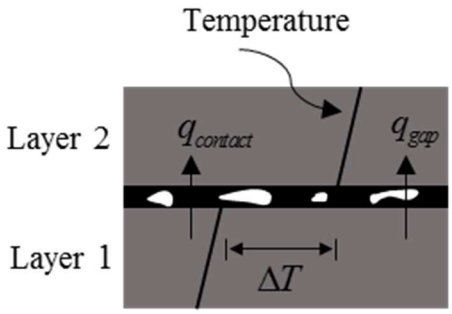

Figure 2-2: Interfacial temperature jump due to the interfacial thermal resistance.

The concept of thermally imperfect interface characterized by an interfacial thermal resistance has been frequently used in the literature to account for the behavior described above [7, 48-50]. This model enforces the equality of the heat fluxes which enter and leave the interface and assumes that the heat flux through the interface is proportional to the interfacial temperature jump; the interfacial thermal conductance H is the proportionality factor and should then account for the various modes of heat transfer through the interface [47]. An interfacial thermal resistance is then introduced which is the reciprocal of the interfacial thermal conductance, $R = 1/H$. If $R = 0$, the model describes perfect interfaces, where the temperature is continuous at the interface. Impermeable interfaces, where the heat flux vanishes, can be modelled by setting $H = 0$. The model can also be used to efficiently describe the thermal behavior of thin adhesive layers when they are represented as interfaces, to reduce the computational cost, and H will then be related to the conductivity and thickness of the adhesive. Pelassa et al. [7] employed the concept of interfacial thermal resistance and assumed the interfaces to be mechanically imperfect and described by linear traction laws to extend the thermo-elasticity model presented in [6] to multilayered plates with thermally and/or mechanically imperfect interfaces.

2.2.3 Matrix formulations in thermo-elasticity: the transfer matrix method

Most of the aforementioned thermo-elasticity theories are based on two main steps. First, the general forms of the field variables which satisfy the edge boundary conditions and the governing field equations are obtained for a generic layer. Then, the unknown constants in the solutions of each layer are calculated by imposing continuity conditions at the layer interfaces and boundary conditions at the top and bottom surfaces of the plate. For a plate composed of *n* layers, a system of 4×*n* and 6×*n* algebraic equations need to be solved for cylindrical bending and general plate problems, respectively [8, 29]. Therefore, solving the system of equations becomes cumbersome when the number of layers increases and this restricts the applicability of the models.

The transfer matrix method was originally formulated by Thomson in [51] to solve the problem of the propagation of plane elastic waves in a layered medium immersed in a fluid. The method is the first attempt in the literature to methodically extend the solution derived for layer to a multilayered medium. Thomson derives a local transfer matrix, which relates the displacements and transverse stresses at the bottom and top surfaces of a generic layer. The local transfer matrix is then related to that of the adjacent layer by imposing continuity conditions at the interface. Starting from the uppermost layer and using the local

matrices and continuity conditions at the interfaces, a global transfer matrix is derived which relates the field variables at the bottom surface of the medium to those at the top. The solution for a medium with any arbitrary number of layers is then obtained through the imposition of the boundary conditions only. A small mistake in the interfacial continuity conditions in [51] was later corrected by Haskell and the method became known as the Thomson-Haskell method [52]. Applications of the method in the ultrasonic and seismology fields have been reviewed in [53].

The applications of the transfer matrix method have not been restricted to wave propagation problems. A matrix technique was employed within the state-space approach to efficiently solve, using a mixed formulation, the three-dimensional elasticity problem of a simply supported multilayered plate subjected to transverse loadings in [13] and to compressive in-plane loadings in [14] (buckling problem). Solutions were obtained for perfectly bonded, homogeneous and orthotropic layers, with principal material axes parallel to the geometrical axes. The transfer matrix method was later applied to multilayered plates with mechanically imperfect interfaces governed by linear interfacial traction laws in [12, 15]. The solutions in [12-15] however are derived and presented only in matrix form, can be obtained through many matrix multiplications and no expanded explicit expressions are given for the field variables; the solution then remains quite complex. Applications of the transfer matrix method to the solution of stationary thermo-elasticity problems can be found in [16-18] for simply supported rectangular multilayered plates and cylindrical arches with perfectly bonded isotropic layers in perfect thermal contact. As for the previous applications, solutions are derived only in terms of matrix multiplications and interfacial mechanical or thermal imperfections are not considered.

Therefore, there is a need in the literature for explicit expressions, to be used to easily generate exact solutions for laminated composites with an arbitrary number of imperfectly bonded layers in imperfect thermal contact. The exact solutions can be then used to assess the accuracy of numerical and approximate models and to perform parametric analyses. Currently, due to the absence of such explicit expressions in the literature, a few classical examples, which have been presented in some original papers for fully bonded layers in perfect thermal contact, e.g. [8, 10, 29, 33] are often used to verify theories which are based on different assumptions and account, for instance, of interfacial imperfections and this may lead to misjudgments on their accuracy and range of validity (see [11] for a discussion on this problem).

2.3 STRUCTURAL THEORIES FOR MULTILAYERED COMPOSITES

The in-plane dimensions of laminated composite structures are usually much larger than their thickness dimension. This feature allows to formulate structural theories based on a priori assumptions on through the thickness variations of the primary variables (axiomatic approach). In displacement based structural theories, the primary variables are the generalized displacements (e.g., axial displacements, rotations), and in mixed theories both generalized displacements and stresses are used as primary variables. These assumptions allow to treat a laminated structure as a two-dimensional problem and reduce the computational cost of modeling complicated structures. Moreover, the structural theories allow to derive approximate solutions for problems for which elasticity solutions are not available. In the remaining part of this chapter, some of the equivalent single layer and the zigzag theories are briefly introduced.

2.3.1 Equivalent single layer theories

Among the displacement based structural models, the equivalent single layer theories (see for example [54, 55], and [56, 57] for recent reviews) assume either a polynomial or non-polynomial (e.g. trigonometric, hyperbolic, and exponential functions) expansion of the displacement components in the thickness direction [56]. For cylindrical bending problems in plane $x_2 - x_3$, where x_2 and x_3 are, respectively, the longitudinal and thickness directions, the displacement field of polynomial theories takes the following form [57]:

$$u(x_2, x_3) = \sum_{i=0}^{m} (x_3)^i u_i(x_2) \qquad w(x_2, x_3) = \sum_{j=0}^{n} (x_3)^j w_j(x_2) \tag{2-1}$$

where u and w are the in-plane and transverse displacements, and u_i and w_j are the primary variables. The displacement components are continuous through the thickness with continuous first derivative with respect to the thickness direction, which leads to discontinuous interlaminar stresses in multilayered structures.

The displacement field in Eq. (2-1) for $m = 1$, $n = 0$ and $u_1 = -w_{0,2}$ represents that of the Euler-Bernoulli theory, where the shear deformations are neglected (a comma followed by a subscript denotes a derivative with respect to the corresponding coordinate) [57]. In the Euler-Bernoulli theory it is assumed that plane sections normal to the reference surface remain plane and normal to the reference surface after deformation and do not experience elongation. In the first order shear deformation theory, the transverse shear strain is assumed to be constant through the thickness so $m = 1$, $n = 0$, and u_0, u_1 and w_0 are independent variables [57]. In the first order shear deformation theory it is assumed that plane sections normal to the reference surface do not experience elongation and remain plane but not necessarily normal to the reference surface after deformation. Higher order theories have been formulated by taking more terms in the expansion (e.g., [54]). The transverse compressibility/extensibility of the plate can be incorporated into the formulation by assuming $n \neq 0$ [58].

The displacement field of the equivalent single layer theories does not account for the relative displacement of the adjacent layers. Moreover, the equivalent single layer theories are not able to reproduce the complex stress and displacement fields, with zigzag patterns in the thickness direction, which occur in laminated composite materials due to the different mechanical properties of the layers.

2.3.2 Zigzag theories: perfectly bonded layers

A good compromise between computational simplicity and accuracy, for stress analysis of laminated composite structures, is offered by a class of structural models, known in the literature as zigzag theories. In zigzag theories, the displacement fields of the equivalent single layer theories are enriched by layerwise linear functions, known as zigzag functions, to account for the inhomogeneous material structure. Zigzag functions introduce strain discontinuities at the interfaces and allow to fulfill the interfacial continuity conditions. In this section, two widely used zigzag models are introduced along with a refined zigzag theory.

Murakami's zigzag theory

Within the framework of Reissner's mixed variational theorem [59], Murakami [60] enhanced the in-plane displacement field of the equivalent single layer theory by introducing zigzag functions. His work was motivated by displacement microstructure of laminates with periodic layups. Therefore, he used zigzag

functions with periodic nature, which are independent of the material properties of the layers, depend only on the thickness of the layers, and do not fulfill the condition of continuity of the transverse shear tractions of the interfaces [57].

Adding the Murakami zigzag function to the in-plane displacement field of the first order shear deformation theory introduced in Sect. 2.3.1, yields the following displacements for a generic layer *k*:

$$^{(k)}u\left(x_2,x_3\right)=u_0\left(x_2\right)+x_3u_1\left(x_2\right)+\left(-1\right)^k\zeta_k u_M\left(x_2\right) \qquad ^{(k)}w\left(x_2\right)=w_0\left(x_2\right) \tag{2-2}$$

where $\zeta_k=2\,^{(k)}x_3\,/\,^{(k)}h$ is a dimensionless function (see Figure 2-3), which is linear through the thickness and has values of -1 and 1 at the bottom and top surfaces of the layer, $^{(k)}x_3$ is the distance from the mid-thickness axis of the layer and $^{(k)}h$ is the thickness of the layer. u_M is an additional kinematic variable, which defines the amplitude of the zigzag functions. This zigzag function can be added to any displacement component of any equivalent single layer theory to incorporate the zigzag effects.

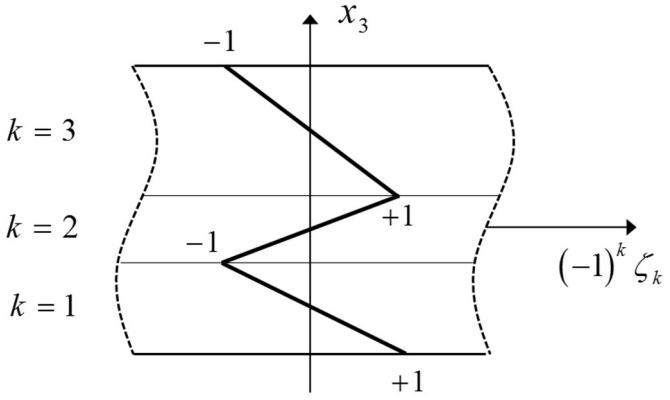

Figure 2-3: Murakami zigzag functions in a three-layer system.

Murakami zigzag theory works well when applied to the laminated composite with periodic stacking sequence, i.e. $\left[+\theta,-\theta,...\right]$ and runs into difficulties, for example, for layups with external soft (lower shear moduli) layers or for sandwiches with large face-to-core stiffness ratios [61].

Di Sciuva's zigzag theory

In [62, 63], Di Sciuva formulated a displacement based zigzag theory in which a different displacement field is assumed for each layer. For cylindrical bending problems in plane x_2-x_3, the displacement field takes the following form for a generic layer *k* (see Figure 2-4):

$$^{(k)}v_2\left(x_2,x_3\right)=v_{02}\left(x_2\right)+x_3\varphi_2\left(x_2\right)+\sum_{i=1}^{k-1}\Omega_2{}^i\left(x_3-x_3{}^i\right) \qquad ^{(k)}v_3\left(x_2\right)=w_0\left(x_2\right) \tag{2-3}$$

where v_{02}, φ_2 and w_0 are the global variables, which define the displacement field of the first-order shear deformation theory (global model), and $\Omega_2{}^k$ is the zigzag function of the layer *k*. Interfacial continuity

conditions are imposed a priori to eliminate the layerwise degrees of freedom, which yields $\Omega_2^k = \left(w_{0,2} + \varphi_2\right)\Lambda_{22}^k$ with Λ_{22}^k known constants only depending on the transverse shear mechanical properties of the layers. Substitution of Ω_2^k into Eq. (2-3) results in a homogenized displacement field in terms of the global displacement variables only. The number of the unknown variables of Di Sciuva's zigzag theory is then equal to that of the first-order shear deformation theory. While Murakami zigzag function $\left(-1\right)^k \zeta_k u_M$ in Eq. (2-2) depends only on the thickness of the layers, Di Sciuva zigzag function accounts for the geometrical and material properties of the layers and is derived by enforcing physical conditions at the interfaces.

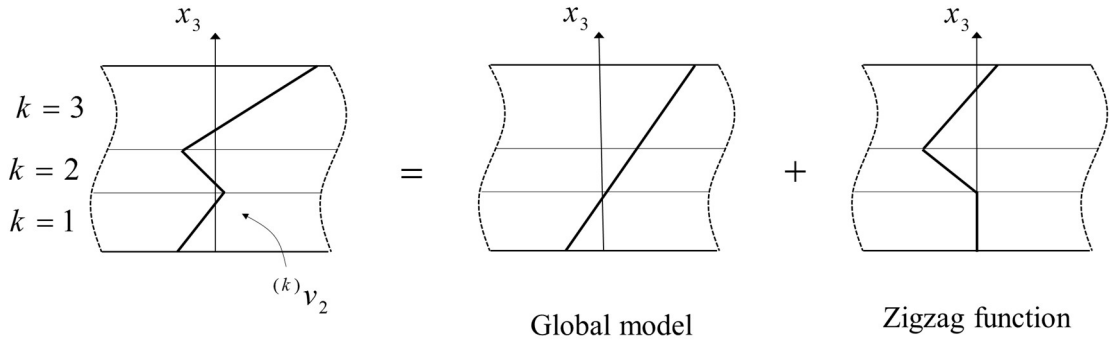

Figure 2-4: Schematic illustration of the displacement field of Di Sciuva's theory for a three-layer system: global model enriched by zigzag functions.

Many researches formulated later zigzag theories inspired by the original Di Sciuva's theory. For instance, in [64, 65] third order shear deformation zigzag theories are formulated. In [66, 67], higher order zigzag theories have been formulated with incorporation of the transverse compressibility/extensibility of layers. In [68-72], zigzag theories have been formulated for laminated plates and shells which use four ply-dependent and five global variables to define the displacement field; the total number of the variables is then reduced to five using the interfacial continuity conditions. In [73], a higher order zigzag theory has been formulated with improved approximations for the transverse displacements of laminated shells under thermal loadings.

Di Sciuva's theory has two drawbacks. First, its finite element implementation requires C^1-continuous shape functions for the transverse displacements, which is undesirable especially for plate and shell problems. Second, the transverse shear stress, strain and resultant, obtained from the constitutive equations, vanish along clamped boundaries [27, 74]. To facilitate the finite element implementation, Di Sciuva's theory has been modified in [74, 75] to formulate zigzag models which require only C^0-continuous shape functions. In the next section, a recently formulated refined zigzag theory [27, 76] will be introduced, which overcomes both limitations of Di Sciuva's theory.

Refined zigzag theory

A refined zigzag theory is formulated in [27, 76] by enriching the displacement field of the first order shear deformation theory through piecewise linear zigzag functions, which vanish at the top and bottom surfaces

of the plate (see Figure 2-5). For cylindrical bending problems in plane $x_2 - x_3$, displacement field of the refined zigzag theory for a generic layer *k* is:

$$^{(k)}v_2\left(x_2,x_3\right)=v_{02}\left(x_2\right)+x_3\varphi_2\left(x_2\right)+{}^{(k)}\phi\left(x_3\right)\theta_2\left(x_2\right) \qquad {}^{(k)}v_3\left(x_2\right)=w_0\left(x_2\right) \tag{2-4}$$

where v_{02}, φ_2 and w_0 are the global variables, which define the displacement field of the first-order shear deformation theory, $^{(k)}\phi\left(x_3\right)$ is a piecewise linear zigzag function and θ_2 is the amplitude of the zigzag contribution into the longitudinal displacement. The zigzag functions can be fully defined in terms of their values at the interfaces, ϕ^k for $k = 0, \ldots, n$, with n the number of layers; ϕ^0 and ϕ^n are imposed to be zero at the top and bottom surfaces of the domain. The interfacial values of the zigzag functions are determined a priory without enforcing the continuity of the transverse shear tractions at the layer interfaces.

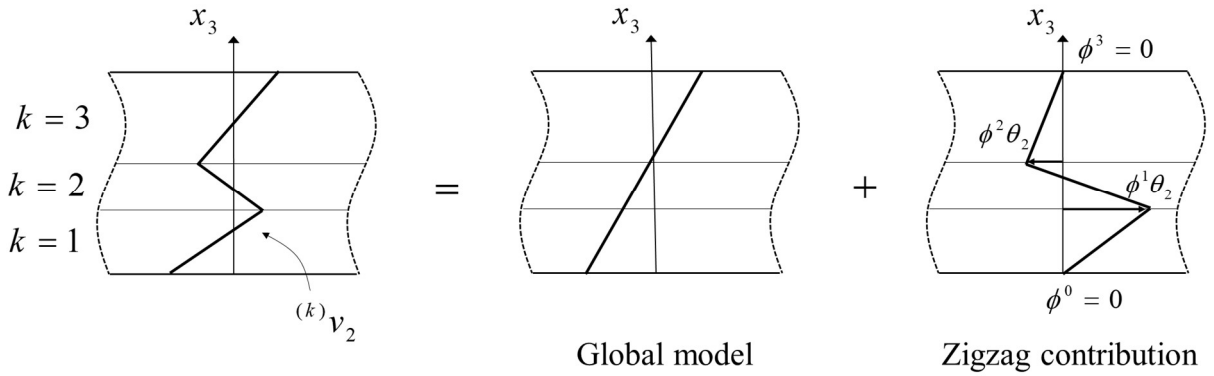

Figure 2-5: Schematic illustration of the displacement field of the refined zigzag theory for a three-layer system: global model enriched by zigzag contribution.

The refined zigzag theory requires only C^0-continuous shape functions for finite element implementation, and uses more kinematic variables compared to that of Di Sciuva's zigzag theories. The refined zigzag theory is proved to be accurate in predicting displacements and stresses in highly anisotropic thick laminates and sandwiches with clamped boundaries [27, 76]. The extension of the refined zigzag theory to laminated shells is presented in [77]. In [78], a refined zigzag theory is formulated within the framework of Reissner's mixed variational theorem, and the approximation of the transverse shear stresses is made a priori using Cauchy's equilibrium equation and continuity conditions at the layer interfaces. The mixed model allows to accurately predict the transverse shear stress without using a posteriori integration procedure [78].

2.3.3 Zigzag theories: imperfectly bonded layers

All the aforementioned zigzag theories have been formulated for perfectly bonded laminated composite structures. In [74], the presence of a delamination has been modeled through the introduction of a very thin layer with negligible material stiffnesses. In [79-82], the presence of multiple zero-thickness imperfect interfaces has been incorporated into the displacement field of zigzag theories using Heaviside unit step functions, which allows discontinuity in the displacement field. The theories only account for the relative

sliding displacements of the adjacent layers and use the spring-layer model to describe the mechanical behavior of the interfaces; the law relates the interfacial shear tractions to the relative sliding displacements of the layers. The a priori imposition of the interfacial continuity conditions allows to define the displacement field in terms of the global variables only. In [83-85], displacement jumps across delaminations are considered as unknown variables and are added to the displacement field of a third order zigzag theory, to perform buckling and dynamic analysis on laminated plates and shells with delaminations; the number of variables in these theories depend on the number of delaminations and therefore, the theories become computationally expensive for structures with multiple delaminations.

The refined zigzag theory have been used in [86-89] to model delamination fracture in laminated composite structures. In these theories, delaminations are represented by very thin layers and the nonlinear deformations at the vicinity of the delaminations are modeled through continuum damage mechanics. The applications have been restricted to delamination problems under mode II loading, since the theories neglect the transverse normal strain and compressibility/extensibility of the layers.

A multiscale structural model, based on the Di Sciuva's zigzag theory [62, 63], has been formulated in [11, 25] for laminated composite plates with mixed mode cohesive interfaces and delaminations subjected to dynamically applied loads, by reconsidering the original idea of theories in [80-82]. The model follows the approach proposed in [90] to account for interfacial relative opening displacements and couples a first order shear and first order normal deformation theory [58] (coarse-grained model), which defines the global fields, to a discrete layer cohesive crack theory (detailed small-scale model), which describes the local fields. Piecewise linear interfacial laws, which relate the interfacial tractions to the interfacial relative displacements, are used to approximate nonlinear cohesive traction laws and to represent all nonlinear mechanisms taking place at the interfaces, e.g. brittle, cohesive and bridging fracture and contact. A homogenization technique, which imposes continuity of the tractions at the layer interfaces and the cohesive traction laws, is then applied to define the local variables as functions of the global ones. The model then removes the need for the through-thickness discretization of conventional discrete layer cohesive crack models; the number of unknown functions in the model is independent of the number of layers, cohesive interfaces and delaminations, and is equal to that of the global model. The model was proven to be accurate in predicting the local and global fields in layered plates with continuous, imperfect and fully debonded interfaces and subjected to stationary thermo-mechanical loads [7, 11, 25, 26] and was used in [91] to study propagation of plane strain harmonic waves in multilayered plates with imperfect interfaces. In [26], the multiscale structural model was applied to a delaminated cantilever homogeneous wide plate subjected to concentrated end load, to preliminary assess the applicability of the model to study delamination fracture problems.

2.3.4 Homogenized structural theory ([25])

In this section, the homogenized structural theory in [25] is briefly presented for wide plates with mixed mode cohesive interfaces and delaminations subjected to static loads; the theory in [25] has been formulated for wide plates subjected to dynamically applied loads. The simplified version of the model for plates with

sliding only interfaces, which will be used in Chapter 4 to study mode II dominant delamination problems in bi-material wide plates, is also presented.

Figure 2-6(a) depicts a portion of a rectangular multilayered plate with global thickness *h*, in-plane dimensions L_1 and $L_2 = L$ with $L_1 >> L_2$, and $x_1 - x_2 - x_3$ a system of Cartesian coordinates with origin at the left edge. The plane $x_3 = 0$ defines the reference surface of the plate, $\mathscr{S}$.The plate is composed of *n* linearly elastic, homogenous and orthotropic layers with principal material axes parallel to the geometrical axes, and is subjected to distributed loads, which are independent of x_1, acting on the upper and lower and lateral bounding surfaces, S^+, S^- and B. The plate deforms in cylindrical bending parallel to the plane $x_2 - x_3$. The layers are joined by $n-1$ interfaces, which are zero-thickness mathematical surfaces where material properties and displacements may be discontinuous while interfacial tractions are continuous. The layer *k*, with *k* = 1, … *n* numbered from bottom to top, is defined by x_3^{k-1} and x_3^k, the coordinates of its lower and upper surfaces, ${}^{(k)}\mathscr{S}^-$ and ${}^{(k)}\mathscr{S}^+$, and has thickness ${}^{(k)}h$ (the superscript (*k*) on the left of a quantity shows association with the layer *k*, while the superscript *k* on the right identifies the interface between layers *k* and $k+1$). Under these assumptions, the displacement components in each layer simplify as ${}^{(k)}v_1 = 0$, ${}^{(k)}v_2 = {}^{(k)}v_2(x_2, x_3)$ and ${}^{(k)}v_3 = {}^{(k)}w(x_2, x_3)$ where ${}^{(k)}v_i$ is the displacement component in the layer *k* in x_i direction and *i* = 1, 2, 3.

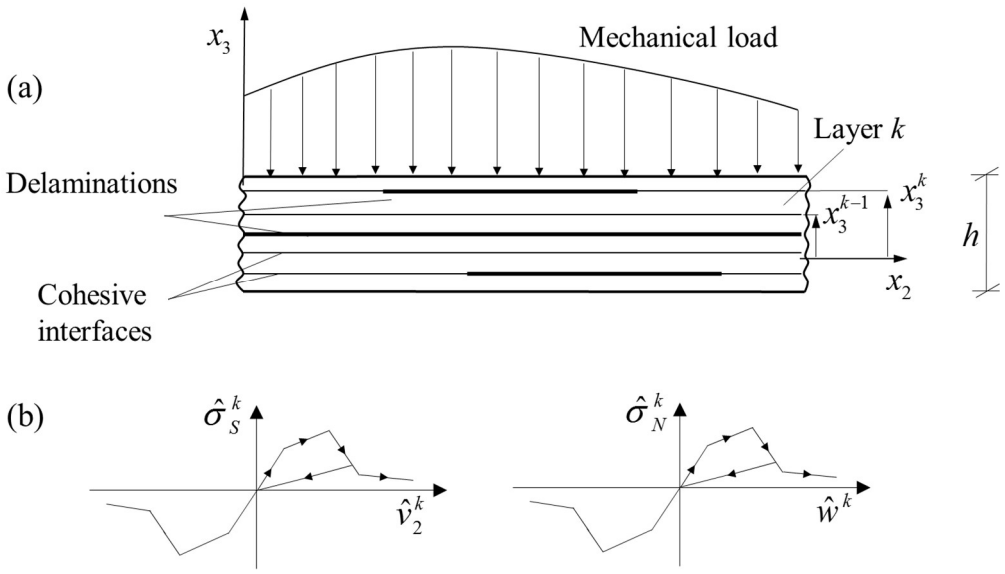

Figure 2-6: (a) Laminated composite plate with multiple delaminations and cohesive interfaces. (b) Exemplary piecewise linear cohesive traction law.

The constitutive equations for the layer *k* are those of the 3D elasticity, particularized to plane-strain conditions:

$$\begin{aligned} {}^{(k)}\sigma_{22} &= {}^{(k)}C_{22}\,{}^{(k)}\varepsilon_{22} + {}^{(k)}C_{23}\,{}^{(k)}\varepsilon_{33} \\ {}^{(k)}\sigma_{23} &= {}^{(k)}C_{44}\,2\,{}^{(k)}\varepsilon_{23} \\ {}^{(k)}\sigma_{33} &= {}^{(k)}C_{23}\,{}^{(k)}\varepsilon_{22} + {}^{(k)}C_{33}\,{}^{(k)}\varepsilon_{33} \end{aligned} \tag{2-5}$$

with ${}^{(k)}\sigma_{ij}$ and ${}^{(k)}\varepsilon_{ij}$ the stress and strain components, and ${}^{(k)}C_{ij}$ are the coefficients of the stiffness matrix in engineering notation.

The mechanical behavior of the interfaces is described through the interfacial traction laws which relate the interfacial tractions, acting along the surface of the layer *k* at the interface with unit positive normal vector, ${}^{(k)}\mathscr{S}^{+}$,

$$\begin{aligned}\hat{\sigma}_S^k &= \hat{\sigma}_{23}^k\left(x_2\right) = {}^{(k)}\sigma_{23}\left(x_2, x_3 = x_3^k\right)\\ \hat{\sigma}_N^k &= \hat{\sigma}_{33}^k\left(x_2\right) = {}^{(k)}\sigma_{33}\left(x_2, x_3 = x_3^k\right)\end{aligned} \tag{2-6}$$

to the interfacial relative sliding and opening displacements:

$$\begin{aligned}\hat{v}_2^k(x_2) &= {}^{(k+1)}v_2(x_2, x_3 = x_3^k) - {}^{(k)}v_2(x_2, x_3 = x_3^k)\\ \hat{w}^k(x_2) &= {}^{(k+1)}w(x_2, x_3 = x_3^k) - {}^{(k)}w(x_2, x_3 = x_3^k)\end{aligned} \tag{2-7}$$

Generally nonlinear traction laws can be approximated as piecewise linear functions so that an arbitrary piece of the law is defined by the affine function (Figure 2-6(b)) [25]:

$$\begin{aligned}\hat{\sigma}_S^k(x_2) &= K_S^k \hat{v}_2^k(x_2) + t_S^k \qquad & \hat{\sigma}_N^k(x_2) &= K_N^k \hat{w}^k(x_2) + t_N^k\\ \hat{v}_2^k(x_2) &= B_S^k\left(\hat{\sigma}_S^k(x_2) - t_S^k\right) \qquad & \hat{w}^k(x_2) &= B_N^k\left(\hat{\sigma}_N^k(x_2) - t_N^k\right)\end{aligned} \tag{2-8}$$

with K_S^k, K_N^k and B_S^k, B_N^k the interfacial tangential and normal stiffnesses and compliances, t_S^k and t_N^k constant tractions. The interfacial traction laws in Eq. (2-8) assume no coupling between in-plane and out of plane behavior.

Purely elastic interfaces which can represent an adhesive layer, are modeled by a single branch with $t_S^k = t_N^k = 0$. Perfectly bonded interfaces are described by $t_S^k = t_N^k = 0$ and $B_S^k = B_N^k = 0$ which result in $\hat{v}_2^k = \hat{w}_2^k = 0$. Fully debonded interfaces are modeled by $t_S^k = t_N^k = 0$ and $K_S^k = K_N^k = 0$ which result in $\hat{\sigma}_S^k = \hat{\sigma}_N^k = 0$. For t_S^k, $t_N^k \neq 0$ and $K_S^k = K_N^k = 0$, the law could represent plastic deformations of the interlayer. The model is presented here for an arbitrary branch of the interfacial traction law, (2-8), which provides the essential tools for solving plates with nonlinear cohesive interfaces.

Homogenized displacements, strain and stress components ([25])

The following two length scales displacement field is assumed in the layer *k*, which is a superposition of the first order shear and first order normal deformation theory (coarse-grained model) and local perturbations (small-scale model) [25]:

$$
\begin{aligned}
{}^{(k)}v_2(x_2,x_3) &= v_{02}(x_2) + x_3\varphi_2(x_2) + \sum_{i=1}^{k-1}\Omega_2{}^i(x_2)(x_3 - x_3{}^i) + \sum_{i=1}^{k-1}\hat{v}_2{}^i(x_2) \\
{}^{(k)}w(x_2,x_3) &= w_0(x_2) + x_3\varphi_3(x_2) + \sum_{i=1}^{k-1}\Omega_3{}^i(x_2)(x_3 - x_3{}^i) + \sum_{i=1}^{k-1}\hat{w}{}^i(x_2)
\end{aligned}
\tag{2-9}
$$

The global variables, $v_{02}(x_2)$, $\varphi_2(x_2)$ and $w_0(x_2)$, define the displacement field of the first-order shear deformation theory, which is continuous with continuous first derivative in the thickness direction; when the reference surface $x_3 = 0$ is placed at the mid-thickness of the first layer, the global variables then define the displacement components of points on the reference surface and the rotations of its normal axes; $\varphi_3(x_2)$ is the constant strain in the transverse direction, which is needed to capture, in the simplest way possible, the effect of the transverse normal compressibility/extensibility and to model opening or elastic contact along the delaminations. The third and fourth terms on the right hand side of Eq. (2-9) are the local variables and account for the zigzag contribution due to the inhomogeneous material structure through the zigzag functions $\sum_{i=1}^{k-1}\Omega_2{}^i(x_2)(x_3 - x_3{}^i)$ and $\sum_{i=1}^{k-1}\Omega_3{}^i(x_2)(x_3 - x_3{}^i)$, and the interfacial sliding and opening jumps due to the cohesive interface through $\sum_{i=1}^{k-1}\hat{v}_2{}^i(x_2)$ and $\sum_{i=1}^{k-1}\hat{w}{}^i(x_2)$.

The strain components are derived from the displacement field in Eq. (2-9) through the linear strain-displacement relationships:

$$
\begin{aligned}
{}^{(k)}\varepsilon_{22} &= v_{02},_2 + x_3\varphi_2,_2 + \sum_{i=1}^{k-1}\Omega_2{}^i,_2\,(x_3 - x_3{}^i) + \sum_{i=1}^{k-1}\hat{v}_2{}^i,_2 \\
2\,{}^{(k)}\varepsilon_{23} &= w_0,_2 + x_3\varphi_3,_2 + \sum_{i=1}^{k-1}\left[\Omega_3{}^i,_2\,(x_3 - x_3{}^i) + \Omega_2{}^i\right] + \sum_{i=1}^{k-1}\hat{w}{}^i,_2 \\
{}^{(k)}\varepsilon_{33} &= \varphi_3 + \sum_{i=1}^{k-1}\Omega_3{}^i
\end{aligned}
\tag{2-10}
$$

The stress components are derived by substituting the strain components from Eq. (2-10) into the constitutive equations (2-1). The $2\times(n-1)$ zigzag functions $\Omega_2{}^k$ and $\Omega_3{}^k$ for k = 1, …, $n-1$ are then derived by imposing continuity of shear and normal tractions at the layer interfaces, which yields [25]:

$$
\begin{aligned}
{}^{(k)}\sigma_{23}\left(x_3^k\right) &= {}^{(k+1)}\sigma_{23}\left(x_3^k\right) \\
{}^{(k)}\sigma_{33}\left(x_3^k\right) &= {}^{(k+1)}\sigma_{33}\left(x_3^k\right)
\end{aligned}
\tag{2-11}
$$

for k = 1, …, $n-1$. The presence of the zigzag functions in both algebraic and differential forms in Eq. (2-10) complicates the derivation of the zigzag functions. Following [90], for the purpose of determining $\Omega_3{}^k$ only, it is assumed that the effect of ε_{22} on σ_{33} in Eq. (2-1) is negligible with respect to that of ε_{33}. Under this assumption, the following forms are derived for the zigzag functions of the layer k [25]:

$$\Omega_2{}^k = \left(w_0{}_{,2} + \varphi_2 + x_3^1 \varphi_3{}_{,2}\right)\Lambda_{22}^{(1;k)} + \varphi_3{}_{,2}\sum_{l=2}^{k}\Lambda_{22}^{(l;k)}\left(x_3^l - x_3^{l-1}\right)\left(1+\sum_{j=1}^{l-1}\Lambda_{33}^{(j)}\right) - \hat{w}^k{}_{,2}$$
$$\Omega_3{}^k = \Lambda_{33}^{(k)}\varphi_3 \tag{2-12}$$

where:

$$\Lambda_{33}^{(k)} = -{}^{(1)}C_{33}\,\frac{{}^{(k+1)}C_{33} - {}^{(k)}C_{33}}{{}^{(k+1)}C_{33}\;{}^{(k)}C_{33}}$$
$$\Lambda_{22}^{(\mathrm{i};j)} = {}^{(i)}C_{55}\left(\frac{1}{{}^{(j+1)}C_{44}} - \frac{1}{{}^{(j)}C_{44}}\right) \tag{2-13}$$

Once the zigzag functions $\Omega_2{}^k$ and $\Omega_3{}^k$ for $k = 1, \ldots, n-1$ have been defined, the interfacial relative displacements at each cohesive interface are derived in terms of the global variables through the interfacial constitutive laws in Eq. (2-8), through Eqs. (2-1), (2-6), (2-10) and (2-12). The expressions for the displacement jumps for kth interface are:

$$\hat{v}_2^k = \left(\varphi_2 + w_0{}_{,2}\right)\Psi_{22}^k + \varphi_3{}_{,2}\,\Phi_{22}^k - B_S^k t_S^k$$
$$\hat{w}^k = \varphi_3\Psi_{33}^k - B_N^k t_N^k \tag{2-14}$$

where

$$\Psi_{22}^k = {}^{(k+1)}C_{44}B_S^k\left(1+\sum_{j=1}^{k}\Lambda_{22}^{(1;j)}\right)$$
$$\Phi_{22}^k = {}^{(k+1)}C_{44}B_S^k\left\{x_3^k + \sum_{j=1}^{k}\left[\Lambda_{22}^{(1;j)}x_3^1 + \Lambda_{33}^{(j)}\left(x_3^k - x_3^j\right) + \sum_{l=2}^{j}\Lambda_{22}^{(l;i)}\left(x_3{}^l - x_3{}^{l-1}\right)\left(1+\sum_{i=1}^{l-1}\Lambda_{33}^{(i)}\right)\right]\right\} \tag{2-15}$$
$$\Psi_{33}^k = {}^{(k+1)}C_{33}B_N^k\left(1+\sum_{j=1}^{k}\Lambda_{33}^{(j)}\right)$$

Substituting the small-scale variables from Eqs. (2-12) and (2-14) into Eq. (2-9) yields the homogenized displacement field, which is defined only in terms of the global variables, v_{02}, φ_2, w_0 and φ_3 [25]:

$${}^{(k)}v_2 = v_{02} + \varphi_2 x_3 + \left(\varphi_2 + w_0{}_{,2}\right)R_{S22}^k + \varphi_3{}_{,2}\,R_{N22}^k - \sum_{i=1}^{k-1}B_S^i t_S^i$$
$${}^{(k)}w = w_0 + \varphi_3\left\{x_3 + \sum_{i=1}^{k-1}\left[\Lambda_{33}^{(i)}\left(x_3 - x_3^i\right) + \Psi_{33}^i\right]\right\} - \sum_{i=1}^{k-1}B_N^i t_N^i \tag{2-16}$$

with

$$R_{S22}^{k}=\sum_{i=1}^{k-1}\left[\Lambda_{22}^{(1;i)}\left(x_3-x_3^{i}\right)+\Psi_{22}^{i}\right]$$
$$R_{N22}^{k}=\sum_{i=1}^{k-1}\left\{\left[\Lambda_{22}^{(1;i)}x_3^{\,1}+\sum_{l=2}^{i}\Lambda_{22}^{(l;i)}\left(x_3^{\,l}-x_3^{\,l-1}\right)\left(1+\sum_{j=1}^{l-1}\Lambda_{33}^{(j)}\right)-\Psi_{33}^{i}\right]\left(x_3-x_3^{i}\right)+\Phi_{22}^{i}\right\} \tag{2-17}$$

The longitudinal and transverse displacements in Eq. (2-16) are piecewise linear through the thickness and discontinuous at the imperfect interfaces.

The strain components in the layer *k* are derived from the homogenized displacement field in Eq. (2-16) through the linear strain-displacement relationships:

$$^{(k)}\varepsilon_{22}=v_{02},_2+\varphi_2,_2\,x_3+\left(\varphi_2,_2+w_0,_{22}\right)R_{S22}^{k}+\varphi_3,_{22}\,R_{N22}^{k}$$
$$^{(k)}\varepsilon_{33}=\varphi_3\left(1+\sum_{i=1}^{k-1}\Lambda_{33}^{(i)}\right)$$
$$2\,^{(k)}\varepsilon_{23}=\left(\varphi_2+w_0,_2\right)\left(1+R_{S22}^{k},_3\right)+\varphi_3,_2\left[x_3+\sum_{i=1}^{k-1}\left(\Lambda_{33}^{(i)}\left(x_3-x_3^{i}\right)+\Psi_{33}^{i}\right)+R_{N22}^{k},_3\right] \tag{2-18}$$

The axial and transverse shear strains in Eq. (2-18) are piecewise linear through the thickness and discontinuous at the interfaces, while the transverse normal strain is piecewise constant through the thickness.

The stress components in the layers are derived by substituting the strain components from Eq. (2-18) into the constitutive equations (2-1). The bending and transverse normal stresses are piecewise linear through the thickness and discontinuous at the interfaces, whereas the transverse shear stress is piecewise linear through the thickness and continuous at the interfaces. Discontinuity of the transverse normal stresses at the interfaces are due to neglecting the effect of ε_{22} on σ_{33} for determining $\Omega_3{}^{k}$.

The interfacial tractions in terms of the global variable are:

$$\hat{\sigma}_S^{k}=K_S^{k}\left[\left(\varphi_2+w_0,_2\right)\Psi_{22}^{k}+\varphi_3,_2\,\Phi_{22}^{k}\right]$$
$$\hat{\sigma}_N^{k}=K_N^{k}\Psi_{33}^{k}\varphi_3 \tag{2-19}$$

Homogenized equilibrium equations and boundary conditions ([25])

The homogenized equilibrium equations and boundary conditions are derived using the Principle of Virtual Works [25]:

$$\int_V\left(\sigma_{22}\delta\varepsilon_{22}+2\sigma_{23}\delta\varepsilon_{23}+\sigma_{33}\delta\varepsilon_{33}\right)dV+\sum_{k=1}^{n-1}\int_{(k)^{+}}\left(\hat{\sigma}_S^{k}\delta\hat{v}_2^{k}+\hat{\sigma}_N^{k}\delta\hat{w}^{k}\right)dS+$$
$$+\sum_{k=1}^{n-1}\int_{(k)^{+}}\left(t_S^{k}\delta\hat{v}_2^{k}+t_N^{k}\delta\hat{w}^{k}\right)dS-\int_{S^{+}}F_i^{S^{+}}\delta^{(n)}v_i\,dS-\int_{S^{-}}F_i^{S^{-}}\delta^{(1)}v_i\,dS-\int_B F_i^{B}\delta v_i\,dB=0 \tag{2-20}$$

where ν is the volume of the plate. $F_i^{S^+}$, $F_i^{S^-}$ and F_i^B with i = 2, 3 are the components of the tractions acting along the boundary surfaces of the plate, S^+, S^- and B. The δ symbol is the variational operator and the virtual displacements are independent and arbitrary. The second and third terms on the left hand side of Eq. (2-20) define energy contributions due to the interfacial tractions on the interfaces.

Virtual strains and displacements are defined in terms of the global variables through Eqs. (2-14), (2-16) and (2-18), and are substituted in Eq. (2-20). Applying Green's theorem wherever possible, Eq. (2-20) yields the equilibrium equations and boundary conditions.

The equilibrium equations conditions are presented here in a form similar to that of the first order shear and first order normal deformation theory [58]:

$$\begin{aligned}
&\delta v_{02} : N_{22},_2 + f_2 = 0 \\
&\delta \varphi_2 : M^b_{22},_2 - Q_{2g} + f_{2m} = 0 \\
&\delta w_0 : Q_{2g},_2 + f_3 = 0 \\
&\delta \varphi_3 : V_{3g} - M_{3g},_2 + f_{3m} = 0
\end{aligned} \tag{2-21}$$

The stress resultants and loading terms in Eq. (2-21) are:

- normal force and bending moment:

$$\left(N_{22}, M^b_{22}\right) = \sum_{k=1}^{n} \int_{x_3^{k-1}}^{x_3^k} {}^{(k)}\sigma_{22}\left(1, x_3\right) dx_3 \tag{2-22}$$

- generalized transverse shear force:

$$Q_{2g} = Q_2^b + Q_2^z - M^{zS}_{22},_2 - \hat{\sigma}_2 \tag{2-23}$$

- transverse shear force:

$$Q_2^b = \sum_{k=1}^{n} \int_{x_3^{k-1}}^{x_3^k} {}^{(k)}\sigma_{23} dx_3 \tag{2-24}$$

- higher order stress resultants due to the transverse normal stress:

$$\begin{aligned}
&V_{3g} = V_3 + V_3^z + \sum_{l=1}^{n-1} \left(\hat{\sigma}_N^l + t_N^l\right) \Psi^l_{33}; \qquad M_{3g} = M_3^b + M_3^z - R^{zS}_{33,2} - \hat{\sigma}_3 \\
&V_3 = \sum_{k=1}^{n} \int_{x_3^{k-1}}^{x_3^k} {}^{(k)}\sigma_{33} dx_3 \; ; \qquad M_3^b = \sum_{k=1}^{n} \int_{x_3^{k-1}}^{x_3^k} {}^{(k)}\sigma_{23} x_3 dx_3
\end{aligned} \tag{2-25}$$

- stress resultants, load and load couples associated to the multilayered structure and cohesive interfaces:

$$Q_2^z = \sum_{k=1}^{n} \int_{x_3^{k-1}}^{x_3^k} {}^{(k)}\sigma_{23} \sum_{i=1}^{k-1} \Lambda_{22}^{(1;i)} dx_3 \; ; \qquad M^{zS}_{22} = \sum_{k=1}^{n} \int_{x_3^{k-1}}^{x_3^k} {}^{(k)}\sigma_{22} R^k_{S22} dx_3 \tag{2-26}$$

$$\hat{\sigma}_2 = -\sum_{l=1}^{n-1}\left(\hat{\sigma}_S^l + t_S^l\right)\Psi_{22}^l; \qquad V_3^z = \sum_{k=1}^{n}\int_{x_3^{k-1}}^{x_3^k} {}^{(k)}\sigma_{33}\sum_{i=1}^{k-1}\Lambda_{33}^{(i)}dx_3$$

$$\hat{\sigma}_3 = -\sum_{l=1}^{n-1}\left(\hat{\sigma}_S^l + t_S^l\right)\Phi_{22}^l; \qquad R_{33}^{zS} = \sum_{k=1}^{n}\int_{x_3^{k-1}}^{x_3^k} {}^{(k)}\sigma_{22}R_{N22}^k dx_3$$

$$M_3^z = \sum_{k=1}^{n}\int_{x_3^{k-1}}^{x_3^k} {}^{(k)}\sigma_{23}\left\{\sum_{i=1}^{k-1}[\Lambda_{33}^{(i)}(x_3 - x_3^i) + \Psi_{33}^i] + R_{N22}^k{}_{,3}\right\}dx_3$$

- loading terms

$$f_2 = F_2^{S+} + F_2^{S-};\ f_{2m} = F_2^{S+}x_3^n + F_2^{S-}x_3^0 + F_2^{S+}R_{S22}^n\Big|_{x_3^n};\ f_3 = F_3^{S+} + F_3^{S-} - F_2^{S+}{}_{,2}\,R_{S22}^n\Big|_{x_3^n}$$

$$f_{3m} = -F_3^{S+}x_3^n - F_3^{S-}x_3^0 - F_3^{S+}\sum_{i=1}^{n-1}\left[\Lambda_{33}^{(i)}\left(x_3^n - x_3^i\right) + \Psi_{33}^i\right] + F_2^{S+}{}_{,2}\,R_{N22}^n\Big|_{x_3^n} \tag{2-27}$$

The generalized transverse shear force, Q_{2g} in Eq. (2-23), has additional contributions to Q_2^b, which are due to the discontinuities of material properties, M_{22}^{zS}, Q_2^z, and displacements at the interface, M_{22}^{zS}, $\hat{\sigma}_2$. The introduction of Q_{2g} is physically important since it is statically equivalent at any arbitrary section of the plate with outward normal $\boldsymbol{n} = \{0, \pm 1, 0\}^T$, to the vertical equilibrant of the external forces acting on the portion of the plate to the right of the section.

The homogenized boundary conditions at the plate edges are:

$$\begin{aligned}
&N_{22}n_2 = \tilde{N}_2 && \text{or} && v_{02} = \tilde{v}_{02}\\
&M_{22}^b n_2 = \tilde{M}_2^b && \text{or} && \varphi_2 = \tilde{\varphi}_2\\
&Q_{2g}n_2 = \tilde{N}_3 + f_{2mbc}n_2 && \text{or} && w_0 = \tilde{w}_0\\
&M_{3g}n_2 = \tilde{M}_{3g} + f_{3mbc}n_2 && \text{or} && \varphi_3 = \tilde{\varphi}_3\\
&M_{22}^{zS}n_2 = \tilde{M}_2^{zS} && \text{or} && w_{0,2} = \tilde{w}_{0,2}\\
&R_{33}^{zS}n_2 = \tilde{R}_3^{zS} && \text{or} && \varphi_{3,2} = \tilde{\varphi}_{3,2}
\end{aligned} \tag{2-28}$$

with n_2 the component of the outward normal. The terms with the tilde define prescribed values of displacements, forces and couples at the plate edges:

$$\begin{aligned}
&\left(\tilde{N}_j, \tilde{M}_j^b\right) = \sum_{k=1}^{n}\int_{x_3^{k-1}}^{x_3^k} {}^{(k)}F_j^B\left(1, x_3\right)dx_3 && f_{2mbc} = F_2^{S+}R_{S22}^n\Big|_{x_3^n}\\
&\tilde{M}_{3g} = \tilde{M}_3^b + \tilde{M}_3^z + \tilde{M}_3^S && \tilde{M}_3^z = \sum_{k=1}^{n}\int_{x_3^{k-1}}^{x_3^k} {}^{(k)}F_3^B\sum_{i=1}^{k-1}\Lambda_{33}^{(i)}(x_3 - x_3^i)dx_3\\
&\tilde{M}_3^S = \sum_{k=1}^{n}\int_{x_3^{k-1}}^{x_3^k} {}^{(k)}F_3^B\sum_{i=1}^{k-1}\Psi_{33}^i dx_3 && f_{3mbc} = F_2^{S+}R_{N22}^n\Big|_{x_3^n}\\
&\tilde{M}_2^{zS} = \sum_{k=1}^{n}\int_{x_3^{k-1}}^{x_3^k} {}^{(k)}F_2^B R_{S22}^k dx_3 && \tilde{R}_3^{zS} = \sum_{k=1}^{n}\int_{x_3^{k-1}}^{x_3^k} {}^{(k)}F_2^B R_{N22}^k dx_3
\end{aligned} \tag{2-29}$$

for j = 2, 3. Along a clamped support, where $\varphi_2 = w_{0,2} = \varphi_{3,2} = 0$, Eq. (2-18) shows that the transverse shear strain and stress vanish and the model then neglects the shear deformations at a clamped end, similar to the original zigzag theory for fully bonded plates in [62, 63].

The importance of the introduction of the generalized shear force, Q_{2g} ,was demonstrated in [26], where some of the previously observed anomalies in the original zigzag theory [62, 63] at the clamped supports, were clarified. In [27], the original zigzag theory [62, 63] was used to study a multilayered cantilever beam subjected to a concentrated force at the free end and it was found that the shear force increases from zero at the clamped end, due to vanishing shear strain and stress, to a value higher than the applied load. This apparent inconsistency is explained by Eqs. (2-21), (2-23) and (2-28), which demonstrate that the generalized shear force defined in Eq. (2-23), is constant, due to the linear distribution of the bending moment, and equals the applied force at any cross section of the beam including the clamped end [26].

The equilibrium equations (2-21) and boundary conditions (2-28) can be defined in terms of the displacements through Eqs. (2-1), (2-14), (2-18) and (2-19).

Displacement field, equilibrium equations and boundary conditions for plates with sliding interfaces ([25])

The displacement field in Eq. (2-9), the equilibrium equations (2-21) and boundary conditions (2-28) are presented here for plate with interfaces which are rigid against mode I (opening) relative displacements, $B_N^k = 0$, so that $\hat{w}^k = 0$ for $k = 1, \ldots, n-1$. The assumption of sliding only interfaces is exact for interfaces under pure mode II loading, e.g. a single interface in a plate with symmetric layup subjected to anti-symmetric loading about the interface plane. The assumption is acceptable for plates with continuous interfaces, when the interfacial normal tractions are small compared to the tangential tractions and interfacial opening is prevented by a through-thickness reinforcements or other means. The simplified version of the model for plates with sliding only interfaces, will be used in Chapter 4 to study mode II dominant delamination problems in bi-material wide plates.

For plates with sliding only interfaces, the transverse compressibility/extensibility of the layers is neglected, $\varphi_3 = 0$ and $\Lambda_{33} = 0$; therefore, the transverse displacement in Eq. (2-9) becomes constant through the thickness, ${}^{(k)}w(x_2) = w_0(x_2)$ for $k = 1, \ldots, n$. In addition, the normal stress ${}^{(k)}\sigma_{33}$ is assumed to be negligible compared to the other stress components and the constitutive equation (2-1) modifies in ${}^{(k)}\sigma_{22} = {}^{(k)}\overline{C}_{22}\,{}^{(k)}\varepsilon_{22}$, with ${}^{(k)}\overline{C}_{22} = {}^{(k)}\left(C_{22} - C_{23}C_{32}/C_{33}\right)$.

The displacement field in Eq. (2-9), particularized to plates with sliding only interfaces is:

$$\begin{aligned} {}^{(k)}v_2(x_2,x_3) &= v_{02}(x_2) + x_3\varphi_2(x_2) + \sum_{i=1}^{k-1}\Omega_2{}^i(x_2)(x_3 - x_3{}^i) + \sum_{i=1}^{k-1}\hat{v}_2{}^i(x_2) \\ {}^{(k)}w(x_2,x_3) &= w_0(x_2) \end{aligned} \tag{2-30}$$

where $\Omega_2{}^i$ and $\hat{v}_2{}^i$ are defined in Eqs. (2-12) and (2-14) with $\varphi_3 = \hat{w}^k = 0$. The homogenized displacement field in Eq. (2-16), particularized to plates with sliding only interfaces is:

$$
\begin{aligned}
&{}^{(k)}v_2 = v_{02} + \varphi_2 x_3 + \left(\varphi_2 + w_{0,2}\right) R^k_{S22} - \sum_{i=1}^{k-1} B^i_S t^i_S \\
&{}^{(k)}w = w_0
\end{aligned}
\tag{2-31}
$$

where R^k_{S22} is given in Eq. (2-17).

The equilibrium equations in terms of displacement for plates with sliding only interfaces are [25]:

$$
\begin{aligned}
&C^0_{22} v_{02,22} + (C^1_{22} + C^{0S}_{22})\varphi_{2,22} + C^{0S}_{22} w_{0,222} + f_2 = 0 \\
&(C^1_{22} + C^{0S}_{22}) v_{02,22} + (C^2_{22} + 2C^{1S}_{22} + C^{S2}_{22})\varphi_{2,22} + (C^{1S}_{22} + C^{S2}_{22}) w_{0,222} \\
&-[k_{44} C^P_{44} + C^S_{22}](w_{0,2} + \varphi_2) - C^C_{22} + f_{2m} = 0 \\
&C^{0S}_{22} v_{02,222} + (C^{1S}_{22} + C^{S2}_{22})\varphi_{2,222} + C^{S2}_{22} w_{0,2222} - [k_{44} C^P_{44} + C^S_{22}](w_{0,22} + \varphi_{2,2}) - f_3 = 0
\end{aligned}
\tag{2-32}
$$

where the coefficients, C^r_{22}, C^{rS}_{22}, C^{S2}_{22}, C^P_{44}, C^S_{22} and C^C_{22} for $r = 0, 1, 2,$ can be calculated a priori, depend on the geometry, the layup and the status of the interfaces:

$$
\begin{aligned}
&C^r_{22} = \sum_{k=1}^{n} {}^{(k)}\overline{C}_{22} \int_{x_3^{k-1}}^{x_3^k} (x_3)^r dx_3 \qquad C^{rS}_{22} = \sum_{k=1}^{n} {}^{(k)}\overline{C}_{22} \int_{x_3^{k-1}}^{x_3^k} (x_3)^r R^k_{S22} dx_3 \\
&C^{S2}_{22} = \sum_{k=1}^{n} {}^{(k)}\overline{C}_{22} \int_{x_3^{k-1}}^{x_3^k} (R^k_{S22})^2 dx_3 \qquad C^P_{44} = \sum_{k=1}^{n} {}^{(k)}C_{44} \int_{x_3^{k-1}}^{x_3^k} \left(1 + R^k_{S22,3}\right)^2 dx_3 \\
&C^S_{22} = \sum_{k=1}^{n-1} K^k_S \left(\Psi^k_{22}\right)^2 \qquad C^C_{22} = \sum_{k=1}^{n-1} t^k_S \Psi^k_{22}
\end{aligned}
\tag{2-33}
$$

A shear correction factor, k_{44}, has been introduced in Eq. (2-32) to improve the approximate description of the shear [25]. The correction factor is defined, following the classical approach used in the first order theories, as $k_{44} = \left(Q^b_2 + Q^z_2\right) \Big/ \left[C^p_{44}\left(\varphi_2 + w_{0,2}\right)\right]$. The introduction of the shear correction factor has some advantages. It allows to recover the constitutive equations of the equivalent single layer first order shear deformation theory in the limiting case of a fully bonded and homogeneous plate, for which $k_{44} = 5/6$ is required. Also, in a plate with imperfect interfaces, where the transverse shear strains and stresses in the layers will progressively reduce on decreasing the interfacial stiffness, as it can be understood from Eqs. (2-8), (2-18) and (2-19), the shear correction factor may be used to account for the missing contribution of the shear deformations in the equilibrium equations of the model [25]. In general, the shear correction factor is a problem dependent parameter and depends on the stacking sequence, geometry, material and interfacial properties and loading conditions. If the shear correction factor is not needed, for instance in bending problem of fully bonded multilayered plates subjected to static loadings, the shear correction factor should be equal to 1.

The boundary conditions (2-28) for plates with sliding only interfaces simplify as:

$$
\begin{aligned}
&N_{22}n_2 = \tilde{N}_2 && \text{or} && v_{02} = \tilde{v}_{02} \\
&M^{b}_{22}n_2 = \tilde{M}^{b}_{2} && \text{or} && \varphi_2 = \tilde{\varphi}_2 \\
&Q_{2g}n_2 = \tilde{N}_3 + f_{2mbc}n_2 && \text{or} && w_0 = \tilde{w}_0 \\
&M^{zS}_{22}n_2 = \tilde{M}^{zS}_{2} && \text{or} && w_{0,2} = \tilde{w}_{0,2}
\end{aligned}
\tag{2-34}
$$

A MATRIX TECHNIQUE FOR THERMO-ELASTIC ANALYSIS OF MULTILAYERED STRUCTURES

3.1 INTRODUCTION

In this chapter a matrix technique is formulated aimed at efficiently obtaining exact solutions for thermo-mechanical problems in simply supported multilayered plates and beams with an arbitrary number of imperfectly bonded layers in imperfect thermal contact, and subjected to stationary sinusoidal thermo-mechanical loading. The technique is based on the theoretical formulation developed in [7], which uses a classical displacement approach, and on the transfer matrix method formulated in [51]. The model in [7] follows the models formulated in [6, 29, 37] for fully bonded layers and perfect thermal contact. Imperfect interfaces, which are zero-thickness mathematical surfaces where interfacial tractions and heat flux are continuous while displacements and temperature may be discontinuous, are introduced in the model in [7] to account for the presence of damage regions, delaminations or thin interlayers, e.g. adhesives.

The applications of matrix techniques in elasticity problems of simply supported multilayered plates subjected to mechanical and/or thermal loadings can be found in [12-18], where the solutions are derived and presented only in the matrix form, can be obtained through many matrix multiplications and no explicit expression is given for the field variables; therefore, the solution remains quite complex. Moreover, none of them consider the presence of thermally imperfect interfaces.

Novel explicit expressions are derived for two-dimensional and three-dimensional problems. The expressions can be used to solve problems with load distributions other than sinusoidal using Fourier series and the principle of superposition. The expressions are applicable to the limiting cases of perfectly bonded layers in perfect thermal contact and fully debonded layers or impermeable interfaces. For purely mechanical loading and plates with orthotropic layers, the explicit expressions derived in this chapter coincide with the expanded forms of the matrix expressions in [12]; the solution presented here is applicable also to plates containing isotropic layers. Different applications to composite laminates and sandwiches are also presented; the influence of interfacial imperfections and length-to-thickness ratio on local fields is highlighted.

In Sect. 3.2, the two-dimensional problem is solved. In Sect. 3.3, closed-form and explicit expressions are derived for plates with finite dimensions. The conclusions are presented in Sect. 3.4.

3.2 CLOSED-FORM 2D THERMO-ELASTICITY SOLUTIONS FOR MULTILAYERED WIDE PLATES WITH IMPERFECT INTERFACES AND IMPERFECT THERMAL CONTACT

The multilayered plate illustrated in Figure 3-1 is assumed to be under plane conditions parallel to the plane $x_2 - x_3$, with $x_1 - x_2 - x_3$ a system of Cartesian coordinates with origin at the left edge. The plate is simply

supported at $x_2 = 0, L$, has global thickness h and is composed of n layers. The kth layer, with $k = 1, \ldots n$ numbered from bottom to top, is defined by the coordinates of its lower and upper surfaces, x_3^{k-1} and x_3^k, and has thickness ${}^{(k)}h$ (the superscript (k) on the left of a quantity shows association with the layer k, while the superscript k on the right identifies the interface between layers k and k+1). The plate is subjected to thermo-mechanical loadings: $f_3\left(x_2, x_3 = x_3^n\right) = f_u \sin\left(px_2\right)$ and $f_3\left(x_2, x_3 = x_3^0\right) = f_l \sin\left(px_2\right)$ are normal surface tractions acting on the upper and lower surfaces, and $T\left(x_2, x_3 = x_3^n\right) = T_u \sin\left(px_2\right)$ and $T\left(x_2, x_3 = x_3^0\right) = T_l \sin\left(px_2\right)$ are applied temperatures, with $p = m\pi/L$ and $m \in \mathbb{N}$.

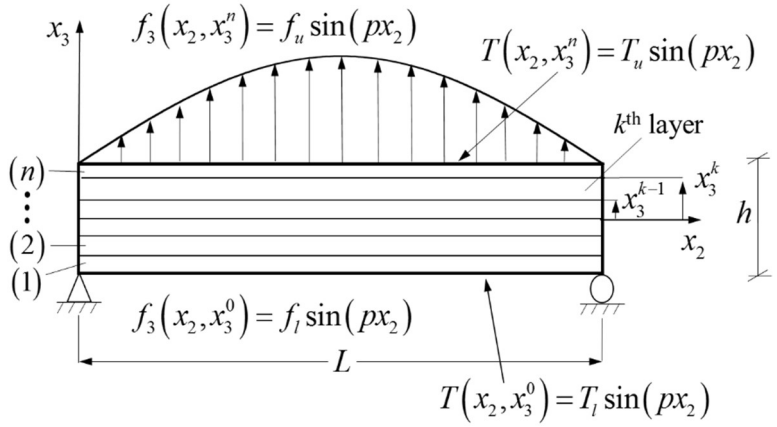

Figure 3-1: Simply supported multilayered plate subjected to thermo-mechanical loadings. Surface tractions correspond to the case $p = \pi/L$, $(m = 1)$.

The layers are linearly elastic, homogenous and orthotropic with principal material axes parallel to the geometrical axes. Coupling between elastic deformations and heat transfer is neglected and the thermal conditions are assumed to be stationary. For plane-strain conditions, the constitutive equations of a generic layer k are:

$$\begin{Bmatrix} {}^{(k)}\sigma_{22} \\ {}^{(k)}\sigma_{33} \\ {}^{(k)}\sigma_{23} \end{Bmatrix} = {}^{(k)}[C] \begin{Bmatrix} {}^{(k)}\varepsilon_{22} - \alpha_2 T \\ {}^{(k)}\varepsilon_{33} - \alpha_3 T \\ 2{}^{(k)}\varepsilon_{23} \end{Bmatrix} - \begin{Bmatrix} C_{12}\alpha_1 T \\ C_{13}\alpha_1 T \\ 0 \end{Bmatrix}$$
$$ {}^{(k)}[C] = \begin{bmatrix} C_{22} & C_{23} & 0 \\ C_{23} & C_{33} & 0 \\ 0 & 0 & C_{55} \end{bmatrix} \tag{3-1}$$

where ${}^{(k)}\sigma_{ij} = {}^{(k)}\sigma_{ij}(x_2, x_3)$ and ${}^{(k)}\varepsilon_{ij} = {}^{(k)}\varepsilon_{ij}(x_2, x_3)$ (for i, j = 2, 3) are Cauchy stress and linear strain components, ${}^{(k)}C_{ij}$ (for $i, j = 1, 2, 3, 5$) are stiffness coefficients, ${}^{(k)}\alpha_i$ are coefficients of thermal expansion along the x_i direction and ${}^{(k)}T = {}^{(k)}T(x_2, x_3)$ is the temperature increment in the layer k. The constitutive

equations for plane-stress conditions can be obtained by replacing ${}^{(k)}C_{ij}$ for $i, j =$ 2, 3 and ${}^{(k)}\alpha_1$ in Eq. (3-1) with ${}^{(k)}C_{ij} - {}^{(k)}C_{1i}\,{}^{(k)}C_{1j} \big/ {}^{(k)}C_{11}$ and 0, respectively.

The displacement components in the layer k are ${}^{(k)}v_i$ with i = 2, 3. The layers are joined by interfaces, which are zero-thickness mathematical surfaces where material properties, displacements and temperature may be discontinuous while interfacial tractions and heat flux are continuous. The interfaces are introduced to account for the presence of damage regions, delaminations or thin interlayers, e.g. adhesives [7]. In this work, the constitutive equations of the interfaces are defined by linear uncoupled traction laws which relate the interfacial tractions to the relative displacements of the adjacent layers:

$$\begin{aligned} \hat{\sigma}_2^k(x_2) &= K_S^k\ \hat{v}_2^k(x_2, x_3 = x_3^k) \\ \hat{\sigma}_3^k(x_2) &= K_N^k\ \hat{v}_3^k(x_2, x_3 = x_3^k) \end{aligned} \tag{3-2}$$

where $\hat{\sigma}_2^k$ and $\hat{\sigma}_3^k$ are the interfacial tangential and normal tractions acting on the upper surface of the layer k with unit positive normal vector, K_S^k and K_N^k are tangential and normal stiffnesses and $\hat{v}_2^k$ and $\hat{v}_3^k$ are the relative displacements between the layers k and k + 1 at the interface:

$$\hat{v}_i^k(x_2) = {}^{(k+1)}v_i(x_2, x_3 = x_3^k) - {}^{(k)}v_i(x_2, x_3 = x_3^k) \tag{3-3}$$

with ${}^{(k)}v_i$ the displacement component in the layer k and i = 2, 3. The limiting case of a perfectly bonded interface is described by $1/K_S^k = 1/K_N^k = 0$, which leads to a continuous displacement field with $\hat{v}_2^k = \hat{v}_3^k = 0$; an interface which allows free sliding displacements in constrained contact is defined by $1/K_N^k = 0$ and $K_S^k = 0$, which yield $\hat{\sigma}_2^k = 0$ and $\hat{v}_3^k = 0$.

The thermal behavior of the interfaces is described in this work by a thermal resistance, R^k, which is independent of the interfacial displacements and controls the heat flux and the temperature at the interface [47]. The jump in temperature between layers k and k + 1 is related to the heat flux through the interface through the interfacial thermal resistance:

$${}^{(k)}q_3(x_2, x_3 = x_3^k)R^k = -\left[{}^{(k+1)}T(x_2, x_3 = x_3^k) - {}^{(k)}T(x_2, x_3 = x_3^k)\right] \tag{3-4}$$

where ${}^{(k)}q_3(x_2, x_3 = x_3^k) = -{}^{(k)}K_3\,{}^{(k)}T(x_2, x_3 = x_3^k)_{,3}$ is the heat flux in the layer k at $x_3 = x_3^k$, and ${}^{(k)}K_i$ is its thermal conductivity in the x_i direction. Here and throughout the derivation, a comma followed by a subscript denotes a partial derivative with respect to the corresponding coordinate. The limiting case corresponding to perfect thermal contact, where the temperature is continuous across the interface is described by $R^k = 0$, and an impermeable interface, where the heat flux through the interface vanishes, by a vanishing thermal conductance $1/R^k = 0$.

3.2.1 Heat conduction and thermo-elastic problems

In this section, heat conduction and equilibrium equations are presented for a generic layer *k* along with the associated thermal and mechanical boundary and continuity conditions. The two-dimensional steady-state heat conduction equation, in the absence of internal heat generation, for the layer *k* is given by:

$$\frac{{}^{(k)}K_2}{{}^{(k)}K_3}\frac{\partial^2\,{}^{(k)}T(x_2,x_3)}{\partial x_2^2}+\frac{\partial^2\,{}^{(k)}T(x_2,x_3)}{\partial x_3^2}=0 \tag{3-5}$$

where ${}^{(k)}K_i$ is the thermal conductivity of the layer *k* in the x_i direction. The solution of the heat conduction equation must satisfy the continuity conditions at the layer interfaces, also accounting for the interfacial thermal laws Eq. (3-4)

$$\begin{aligned}&\frac{{}^{(k)}K_3}{{}^{(k+1)}K_3}\,{}^{(k)}T(x_2,x_3^k),_3={}^{(k+1)}T(x_2,x_3^k),_3\\&{}^{(k+1)}T(x_2,x_3^k)-{}^{(k)}T(x_2,x_3^k)=-{}^{(k)}q_3(x_2,x_3^k)R^k\end{aligned} \tag{3-6}$$

for *k* = 1, …, $n-1$, and the boundary conditions at the upper and lower surfaces of the plate and at the plate edges:

$$\begin{aligned}&{}^{(n)}T(x_2,x_3=x_3^n)=T_u\sin(px_2)\\&{}^{(1)}T(x_2,x_3=x_3^0)=T_l\sin(px_2)\\&{}^{(k)}T(x_2=0\text{ and }L,x_3)=0,\text{ for }k=1,\ldots,n\end{aligned} \tag{3-7}$$

The two-dimensional equilibrium equations for the layer *k*, in the absence of body forces, are:

$$\begin{aligned}&{}^{(k)}\sigma_{22},_2+{}^{(k)}\sigma_{32},_3=0\\&{}^{(k)}\sigma_{33},_3+{}^{(k)}\sigma_{23},_2=0\end{aligned} \tag{3-8}$$

and the compatibility equations:

$${}^{(k)}\varepsilon_{22}={}^{(k)}v_2,_2;\ {}^{(k)}\varepsilon_{33}={}^{(k)}v_3,_3;\ \ 2\,{}^{(k)}\varepsilon_{23}={}^{(k)}v_2,_3+{}^{(k)}v_3,_2 \tag{3-9}$$

Using the constitutive and compatibility equations, (3-1) and (3-9), the equilibrium equations are restated in terms of displacement variables, ${}^{(k)}v_2$ and ${}^{(k)}v_3$:

$$\begin{aligned}&{}^{(k)}C_{22}\,{}^{(k)}v_2,_{22}+{}^{(k)}(C_{23}+C_{55})\,{}^{(k)}v_3,_{23}+{}^{(k)}C_{55}\,{}^{(k)}v_2,_{33}\\&\qquad={}^{(k)}(C_{12}\alpha_1+C_{22}\alpha_2+C_{23}\alpha_3)\,{}^{(k)}T,_2\\&{}^{(k)}C_{33}\,{}^{(k)}v_3,_{33}+{}^{(k)}(C_{23}+C_{55})\,{}^{(k)}v_2,_{23}+{}^{(k)}C_{55}\,{}^{(k)}v_3,_{22}\\&\qquad={}^{(k)}(C_{13}\alpha_1+C_{23}\alpha_2+C_{33}\alpha_3)\,{}^{(k)}T,_3\end{aligned} \tag{3-10}$$

The continuity conditions on interfacial tractions and relative displacements, also accounting for the interfacial tractions laws Eqs. (3-2), are expressed in terms of stresses in the layers as:

$$
\begin{aligned}
&{}^{(k)}\sigma_{23}(x_2, x_3^k) = {}^{(k+1)}\sigma_{23}(x_2, x_3^k) \\
&{}^{(k)}\sigma_{33}(x_2, x_3^k) = {}^{(k+1)}\sigma_{33}(x_2, x_3^k) \\
&{}^{(k+1)}v_2(x_2, x_3^k) - {}^{(k)}v_2(x_2, x_3^k) = \frac{1}{K_S^k}\,{}^{(k)}\sigma_{23}(x_2, x_3^k) \\
&{}^{(k+1)}v_3(x_2, x_3^k) - {}^{(k)}v_3(x_2, x_3^k) = \frac{1}{K_N^k}\,{}^{(k)}\sigma_{33}(x_2, x_3^k)
\end{aligned}
\tag{3-11}
$$

for $k = 1, \ldots, n-1$. The boundary conditions at the upper and lower surfaces of the plate and at the plate edges impose:

$$
\begin{aligned}
&{}^{(n)}\sigma_{33}(x_2, x_3 = x_3^n) = f_u \sin(px_2) \\
&{}^{(n)}\sigma_{23}(x_2, x_3 = x_3^n) = 0 \\
&{}^{(1)}\sigma_{33}(x_2, x_3 = x_3^0) = -f_l \sin(px_2) \\
&{}^{(1)}\sigma_{23}(x_2, x_3 = x_3^0) = 0 \\
&{}^{(k)}\sigma_{22}(x_2 = 0 \text{ and } L, x_3) = 0, \text{ for } k = 1, \ldots, n \\
&{}^{(k)}v_3(x_2 = 0 \text{ and } L, x_3) = 0, \text{ for } k = 1, \ldots, n
\end{aligned}
\tag{3-12}
$$

Following Buckingham's Π theorem [92] and choosing as independent fundamental units ${}^{(1)}\alpha_2$, ${}^{(1)}C_{22}$ and h, the equations (3-5)-(3-12) can be defined in dimensionless forms to highlight self-similar behaviors and the dimensionless groups which control the response of the plate. This is done by first defining the dimensionless forms of all quantities. The dimensionless temperature in the layer *k*, for instance, is given by ${}^{(1)}\alpha_2\,{}^{(k)}T$; and the dimensionless forms of x_i, v_i and K_S^k are x_i/h, v_i/h and $K_S^k h / {}^{(1)}C_{22}$. The thermal conductivities always appear through the dimensionless group ${}^{(k)}K_i / {}^{(k)}K_j$, due to the assumption of stationary conditions, and heat flux and thermal resistance through the group ${}^{(k)}q_3(x_2, x_3^k)R^k$, whose dimensionless form is ${}^{(1)}\alpha_2\,{}^{(k)}q_3 R^k$. The list of dimensionless quantities is given in Table 3-1.

Table 3-1: Dimensionless quantities (with ${}^{(1)}\alpha_2$, h and ${}^{(1)}C_{22}$ as fundamental units).

Dimensional quantity/group	Dimensionless quantity/group	Dimensional quantity/group	Dimensionless quantity/group
${}^{(k)}C_{ij}$	${}^{(k)}C_{ij} \,/\, {}^{(1)}C_{22}$	$R^k\, {}^{(k)}q_3$	${}^{(1)}\alpha_2 R^k\, {}^{(k)}q_3$
$\left({}^{(k)}\sigma_{ij}, \hat{\sigma}_i^k\right)$	$\frac{1}{{}^{(1)}C_{22}}\left({}^{(k)}\sigma_{ij}, \hat{\sigma}_i^k\right)$	$R^k\, {}^{(k)}K_3$	$R^k\, {}^{(k)}K_3 / h$
${}^{(k)}\alpha_i$	${}^{(k)}\alpha_i / {}^{(1)}\alpha_2$	$\left(K_S^k, K_N^k\right)$	$\frac{h}{{}^{(1)}C_{22}}\left(K_S^k, K_N^k\right)$
$\left(x_i, x_3^k, L\right)$	$\frac{1}{h}\left(x_i, x_3^k, L\right)$	$\left({}^{(k)}B_i, {}^{(k)}D_i, {}^{(k)}a_{ij}\right)$	$\frac{1}{h}\left({}^{(k)}B_i, {}^{(k)}D_i, {}^{(k)}a_{ij}\right)$
${}^{(k)}T$	${}^{(1)}\alpha_2\, {}^{(k)}T$	${}^{(k)}\gamma_j$	$h^2\, {}^{(k)}\gamma_j$
f	$f / {}^{(1)}C_{22}$	${}^{(k)}A_0$	$\left(1/{}^{(1)}C_{22}\right)^2\, {}^{(k)}A_0$
$\left({}^{(k)}c_1, {}^{(k)}c_2\right)$	${}^{(1)}\alpha_2\left({}^{(k)}c_1, {}^{(k)}c_2\right)$	${}^{(k)}A_1$	$\left(h/{}^{(1)}C_{22}\right)^2\, {}^{(k)}A_1$
$\left({}^{(k)}s, {}^{(k)}m_j, {}^{(k)}t, p\right)$	$h\left({}^{(k)}s, {}^{(k)}m_j, {}^{(k)}t, p\right)$	${}^{(k)}A_2$	$\left(h^2/{}^{(1)}C_{22}\right)^2\, {}^{(k)}A_2$
$\left({}^{(k)}v_i, \hat{v}_i^k, {}^{(k)}V, {}^{(k)}W\right)$	$\frac{1}{h}\left({}^{(k)}v_i, \hat{v}_i^k, {}^{(k)}V, {}^{(k)}W\right)$	${}^{(k)}\Delta$	$\left(h/{}^{(1)}C_{22}\right)^4\, {}^{(k)}\Delta$

Equation (3-10), for instance, is dimensionalized by multiplying both sides by $h/{}^{(1)}C_{22}$ so that:

$$\frac{{}^{(k)}C_{22}}{{}^{(1)}C_{22}} h\, {}^{(k)}v_{2,22} + \frac{{}^{(k)}\left(C_{23}+C_{55}\right)}{{}^{(1)}C_{22}} h\, {}^{(k)}v_{3,23} + \frac{{}^{(k)}C_{55}}{{}^{(1)}C_{22}} h\, {}^{(k)}v_{2,33} = \frac{{}^{(k)}\left(C_{12}\alpha_1 / {}^{(1)}\alpha_1 + C_{22}\alpha_2 / {}^{(1)}\alpha_1 + C_{23}\alpha_3 / {}^{(1)}\alpha_1\right)}{{}^{(1)}C_{22}} {}^{(1)}\alpha_1 h\, {}^{(k)}T_{,2} \tag{3-13}$$

Comparing Eqs. (3-13) and (3-10) shows that Eq. (3-10) can be interpreted as a dimensionless equation provided its terms are interpreted as their respective dimensionless forms in Table 3-1. The formulation of the problem in the remaining of the chapter can be used, similarly, in dimensional or dimensionless form.

3.2.2 Solution of the heat conduction problem through the transfer matrix method

The general solution of the heat conduction equation (3-5) in layer *k*, which satisfies the thermal boundary conditions at the plate edges, Eq. (3-7), is obtained using the method of separation of variables [7]

$${}^{(k)}T(x_2, x_3) = {}^{(k)}F(x_3)\sin(px_2) \tag{3-14}$$

with:

$$
\begin{aligned}
{}^{(k)}F(x_3) &= ({}^{(k)}c_1 e^{{}^{(k)}sx_3} + {}^{(k)}c_2 e^{-{}^{(k)}sx_3}) \\
{}^{(k)}s &= p\sqrt{\frac{{}^{(k)}K_2}{{}^{(k)}K_3}}, \quad p = \frac{m\pi}{L}
\end{aligned}
\tag{3-15}
$$

where ${}^{(k)}c_1$ and ${}^{(k)}c_2$ are integration constants (dimensionless forms in Table 3-1). Equation (3-14) and the thermal continuity and boundary conditions, Eqs. (3-6) and (3-7), yield an algebraic system of $2\times n$ coupled equations in the $2\times n$ unknown constants ${}^{(k)}c_1$ and ${}^{(k)}c_2$, for $k = 1, \ldots, n$.

The transfer matrix method is used here for an efficient closed-form derivation of the unknowns. The method first derives explicit expressions which relate the unknowns in layer k to those of the first layer; then defines the two unknowns, ${}^{(1)}c_1$ and ${}^{(1)}c_2$, through the boundary conditions at the top and bottom surfaces of the laminate.

The matrix forms of the temperature distribution in the layer k, Eqs. (3-14) and (3-15), and its gradient in the x_3 direction, ${}^{(k)}T(x_2,x_3),_3$, are:

$$
{}^{(k)}\begin{bmatrix} T(x_2,x_3) \\ T(x_2,x_3),_3 \end{bmatrix} = {}^{(k)}G(x_3)\sin(px_2)
\tag{3-16}
$$

where:

$$
{}^{(k)}G(x_3) = {}^{(k)}D(x_3)\,{}^{(k)}\begin{bmatrix} c_1 \\ c_2 \end{bmatrix}
\tag{3-17}
$$

$$
{}^{(k)}D(x_3) = {}^{(k)}\begin{bmatrix} e^{sx_3} & e^{-sx_3} \\ se^{sx_3} & -se^{-sx_3} \end{bmatrix}
\tag{3-18}
$$

with ${}^{(k)}D(x_3)$ a 2×2 matrix whose elements depend on ${}^{(k)}s$ and x_3. In order to establish a relationship between ${}^{(k)}c_1$ and ${}^{(k)}c_2$, and the constants of the first layer, the 2×1 matrix ${}^{(k)}G$ is related to the matrix ${}^{(1)}G$ of the first layer (Figure 3-2). The procedure necessitates two main relationships, namely the local transfer matrix, which relates the values of the matrix ${}^{(k)}G$ at the upper and lower surfaces of the layer, and the interfacial continuity conditions expressed in terms of matrix ${}^{(k)}G$.

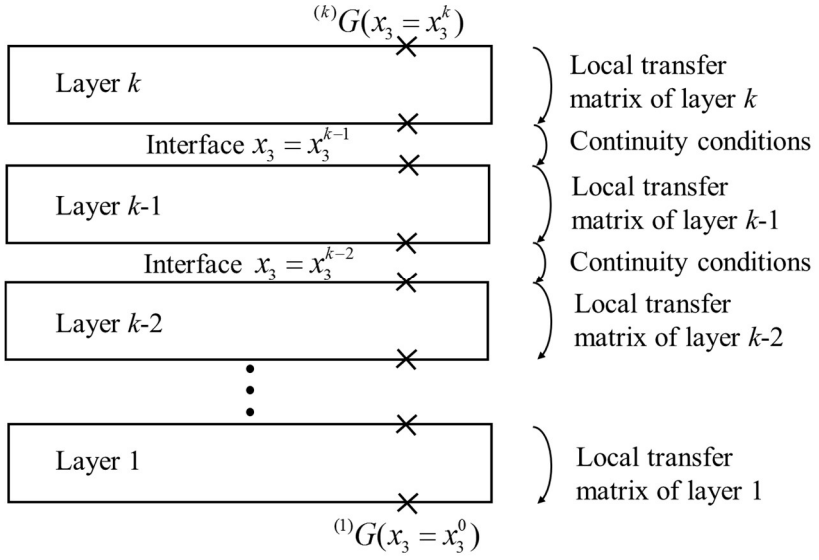

Figure 3-2: Schematic of the Transfer Matrix Method.

Local transfer matrix of a generic layer

The vector $^{(k)}\left[c_1, c_2\right]^T$ is expressed as function of $^{(k)}G$ by setting $x_3 = x_3^{k-1}$ in Eq. (3-17):

$$^{(k)}\begin{bmatrix} c_1 \\ c_2 \end{bmatrix} = {}^{(k)}D^{-1}(x_3^{k-1})\,{}^{(k)}G(x_3^{k-1}) \tag{3-19}$$

where the superscript -1 at the right of a matrix denotes its inverse. The local transfer matrix is then obtained by substituting Eq. (3-19) into Eq. (3-17) and setting $x_3 = x_3^k$:

$$^{(k)}G(x_3^k) = {}^{(k)}D(x_3^k)\,{}^{(k)}D^{-1}(x_3^{k-1})\,{}^{(k)}G(x_3^{k-1}) \tag{3-20}$$

where $^{(k)}D(x_3^k)\,{}^{(k)}D^{-1}(x_3^{k-1})$ is the local 2×2 transfer matrix which relates the values of $^{(k)}G$ calculated at the upper and lower surfaces of the layer.

Continuity conditions and global transfer matrix

The continuity conditions at the interface $x_3 = x_3^{k-1}$, between the layer k and $k-1$, Eq. (3-6), are expressed in terms of matrix $^{(k)}G$ as:

$$\begin{aligned} {}^{(k)}G(x_3^{k-1}) &= \left(J^{k-1}\right){}^{(k-1)}G(x_3^{k-1}) \\ J^{k-1} &= \begin{bmatrix} 1 & {}^{(k-1)}K_3 R^{k-1} \\ 0 & {}^{(k-1)}K_3 \,/\, {}^{(k)}K_3 \end{bmatrix} \end{aligned} \tag{3-21}$$

where the 2×2 interfacial transfer matrix J^{k-1} depends on the interfacial thermal resistance and the thermal conductivities of the layers k and $k-1$. Substitution of $^{(k)}G(x_3^{k-1})$ from Eq. (3-21) into Eq. (3-20) gives

a relationship between the matrices G of the layers k and $k-1$. The local transfer matrix of the layer $k-1$ is then used to extend the previous relationship and further relate the matrix ${}^{(k)}G$ calculated at the upper surface of the layer k to that of the layer $k-1$ calculated at its lower surface (Figure 3-2). Repeating this procedure, an explicit relationship between ${}^{(k)}G(x_3^k)$ and ${}^{(1)}G(x_3^0)$ is derived:

$${}^{(k)}G(x_3^k) = \left(J^k\right)^{-1} \prod_{i=k}^{1} \left\{ \left(J^i\right) {}^{(i)}D(x_3^i) \, {}^{(i)}D^{-1}(x_3^{i-1}) \right\} {}^{(1)}G(x_3^0) \tag{3-22}$$

where the symbol $\prod_{i=k}^{1} \{\bullet\}$ defines the product of the terms in brackets. The explicit relationships between ${}^{(k)}c_1$ and ${}^{(k)}c_2$, and the constants of the first layer, are then obtained by substituting ${}^{(k)}G(x_3^k)$ and ${}^{(1)}G(x_3^0)$ in Eq. (3-17) into Eq. (3-22):

$${}^{(k)}\begin{bmatrix} c_1 \\ c_2 \end{bmatrix} = {}^{(k)}D^{-1}(x_3^k)\left(J^k\right)^{-1} \prod_{i=k}^{1} \left\{ \left(J^i\right) {}^{(i)}D(x_3^i) \, {}^{(i)}D^{-1}(x_3^{i-1}) \right\} {}^{(1)}D(x_3^0) \; {}^{(1)}\begin{bmatrix} c_1 \\ c_2 \end{bmatrix} \tag{3-23}$$

with $k = 1, \ldots, n$. The boundary conditions are then applied to define the constants of the first layer. The condition at the bottom surface directly depends on ${}^{(1)}c_1$ and ${}^{(1)}c_2$ while the one at the top is restated in terms of ${}^{(1)}c_1$ and ${}^{(1)}c_2$ using Eq. (3-23) for $k = n$. Explicit expressions have been derived for ${}^{(1)}c_1$ and ${}^{(1)}c_2$, through the procedure presented in the Appendix A:

$$\begin{aligned} {}^{(1)}c_1 &= \frac{T_u - T_l e^{{}^{(1)}sx_3^0} \, {}^{(n)}\left(F_{12} e^{sx_3^n} + F_{22} e^{-sx_3^n} \right)}{{}^{(n)}\left(F_{11} e^{sx_3^n} + F_{21} e^{-sx_3^n} \right) - e^{2\,{}^{(1)}sx_3^0} \, {}^{(n)}\left(F_{12} e^{sx_3^n} + F_{22} e^{-sx_3^n} \right)} \\ {}^{(1)}c_2 &= \frac{T_l - {}^{(1)}c_1 e^{{}^{(1)}sx_3^0}}{e^{-{}^{(1)}sx_3^0}} \end{aligned} \tag{3-24}$$

with ${}^{(n)}F_{ij}$ given in the Appendix A, Eq. (A-2). The constants in the remaining layers are calculated using Eq. (3-23) or its expanded version:

$$\begin{aligned} {}^{(k)}c_1 &= {}^{(k)}F_{11} \, {}^{(1)}c_1 + {}^{(k)}F_{12} \, {}^{(1)}c_2 \\ {}^{(k)}c_2 &= {}^{(k)}F_{21} \, {}^{(1)}c_1 + {}^{(k)}F_{22} \, {}^{(1)}c_2 \end{aligned} . \tag{3-25}$$

The temperature in the layers is then defined by Eqs. (3-14) and (3-15).

3.2.3 Solution of the thermo-elastic problem through the transfer matrix method

The displacement components in the layer k are obtained by summing particular and complementary solutions of the governing equilibrium equations (3-10), for $i = 2, 3$:

$$ {}^{(k)}v_i(x_2,x_3) = {}^{(k)}v_{ip}(x_2,x_3) + {}^{(k)}v_{ic}(x_2,x_3) \tag{3-26} $$

In the absence of thermal loads, the particular solution is ${}^{(k)}v_{ip}(x_2,x_3) = 0$.

Particular solution for layer k

A particular solution of the equilibrium equations (3-10) for the layer *k*, with ${}^{(k)}T = {}^{(k)}T(x_2,x_3)$ prescribed by the previous solution of the heat conduction problem, which satisfies the edge boundary conditions in Eq. (3-12), is [7]:

$$ \begin{aligned} {}^{(k)}v_{2p}(x_2,x_3) &= ({}^{(k)}B_1 e^{{}^{(k)}sx_3} + {}^{(k)}B_2 e^{-{}^{(k)}sx_3})\cos(px_2) \\ {}^{(k)}v_{3p}(x_2,x_3) &= ({}^{(k)}D_1 e^{{}^{(k)}sx_3} + {}^{(k)}D_2 e^{-{}^{(k)}sx_3})\sin(px_2) \end{aligned} \tag{3-27} $$

where ${}^{(k)}B_1$, ${}^{(k)}B_2$, ${}^{(k)}D_1$ and ${}^{(k)}D_2$ are unknown constants and ${}^{(k)}s$ is given in Eq. (3-15). Substituting (3-27) into (3-10), collecting the terms multiplying $e^{{}^{(k)}sx_3}$ and $e^{-{}^{(k)}sx_3}$ and equating them to zero, result in four algebraic equations for the unknown constants, Eq. (B-1) in Appendix B.

Complementary solution for layer k

A solution of the complementary problem, which satisfies the boundary conditions at the plate edges in Eq. (3-12) is obtained using the separation of variables [7]:

$$ \begin{aligned} {}^{(k)}v_{2c}(x_2,x_3) &= {}^{(k)}V(x_3)\cos(px_2) \\ {}^{(k)}v_{3c}(x_2,x_3) &= {}^{(k)}W(x_3)\sin(px_2) \end{aligned} \tag{3-28} $$

with:

$$ \left[{}^{(k)}V(x_3), {}^{(k)}W(x_3) \right] = \left[{}^{(k)}V_0, {}^{(k)}W_0 \right] e^{{}^{(k)}tx_3} \tag{3-29} $$

where ${}^{(k)}V_0$ and ${}^{(k)}W_0$ are unknown constants and ${}^{(k)}t$ is the root of the associated characteristic equation which is defined below. Substituting Eqs. (3-28) and (3-29) in the homogenous part of Eq. (3-10) results in the following system of algebraic equations:

$$ \begin{aligned} {}^{(k)}\left[(C_{22}p^2 - C_{55}t^2)V_0 - (C_{23} + C_{55})ptW_0 \right] &= 0 \\ {}^{(k)}\left[(C_{23} + C_{55})ptV_0 + (C_{55}p^2 - C_{33}t^2)W_0 \right] &= 0 \end{aligned} \tag{3-30} $$

The non-trivial solution of the system is obtained by imposing the determinant of the coefficients to be zero. This yields the characteristic equation for the layer *k*:

$$^{(k)}(A_0\gamma^2 + A_1\gamma + A_2) = 0 \tag{3-31}$$

where:

$$\begin{aligned} ^{(k)}\gamma &= {}^{(k)}t^2 \\ ^{(k)}A_0 &= {}^{(k)}(C_{33}C_{55}) \\ ^{(k)}A_1 &= {}^{(k)}\left[(C_{23}+C_{55})^2 - C_{22}C_{33} - C_{55}^2\right]p^2 \\ ^{(k)}A_2 &= {}^{(k)}(C_{22}C_{55})p^4 \end{aligned} \tag{3-32}$$

The nature of the solution $^{(k)}\gamma = {}^{(k)}t^2 = {}^{(k)}\left(-A_1 \pm \sqrt{\Delta}\right)\Big/ 2\,{}^{(k)}A_0$ is controlled by the discriminant $^{(k)}\Delta = {}^{(k)}(A_1^2 - 4A_0A_2)$. When $^{(k)}\Delta$ is positive, $^{(k)}V(x_3)$ and $^{(k)}W(x_3)$ are:

$$\begin{aligned} ^{(k)}V(x_3) &= \sum_{j=1}^{2} {}^{(k)}V_j(x_3) \\ ^{(k)}W(x_3) &= \sum_{j=1}^{2} {}^{(k)}\beta_j\, {}^{(k)}W_j(x_3) \end{aligned} \tag{3-33}$$

with

$$\begin{aligned} ^{(k)}V_j(x_3) &= {}^{(k)}a_{1j}\, {}^{(k)}X_j(x_3) + {}^{(k)}a_{2j}\, {}^{(k)}Y_j(x_3) \\ ^{(k)}W_j(x_3) &= {}^{(k)}\lambda\, {}^{(k)}a_{2j}\, {}^{(k)}X_j(x_3) + {}^{(k)}a_{1j}\, {}^{(k)}Y_j(x_3) \\ ^{(k)}\beta_j &= {}^{(k)}\left[\frac{(C_{23}+C_{55})pm_j}{C_{33}m_j^2 - \lambda C_{55}p^2}\right] \\ ^{(k)}m_j &= \sqrt{\left|{}^{(k)}\gamma_j\right|} \end{aligned} \tag{3-34}$$

and

$$\begin{cases} ^{(k)}X_j(x_3) = \cosh(^{(k)}m_j x_3) \\ ^{(k)}Y_j(x_3) = \sinh(^{(k)}m_j x_3) \quad \text{if } ^{(k)}\gamma_j > 0 \\ ^{(k)}\lambda = 1 \end{cases}$$

$$\begin{cases} ^{(k)}X_j(x_3) = \cos(^{(k)}m_j x_3) \\ ^{(k)}Y_j(x_3) = \sin(^{(k)}m_j x_3) \quad \text{if } ^{(k)}\gamma_j < 0 \\ ^{(k)}\lambda = -1 \end{cases} \tag{3-35}$$

The displacement components in each layer then depend on four unknown constants, $^{(k)}a_{11}$, $^{(k)}a_{21}$, $^{(k)}a_{12}$ and $^{(k)}a_{22}$, which leads to a total of $4\times n$ unknowns for the plate. Solutions for the cases of negative and zero discriminants are presented in matrix form in Appendix C.

In the classical approach, the unknowns are obtained by imposing continuity and boundary conditions, which lead to a system of 4×*n* coupled algebraic equations. Here the transfer matrix method is applied to first derive explicit relations between the unknowns of the generic layer and those of the first layer; the four unknown constants ${}^{(1)}a_{11}$, ${}^{(1)}a_{21}$, ${}^{(1)}a_{12}$ and ${}^{(1)}a_{22}$ are then defined through the application of the boundary conditions.

From Eqs. (3-27), (3-33) and (3-34), the displacements of the layer *k*, are:

$$\begin{aligned}
{}^{(k)}v_2(x_2,x_3) &= \Big[{}^{(k)}B_1 e^{{}^{(k)}sx_3} + {}^{(k)}B_2 e^{-{}^{(k)}sx_3} + \\
&+ {}^{(k)}V(x_3, {}^{(k)}a_{11}, {}^{(k)}a_{12}, {}^{(k)}a_{21}, {}^{(k)}a_{11}) \Big] \cos(px_2) \\
{}^{(k)}v_3(x_2,x_3) &= \Big[{}^{(k)}D_1 e^{{}^{(k)}sx_3} + {}^{(k)}D_2 e^{-{}^{(k)}sx_3} + \\
&+ {}^{(k)}W(x_3, {}^{(k)}a_{11}, {}^{(k)}a_{12}, {}^{(k)}a_{21}, {}^{(k)}a_{11}) \Big] \sin(px_2)
\end{aligned} \tag{3-36}$$

where the constants ${}^{(k)}B_1$, ${}^{(k)}B_2$, ${}^{(k)}D_1$ and ${}^{(k)}D_2$ are defined in Appendix B. Normal and transverse shear stress components are derived from the equation above using constitutive and compatibility equations (3-1) and (3-9). Displacements and transverse stresses are then collected in the following matrix form:

$${}^{(k)}\begin{bmatrix} v_2(x_2,x_3) \\ v_3(x_2,x_3) \\ \sigma_{33}(x_2,x_3) \\ \sigma_{23}(x_2,x_3) \end{bmatrix} = C(x_2)\,{}^{(k)}M(x_3) \tag{3-37}$$

where $C(x_2)$ and ${}^{(k)}M(x_3)$ are 4×4 and 4×1 matrices defined as follows:

$$C(x_2) = \begin{bmatrix} \cos(px_2) & 0 & 0 & 0 \\ 0 & \sin(px_2) & 0 & 0 \\ 0 & 0 & \sin(px_2) & 0 \\ 0 & 0 & 0 & \cos(px_2) \end{bmatrix} \tag{3-38}$$

$${}^{(k)}M(x_3) = {}^{(k)}Q(x_3) + {}^{(k)}E(x_3)\,{}^{(k)}\left[a_{11}, a_{21}, a_{12}, a_{22}\right]^T \tag{3-39}$$

The 4×1 matrix ${}^{(k)}Q(x_3)$ is independent of the unknowns with elements:

$$
\begin{aligned}
{}^{(k)}Q_1(x_3) &= {}^{(k)}\left(B_1 e^{sx_3} + B_2 e^{-sx_3}\right) \\
{}^{(k)}Q_2(x_3) &= {}^{(k)}\left(D_1 e^{sx_3} + D_2 e^{-sx_3}\right) \\
{}^{(k)}Q_3(x_3) &= {}^{(k)}\left\{-C_{23}p\left(B_1 e^{sx_3} + B_2 e^{-sx_3}\right) + C_{33}s\left(D_1 e^{sx_3} - D_2 e^{-sx_3}\right) - \right. \\
&\left. -\left(c_1 e^{sx_3} + c_2 e^{-sx_3}\right)\left(C_{23}\alpha_2 + C_{13}\alpha_1 + C_{33}\alpha_3\right)\right\} \\
{}^{(k)}Q_4(x_3) &= {}^{(k)}C_{55}\,{}^{(k)}\left[s\left(B_1 e^{sx_3} - B_2 e^{-sx_3}\right) + p\left(D_1 e^{sx_3} + D_2 e^{-sx_3}\right)\right]
\end{aligned}
\tag{3-40}
$$

The 4×4 matrix ${}^{(k)}E(x_3)$ is related to the complementary solution and depends on the sign of the discriminant. Expressions for ${}^{(k)}E(x_3)$ in the different cases are given in Appendix C.

Local transfer matrix of a generic layer

The local transfer matrix, which provides a relationship between the values of the matrix ${}^{(k)}M$ at the top and bottom surfaces of the layer is derived following what done for the heat condition problem

$$
{}^{(k)}M(x_3^k) = {}^{(k)}E(x_3^k)\,{}^{(k)}E^{-1}(x_3^{k-1})\left[{}^{(k)}M(x_3^{k-1}) - {}^{(k)}Q(x_3^{k-1})\right] + {}^{(k)}Q(x_3^k) \tag{3-41}
$$

Continuity conditions and global transfer matrix

The continuity conditions between the layer k and $k-1$, Eq. (3-11), are written in matrix form:

$$
{}^{(k)}M(x_3^{k-1}) = \left(B^{k-1}\right)\,{}^{(k-1)}M(x_3^{k-1}) \tag{3-42}
$$

with the interfacial transfer matrix:

$$
B^{k-1} = \begin{bmatrix} 1 & 0 & 0 & 1/K_S^{k-1} \\ 0 & 1 & 1/K_N^{k-1} & 0 \\ 0 & 0 & 1 & 0 \\ 0 & 0 & 0 & 1 \end{bmatrix} \tag{3-43}
$$

For perfect bonding of the layers $1/K_S^{k-1} = 1/K_N^{k-1} = 0$ and B is the identity matrix. The procedure used for the solution of the heat conduction problem (Figure 3-2), is used to derive a relationship between ${}^{(k)}M\,(x_3 = x_3^k)$ and ${}^{(1)}M\,(x_3 = x_3^0)$:

$$
\begin{aligned}
&{}^{(k)}M(x_3^k) = \left(B^k\right)^{-1}\left\{\prod_{i=k}^{1}\left\{\left(B^i\right){}^{(i)}E(x_3^i){}^{(i)}E^{-1}(x_3^{i-1})\right\}\right\}\left\{{}^{(1)}M(x_3^0) - {}^{(1)}Q(x_3^0)\right\} \\
&+\sum_{i=2}^{k}\left(\prod_{j=k}^{i}\left\{\left(B^j\right){}^{(j)}E(x_3^j){}^{(j)}E^{-1}(x_3^{j-1})\right\}\left\{\left(B^{i-1}\right){}^{(i-1)}Q(x_3^{i-1}) - {}^{(i)}Q(x_3^{i-1})\right\}\right)\Bigg\} \\
&+\ {}^{(k)}Q(x_3^k)
\end{aligned}
\tag{3-44}
$$

The explicit expressions relating the four unknown constants, ${}^{(k)}a_{11}$, ${}^{(k)}a_{21}$, ${}^{(k)}a_{12}$ and ${}^{(k)}a_{22}$ in Eq. (3-33), to those of the first layer are then derived substituting ${}^{(k)}M(x_3^k)$ and ${}^{(1)}M(x_3^0)$ defined by Eq. (3-41), into Eq. (3-44):

$$
\begin{aligned}
&{}^{(k)}\begin{bmatrix} a_{11} \\ a_{21} \\ a_{12} \\ a_{22} \end{bmatrix} = {}^{(k)}E^{-1}(x_3^k)\left(B^k\right)^{-1}\left\{\prod_{i=k}^{1}\left\{\left(B^i\right){}^{(i)}E(x_3^i){}^{(i)}E^{-1}(x_3^{i-1})\right\}\right\}{}^{(1)}E(x_3^0)\ {}^{(1)}\begin{bmatrix} a_{11} \\ a_{21} \\ a_{12} \\ a_{22} \end{bmatrix} \\
&+\sum_{i=2}^{k}\left(\prod_{j=k}^{i}\left\{\left(B^j\right){}^{(j)}E(x_3^j){}^{(j)}E^{-1}(x_3^{j-1})\right\}\left\{\left(B^{i-1}\right){}^{(i-1)}Q(x_3^{i-1}) - {}^{(i)}Q(x_3^{i-1})\right\}\right)
\end{aligned}
\tag{3-45}
$$

for $k = 2, \ldots, n$. For fully bonded layers, the matrix $B = I$ in Eq. (3-45) can be omitted. The constants of the first layer may then be defined using the four boundary conditions (3-12) at the top and bottom surfaces of the laminate and Eq. (3-45) for $k = n$, which lead to an algebraic system of four equations. A different approach is presented in Appendix D, which avoids the derivation of the constants and provides explicit expressions of displacements and stresses directly:

$$
\begin{aligned}
&{}^{(k)}v_2(x_2,x_3) = \\
&\left\{{}^{(k)}Q_1(x_3) + \sum_{l=1}^{4}\left[\sum_{r=1}^{4}{}^{(k)}P_{1r}(x_3){}^{(k)}\Omega_{rl}\right]\left({}^{(1)}M_l(x_3^0) - {}^{(1)}Q_l(x_3^0)\right) + \sum_{t=1}^{4}{}^{(k)}P_{1t}(x_3){}^{(k)}S_t\right\}\cos(px_2) \\
&{}^{(k)}v_3(x_2,x_3) = \\
&\left\{{}^{(k)}Q_2(x_3) + \sum_{l=1}^{4}\left[\sum_{r=1}^{4}{}^{(k)}P_{2r}(x_3){}^{(k)}\Omega_{rl}\right]\left({}^{(1)}M_l(x_3^0) - {}^{(1)}Q_l(x_3^0)\right) + \sum_{t=1}^{4}{}^{(k)}P_{2t}(x_3){}^{(k)}S_t\right\}\sin(px_2) \\
&{}^{(k)}\sigma_{33}(x_2,x_3) = \\
&\left\{{}^{(k)}Q_3(x_3) + \sum_{l=1}^{4}\left[\sum_{r=1}^{4}{}^{(k)}P_{3r}(x_3){}^{(k)}\Omega_{rl}\right]\left({}^{(1)}M_l(x_3^0) - {}^{(1)}Q_l(x_3^0)\right) + \sum_{t=1}^{4}{}^{(k)}P_{3t}(x_3){}^{(k)}S_t\right\}\sin(px_2) \\
&{}^{(k)}\sigma_{23}(x_2,x_3) = \\
&\left\{{}^{(k)}Q_4(x_3) + \sum_{l=1}^{4}\left[\sum_{r=1}^{4}{}^{(k)}P_{4r}(x_3){}^{(k)}\Omega_{rl}\right]\left({}^{(1)}M_l(x_3^0) - {}^{(1)}Q_l(x_3^0)\right) + \sum_{t=1}^{4}{}^{(k)}P_{4t}(x_3){}^{(k)}S_t\right\}\cos(px_2)
\end{aligned}
\tag{3-46}
$$

$$
\begin{aligned}
&{}^{(k)}\sigma_{22}(x_2,x_3) = \\
&\left\{-p\,{}^{(k)}C_{22}\left[{}^{(k)}Q_1(x_3)+\sum_{l=1}^{4}\left[\sum_{r=1}^{4}{}^{(k)}P_{1r}(x_3)\,{}^{(k)}\Omega_{rl}\right]\left({}^{(1)}M_l(x_3^0)-{}^{(1)}Q_l(x_3^0)\right)+\sum_{t=1}^{4}{}^{(k)}P_{1t}(x_3)\,{}^{(k)}S_t\right]\right. \\
&\left.+{}^{(k)}C_{23}\left[{}^{(k)}Q_2(x_3),_3+\sum_{l=1}^{4}\left[\sum_{r=1}^{4}{}^{(k)}P_{2r}(x_3),_3\,{}^{(k)}\Omega_{rl}\right]\left({}^{(1)}M_l(x_3^0)-{}^{(1)}Q_l(x_3^0)\right)+\sum_{t=1}^{4}{}^{(k)}P_{2t}(x_3),_3\,{}^{(k)}S_t\right]\right\} \\
&\times\sin(px_2)-{}^{(k)}\left(C_{12}\alpha_1+C_{22}\alpha_2+C_{23}\alpha_3\right){}^{(k)}T(x_2,x_3)
\end{aligned}
$$

with

$$
{}^{(k)}P_{ir}(x_3)=\sum_{d=1}^{4}\left[\sum_{j=1}^{4}{}^{(k)}E_{ij}(x_3)\,{}^{(k)}E^{-1}{}_{jd}(x_3^k)\right]\left(B^k\right)^{-1}{}_{dr} \tag{3-47}
$$

The constants ${}^{(1)}M_l(x_3^0)$, ${}^{(k)}\Omega_{rl}$ and ${}^{(k)}S_t$ are given in Eqs. (D-3) and (D-5) in the Appendix D; ${}^{(k)}Q_l(x_3)$ and B^k in Eqs. (3-40) and (3-43); ${}^{(k)}E_{ij}(x_3)$ in Appendix C; ${}^{(k)}T(x_2,x_3)$ is defined in (3-14), (3-15), (3-24) and (3-25).

For fully bonded layers, Eq. (3-47) modifies as:

$$
{}^{(k)}P_{ir}(x_3)=\sum_{j=1}^{4}{}^{(k)}E_{ij}(x_3)\,{}^{(k)}E^{-1}{}_{jr}(x_3^k) \tag{3-48}
$$

3.2.4 Application to simply supported plates and sandwiches subjected to mechanical loading

The explicit expressions derived above are easily applied to solve special problems. For purely mechanical loading, $T_l = T_u = 0$, and for purely thermal loading, $f_l = f_u = 0$. If the equations are used as dimensionless equations, using the notation in Table 3-1, parametric analyses can be performed and the results collected in tables and diagram to describe the response of a class of materials and interfacial imperfections. In this section, exact solutions for two simply supported cross-ply laminates and one sandwich plate under plane-strain conditions and subjected to sinusoidal transverse loading are presented. The results are given in tables using at least four digits in order to generate benchmark solutions with enough precision for verification of approximate structural theories. The dimensionless quantities are easily related to the dimensionless groups used in the derivation, e.g. $v_2E_T/hf_u = \left(v_2/h\right)\left({}^{(1)}C_{22}/f_u\right)\left(E_T/{}^{(1)}C_{22}\right)$. The results are also presented in graph form, to highlight the important influence of the interfacial imperfections on stress and displacement fields. Dimensionless stresses and displacements are given for different length-to-thickness ratios and interfacial stiffnesses. In the examples, the interfaces have the same interfacial stiffnesses and three cases of perfect bonding, sliding interfaces in constrained contact and partial bonding are examined.

In order to avoid interpenetration between the layers, the results presented for the cases with $1/K_N \neq 0$, are valid only for positive applied surface tractions. The model presented in the previous section and the

results are valid under the assumption of infinitesimal strains and displacements, which must be verified in each layer. The validity of this assumption and the range of values of the applied load for which the solutions in the tables are correct can be verified by using the maximum dimensionless transverse displacements and stresses given in the tables.

Plate with 3-layers and a symmetric layup

The first example is a simply supported anisotropic plate with three layers of equal thickness, symmetrically stacked and joined by two interfaces. The length and thickness of the plate are *L* and *h*, respectively, and the origin of the coordinate system is placed at mid-thickness of the left edge of the plate. The elastic constants of the layers are $E_L/E_T = 17$, $G_{LT}/E_T = 0.7$, $G_{TT}/E_T = 0.6$, $\nu_{LT} = 0.28$ and $\nu_{TT} = 0.4$ (subscripts *L* and *T* indicate in-plane principal material directions), and the stacking sequence of $(0,90,0)$. The assumed ratios between the elastic constants of the layers could represent a graphite-epoxy laminate. The plate is subjected to normally applied tractions $f_3 = f_u \sin(\pi x_2/L)$ acting on the upper surface . Results are presented in Table 3-2 for three length-to-thickness ratios equal to 4, 10, 20. The results are tabulated for perfectly bonded interfaces, $1/K_S = 1/K_N = 0$, sliding interfaces in constrained contact, $1/K_N = 0$ and $K_S = 0$, and partial bonding with dimensionless interfacial stiffnesses $K_S h/E_T = 0.2$ and $K_N h/E_T = 0.5$ (see Eq. (3-2) for the interfacial traction laws used in the model). The ratio between the interfacial normal and tangential stiffnesses for this latter case is 2.5 and could represent layers joined by thin elastic and isotropic adhesive interlayers.

Table 3-2: Simply supported three-layer plate $(0,90,0)$ under plane-strain conditions: normal surface tractions $f_3 = f_u \sin(\pi x_2/L)$ acting on upper surface. Elastic constants: $E_L/E_T = 17$, $G_{LT}/E_T = 0.7$, $G_{TT}/E_T = 0.6$, $\nu_{LT} = 0.28$ and $\nu_{TT} = 0.4$. Subscripts *l* and *u* correspond to values below and above the interface.

T3-2-1: Perfect bonding: $1/K_S = 0$ **and** $1/K_N = 0$

$\frac{L}{h}$	x_3/h							
	-1/2	-1/3	-1/6$_l$	-1/6$_u$	1/6$_l$	1/6$_u$	1/3	1/2
	Dimensionless longitudinal displacements: $v_2 E_T/(f_u h)$ *at* $x_2 = 0$							
4	0.915	0.458	0.194	0.194	-0.118	-0.118	-0.414	-0.914
10	12.21	7.710	3.718	3.718	-3.595	-3.595	-7.602	-12.12
20	94.88	62.38	30.90	30.90	-30.67	-30.67	-62.16	-94.68
	Dimensionless transverse displacements: $v_3 E_T/(f_u h)$ *at* $x_2 = L/2$							
4	4.648	4.686	4.727	4.727	4.870	4.870	4.971	5.072
10	92.67	92.88	93.02	93.02	93.16	93.16	93.16	93.09
20	1268	1269	1269	1269	1269	1269	1269	1268
	Dimensionless bending stresses: σ_{22}/f_u *at* $x_2 = L/2$							
4	-12.27	-6.111	-2.487	-0.040	0.387	1.872	5.913	12.66
10	-65.52	-41.34	-19.84	-1.063	1.431	19.58	41.15	65.44
20	-254.5	-167.3	-82.78	-4.766	5.138	82.58	167.1	254.4

$\frac{L}{h}$	x_3/h									
	-5/12	-1/3	-1/4	-1/6	-1/12	1/12	1/6	1/4	1/3	5/12
	Dimensionless transverse shear stresses [a]*:* σ_{23}/f_u *at* $x_2 = 0$									
4	0.682	1.164	1.495	1.709	1.708	1.686	1.665	1.485	1.174	0.696
10	1.549	2.783	3.720	4.376	4.395	4.386	4.356	3.707	2.775	1.546
20	3.043	5.515	7.426	8.784	8.830	8.825	8.774	7.419	5.510	3.040

$\frac{L}{h}$	x_3/h									
	-1/2	-7/18	-5/18	-1/6	-1/18	1/18	1/6	5/18	7/18	1/2
	Dimensionless transverse normal stresses: σ_{33}/f_u *at* $x_2 = L/2$									
4	0.000	0.040	0.141	0.278	0.427	0.576	0.722	0.857	0.959	1.000
10	0.000	0.036	0.133	0.271	0.424	0.577	0.730	0.867	0.964	1.000
20	0.000	0.036	0.131	0.269	0.423	0.577	0.731	0.869	0.964	1.000

T3-2-2: Partial bonding: $K_S h/E_T = 0.2$ **and** $K_N h/E_T = 0.5$ **(** $f_u > 0$ **)**

$\frac{L}{h}$	x_3/h								
	-1/2	-1/3	$-1/6_l$	$-1/6_u$	$1/6_l$	$1/6_u$	1/3	1/2	
	Dimensionless longitudinal displacements: $v_2 E_T/(f_u h)$ *at* $x_2 = 0$								
4	2.079	0.208	-1.579	2.229	-1.875	1.864	-0.173	-2.308	
10	18.86	6.336	-5.772	12.20	-11.90	5.991	-6.233	-18.88	
20	110.6	59.11	8.559	50.18	-49.86	-8.286	-58.90	-110.5	
	Dimensionless transverse displacements: $v_3 E_T/(f_u h)$ *at* $x_2 = L/2$								
4	16.51	16.57	16.58	17.33	17.48	18.66	18.80	18.86	
10	248.4	248.7	248.7	249.3	249.5	250.8	251.0	250.8	
20	1998	1998	1999	1999	2000	2001	2001	2000	
	Dimensionless bending stresses: σ_{22}/f_u *at* $x_2 = L/2$								
4	-27.88	-2.728	21.32	-1.607	1.719	-24.76	2.640	31.36	
10	-101.2	-33.95	31.09	-3.724	4.036	-31.87	33.79	101.7	
20	-296.8	-158.6	-22.85	-7.805	8.161	22.51	158.4	296.8	

$\frac{L}{h}$	x_3/h									
	-5/12	-1/3	-1/4	-1/6	-1/12	1/12	1/6	1/4	1/3	5/12
	Dimensionless transverse shear stresses [b]*:* σ_{23}/f_u *at* $x_2 = 0$									
4	1.377	1.939	1.740	0.762	0.840	0.833	0.748	1.894	2.151	1.541
10	2.199	3.519	3.982	3.594	3.666	3.658	3.578	3.982	3.528	2.208
20	3.429	5.953	7.583	8.324	8.400	8.396	8.315	7.577	5.950	3.428

$\frac{L}{h}$	x_3/h									
	-1/2	-7/18	-5/18	-1/6	-1/18	1/18	1/6	5/18	7/18	1/2
	Dimensionless transverse normal stresses: σ_{33}/f_u *at* $x_2 = L/2$									
4	0.000	0.083	0.247	0.373	0.445	0.520	0.590	0.725	0.907	1.000
10	0.000	0.052	0.173	0.309	0.436	0.564	0.691	0.827	0.947	1.000
20	0.000	0.040	0.143	0.280	0.427	0.574	0.720	0.857	0.960	1.000

T3-2-3: Sliding interfaces in constrained contact : $K_S = 0$ **and** $1/K_N = 0$

$\frac{L}{h}$	x_3/h							
	-1/2	-1/3	$-1/6_l$	$-1/6_u$	$1/6_l$	$1/6_u$	1/3	1/2
	Dimensionless longitudinal displacements: $v_2 E_T/(f_u h)$ *at* $x_2 = 0$							
4	3.222	0.008	-3.210	3.889	-3.384	3.269	0.024	-3.233
10	49.70	0.018	-49.67	51.36	-50.07	49.75	0.057	-49.64
20	396.6	0.036	-396.5	399.9	-397.3	396.7	0.112	-396.5
	Dimensionless transverse displacements: $v_3 E_T/(f_u h)$ *at* $x_2 = L/2$							
4	27.84	27.93	27.90	27.90	28.07	28.07	28.23	28.28
10	969.6	970.1	969.6	969.6	969.8	969.8	970.4	970.0
20	15230	15232	15230	15230	15231	15231	15233	15231
	Dimensionless bending stresses: σ_{22}/f_u *at* $x_2 = L/2$							
4	-43.21	-0.009	43.25	-2.873	2.879	-43.64	-0.030	43.76
10	-266.7	-0.002	266.7	-16.01	16.01	-266.7	-0.005	266.8
20	-1064	0.000	1064	-62.91	62.91	-1064	-0.001	1064

$\frac{L}{h}$	x_3/h									
	-5/12	-1/3	-1/4	-1/6	-1/12	1/12	1/6	1/4	1/3	5/12
	Dimensionless transverse shear stresses [c]*:* σ_{23}/f_u *at* $x_2 = 0$									
4	2.070	2.737	2.071	0.000	0.141	0.141	0.000	2.091	2.767	2.094
10	5.215	6.944	5.215	0.000	0.314	0.314	0.000	5.216	6.946	5.217
20	10.43	13.91	10.43	0.000	0.618	0.618	0.000	10.43	13.91	10.43

$\frac{L}{h}$	x_3/h									
	-1/2	-7/18	-5/18	-1/6	-1/18	1/18	1/6	5/18	7/18	1/2
	Dimensionless transverse normal stresses: σ_{33}/f_u *at* $x_2 = L/2$									
4	0.000	0.125	0.356	0.481	0.489	0.505	0.514	0.640	0.873	1.000
10	0.000	0.126	0.359	0.485	0.493	0.507	0.515	0.641	0.874	1.000
20	0.000	0.126	0.360	0.486	0.493	0.507	0.514	0.640	0.874	1.000

[a] Maxima $(x_3/h, \sigma_{23\max}/f_u)$: (-0.134, 1.710) for $L/h = 4$, (-0.024, 4.399) for $L/h = 10$ and (-0.006, 8.844) for $L/h = 20$.

[b] Maxima $(x_3/h, \sigma_{23\max}/f_u)$: (0.317, 2.168) for $L/h = 4$, (-0.246, 3.983) for $L/h = 10$ and (-0.004, 8.424) for $L/h = 20$.

[c] Maxima $(x_3/h, \sigma_{23\max}/f_u)$: (0.333, 2.767) for $L/h = 4$, (0.333, 6.946) for $L/h = 10$ and (0.333, 13.91) for $L/h = 20$.

Figure 3-3 and Figure 3-4 highlight the influence of the interfacial imperfections on the field variables: both longitudinal and transverse displacements may become discontinuous at the interfaces and the stress distributions are substantially modified with changes in position and value of the maxima.

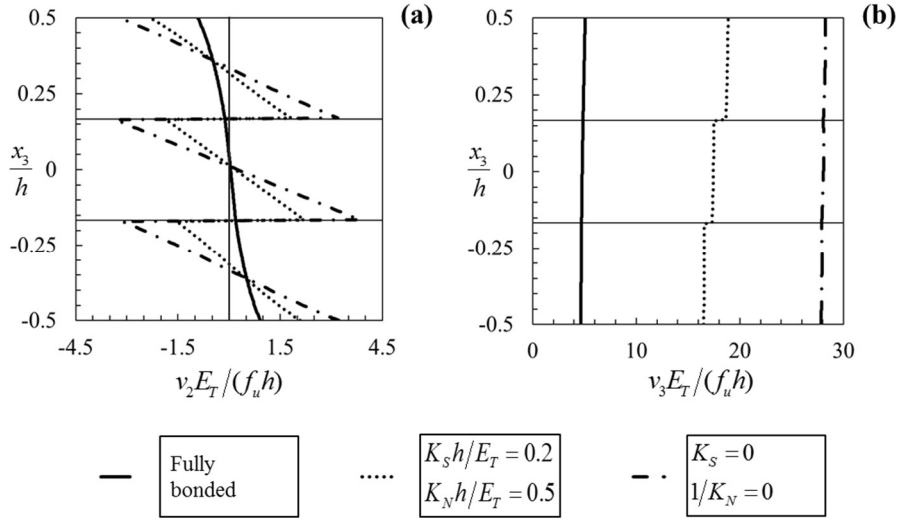

Figure 3-3: (a) Longitudinal at $x_2 = 0$ and (b) transverse at $x_2 = L/2$ displacements through thickness in a simply supported three-layer plate $(0,90,0)$ under plane-strain conditions, $L/h = 4$, normal surface tractions $f_3 = f_u \sin(\pi x_2/L)$ acting on upper surface. Elastic constants: $E_L/E_T = 17$, $G_{LT}/E_T = 0.7$, $G_{TT}/E_T = 0.6$, $\nu_{LT} = 0.28$ and $\nu_{TT} = 0.4$.

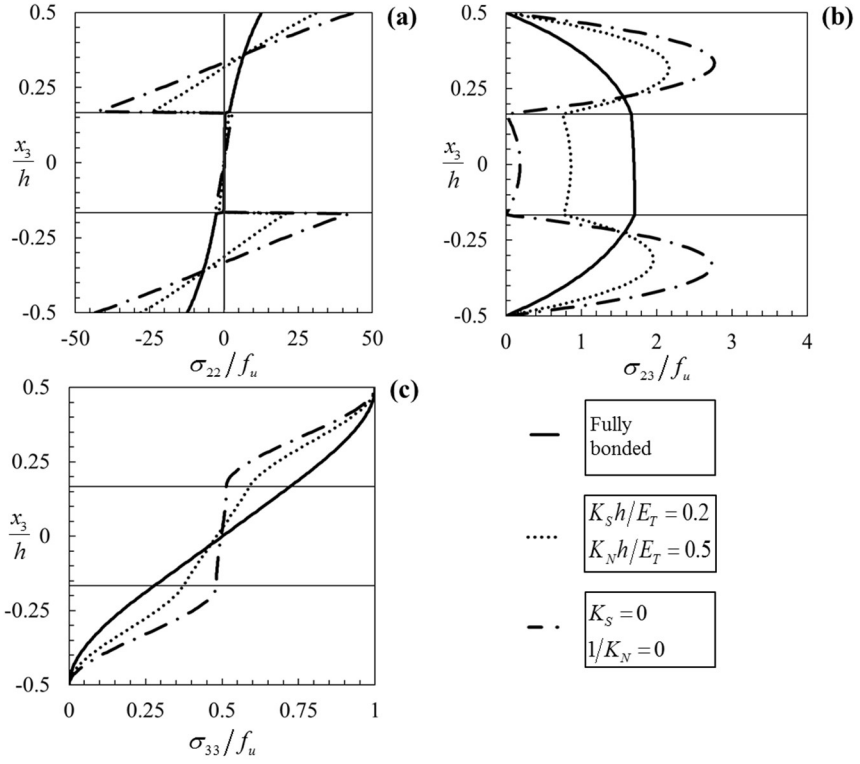

Figure 3-4: (a) Bending at $x_2 = L/2$, (b) transverse shear at $x_2 = 0$ and (c) transverse normal at $x_2 = L/2$ stresses through thickness in a simply supported three-layer plate $(0,90,0)$ under plane-strain conditions, $L/h = 4$, normal

surface tractions $f_3 = f_u \sin(\pi x_2/L)$ acting on upper surface. Elastic constants: $E_L/E_T = 17$, $G_{LT}/E_T = 0.7$, $G_{TT}/E_T = 0.6$, $\nu_{LT} = 0.28$ and $\nu_{TT} = 0.4$.

Plate with 5-layers and a symmetric layup

The second example is a simply supported symmetrically laminated plate with length *L* and thickness *h*. The layup consists of five layers of equal thickness and joined by four identical interfaces; the stacking sequence is $(0,90,0,90,0)$. The origin of the coordinate system is assumed to be at mid-thickness of the left edge and the elastic constants of the layers are $E_L/E_T = 17$, $G_{LT}/E_T = 0.7$, $G_{TT}/E_T = 0.6$, $\nu_{LT} = 0.28$ and $\nu_{TT} = 0.4$. The plate is subjected to normal surface tractions $f_3 = f_u \sin(\pi x_2/L)$ on the upper surface. Results in the tables are given for three length-to-thickness ratios of 4, 10, 20 and for laminates with perfect interfaces, imperfect interfaces with $K_S h/E_T = 0.1$ and $K_N h/E_T = 0.25$, and sliding interfaces in constrained contact with $1/K_N = 0$ and $K_S = 0$.

Table 3-3: Simply supported five-layer plate $(0,90,0,90,0)$ under plane-strain conditions: normal surface tractions $f_3 = f_u \sin(\pi x_2/L)$ acting on upper surface. Elastic constants: $E_L/E_T = 17$, $G_{LT}/E_T = 0.7$, $G_{TT}/E_T = 0.6$, $\nu_{LT} = 0.28$ and $\nu_{TT} = 0.4$. Subscripts *l* and *u* correspond to values below and above the interface.

T3-3-1: Perfect bonding: $1/K_S = 0$ **and** $1/K_N = 0$

$\frac{L}{h}$	x_3/h							
	-1/2	-3/10$_l$	-3/10$_u$	-1/10$_u$	1/10$_u$	3/10$_l$	3/10$_u$	1/2
	Dimensionless longitudinal displacements: $v_2 E_T/(f_u h)$ *at* $x_2 = 0$							
4	1.016	0.482	0.482	0.205	-0.129	-0.426	-0.426	-1.011
10	14.42	8.295	8.295	2.854	-2.721	-8.173	-8.173	-14.32
20	113.4	67.31	67.31	22.60	-22.36	-67.07	-67.07	-113.2
	Dimensionless transverse displacements: $v_3 E_T/(f_u h)$ *at* $x_2 = L/2$							
4	4.905	4.957	4.957	5.021	5.106	5.212	5.212	5.329
10	106.7	107.0	107.0	107.2	107.2	107.2	107.2	107.1
20	1503	1505	1505	1505	1505	1505	1505	1504
	Dimensionless bending stresses: σ_{22}/f_u *at* $x_2 = L/2$							
4	-13.62	-6.414	-0.326	-2.604	0.356	0.688	6.055	13.96
10	-77.35	-44.46	-2.565	-15.17	1.114	2.933	44.20	77.21
20	-304.2	-180.5	-10.57	-60.50	3.784	10.94	180.3	303.9

$\frac{L}{h}$	x_3/h									
	-13/30	-11/30	-3/10	-1/10	-1/30	1/30	1/10	3/10	11/30	13/30
	Dimensionless transverse shear stresses [a]*:* σ_{23}/f_u *at* $x_2 = 0$									
4	0.630	1.120	1.502	1.528	1.624	1.640	1.577	1.495	1.128	0.641
10	1.497	2.759	3.797	3.901	4.114	4.117	3.912	3.785	2.751	1.494
20	2.965	5.496	7.599	7.818	8.241	8.242	7.822	7.591	5.491	2.963

$\frac{L}{h}$	x_3/h									
	-13/30	-11/30	-3/10	-1/10	-1/30	1/30	1/10	3/10	11/30	13/30
	Dimensionless transverse normal stresses: σ_{33}/f_u *at* $x_2 = L/2$									
4	0.017	0.064	0.133	0.371	0.454	0.540	0.624	0.866	0.936	0.982
10	0.016	0.061	0.130	0.373	0.457	0.543	0.628	0.870	0.939	0.984
20	0.016	0.061	0.130	0.372	0.457	0.543	0.628	0.871	0.939	0.984

T3-3-2: Partial bonding: $K_S h/E_T = 0.1$ **and** $K_N h/E_T = 0.25$ **(**$f_u > 0$**)**

$\frac{L}{h}$	x_3/h								
	-1/2	$-3/10_l$	$-3/10_u$	$-1/10_u$	$1/10_u$	$3/10_l$	$3/10_u$	1/2	
	Dimensionless longitudinal displacements: $v_2 E_T/(f_u h)$ *at* $x_2 = 0$								
4	3.477	-2.838	3.522	3.328	3.813	-3.425	3.437	-4.072	
10	27.64	-8.907	22.40	18.23	14.35	-22.17	9.216	-27.85	
20	144.2	27.39	99.56	58.09	16.56	-99.24	-27.09	-144.2	
	Dimensionless transverse displacements: $v_3 E_T/(f_u h)$ *at* $x_2 = L/2$								
4	42.74	42.77	43.66	45.06	47.62	47.74	50.71	50.83	
10	593.2	593.4	594.1	595.7	598.3	598.3	601.7	601.6	
20	3758	3759	3759	3761	3764	3764	3767	3766	
	Dimensionless bending stresses: σ_{22}/f_u *at* $x_2 = L/2$								
4	-46.64	38.16	-2.688	-44.51	-2.757	3.004	-45.81	55.02	
10	-148.3	47.85	-7.004	-97.65	-4.271	7.336	-49.12	149.8	
20	-386.9	-73.43	-15.65	-155.7	-2.357	16.01	73.02	387.1	

$\frac{L}{h}$	x_3/h									
	-13/30	-11/30	-3/10	-1/10	-1/30	1/30	1/10	3/10	11/30	13/30
	Dimensionless transverse shear stresses [b]*:* σ_{23}/f_u *at* $x_2 = 0$									
4	1.678	1.886	0.636	0.644	2.188	2.208	0.705	0.686	2.196	1.972
10	2.412	3.452	3.131	3.209	4.573	4.581	3.235	3.138	3.477	2.434
20	3.500	5.903	7.216	7.420	8.507	8.510	7.429	7.214	5.905	3.502

$\frac{L}{h}$	x_3/h									
	-13/30	-11/30	-3/10	-1/10	-1/30	1/30	1/10	3/10	11/30	13/30
	Dimensionless transverse normal stresses: σ_{33}/f_u *at* $x_2 = L/2$									
4	0.051	0.150	0.223	0.334	0.415	0.537	0.620	0.741	0.824	0.941
10	0.028	0.091	0.163	0.366	0.450	0.548	0.632	0.836	0.908	0.972
20	0.019	0.069	0.139	0.371	0.455	0.545	0.629	0.861	0.930	0.981

T3-3-3: Sliding interfaces in constrained contact : $K_S = 0$ **and** $1/K_N = 0$

$\frac{L}{h}$	x_3/h							
	-1/2	$-3/10_l$	$-3/10_u$	$-1/10_u$	$1/10_u$	$3/10_l$	$3/10_u$	1/2
	Dimensionless longitudinal displacements: $v_2 E_T/(f_u h)$ *at* $x_2 = 0$							
4	5.846	-5.838	6.285	5.865	6.473	-5.787	5.892	-5.847
10	90.96	-90.94	92.06	90.99	92.50	-90.77	91.02	-90.90
20	727.1	-727.0	729.3	727.1	730.1	-726.7	727.2	-726.9
	Dimensionless transverse displacements: $v_3 E_T/(f_u h)$ *at* $x_2 = L/2$							
4	78.01	78.04	78.04	78.11	78.19	78.32	78.32	78.46
10	2918	2918	2918	2918	2918	2918	2918	2918
20	46377	46377	46377	46377	46377	46377	46377	46377
	Dimensionless bending stresses: σ_{22}/f_u *at* $x_2 = L/2$							
4	-78.42	78.43	-4.829	-78.53	-4.840	4.842	-78.77	78.82
10	-488.1	488.1	-28.92	-488.1	-28.93	28.93	-488.1	488.1
20	-1951	1951	-115.0	-1951	-115.0	115.0	-1951	1951

$\frac{L}{h}$	x_3/h									
	-13/30	-11/30	-3/10	-1/10	-1/30	1/30	1/10	3/10	11/30	13/30
	Dimensionless transverse shear stresses [c]: σ_{23}/f_u *at* $x_2 = 0$									
4	2.708	2.708	0.000	0.000	2.712	2.713	0.000	0.000	2.721	2.721
10	6.803	6.803	0.000	0.000	6.803	6.803	0.000	0.000	6.804	6.804
20	13.61	13.61	0.000	0.000	13.61	13.61	0.000	0.000	13.61	13.61

$\frac{L}{h}$	x_3/h									
	-13/30	-11/30	-3/10	-1/10	-1/30	1/30	1/10	3/10	11/30	13/30
	Dimensionless transverse normal stresses: σ_{33}/f_u *at* $x_2 = L/2$									
4	0.083	0.236	0.319	0.339	0.422	0.576	0.659	0.679	0.762	0.917
10	0.083	0.237	0.321	0.340	0.423	0.577	0.660	0.679	0.762	0.917
20	0.083	0.238	0.321	0.340	0.423	0.577	0.660	0.679	0.762	0.917

[a] Maxima $(x_3/h, \sigma_{23\max}/f_u)$: (0.014, 1.643) for $L/h = 4$, (0.001, 4.142) for $L/h = 10$ and (0.000, 8.294) for $L/h = 20$.

[b] Maxima $(x_3/h, \sigma_{23\max}/f_u)$: (0.001, 2.386) for $L/h = 4$, (0.000, 4.746) for $L/h = 10$ and (0.000, 8.644) for $L/h = 20$.

[c] Maxima $(x_3/h, \sigma_{23\max}/f_u)$: (0.400, 3.057) for $L/h = 4$, (0.400, 7.652) for $L/h = 10$ and (0.400, 15.31) for $L/h = 20$.

Figure 3-5 and Figure 3-6 highlight the influence of the interfacial imperfections on the field variables: both longitudinal and transverse displacements may become discontinuous at the interfaces and the stress distributions are substantially modified with changes in position and value of the maxima.

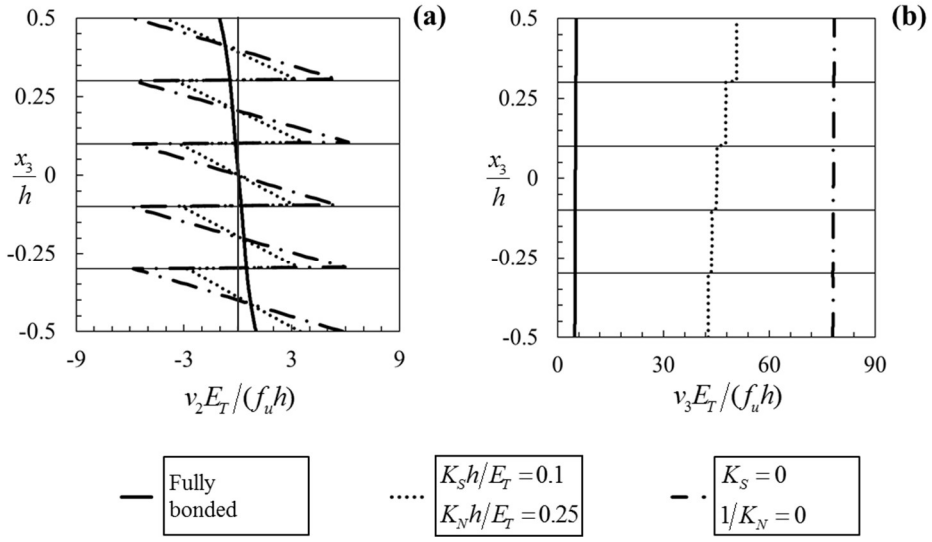

Figure 3-5: (a) Longitudinal at $x_2 = 0$ and (b) transverse at $x_2 = L/2$ displacements through thickness in a simply supported five-layer plate $(0,90,0,90,0)$ under plane-strain conditions, $L/h = 4$, normal surface tractions $f_3 = f_u \sin(\pi x_2/L)$ acting on upper surface. Elastic constants: $E_L/E_T = 17$, $G_{LT}/E_T = 0.7$, $G_{TT}/E_T = 0.6$, $\nu_{LT} = 0.28$ and $\nu_{TT} = 0.4$.

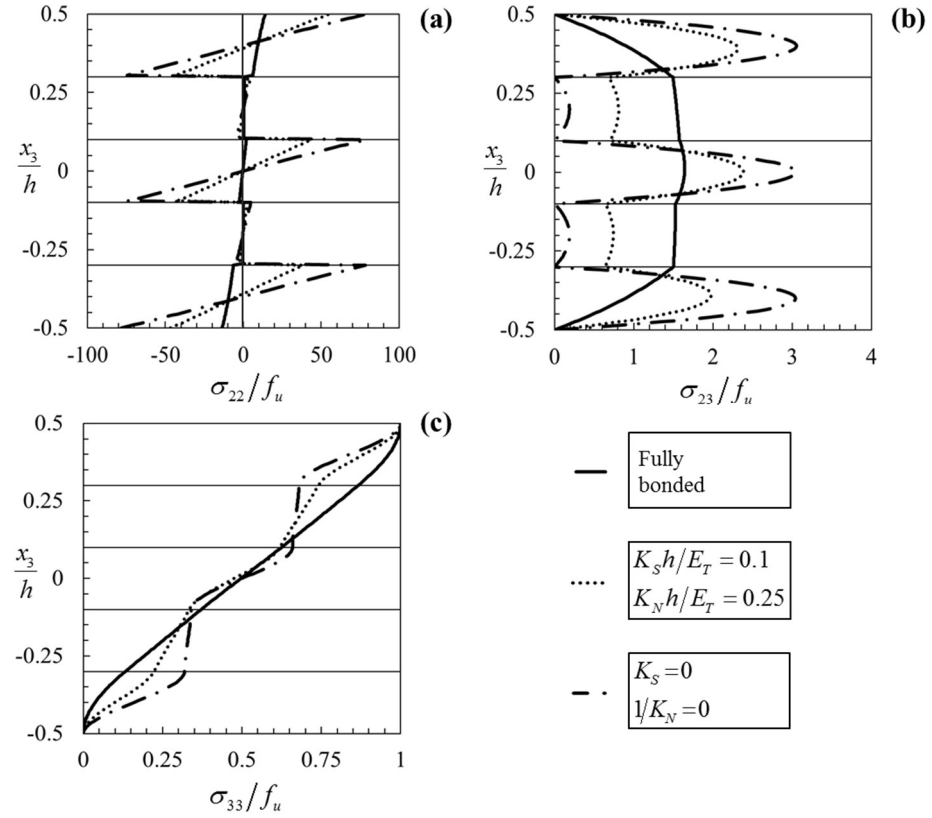

Figure 3-6: (a) Bending at $x_2 = L/2$, (b) transverse shear at $x_2 = 0$ and (c) transverse normal at $x_2 = L/2$ stresses through thickness in a simply supported five-layer plate $(0,90,0,90,0)$ under plane-strain conditions, $L/h = 4$,

normal surface tractions $f_3 = f_u \sin(\pi x_2/L)$ acting on upper surface. Elastic constants: $E_L/E_T = 17$, $G_{LT}/E_T = 0.7$, $G_{TT}/E_T = 0.6$, $\nu_{LT} = 0.28$ and $\nu_{TT} = 0.4$.

Sandwich plate with imperfect bonding at the core-face sheets interfaces

The third example is a symmetric sandwich plate with thickness of face sheets and core $0.1h$ and $0.8h$, respectively, and subjected to normal tractions $f_3 = f_u \sin(\pi x_2/L)$ acting on the upper surface on varying the interfacial conditions. Faces and core are assumed to be transversally isotropic in the planes $x_1 - x_3$ and $x_1 - x_2$ respectively. The origin of the coordinate system is assumed to be at mid-thickness of the left edge and the elastic constants of faces and core are $E_2^f/E_3^f = 17$, $G_{23}^f/E_3^f = 0.7$, $\nu_{23}^f = \nu_{21}^f = 0.28$, and $\nu_{31}^f = 0.4$; $E_2^c/E_3^f = 0.016$, $E_3^c/E_3^f = 0.026$, $G_{23}^c/E_3^f = 0.006$ and $\nu_{23}^c = \nu_{21}^c = \nu_{31}^c = 0.32$ which could represent unidirectionally reinforced graphite-epoxy face sheets with fibers aligned along the x_2 axis and a foam core. Results are presented for $L/h = 4$, 6 and 8, and for perfectly bonded layers, partially bonded layers with $K_S h/E_3^f = 0.005$ and $K_N h/E_3^f = 0.0125$, and layers free to slide in constrained contact.

Table 3-4: Simply supported symmetric sandwich plate under plane-strain conditions with thickness of face sheets and core $0.1h$ and $0.8h$: normal surface tractions $f_3 = f_u \sin(\pi x_2/L)$ acting on upper surface. Elastic constants $E_2^f/E_3^f = 17$, $G_{23}^f/E_3^f = 0.7$, $\nu_{23}^f = \nu_{21}^f = 0.28$, and $\nu_{31}^f = 0.4$, $E_2^c/E_3^f = 0.016$, $E_3^c/E_3^f = 0.026$, $G_{23}^c/E_3^f = 0.006$ and $\nu_{23}^c = \nu_{21}^c = \nu_{31}^c = 0.32$. Subscripts *l* and *u* correspond to values below and above the interface.

T3-4-1: Perfect bonding: $1/K_S = 0$ **and** $1/K_N = 0$

$\frac{L}{h}$	x_3/h									
	-1/2	-9/20	-2/5$_l$	-2/5$_u$	-4/15	4/15	2/5$_l$	2/5$_u$	9/20	1/2
	Dimensionless longitudinal displacements: $v_2 E_3^f/(f_u h)$ *at* $x_2 = 0$									
4	9.062	1.088	-6.847	-6.847	-3.068	6.734	7.420	7.420	-0.948	-9.354
6	18.22	4.076	-9.997	-9.997	-5.623	8.295	10.50	10.50	-3.853	-18.27
8	30.50	10.08	-10.25	-10.25	-6.038	8.203	10.77	10.77	-9.772	-30.40
	Dimensionless transverse displacements: $v_3 E_3^f/(f_u h)$ *at* $x_2 = L/2$									
4	206.1	206.2	206.1	206.1	206.6	214.1	217.1	217.1	217.2	217.2
6	544.4	544.5	544.5	544.5	544.8	552.0	555.1	555.1	555.2	555.1
8	1046	1046	1046	1046	1046	1053	1056	1056	1056	1056
$\frac{L}{h}$	x_3/h									
	-1/2	-19/40	-17/40	-2/5$_l$	-2/5$_u$	2/5$_l$	2/5$_u$	17/40	19/40	1/2
	Dimensionless bending stresses: σ_{22}/f_u *at* $x_2 = L/2$									
4	-121.6	-67.75	38.49	91.90	0.162	0.256	-99.20	-42.87	69.16	125.9
6	-162.9	-99.47	26.45	89.44	0.139	0.283	-93.57	-29.31	99.12	163.8
8	-204.5	-135.9	0.617	68.80	0.109	0.314	-71.85	-2.962	135.0	204.3
$\frac{L}{h}$	x_3/h									
	-19/40	-9/20	-17/40	-2/5	-1/5	1/5	2/5	17/40	9/20	19/40
	Dimensionless transverse shear stress [a]*:* σ_{23}/f_u *at* $x_2 = 0$									
4	1.857	2.665	2.430	1.151	1.126	1.070	1.034	2.428	2.720	1.913
6	1.717	2.606	2.671	1.913	1.897	1.856	1.829	2.633	2.597	1.720
8	1.671	2.669	2.998	2.657	2.647	2.615	2.593	2.960	2.651	1.665
$\frac{L}{h}$	x_3/h									
	-9/20	-2/5	-3/10	-1/5	-1/10	1/10	1/5	3/10	2/5	9/20
	Dimensionless transverse normal stresses: σ_{33}/f_u *at* $x_2 = L/2$									
4	0.066	0.155	0.245	0.333	0.421	0.594	0.679	0.762	0.844	0.932
6	0.041	0.108	0.208	0.307	0.406	0.603	0.700	0.797	0.893	0.959
8	0.031	0.087	0.192	0.296	0.399	0.606	0.709	0.812	0.914	0.970

T3-4-2: Partial bonding: $K_S h/E_3^f = 0.005$ **and** $K_N h/E_3^f = 0.0125$ **(** $f_u > 0$ **)**

$\frac{L}{h}$	x_3/h									
	-1/2	-9/20	$-2/5_l$	$-2/5_u$	-4/15	4/15	$2/5_l$	$2/5_u$	9/20	1/2
	Dimensionless longitudinal displacements: $v_2 E_3^f/(f_u h)$ *at* $x_2 = 0$									
4	17.18	0.566	-16.02	103.3	70.65	-54.17	-88.85	19.54	-0.486	-20.54
6	41.63	2.821	-35.94	228.6	153.9	-138.2	-214.6	38.49	-2.655	-43.84
8	70.92	8.001	-54.85	367.0	245.9	-232.1	-354.7	56.89	-7.746	-72.45
	Dimensionless transverse displacements: $v_3 E_3^f/(f_u h)$ *at* $x_2 = L/2$									
4	428.5	428.6	428.5	448.6	453.5	461.7	460.8	517.1	517.2	517.1
6	1492	1492	1492	1507	1514	1521	1519	1583	1583	1583
8	3216	3217	3216	3228	3236	3243	3240	3307	3308	3307
$\frac{L}{h}$	x_3/h									
	-1/2	-19/40	-17/40	$-2/5_l$	$-2/5_u$	$2/5_l$	$2/5_u$	17/40	19/40	1/2
	Dimensionless bending stresses: σ_{22}/f_u *at* $x_2 = L/2$									
4	-230.4	-118.4	103.3	215.0	-1.338	1.544	-261.9	-126.9	140.7	275.9
6	-372.3	-198.3	147.9	321.5	-2.051	2.343	-343.8	-159.6	207.8	392.4
8	-475.6	-264.3	157.0	367.9	-2.505	2.845	-381.2	-164.3	269.0	486.3
$\frac{L}{h}$	x_3/h									
	-19/40	-9/20	-17/40	-2/5	-1/5	1/5	2/5	17/40	9/20	19/40
	Dimensionless transverse shear stress [b]*:* σ_{23}/f_u *at* $x_2 = 0$									
4	3.422	4.658	3.719	0.596	0.749	0.724	0.542	4.356	5.534	4.087
6	3.734	5.196	4.394	1.323	1.480	1.452	1.265	4.559	5.445	3.928
8	3.632	5.192	4.685	2.109	2.253	2.228	2.058	4.735	5.284	3.707
$\frac{L}{h}$	x_3/h									
	-9/20	-2/5	-3/10	-1/5	-1/10	1/10	1/5	3/10	2/5	9/20
	Dimensionless transverse normal stresses: σ_{33}/f_u *at* $x_2 = L/2$									
4	0.120	0.252	0.302	0.359	0.419	0.543	0.602	0.656	0.703	0.857
6	0.088	0.193	0.265	0.341	0.419	0.578	0.656	0.730	0.799	0.908
8	0.065	0.150	0.234	0.322	0.411	0.591	0.679	0.765	0.848	0.934

T3-4-3: Sliding interfaces in constrained contact : $K_S = 0$ and $1/K_N = 0$

$\frac{L}{h}$	x_3/h									
	-1/2	-9/20	-2/5$_l$	-2/5$_u$	-4/15	4/15	2/5$_l$	2/5$_u$	9/20	1/2
	Dimensionless longitudinal displacements: $v_2 E_3^f / (f_u h)$ *at* $x_2 = 0$									
4	28.80	0.006	-28.79	231.5	156.3	-126.3	-202.7	29.37	0.024	-29.33
6	97.09	0.009	-97.08	776.6	520.4	-474.9	-731.9	97.50	0.035	-97.43
8	229.7	0.012	-229.7	1837	1228	-1167	-1776	230.0	0.047	-230.0
	Dimensionless transverse displacements: $v_3 E_3^f / (f_u h)$ *at* $x_2 = L/2$									
4	742.2	742.5	742.3	742.3	752.3	761.9	756.6	756.6	756.8	756.6
6	3729	3729	3729	3729	3749	3759	3743	3743	3744	3743
8	11735	11736	11735	11735	11771	11780	11749	11749	11750	11749
$\frac{L}{h}$	x_3/h									
	-1/2	-19/40	-17/40	-2/5$_l$	-2/5$_u$	2/5$_l$	2/5$_u$	17/40	19/40	1/2
	Dimensionless bending stresses: σ_{22} / f_u *at* $x_2 = L/2$									
4	-386.3	-192.3	192.3	386.3	-3.072	3.092	-393.8	-196.0	196.0	393.7
6	-868.2	-433.2	433.2	868.2	-7.079	7.088	-871.6	-434.9	434.9	871.6
8	-1541	-769.5	769.5	1541	-12.69	12.69	-1543	-770.4	770.4	1543
$\frac{L}{h}$	x_3/h									
	-19/40	-9/20	-17/40	-2/5	-1/5	1/5	2/5	17/40	9/20	19/40
	Dimensionless transverse shear stress [c]*:* σ_{23} / f_u *at* $x_2 = 0$									
4	5.676	7.562	5.676	0.000	0.358	0.359	0.000	5.785	7.708	5.786
6	8.515	11.35	8.515	0.000	0.553	0.553	0.000	8.548	11.39	8.548
8	11.34	15.11	11.34	0.000	0.745	0.745	0.000	11.35	15.13	11.35
$\frac{L}{h}$	x_3/h									
	-9/20	-2/5	-3/10	-1/5	-1/10	1/10	1/5	3/10	2/5	9/20
	Dimensionless transverse normal stresses: σ_{33} / f_u *at* $x_2 = L/2$									
4	0.198	0.396	0.405	0.428	0.459	0.533	0.565	0.587	0.596	0.798
6	0.198	0.396	0.405	0.429	0.461	0.537	0.570	0.593	0.602	0.801
8	0.198	0.396	0.405	0.428	0.462	0.538	0.571	0.595	0.604	0.802

[a] Maxima $(x_3 / h, \sigma_{23\max} / f_u)$: (0.444, 2.750) for $L/h = 4$, (-0.436, 2.744) for $L/h = 6$ and (-0.425, 2.998) for $L/h = 8$.

[b] Maxima $(x_3 / h, \sigma_{23\max} / f_u)$: (0.449, 5.538) for $L/h = 4$, (0.447, 5.466) for $L/h = 6$ and (0.444, 5.346) for $L/h = 8$.

[c] Maxima $(x_3 / h, \sigma_{23\max} / f_u)$: (0.450, 7.708) for $L/h = 4$, (0.450, 11.394) for $L/h = 6$ and (0.450, 15.133) for $L/h = 8$.

The diagrams in Figure 3-7 show results for $L/h = 4$. In the presence of interfacial imperfections, longitudinal and transverse displacements are discontinuous at the interfaces and the stress distributions are modified with changes in location and value of the maxima with respect to the fully bonded case. The presence of interfacial imperfections reduces the transverse shear stresses at the both interfaces at the expenses of an increase in the transverse shear stresses of the face sheets. The transverse normal stress at the lower interface of the sandwich plate increases in the presence of interfacial imperfections.

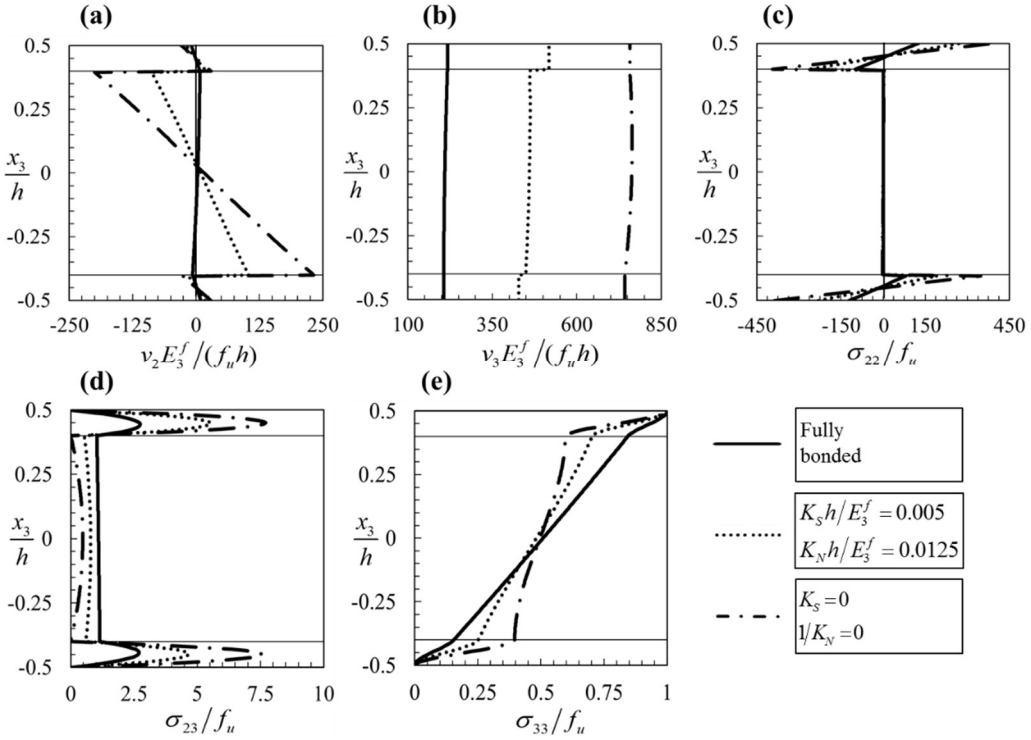

Figure 3-7: (a) longitudinal at $x_2 = 0$, (b) transverse at $x_2 = L/2$ displacements, (c) bending at $x_2 = L/2$, (d) transverse shear at $x_2 = 0$ and (e) transverse normal at $x_2 = L/2$ stresses through thickness in a simply supported symmetric sandwich plate under plane-strain conditions, $L/h = 4$, normal surface tractions $f_3 = f_u \sin(\pi x_2/L)$ acting on upper surface. Thickness of face sheets and core $0.1h$ and $0.8h$. Elastic constants: $E_2^f/E_3^f = 17$, $G_{23}^f/E_3^f = 0.7$, $\nu_{23}^f = \nu_{21}^f = 0.28$, and $\nu_{31}^f = 0.4$, $E_2^c/E_3^f = 0.016$, $E_3^c/E_3^f = 0.026$, $G_{23}^c/E_3^f = 0.006$ and $\nu_{23}^c = \nu_{21}^c = \nu_{31}^c = 0.32$.

3.2.5 Application to simply supported plates subjected to thermal loading

This section presents exact solutions of temperature, displacements and stresses in a simply supported symmetrically laminated plate under plane-strain conditions subjected to sinusoidal thermal loading. The plate has thickness *h* and length *L* and is composed of three layers of equal thickness, joined by two identical interfaces. The origin of the coordinate system is at the mid-thickness. The stacking sequence of the plate is $(0,90,0)$ and the thermo-elastic constants of the layers are $E_L/E_T = 17$, $G_{LT}/E_T = 0.7$, $G_{TT}/E_T = 0.6$, $\nu_{LT} = 0.28$, $\nu_{TT} = 0.4$, $\alpha_T/\alpha_L = 1125$ and $K_T/K_L = 0.16$ (subscripts L and T indicate in-plane principal material directions). The assumed thermo-elastic constants could represent a graphite-epoxy laminate with a large ratio between the coefficients of thermal expansion in the principal material directions. This example provides a severe test for the approximate structural theories. Results are presented in tables and figures for a plate subjected to thermal loading $T = -T_0 \sin(\pi x_2/L)$ on the upper surface, with T_0 a positive constant; the temperature increment at the lower surface of the plate is assumed to be zero. Results in Table 3-5 correspond to layers in perfect thermal contact, $R = 0$, and those in Table 3-6 to layers with interfacial thermal resistance, $RK_L/h = 10$. Dimensionless stresses and displacements are presented for three length-to-thickness ratios equal to 4, 10, 20 and for three cases of perfect bonding, $1/K_S = 1/K_N = 0$, partial bonding

with dimensionless interfacial stiffnesses equal to $K_S h/E_T = 0.1$ and $K_N h/E_T = 0.25$, and sliding interfaces in constrained contact, $K_S = 0$ and $1/K_N = 0$. The assumed applied temperature implies no interpenetration of the layers at the interfaces for all interfacial stiffnesses, including the case $1/K_N \neq 0$; for constrained contact the results apply also to $T_0 < 0$.

Table 3-5: Simply supported three-layer plate $(0,90,0)$ under plane-strain conditions: applied temperature $T = -T_0 \sin(\pi x_2/L)$ on upper surface . Thermo-elastic constants: $E_L/E_T = 17$, $G_{LT}/E_T = 0.7$, $G_{TT}/E_T = 0.6$, $\nu_{LT} = 0.28$, $\nu_{TT} = 0.4$, $\alpha_T/\alpha_L = 1125$ and $K_T/K_L = 0.16$. Perfect thermal contact, $R = 0$. Subscripts *l* and *u* correspond to values below and above the interface.

T3-5-1: Perfect mechanical bonding: $1/K_S = 1/K_N = 0$; **Perfect thermal contact:** $R = 0$

$\frac{L}{h}$	x_3/h									
	-1/2	-7/18	-5/18	$-1/6_l$	$-1/6_u$	$1/6_l$	$1/6_u$	5/18	7/18	1/2
	Dimensionless longitudinal displacements: $v_2/(\alpha_L T_0 h)$ *at* $x_2 = 0$									
4	31.27	20.90	15.24	14.10	14.10	17.74	17.74	23.29	40.32	73.69
10	53.52	54.20	56.91	62.20	62.20	82.75	82.75	92.29	107.8	130.2
20	96.41	108.3	121.2	135.4	135.4	180.7	180.7	197.2	216.9	240.0
	Dimensionless transverse displacements: $v_3/(\alpha_L T_0 h)$ *at* $x_2 = L/2$									
4	149.0	143.1	123.2	88.45	88.45	-114.7	-114.7	-219.0	-346.8	-503.5
10	5.185	-3.273	-30.15	-75.60	-75.60	-325.3	-325.3	-447.1	-589.1	-752.3
20	-656.9	-665.8	-693.9	-741.2	-741.2	-998.8	-998.8	-1123	-1268	-1432
	Dimensionless bending stresses: $\sigma_{22}/(\alpha_L T_0 E_T)$ *at* $x_2 = L/2$									
4	-419.4	-253.7	-149.3	-102.3	274.5	606.8	-51.82	-88.97	-269.3	-654.9
10	-287.1	-255.8	-235.0	-227.3	339.7	702.8	-228.5	-242.5	-286.4	-365.0
20	-258.7	-254.0	-251.9	-253.4	351.0	718.8	-264.2	-271.5	-286.5	-310.3
$\frac{L}{h}$	x_3/h									
	-5/12	-1/3	-1/4	-1/6	-1/12	1/12	1/6	1/4	1/3	5/12
	Dimensionless transverse shear stress [a]: $\sigma_{23}/(\alpha_L T_0 E_T)$ *at* $x_2 = 0$									
4	22.97	38.61	49.12	56.60	36.00	-21.28	-58.18	-54.63	-47.68	-31.86
10	7.187	13.81	20.02	26.01	15.93	-11.33	-28.53	-22.48	-16.02	-8.692
20	3.360	6.680	9.980	13.29	8.090	-5.909	-14.72	-11.23	-7.656	-3.933
	Dimensionless transverse normal stresses: $\sigma_{33}/(\alpha_L T_0 E_T)$ *at* $x_2 = L/2$									
4	0.798	2.847	5.740	9.211	12.27	13.47	10.90	7.203	3.822	1.154
10	0.095	0.371	0.815	1.417	1.972	2.133	1.617	0.949	0.443	0.117
20	0.022	0.088	0.197	0.349	0.490	0.529	0.396	0.226	0.102	0.026

T3-5-2: Partial mechanical bonding: $K_S h/E_T = 0.1$ **and** $K_N h/E_T = 0.25$; **Perfect thermal contact:** $R = 0$ ($T_0 > 0$)

$\frac{L}{h}$	x_3/h									
	-1/2	-7/18	-5/18	$-1/6_l$	$-1/6_u$	$1/6_l$	$1/6_u$	5/18	7/18	1/2
	Dimensionless longitudinal displacements: $v_2/(\alpha_L T_0 h)$ *at* $x_2 = 0$									
4	19.92	12.48	8.193	7.138	290.6	297.3	8.676	15.40	32.17	63.77
10	43.30	46.86	52.25	60.07	286.2	315.1	71.28	83.65	101.7	126.5
20	90.10	104.0	118.8	135.0	263.2	314.4	173.4	191.9	213.5	238.6
	Dimensionless transverse displacements: $v_3/(\alpha_L T_0 h)$ *at* $x_2 = L/2$									
4	104.8	98.56	78.22	43.00	63.70	-111.5	-83.56	-188.4	-316.6	-473.6
10	-81.39	-89.97	-116.9	-162.4	-157.6	-397.8	-392.0	-514.0	-656.0	-819.2
20	-772.7	-781.6	-809.7	-857.0	-855.7	-1111	-1109	-1234	-1378	-1542
	Dimensionless bending stresses: $\sigma_{22}/(\alpha_L T_0 E_T)$ *at* $x_2 = L/2$									
4	-267.2	-141.0	-55.46	-10.54	54.72	384.6	68.24	16.16	-160.1	-521.8
10	-232.3	-216.5	-210.0	-216.0	268.9	629.4	-167.0	-196.2	-253.9	-345.5
20	-241.7	-242.4	-245.6	-252.3	330.8	697.7	-244.6	-257.2	-277.5	-306.4
$\frac{L}{h}$	x_3/h									
	-5/12	-1/3	-1/4	-1/6	-1/12	1/12	1/6	1/4	1/3	5/12
	Dimensionless transverse shear stress [b]*:* $\sigma_{23}/(\alpha_L T_0 E_T)$ *at* $x_2 = 0$									
4	14.12	22.57	26.82	28.35	22.10	-6.447	-28.87	-32.69	-32.61	-23.87
10	5.907	11.54	17.05	22.62	14.40	-9.089	-24.38	-19.79	-14.49	-8.054
20	3.165	6.342	9.551	12.82	7.886	-5.573	-14.10	-10.85	-7.453	-3.858
	Dimensionless transverse normal stresses: $\sigma_{33}/(\alpha_L T_0 E_T)$ *at* $x_2 = L/2$									
4	0.497	1.725	3.360	5.176	6.856	8.116	6.990	4.966	2.796	0.885
10	0.078	0.307	0.681	1.200	1.690	1.870	1.437	0.858	0.408	0.110
20	0.021	0.083	0.187	0.333	0.470	0.510	0.383	0.220	0.100	0.026

T3-5-3: Sliding interfaces in constrained contact: $K_S = 0$ **and** $1/K_N = 0$; **Perfect thermal contact:** $R = 0$

$\frac{L}{h}$	x_3/h									
	-1/2	-7/18	-5/18	$-1/6_l$	$-1/6_u$	$1/6_l$	$1/6_u$	5/18	7/18	1/2
	Dimensionless longitudinal displacements: $v_2/(\alpha_L T_0 h)$ *at* $x_2 = 0$									
4	14.56	5.931	-0.756	-5.855	567.3	574.2	-5.392	6.027	25.77	59.16
10	-5.520	4.345	14.79	26.57	1698	1746	16.22	37.02	62.16	92.88
20	-27.66	4.232	36.39	69.28	3494	3599	44.92	82.54	122.4	165.1
	Dimensionless transverse displacements: $v_3/(\alpha_L T_0 h)$ *at* $x_2 = L/2$									
4	112.6	106.1	85.41	49.62	49.62	-97.57	-97.57	-203.0	-331.5	-488.7
10	-281.4	-290.6	-318.1	-364.2	-364.2	-544.4	-544.4	-667.1	-809.8	-973.5
20	-1828	-1838	-1867	-1915	-1915	-2100	-2100	-2226	-2371	-2536
	Dimensionless bending stresses: $\sigma_{22}/(\alpha_L T_0 E_T)$ *at* $x_2 = L/2$									
4	-195.4	-53.29	64.07	162.5	-164.9	164.9	255.7	141.4	-74.36	-460.0
10	29.62	11.61	-9.241	-36.73	-177.3	177.3	127.9	53.86	-41.60	-164.8
20	74.19	25.15	-24.53	-76.05	-179.2	179.2	99.95	36.22	-33.09	-109.3
$\frac{L}{h}$	x_3/h									
	-5/12	-1/3	-1/4	-1/6	-1/12	1/12	1/6	1/4	1/3	5/12
	Dimensionless transverse shear stress [c]: $\sigma_{23}/(\alpha_L T_0 E_T)$ *at* $x_2 = 0$									
4	9.119	11.60	8.328	0.000	8.086	8.087	0.000	-14.39	-22.16	-19.31
10	-0.601	-0.840	-0.670	0.000	3.481	3.481	0.000	-2.667	-3.785	-3.028
20	-0.730	-0.979	-0.740	0.000	1.759	1.759	0.000	-1.002	-1.365	-1.048
	Dimensionless transverse normal stresses: $\sigma_{33}/(\alpha_L T_0 E_T)$ *at* $x_2 = L/2$									
4	0.337	1.049	1.731	2.029	2.323	3.617	3.911	3.412	2.170	0.742
10	-0.009	-0.028	-0.049	-0.059	-0.008	0.214	0.265	0.227	0.139	0.045
20	-0.005	-0.017	-0.029	-0.034	-0.021	0.035	0.048	0.040	0.024	0.008

[a]Maxima $[x_3/h, \sigma_{23\max}/(\alpha_L T_0 E_T)]$: [0.167, -58.18] for $L/h = 4$, [0.167, -28.53] for $L/h = 10$ and [0.167, -14.72] for $L/h = 20$.

[b]Maxima $[x_3/h, \sigma_{23\max}/(\alpha_L T_0 E_T)]$: [0.293, -33.40] for $L/h = 4$, [0.167, -24.38] for $L/h = 10$ and [0.167, -14.10] for $L/h = 20$.

[c]Maxima $[x_3/h, \sigma_{23\max}/(\alpha_L T_0 E_T)]$: [0.358, -22.64] for $L/h = 4$, [0.000, 4.640] for $L/h = 10$ and [0.000, 2.346] for $L/h = 20$.

Table 3-6: Simply supported three-layer plate $(0,90,0)$ under plane-strain conditions: applied temperature $T = -T_0 \sin(\pi x_2/L)$ on upper surface . Thermo-elastic constants: $E_L/E_T = 17$, $G_{LT}/E_T = 0.7$, $G_{TT}/E_T = 0.6$, $\nu_{LT} = 0.28$, $\nu_{TT} = 0.4$, $\alpha_T/\alpha_L = 1125$ and $K_T/K_L = 0.16$. Imperfect thermal contact, $RK_L/h = 10$. Subscripts *l* and *u* correspond to values below and above the interface.

T3-6-1: Perfect mechanical bonding: $1/K_S = 1/K_N = 0$; **Imperfect thermal contact:** $RK_L/h = 10$

$\frac{L}{h}$	x_3/h									
	-1/2	-7/18	-5/18	-1/6$_l$	-1/6$_u$	1/6$_l$	1/6$_u$	5/18	7/18	1/2
	Dimensionless longitudinal displacements: $v_2/(\alpha_L T_0 h)$ *at* $x_2 = 0$									
4	23.91	17.13	13.68	13.05	13.05	15.19	15.19	21.02	39.34	74.53
10	45.18	48.46	53.27	59.84	59.84	82.70	82.70	93.49	111.0	135.8
20	83.21	98.38	114.3	131.2	131.2	183.6	183.6	202.8	225.4	251.8
	Dimensionless transverse displacements: $v_3/(\alpha_L T_0 h)$ *at* $x_2 = L/2$									
4	100.3	99.72	96.46	90.56	90.56	-84.64	-84.64	-218.6	-363.5	-525.8
10	-74.27	-75.74	-81.35	-91.12	-91.12	-334.5	-334.5	-492.0	-655.3	-825.5
20	-850.3	-851.9	-858.0	-868.5	-868.5	-1124	-1124	-1286	-1452	-1624
	Dimensionless bending stresses: $\sigma_{22}/(\alpha_L T_0 E_T)$ *at* $x_2 = L/2$									
4	-320.8	-224.4	-171.8	-156.0	343.3	416.8	50.24	-14.79	-234.8	-666.1
10	-242.4	-251.9	-269.5	-296.3	467.8	547.7	-146.6	-194.9	-276.5	-395.2
20	-223.2	-255.3	-289.4	-326.0	490.9	571.7	-188.1	-230.5	-281.6	-342.1
$\frac{L}{h}$	x_3/h									
	-5/12	-1/3	-1/4	-1/6	-1/12	1/12	1/6	1/4	1/3	5/12
	Dimensionless transverse shear stress [a]: $\sigma_{23}/(\alpha_L T_0 E_T)$ *at* $x_2 = 0$									
4	18.32	32.50	44.09	54.47	31.48	-17.93	-44.53	-47.07	-44.66	-31.44
10	6.421	13.07	20.06	27.53	15.02	-11.53	-25.60	-21.37	-16.03	-9.085
20	3.077	6.474	10.21	14.29	7.733	-6.174	-13.52	-10.86	-7.768	-4.169
	Dimensionless transverse normal stresses: $\sigma_{33}/(\alpha_L T_0 E_T)$ *at* $x_2 = L/2$									
4	0.627	2.308	4.825	8.054	10.87	11.81	9.774	6.764	3.721	1.153
10	0.084	0.338	0.771	1.393	1.951	2.051	1.566	0.950	0.457	0.124
20	0.020	0.082	0.191	0.351	0.495	0.518	0.389	0.229	0.107	0.028

T3-6-2: Partial mechanical bonding: $K_S h/E_T = 0.1$ **and** $K_N h/E_T = 0.25$; **Imperfect thermal contact:** $RK_L/h = 10$ $(T_0 > 0)$

$\frac{L}{h}$	x_3/h									
	-1/2	-7/18	-5/18	$-1/6_l$	$-1/6_u$	$1/6_l$	$1/6_u$	5/18	7/18	1/2
Dimensionless longitudinal displacements: $v_2/(\alpha_L T_0 h)$ *at* $x_2 = 0$										
4	19.50	10.88	4.430	-0.901	260.0	248.0	15.52	17.44	31.23	60.38
10	40.93	42.43	45.28	49.65	285.3	301.9	79.65	88.54	104.0	126.6
20	80.67	94.82	109.7	125.5	262.7	311.9	181.6	199.8	221.4	246.7
Dimensionless transverse displacements: $v_3/(\alpha_L T_0 h)$ *at* $x_2 = L/2$										
4	116.3	115.5	111.9	105.4	125.6	-25.50	-1.901	-136.1	-281.4	-444.1
10	-25.17	-26.71	-32.43	-42.33	-37.47	-271.5	-266.0	-423.6	-587.0	-757.3
20	-792.4	-794.1	-800.2	-810.7	-809.4	-1063	-1061	-1223	-1389	-1560
Dimensionless bending stresses: $\sigma_{22}/(\alpha_L T_0 E_T)$ *at* $x_2 = L/2$										
4	-261.6	-140.6	-48.09	30.06	147.2	231.6	44.21	32.29	-126.2	-476.4
10	-219.6	-219.6	-226.6	-241.7	396.6	478.4	-130.4	-168.3	-239.0	-345.5
20	-216.4	-245.8	-277.1	-310.8	470.2	551.5	-182.8	-222.4	-270.7	-328.2
$\frac{L}{h}$	x_3/h									
	-5/12	-1/3	-1/4	-1/6	-1/12	1/12	1/6	1/4	1/3	5/12
Dimensionless transverse shear stress [b]: $\sigma_{23}/(\alpha_L T_0 E_T)$ *at* $x_2 = 0$										
4	13.92	22.33	26.19	26.09	15.80	-8.817	-23.24	-26.67	-27.83	-21.18
10	5.733	11.50	17.40	23.56	12.91	-9.969	-22.22	-18.51	-13.90	-7.906
20	2.975	6.242	9.817	13.72	7.429	-5.941	-13.03	-10.45	-7.463	-4.002
Dimensionless transverse normal stresses: $\sigma_{33}/(\alpha_L T_0 E_T)$ *at* $x_2 = L/2$										
4	0.489	1.703	3.313	5.045	6.423	6.941	5.899	4.267	2.457	0.794
10	0.075	0.300	0.678	1.214	1.692	1.779	1.359	0.824	0.397	0.108
20	0.019	0.079	0.184	0.338	0.476	0.498	0.374	0.220	0.102	0.027

T3-6-3: Sliding interfaces in constrained contact: $K_S = 0$ **and** $1/K_N = 0$; **Imperfect thermal contact:** $RK_L/h = 10$

$\frac{L}{h}$	x_3/h									
	-1/2	-7/18	-5/18	$-1/6_l$	$-1/6_u$	$1/6_l$	$1/6_u$	5/18	7/18	1/2
	Dimensionless longitudinal displacements: $v_2/(\alpha_L T_0 h)$ *at* $x_2 = 0$									
4	17.26	5.702	-4.640	-15.53	501.8	483.5	6.615	10.65	25.31	54.24
10	6.508	3.565	0.829	-1.675	1677	1679	44.70	51.06	62.86	80.62
20	-2.454	2.351	7.229	12.27	3513	3534	102.0	111.7	124.3	139.9
	Dimensionless transverse displacements: $v_3/(\alpha_L T_0 h)$ *at* $x_2 = L/2$									
4	146.6	145.7	141.8	134.8	134.8	7.827	7.827	-126.9	-272.4	-435.3
10	87.12	85.08	78.77	68.14	68.14	-107.4	-107.4	-265.6	-429.5	-600.4
20	-275.0	-277.2	-284.0	-295.3	-295.3	-479.8	-479.8	-641.9	-808.9	-981.1
	Dimensionless bending stresses: $\sigma_{22}/(\alpha_L T_0 E_T)$ *at* $x_2 = L/2$									
4	-231.5	-71.22	73.24	225.3	-44.58	44.61	162.6	122.9	-46.95	-394.0
10	-34.92	-11.11	11.65	33.29	-43.16	43.16	56.68	32.56	-18.48	-99.04
20	6.584	2.303	-2.157	-7.023	-42.91	42.91	30.84	13.82	-10.22	-41.65
$\frac{L}{h}$	x_3/h									
	-5/12	-1/3	-1/4	-1/6	-1/12	1/12	1/6	1/4	1/3	5/12
	Dimensionless transverse shear stress [c]*:* $\sigma_{23}/(\alpha_L T_0 E_T)$ *at* $x_2 = 0$									
4	11.04	14.52	10.89	0.000	2.187	2.188	0.000	-10.38	-17.35	-15.96
10	0.678	0.893	0.661	0.000	0.847	0.847	0.000	-1.311	-2.019	-1.725
20	-0.065	-0.088	-0.067	0.000	0.421	0.421	0.000	-0.329	-0.473	-0.382
	Dimensionless transverse normal stresses: $\sigma_{33}/(\alpha_L T_0 E_T)$ *at* $x_2 = L/2$									
4	0.405	1.281	2.151	2.549	2.628	2.978	3.058	2.711	1.772	0.622
10	0.010	0.031	0.053	0.062	0.075	0.129	0.141	0.123	0.078	0.026
20	0.000	-0.002	-0.003	-0.003	0.000	0.013	0.017	0.014	0.009	0.003

[a] Maxima $[x_3/h, \sigma_{23\max}/(\alpha_L T_0 E_T)]$: [-0.167, 54.47] for $L/h = 4$, [-0.167, 27.53] for $L/h = 10$ and [-0.167, 14.29] for $L/h = 20$.

[b] Maxima $[x_3/h, \sigma_{23\max}/(\alpha_L T_0 E_T)]$: [0.312, -28.04] for $L/h = 4$, [-0.167, 23.56] for $L/h = 10$ and [-0.167, 13.72] for $L/h = 20$.

[c] Maxima $[x_3/h, \sigma_{23\max}/(\alpha_L T_0 E_T)]$: [0.366, -18.10] for $L/h = 4$, [0.335, -2.056] for $L/h = 10$ and [0.000, 0.562] for $L/h = 20$.

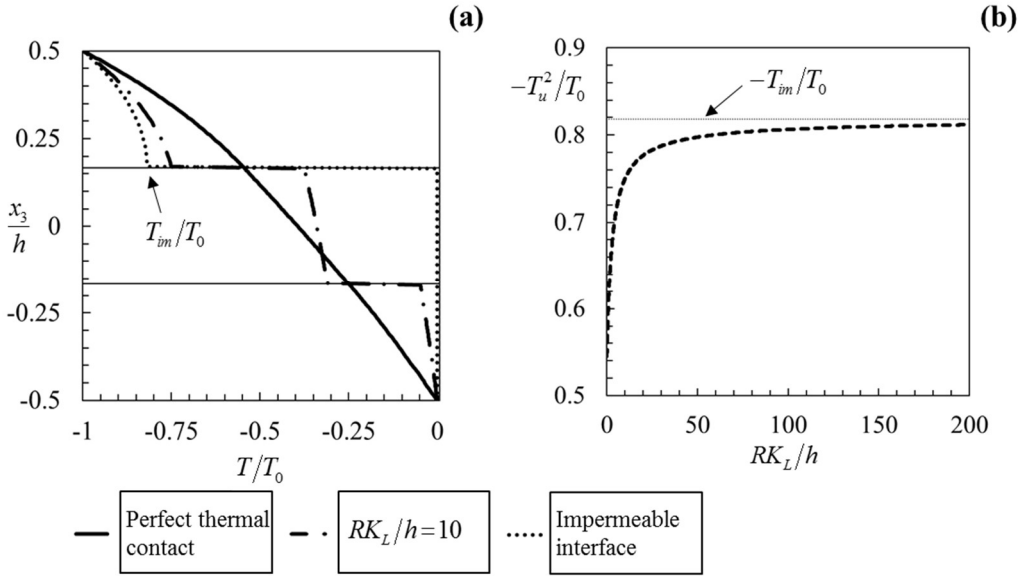

Figure 3-8: (a) Through-thickness temperature distribution at $x_2 = L/2$ in a three-layer plate $(0,90,0)$, $L/h = 4$, applied temperature $T = -T_0 \sin(\pi x_2/L)$ on upper surface, and (b) normalized temperature in the upper layer at the interface at $x_2 = L/2$ on increasing RK_L/h ($RK_L/h = 0$ perfect contact; $h/(RK_L) = 0$ impermeable interface). The thermal conductivities of the layers, $K_T/K_L = 0.16$.

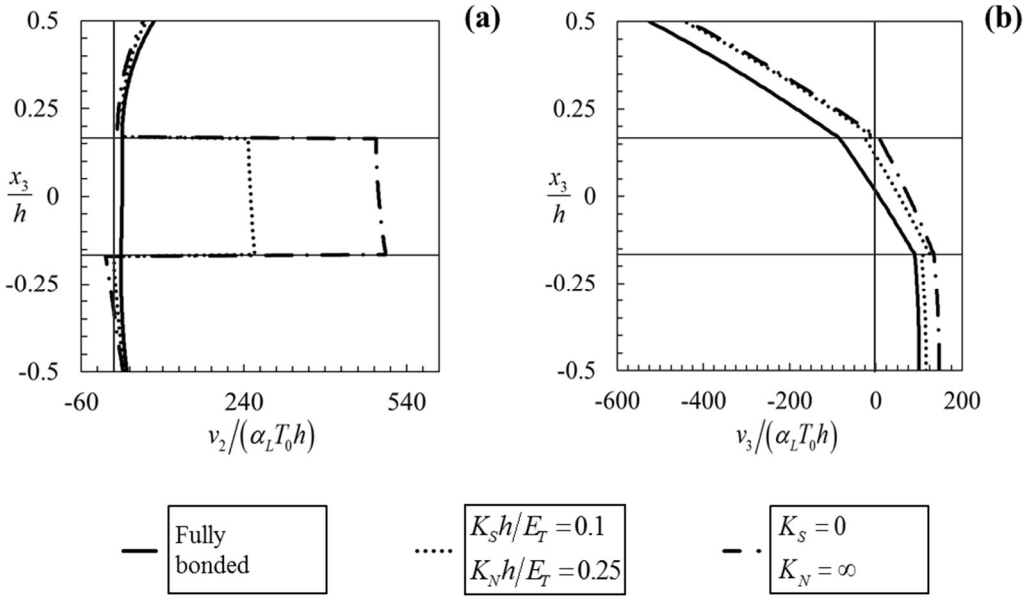

Figure 3-9: (a) Longitudinal at $x_2 = 0$ and (b) transverse at $x_2 = L/2$ displacements through thickness in a simply supported three-layer plate $(0,90,0)$ under plane-strain conditions, $L/h = 4$, applied temperature $T = -T_0 \sin(\pi x_2/L)$ on upper surface. Thermo-elastic constants: $E_L/E_T = 17$, $G_{LT}/E_T = 0.7$, $G_{TT}/E_T = 0.6$, $\nu_{LT} = 0.28$, $\nu_{TT} = 0.4$, $\alpha_T/\alpha_L = 1125$ and $K_T/K_L = 0.16$. Imperfect thermal contact, $RK_L/h = 10$.

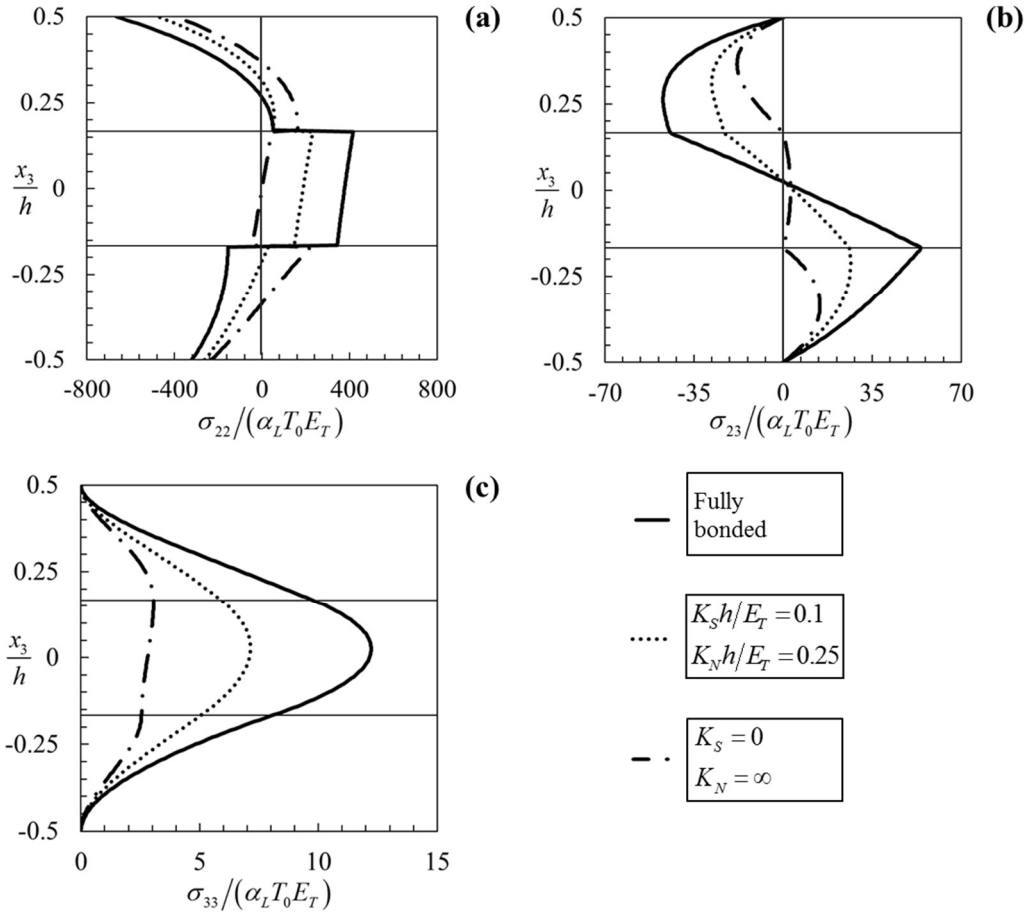

Figure 3-10: (a) Bending at $x_2 = L/2$, (b) transverse shear at $x_2 = 0$ and (c) transverse normal at $x_2 = L/2$ stresses through thickness in a simply supported three-layer plate $(0,90,0)$ under plane-strain conditions, $L/h = 4$, applied temperature $T = -T_0 \sin(\pi x_2/L)$ on upper surface. Thermo-elastic constants: $E_L/E_T = 17$, $G_{LT}/E_T = 0.7$, $G_{TT}/E_T = 0.6$, $\nu_{LT} = 0.28$, $\nu_{TT} = 0.4$, $\alpha_T/\alpha_L = 1125$ and $K_T/K_L = 0.16$. Imperfect thermal contact, $RK_L/h = 10$.

Figure 3-8, Figure 3-9 and Figure 3-10 highlight the influence of the mechanical and thermal interfacial imperfections on the temperature distribution in the layers and the field variables. A non-zero interfacial thermal resistance induces temperature jumps at the layer interfaces (Figure 3-8) and modifies displacement and stress distributions. In the limiting case of an impermeable interface, the temperature in the third layer at the upper interface is given by ${}^{(3)}T_{im}(x_2, x_3 = x_3^2) = -2T_0 e^{{}^{(3)}sh/3} / (1 + e^{2\,{}^{(3)}sh/3}) \sin(\pi x_2/L)$ and tends to the applied temperature on increasing L/h. For large values of L/h, the temperature in the upper layer is ${}^{(3)}T(x_2 = L/2, x_3) = -T_0$.

3.3 CLOSED-FORM 3D THERMO-ELASTICITY SOLUTIONS FOR MULTILAYERED PLATES WITH IMPERFECT INTERFACES AND IMPERFECT THERMAL CONTACT

The matrix formulation developed in Sect. 3.2 is extended here to rectangular plates with finite dimensions. Figure 3-11 shows the multilayered plate with $x_1 - x_2 - x_3$ a system of Cartesian coordinates with origin at the left edge. The plate has global thickness *h* and its length in x_2 and x_1 directions are *a* and *b*,

respectively. The layers are assumed to be linearly elastic, homogenous and orthotropic with principal material axes parallel to the geometrical axes (e.g., cross-ply laminate). The *k*th layer, with $k = 1, \ldots n$ numbered from bottom to top, is defined by the coordinates of its lower and upper surfaces, x_3^{k-1} and x_3^k, and has thickness ${}^{(k)}h$ (the superscript (*k*) on the left of a quantity shows association with the layer *k*, while the superscript *k* on the right identifies the interface between layers *k* and *k*+1). The body is simply supported along four edges and subjected to bi-sinusoidal thermo-mechanical loadings acting on the upper and lower surfaces: $f_3(x_1, x_2, x_3 = x_3^0) = f_l \sin(p_1 x_1)\sin(p_2 x_2)$ and $f_3(x_1, x_2, x_3 = x_3^n)$ $f_u \sin(p_1 x_1)\sin(p_2 x_2)$ are, respectively, normal surface tractions on the lower and upper surfaces of the plate with $p_1 = m_1\pi/b$, $p_2 = m_2\pi/a$, and $m_1, m_2 \in \mathbb{N}$, and the applied temperatures on the lower and upper surfaces of the plate, $T(x_1, x_2, x_3 = x_3^0) = T_l \sin(p_1 x_1)\sin(p_2 x_2)$ and $T(x_1, x_2, x_3 = x_3^n) = T_u \sin(p_1 x_1)\sin(p_2 x_2)$.

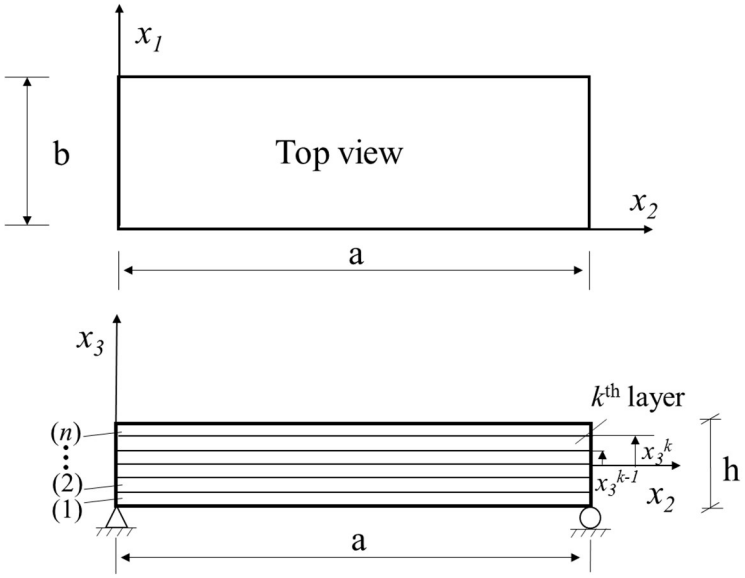

Figure 3-11: Simply supported multilayered plate with thermally and/or mechanically imperfect interfaces.

The constitutive equations of the layer *k*, is:

$$
{}^{(k)}\begin{Bmatrix} \sigma_{11} \\ \sigma_{22} \\ \sigma_{33} \\ \sigma_{13} \\ \sigma_{23} \\ \sigma_{12} \end{Bmatrix} = {}^{(k)}\begin{bmatrix} C_{11} & C_{12} & C_{13} & 0 & 0 & 0 \\ C_{12} & C_{22} & C_{23} & 0 & 0 & 0 \\ C_{13} & C_{23} & C_{33} & 0 & 0 & 0 \\ 0 & 0 & 0 & C_{44} & 0 & 0 \\ 0 & 0 & 0 & 0 & C_{55} & 0 \\ 0 & 0 & 0 & 0 & 0 & C_{66} \end{bmatrix} \begin{Bmatrix} \varepsilon_{11} - \alpha_1 T \\ \varepsilon_{22} - \alpha_2 T \\ \varepsilon_{33} - \alpha_3 T \\ 2\varepsilon_{13} \\ 2\varepsilon_{23} \\ 2\varepsilon_{12} \end{Bmatrix} \tag{3-49}
$$

where ${}^{(k)}\sigma_{ij} = {}^{(k)}\sigma_{ij}(x_1,x_2,x_3)$ and ${}^{(k)}\varepsilon_{ij} = {}^{(k)}\varepsilon_{ij}(x_1,x_2,x_3)$ (for i,j = 1, 2, 3) are Cauchy stress and linear strain components, ${}^{(k)}C_{ij}$ (for i,j = 1, …, 6) are stiffness coefficients, ${}^{(k)}\alpha_i$ are coefficients of thermal expansion along the x_i direction and ${}^{(k)}T = {}^{(k)}T(x_1,x_2,x_3)$ is the temperature increment in the layer k.

The layers are joined by interfaces, which are zero-thickness mathematical surfaces where material properties, displacements and temperature may be discontinuous while interfacial tractions and heat flux are continuous. The constitutive equations of the interfaces are defined by linear uncoupled traction laws which relate the interfacial tractions to the relative displacements of the adjacent layers:

$$\begin{aligned}
\hat{\sigma}_1^k(x_1,x_2,x_3 = x_3^k) &= K_{S1}^k\ \hat{v}_1^k(x_1,x_2,x_3 = x_3^k)\\
\hat{\sigma}_2^k(x_1,x_2,x_3 = x_3^k) &= K_{S2}^k\ \hat{v}_2^k(x_1,x_2,x_3 = x_3^k)\\
\hat{\sigma}_3^k(x_1,x_2,x_3 = x_3^k) &= K_N^k\ \hat{v}_3^k(x_1,x_2,x_3 = x_3^k)
\end{aligned} \tag{3-50}$$

where $\hat{\sigma}_1^k$, $\hat{\sigma}_2^k$ and $\hat{\sigma}_3^k$ are the interfacial tangential and normal tractions acting on the upper surface of the layer k with unit positive normal vector, K_{S1}^k, K_{S2}^k and K_N^k are tangential and normal stiffnesses and $\hat{v}_1^k$, $\hat{v}_2^k$ and $\hat{v}_3^k$ are the relative displacements between the layers k and $k+1$ at the interface:

$$\hat{v}_i^k(x_1,x_2,x_3 = x_3^k) = {}^{(k+1)}v_i(x_1,x_2,x_3 = x_3^k) - {}^{(k)}v_i(x_1,x_2,x_3 = x_3^k) \tag{3-51}$$

with ${}^{(k)}v_i$ the displacement component in the layer k and i = 1, 2, 3. The limiting case of a perfectly bonded layer is described by $1/K_{S1}^k = 1/K_{S2}^k = 1/K_N^k = 0$, which leads to a continuous displacement field and vanishing interfacial jumps; an interface which allows relative sliding displacements in constrained contact is defined by $1/K_N^k = 0$ and $K_{S1}^k = K_{S2}^k = 0$, which yield $\hat{\sigma}_1^k = \hat{\sigma}_2^k = 0$ and $\hat{v}_3^k = 0$.

The thermal behavior of the interfaces is described by a thermal resistance, R^k, which is independent of the interfacial displacements and controls the heat flux and the temperature at the interface [47]. The interfacial thermal jump between layers k and $k+1$ is related to the heat flux through the interface through the interfacial thermal resistance:

$${}^{(k)}q_3(x_1,x_2,x_3 = x_3^k)R^k = -\left[{}^{(k+1)}T(x_1,x_2,x_3 = x_3^k) - {}^{(k)}T(x_1,x_2,x_3 = x_3^k)\right] \tag{3-52}$$

where ${}^{(k)}q_3(x_1,x_2,x_3) = -{}^{(k)}K_3\ {}^{(k)}T(x_1,x_2,x_3)_{,3}$ is the heat flux in the layer k and ${}^{(k)}K_i$ is the thermal conductivity of the layer in the x_i direction. The limiting case corresponding to perfect thermal contact, where the temperature is continuous across the interface is described by $R^k = 0$, and an impermeable interface, where the heat flux through the interface vanishes, by a vanishing thermal conductance $1/R^k = 0$

.

3.3.1 Problem formulation

The equations governing the response of the layer k are [6]:

- Heat conduction in the absence of internal heat generation:

$$\frac{{}^{(k)}K_1}{{}^{(k)}K_3}\frac{\partial^2\,{}^{(k)}T(x_1,x_2,x_3)}{\partial x_1^2}+\frac{{}^{(k)}K_2}{{}^{(k)}K_3}\frac{\partial^2\,{}^{(k)}T(x_1,x_2,x_3)}{\partial x_2^2}+\frac{\partial^2\,{}^{(k)}T(x_1,x_2,x_3)}{\partial x_3^2}=0 \tag{3-53}$$

- Continuity of heat flux and interfacial thermal response:

$$\begin{aligned}&{}^{(k+1)}T(x_1,x_2,x_3^k)-{}^{(k)}T(x_1,x_2,x_3^k)=-R^{k\,(k)}q_3(x_1,x_2,x_3^k)\\&\frac{{}^{(k)}K_3}{{}^{(k+1)}K_3}\,{}^{(k)}T(x_1,x_2,x_3^k),_3={}^{(k+1)}T(x_1,x_2,x_3^k),_3\end{aligned} \tag{3-54}$$

- Thermal boundary conditions:

$$\begin{aligned}&{}^{(n)}T(x_1,x_2,x_3=x_3^n)=T_u\sin\left(p_1x_1\right)\sin\left(p_2x_2\right)\\&{}^{(1)}T(x_1,x_2,x_3=x_3^0)=T_l\sin\left(p_1x_1\right)\sin\left(p_2x_2\right)\\&{}^{(k)}T(x_1,x_2=0\text{ and }a,x_3)=0,\quad\text{for } k=1,\ldots,n\\&{}^{(k)}T(x_1=0\text{ and }b,x_2,x_3)=0,\quad\text{for } k=1,\ldots,n\end{aligned} \tag{3-55}$$

- Strain-displacement equations:

$$\begin{aligned}&{}^{(k)}\varepsilon_{11}={}^{(k)}v_1,_1;\quad {}^{(k)}\varepsilon_{22}={}^{(k)}v_2,_2;\quad {}^{(k)}\varepsilon_{33}={}^{(k)}v_3,_3\\&2\,{}^{(k)}\varepsilon_{13}={}^{(k)}v_1,_3+{}^{(k)}v_3,_1;\quad 2\,{}^{(k)}\varepsilon_{23}={}^{(k)}v_2,_3+{}^{(k)}v_3,_2\\&2\,{}^{(k)}\varepsilon_{12}={}^{(k)}v_2,_1+{}^{(k)}v_1,_2\end{aligned} \tag{3-56}$$

- Equilibrium, Navier equations:

$$\begin{aligned}&{}^{(k)}C_{11}\,{}^{(k)}v_1,_{11}+{}^{(k)}(C_{12}+C_{66})\,{}^{(k)}v_2,_{12}+{}^{(k)}(C_{13}+C_{44})\,{}^{(k)}v_3,_{13}+{}^{(k)}C_{44}\,{}^{(k)}v_1,_{33}\\&+{}^{(k)}C_{66}\,{}^{(k)}v_1,_{22}={}^{(k)}(C_{11}\alpha_1+C_{12}\alpha_2+C_{13}\alpha_3)\,{}^{(k)}T,_1;\\&{}^{(k)}C_{22}\,{}^{(k)}v_2,_{22}+{}^{(k)}(C_{12}+C_{66})\,{}^{(k)}v_1,_{12}+{}^{(k)}(C_{23}+C_{55})\,{}^{(k)}v_3,_{23}+{}^{(k)}C_{55}\,{}^{(k)}v_2,_{33}\\&+{}^{(k)}C_{66}\,{}^{(k)}v_2,_{11}={}^{(k)}(C_{12}\alpha_1+C_{22}\alpha_2+C_{23}\alpha_3)\,{}^{(k)}T,_2;\\&{}^{(k)}C_{33}\,{}^{(k)}v_3,_{33}+{}^{(k)}(C_{23}+C_{55})\,{}^{(k)}v_2,_{23}+{}^{(k)}(C_{13}+C_{44})\,{}^{(k)}v_1,_{13}+{}^{(k)}C_{44}\,{}^{(k)}v_3,_{11}\\&+{}^{(k)}C_{55}\,{}^{(k)}v_3,_{22}={}^{(k)}(C_{13}\alpha_1+C_{23}\alpha_2+C_{33}\alpha_3)\,{}^{(k)}T,_3\end{aligned} \tag{3-57}$$

- Continuity conditions in terms of the stresses and interfacial constitutive response:

$$
\begin{aligned}
&{}^{(k)}\sigma_{13}(x_1,x_2,x_3^k) = {}^{(k+1)}\sigma_{13}(x_1,x_2,x_3^k)\\
&{}^{(k)}\sigma_{23}(x_1,x_2,x_3^k) = {}^{(k+1)}\sigma_{23}(x_1,x_2,x_3^k)\\
&{}^{(k)}\sigma_{33}(x_1,x_2,x_3^k) = {}^{(k+1)}\sigma_{33}(x_1,x_2,x_3^k)\\
&{}^{(k+1)}v_1(x_1,x_2,x_3^k) - {}^{(k)}v_1(x_1,x_2,x_3^k) = \frac{1}{K_{S1}^k}\,{}^{(k)}\sigma_{13}(x_1,x_2,x_3^k)\\
&{}^{(k+1)}v_2(x_1,x_2,x_3^k) - {}^{(k)}v_2(x_1,x_2,x_3^k) = \frac{1}{K_{S2}^k}\,{}^{(k)}\sigma_{23}(x_1,x_2,x_3^k)\\
&{}^{(k+1)}v_3(x_1,x_2,x_3^k) - {}^{(k)}v_3(x_1,x_2,x_3^k) = \frac{1}{K_{N}^k}\,{}^{(k)}\sigma_{33}(x_1,x_2,x_3^k)
\end{aligned}
\tag{3-58}
$$

- Boundary conditions in terms of the stresses and displacements:

$$
\begin{aligned}
&{}^{(n)}\sigma_{33}(x_1,x_2,x_3 = x_3^n) = f_u \sin(p_1x_1)\sin(p_2x_2)\\
&{}^{(n)}\sigma_{23}(x_1,x_2,x_3 = x_3^n) = {}^{(n)}\sigma_{13}(x_1,x_2,x_3 = x_3^n) = 0\\
&{}^{(1)}\sigma_{33}(x_1,x_2,x_3 = x_3^0) = -f_l \sin(p_1x_1)\sin(p_2x_2)\\
&{}^{(1)}\sigma_{23}(x_1,x_2,x_3 = x_3^0) = {}^{(1)}\sigma_{13}(x_1,x_2,x_3 = x_3^0) = 0\\
&{}^{(k)}\sigma_{11}(x_1 = 0 \text{ and } b, x_2, x_3) = 0, \text{ for } k = 1, ..., n\\
&{}^{(k)}\sigma_{22}(x_1, x_2 = 0 \text{ and } a, x_3) = 0, \text{ for } k = 1, ..., n\\
&{}^{(k)}v_2(x_1 = 0 \text{ and } b, x_2, x_3) = 0, \text{ for } k = 1, ..., n\\
&{}^{(k)}v_1(x_1, x_2 = 0 \text{ and } a, x_3) = 0, \text{ for } k = 1, ..., n\\
&{}^{(k)}v_3(x_1 = 0 \text{ and } b, x_2, x_3) = 0, \text{ for } k = 1, ..., n\\
&{}^{(k)}v_3(x_1, x_2 = 0 \text{ and } a, x_3) = 0, \text{ for } k = 1, ..., n
\end{aligned}
\tag{3-59}
$$

3.3.2 Solution of the heat conduction problem through the transfer matrix method

The solution of the heat conduction problem in the layer k, Eq. (3-53), which satisfies the thermal boundary conditions at the plate edges in Eq. (3-55) is obtained using the method of separation of variables [6]:

$$
{}^{(k)}T(x_1,x_2,x_3) = {}^{(k)}F(x_3)\sin(p_1x_1)\sin(p_2x_2) \tag{3-60}
$$

where:

$$
\begin{aligned}
&{}^{(k)}F(x_3) = ({}^{(k)}c_1 e^{{}^{(k)}sx_3} + {}^{(k)}c_2 e^{-{}^{(k)}sx_3})\\
&{}^{(k)}s = \sqrt{\frac{{}^{(k)}K_1(p_1)^2 + {}^{(k)}K_2(p_2)^2}{{}^{(k)}K_3}}
\end{aligned}
\tag{3-61}
$$

The thermal boundary conditions at the upper and lower surfaces of the plate, Eq. (3-55), and the thermal continuity conditions at the layer interfaces, Eq. (3-54), lead to an algebraic system of $2\times n$ coupled equations in the $2\times n$ unknown constants ${}^{(k)}c_1$ and ${}^{(k)}c_2$, for $k = 1, \ldots, n$. The transfer matrix method is used here for the efficient closed form derivation of the $2\times n$ unknown constants.

The temperature distribution, Eqs. (3-60) and (3-61), and its gradient are written in matrix form as:

$$ {}^{(k)}\begin{bmatrix} T(x_2,x_3) \\ T(x_2,x_3),_3 \end{bmatrix} = {}^{(k)}G(x_3)\sin\left(p_1x_1\right)\sin\left(p_2x_2\right) \tag{3-62} $$

where:

$$ {}^{(k)}G(x_3) = {}^{(k)}D(x_3)\ {}^{(k)}\begin{bmatrix} c_1 \\ c_2 \end{bmatrix} \tag{3-63} $$

$$ {}^{(k)}D(x_3) = {}^{(k)}\begin{bmatrix} e^{sx3} & e^{-sx3} \\ se^{sx3} & -se^{-sx3} \end{bmatrix} \tag{3-64} $$

and ${}^{(k)}D(x_3)$ is a 2×2 matrix whose elements are explicit functions of ${}^{(k)}s$ defined in Eq. (3-61) and x_3. In order to stablish a relationship between ${}^{(k)}c_1$ and ${}^{(k)}c_2$, and the constants of the layer $k = 1$, the same procedure as followed for the plane strain problem in Sect. 3.2, is followed here; the local transfer and interfacial matrices remain the same as those of the 2D problem defined in Eqs. (3-20) and (3-21). The relationships between the thermal constants of the layer k and those of the first layer given in Eqs. (3-23) and (3-25) in the matrix and expanded forms, and the expressions given in Eq. (3-24) for the constant of the first layer, hold also for the case of the plate with finite dimensions. Therefore, the temperature distribution is fully defined by Eqs. (3-24), (3-25), (3-60), (3-61) and (A-2) in Appendix A.

3.3.3 Solution of the thermo-elastic problem through the transfer matrix method

The displacement components in the layer k are obtained by summing particular and complementary solutions of the governing equilibrium equations (3-57), for $i = 1, 2, 3$:

$$ {}^{(k)}v_i(x_1,x_2,x_3) = {}^{(k)}v_{ip}(x_1,x_2,x_3) + {}^{(k)}v_{ic}(x_1,x_2,x_3) \tag{3-65} $$

In the absence of thermal loads, the particular solution is ${}^{(k)}v_{ip}(x_1,x_2,x_3) = 0$.

Particular solution for layer k

A particular solution of the equilibrium equations (3-57) for the layer k, with ${}^{(k)}T = {}^{(k)}T(x_1,x_2,x_3)$ prescribed by the previous solution of the heat conduction problem, which satisfies the edge boundary conditions in Eq. (3-59), is [6]:

$$ \begin{aligned} {}^{(k)}v_{1p}(x_1,x_2,x_3) &= ({}^{(k)}A_1e^{{}^{(k)}sx_3} + {}^{(k)}A_2e^{-{}^{(k)}sx_3})\cos\left(p_1x_1\right)\sin\left(p_2x_2\right) \\ {}^{(k)}v_{2p}(x_1,x_2,x_3) &= ({}^{(k)}B_1e^{{}^{(k)}sx_3} + {}^{(k)}B_2e^{-{}^{(k)}sx_3})\sin\left(p_1x_1\right)\cos\left(p_2x_2\right) \\ {}^{(k)}v_{3p}(x_1,x_2,x_3) &= ({}^{(k)}D_1e^{{}^{(k)}sx_3} + {}^{(k)}D_2e^{-{}^{(k)}sx_3})\sin\left(p_1x_1\right)\sin\left(p_2x_2\right) \end{aligned} \tag{3-66} $$

where ${}^{(k)}A_1$, ${}^{(k)}A_2$, ${}^{(k)}B_1$, ${}^{(k)}B_2$, ${}^{(k)}D_1$ and ${}^{(k)}D_2$ are unknown constants and ${}^{(k)}s$ is given in Eq. (3-61). Substituting ${}^{(k)}v_{1p}$, ${}^{(k)}v_{2p}$ and ${}^{(k)}v_{3p}$ from Eq. (3-66) into Eq. (3-57) and collecting the terms multiplying $e^{{}^{(k)}sx_3}$ and $e^{-{}^{(k)}sx_3}$ and equating them to zero, result in a system of six algebraic equations:

$$
\begin{aligned}
&{}^{(k)}\Big[\Big(C_{44}s^2 - C_{11}(p_1)^2 - C_{66}(p_2)^2\Big)A_1 - (C_{12}+C_{66})p_1p_2B_1 + \\
&+(C_{13}+C_{44})p_1sD_1\Big] = p_1\,{}^{(k)}c_1\,{}^{(k)}(C_{11}\alpha_1 + C_{12}\alpha_2 + C_{13}\alpha_3)\\
&{}^{(k)}\Big[-(C_{12}+C_{66})p_1p_2A_1 + \Big(C_{55}s^2 - C_{22}(p_2)^2 - C_{66}(p_1)^2\Big)B_1 + \\
&+(C_{23}+C_{55})p_2sD_1\Big] = p_2\,{}^{(k)}c_1\,{}^{(k)}(C_{12}\alpha_1 + C_{22}\alpha_2 + C_{23}\alpha_3)\\
&{}^{(k)}\Big[-(C_{13}+C_{44})p_1sA_1 + \Big(C_{33}s^2 - C_{44}(p_1)^2 - C_{55}(p_2)^2\Big)D_1 - \\
&-(C_{23}+C_{55})p_2sB_1\Big] = {}^{(k)}s\,{}^{(k)}c_1\,{}^{(k)}(C_{13}\alpha_1 + C_{23}\alpha_2 + C_{33}\alpha_3)\\
&{}^{(k)}\Big[\Big(C_{44}s^2 - C_{11}(p_1)^2 - C_{66}(p_2)^2\Big)A_2 - (C_{12}+C_{66})p_1p_2B_2 - \\
&-(C_{13}+C_{44})p_1sD_2\Big] = p_1\,{}^{(k)}c_2\,{}^{(k)}(C_{11}\alpha_1 + C_{12}\alpha_2 + C_{13}\alpha_3)\\
&{}^{(k)}\Big[-(C_{12}+C_{66})p_1p_2A_2 + \Big(C_{55}s^2 - C_{22}(p_2)^2 - C_{66}(p_1)^2\Big)B_2 - \\
&-(C_{23}+C_{55})p_2sD_2\Big] = p_2\,{}^{(k)}c_2\,{}^{(k)}(C_{12}\alpha_1 + C_{22}\alpha_2 + C_{23}\alpha_3)\\
&{}^{(k)}\Big[-(C_{13}+C_{44})p_1sA_2 - \Big(C_{33}s^2 - C_{44}(p_1)^2 - C_{55}(p_2)^2\Big)D_2 - \\
&-(C_{23}+C_{55})p_2sB_2\Big] = {}^{(k)}s\,{}^{(k)}c_2\,{}^{(k)}(C_{13}\alpha_1 + C_{23}\alpha_2 + C_{33}\alpha_3)
\end{aligned}
\tag{3-67}
$$

which depend on the layer material properties, the integration constants of the thermal problem derived in Sect. 3.3.2 and thermal boundary conditions. Solution of the system of equations (3-67) is:

$$
\begin{aligned}
&{}^{(k)}A_1 = {}^{(k)}c_1\sum_{j=1}^{3}{}^{(k)}O_{1j}^{-1}\,{}^{(k)}X_j;\ {}^{(k)}B_1 = {}^{(k)}c_1\sum_{j=1}^{3}{}^{(k)}O_{2j}^{-1}\,{}^{(k)}X_j;\\
&{}^{(k)}D_1 = {}^{(k)}c_1\sum_{j=1}^{3}{}^{(k)}O_{3j}^{-1}\,{}^{(k)}X_j;\ {}^{(k)}A_2 = \frac{{}^{(k)}c_2}{{}^{(k)}c_1}\,{}^{(k)}A_1;\\
&{}^{(k)}B_2 = \frac{{}^{(k)}c_2}{{}^{(k)}c_1}\,{}^{(k)}B_1;\ {}^{(k)}D_2 = -\frac{{}^{(k)}c_2}{{}^{(k)}c_1}\,{}^{(k)}D_1
\end{aligned}
\tag{3-68}
$$

where:

$$
{}^{(k)}X = {}^{(k)}\begin{bmatrix} p_1\left(C_{11}\alpha_1 + C_{12}\alpha_2 + C_{13}\alpha_3\right) \\ p_2\left(C_{12}\alpha_1 + C_{22}\alpha_2 + C_{23}\alpha_3\right) \\ s\left(C_{13}\alpha_1 + C_{23}\alpha_2 + C_{33}\alpha_3\right) \end{bmatrix}
$$

$$
{}^{(k)}O = {}^{(k)}\begin{bmatrix} C_{44}s^2 - C_{11}\left(p_1\right)^2 - C_{66}\left(p_2\right)^2 & -\left(C_{12}+C_{66}\right)p_1p_2 & \left(C_{13}+C_{44}\right)p_1s \\ -\left(C_{12}+C_{66}\right)p_1p_2 & C_{55}s^2 - C_{22}\left(p_2\right)^2 - C_{66}\left(p_1\right)^2 & \left(C_{23}+C_{55}\right)p_2s \\ -\left(C_{13}+C_{44}\right)p_1s & -\left(C_{23}+C_{55}\right)p_2s & C_{33}s^2 - C_{44}\left(p_1\right)^2 - C_{55}\left(p_2\right)^2 \end{bmatrix} \tag{3-69}
$$

Complementary solution for layer k

A solution for the complementary problem, which satisfies the boundary conditions at the plate edges in Eq. (3-59) is obtained using the method of separation of variables [8]:

$$
\begin{aligned}
{}^{(k)}v_{1c}(x_1,x_2,x_3) &= {}^{(k)}V_c(x_3)\cos\left(p_1x_1\right)\sin\left(p_2x_2\right) \\
{}^{(k)}v_{2c}(x_1,x_2,x_3) &= {}^{(k)}U_c(x_3)\sin\left(p_1x_1\right)\cos\left(p_2x_2\right) \\
{}^{(k)}v_{3c}(x_1,x_2,x_3) &= {}^{(k)}W_c(x_3)\sin\left(p_1x_1\right)\sin\left(p_2x_2\right)
\end{aligned} \tag{3-70}
$$

with:

$$
\left[{}^{(k)}V_c(x_3), {}^{(k)}U_c(x_3), {}^{(k)}W_c(x_3)\right] = \left[{}^{(k)}V_0, {}^{(k)}U_0, {}^{(k)}W_0\right]e^{{}^{(k)}tx_3} \tag{3-71}
$$

where ${}^{(k)}V_0$, ${}^{(k)}U_0$ and ${}^{(k)}W_0$ are unknown constants and ${}^{(k)}t$ is the root of the associated characteristic equation defined below. Substituting Eqs. (3-70) and (3-71) in the homogenous part of Eq. (3-57) yield the following system of algebraic equations:

$$
\begin{aligned}
&{}^{(k)}\left[-\left(C_{12}+C_{66}\right)p_1p_2U_0 + \left(C_{44}t^2 - C_{11}\left(p_1\right)^2 - C_{66}\left(p_2\right)^2\right)V_0 + \left(C_{13}+C_{44}\right)p_1tW_0\right] = 0 \\
&{}^{(k)}\left[\left(C_{55}t^2 - C_{22}\left(p_2\right)^2 - C_{66}\left(p_1\right)^2\right)U_0 - \left(C_{12}+C_{66}\right)p_1p_2V_0 + \left(C_{23}+C_{55}\right)p_2tW_0\right] = 0 \\
&{}^{(k)}\left[\left(C_{23}+C_{55}\right)p_2tU_0 + \left(C_{13}+C_{44}\right)p_1tV_0 - \left(C_{33}t^2 - C_{44}\left(p_1\right)^2 - C_{55}\left(p_2\right)^2\right)W_0\right] = 0
\end{aligned} \tag{3-72}
$$

The non-trivial solution of the system is obtained by imposing the determinant of the coefficients to be zero. This yields the characteristic equation for the layer k [8]:

$$
{}^{(k)}\left(-At^6 + Bt^4 + Ct^2 + D\right) = 0 \tag{3-73}
$$

where:

$$
\begin{aligned}
&{}^{(k)}A = {}^{(k)}\left(C_{33}C_{44}C_{55}\right)\\
&{}^{(k)}B = \left(p_1\right)^2\,{}^{(k)}\left[C_{55}\left(C_{11}C_{33}-C_{13}^{\ 2}\right)+C_{44}\left(C_{33}C_{66}-2C_{13}C_{55}\right)\right]+\\
&\left(p_2\right)^2\,{}^{(k)}\left[C_{44}\left(C_{22}C_{33}-C_{23}^{\ 2}\right)+C_{55}\left(C_{33}C_{66}-2C_{23}C_{44}\right)\right]\\
&{}^{(k)}C = -\left(p_1\right)^4\,{}^{(k)}\left[C_{66}\left(C_{11}C_{33}-C_{13}^{\ 2}\right)+C_{44}\left(C_{11}C_{55}-2C_{13}C_{66}\right)\right]-\\
&\left(p_2\right)^4\,{}^{(k)}\left[C_{66}\left(C_{22}C_{33}-C_{23}^{\ 2}\right)+C_{55}\left(C_{22}C_{44}-2C_{23}C_{66}\right)\right]+\\
&\left(p_1\right)^2\left(p_2\right)^2\,{}^{(k)}\left[-C_{22}\left(C_{11}C_{33}-C_{13}^{\ 2}\right)-2\left(C_{23}+C_{55}\right)\left(C_{13}+C_{44}\right)\left(C_{12}+C_{66}\right)-2\,{}^{(k)}\left(C_{44}C_{55}C_{66}\right)+\right.\\
&\left.+2\,{}^{(k)}\left(C_{22}C_{13}C_{44}\right)+C_{12}C_{33}\left(C_{12}+2C_{66}\right)+C_{23}C_{11}\left(C_{23}+2C_{55}\right)\right]\\
&{}^{(k)}D = {}^{(k)}\left(C_{22}C_{55}C_{66}\right)\left(p_2\right)^6+{}^{(k)}\left[C_{55}\left(C_{11}C_{22}-C_{12}^{\ 2}\right)+C_{66}\left(C_{22}C_{44}-2C_{12}C_{55}\right)\right]\left(p_1\right)^2\left(p_2\right)^4\\
&+{}^{(k)}\left[C_{44}\left(C_{11}C_{22}-C_{12}^{\ 2}\right)+C_{66}\left(C_{11}C_{55}-2C_{12}C_{44}\right)\right]\left(p_1\right)^4\left(p_2\right)^2+{}^{(k)}\left(C_{11}C_{44}C_{66}\right)\left(p_1\right)^6
\end{aligned}
\tag{3-74}
$$

The characteristic equation (3-73) is put into the standard cubic form by introducing ${}^{(k)}\gamma = {}^{(k)}t^2 - {}^{(k)}\left(\frac{B}{3A}\right)$ [8]:

$$
\begin{aligned}
&{}^{(k)}\left(\gamma^3+d\gamma+f\right)=0\\
&{}^{(k)}d = -{}^{(k)}\left[\frac{3CA+B^2}{3A^2}\right]\\
&{}^{(k)}f = -{}^{(k)}\left[\frac{2B^3+9ABC+27DA^2}{27A^3}\right]
\end{aligned}
\tag{3-75}
$$

The discriminant of Eq. (3-75), ${}^{(k)}H = {}^{(k)}\left(\frac{f^2}{4}+\frac{d^3}{27}\right)$, controls the nature of the solution. When the discriminant is negative, the roots of the above cubic equation are real and unequal [8]:

$$
\begin{aligned}
&{}^{(k)}\gamma_j = 2\,{}^{(k)}\left(-\frac{d}{3}\right)^{1/2}\cos\,{}^{(k)}\left[\frac{\phi+2(j-1)\pi}{3}\right]\\
&{}^{(k)}\phi = \cos^{-1}\,{}^{(k)}\left[\frac{-f\sqrt{27}}{2\left(-d\right)^{3/2}}\right]
\end{aligned}
\tag{3-76}
$$

for j=1, 2 and 3. Recalling Eqs. (3-71), (3-72) and ${}^{(k)}\gamma = {}^{(k)}t^2 - {}^{(k)}\left(\frac{B}{3A}\right)$, the displacement functions take the following forms:

$$
\begin{aligned}
{}^{(k)}V_c(x_3) &= \sum_{j=1}^{3} {}^{(k)}\left[L_j U_j(x_3)\right] \\
{}^{(k)}U_c(x_3) &= \sum_{j=1}^{3} {}^{(k)}\left[U_j(x_3)\right] \\
{}^{(k)}W_c(x_3) &= \sum_{j=1}^{3} {}^{(k)}\left[R_j W_j(x_3)\right]
\end{aligned}
\tag{3-77}
$$

where:

$$
\begin{aligned}
{}^{(k)}U_j(x_3) &= {}^{(k)}\left[a_{1j} C_j(x_3) + a_{2j} S_j(x_3)\right] \\
{}^{(k)}W_j(x_3) &= {}^{(k)}\left[a_{2j} C_j(x_3) + \eta a_{1j} S_j(x_3)\right]
\end{aligned}
\tag{3-78}
$$

for j=1, 2, 3. If ${}^{(k)}\left(\gamma_j + \frac{B}{3A}\right) > 0$, then ${}^{(k)}\eta = 1$ and:

$$
\begin{aligned}
{}^{(k)}C_j(x_3) &= \cosh({}^{(k)}m_j x_3) \\
{}^{(k)}S_j(x_3) &= \sinh({}^{(k)}m_j x_3)
\end{aligned}
$$

If ${}^{(k)}\left(\gamma_j + \frac{B}{3A}\right) < 0$, then ${}^{(k)}\eta = -1$ and:

$$
\begin{aligned}
{}^{(k)}C_j(x_3) &= \cos({}^{(k)}m_j x_3) \\
{}^{(k)}S_j(x_3) &= \sin({}^{(k)}m_j x_3)
\end{aligned}
$$

where:

$$
\begin{aligned}
{}^{(k)}m_j &= \left|\gamma_j + \frac{B}{3A}\right|^{1/2} \\
{}^{(k)}L_j &= \frac{p_1 p_2}{{}^{(k)}J_j}\,{}^{(k)}\left\{\eta_j m_j^2\left[C_{33}\left(C_{12}+C_{66}\right)-\left(C_{13}+C_{44}\right)\left(C_{23}+C_{55}\right)\right]-\right. \\
&\left.-\left(C_{12}+C_{66}\right)\left(C_{55}\left(p_2\right)^2+C_{44}\left(p_1\right)^2\right)\right\} \\
{}^{(k)}R_j &= \frac{p_2\,{}^{(k)}m_j}{{}^{(k)}J_j}\,{}^{(k)}\left\{\eta_j m_j^2 C_{44}\left(C_{23}+C_{55}\right)-\left(C_{23}+C_{55}\right)\left(C_{66}\left(p_2\right)^2+C_{11}\left(p_1\right)^2\right)+\right. \\
&\left.+\left(p_1\right)^2\left(C_{13}+C_{44}\right)\left(C_{12}+C_{66}\right)\right\} \\
{}^{(k)}J_j &= {}^{(k)}\left\{C_{33}C_{44}m_j^4+\eta_j m_j^2\left[-\left(p_2\right)^2\left(C_{44}C_{55}+C_{33}C_{66}\right)+\left(p_1\right)^2\left(C_{13}{}^2-C_{11}C_{33}+2C_{13}C_{44}\right)\right]+\right. \\
&\left.+\left(C_{66}\left(p_2\right)^2+C_{11}\left(p_1\right)^2\right)\left(C_{55}\left(p_2\right)^2+C_{44}\left(p_1\right)^2\right)\right\}
\end{aligned}
\tag{3-79}
$$

Solutions for the cases of zero and positive discriminants are presented in matrix form in Appendix E.

The complementary solution for each layer is obtained by substituting ${}^{(k)}V_c(x_3)$, ${}^{(k)}U_c(x_3)$ and ${}^{(k)}W_c(x_3)$ in Eq. (3-77), which depend on six independent unknown constants, ${}^{(k)}a_{11}$, ${}^{(k)}a_{21}$, ${}^{(k)}a_{12}$, ${}^{(k)}a_{22}$, ${}^{(k)}a_{13}$ and ${}^{(k)}a_{23}$, into Eq. (3-70). Therefore, the displacement components in each layer, Eq. (3-65), depend on six unknown constants, which leads to a total of 6×*n* unknowns for the plate. The unknowns are typically obtained using interfacial continuity and boundary conditions, which lead to a system of coupled algebraic equations whose solution becomes computationally cumbersome on increasing the number of layers.

Here, we use the transfer matrix method to solve the problem in closed-form. First, the six unknown constants in the solution of the generic layer *k*, ${}^{(k)}a_{11}$, ${}^{(k)}a_{21}$, ${}^{(k)}a_{12}$, ${}^{(k)}a_{22}$, ${}^{(k)}a_{13}$ and ${}^{(k)}a_{23}$ will be related to those of the first layer. Then, the problem is reduced to finding only six unknown constants ${}^{(1)}a_{11}$, ${}^{(1)}a_{21}$, ${}^{(1)}a_{12}$, ${}^{(1)}a_{22}$, ${}^{(1)}a_{13}$ and ${}^{(1)}a_{23}$ through the application of boundary conditions at the upper and lower surfaces of the plate.

From Eqs. (3-65), (3-66), (3-70) and (3-77), the displacements in the layer *k*, can be written as:

$$
\begin{aligned}
{}^{(k)}v_1(x_1,x_2,x_3) &= \Big[{}^{(k)}A_1 e^{{}^{(k)}sx_3} + {}^{(k)}A_2 e^{-{}^{(k)}sx_3} + \\
&+ {}^{(k)}V_c({}^{(k)}a_{11}, {}^{(k)}a_{21}, {}^{(k)}a_{12}, {}^{(k)}a_{22}, {}^{(k)}a_{13}, {}^{(k)}a_{23}) \Big] \cos(p_1 x_1) \sin(p_2 x_2) \\
{}^{(k)}v_2(x_1,x_2,x_3) &= \Big[{}^{(k)}B_1 e^{{}^{(k)}sx_3} + {}^{(k)}B_2 e^{-{}^{(k)}sx_3} + \\
&+ {}^{(k)}U_c({}^{(k)}a_{11}, {}^{(k)}a_{21}, {}^{(k)}a_{12}, {}^{(k)}a_{22}, {}^{(k)}a_{13}, {}^{(k)}a_{23}) \Big] \sin(p_1 x_1) \cos(p_2 x_2) \\
{}^{(k)}v_3(x_1,x_2,x_3) &= \Big[{}^{(k)}D_1 e^{{}^{(k)}sx_3} + {}^{(k)}D_2 e^{-{}^{(k)}sx_3} + \\
&+ {}^{(k)}W_c({}^{(k)}a_{11}, {}^{(k)}a_{21}, {}^{(k)}a_{12}, {}^{(k)}a_{22}, {}^{(k)}a_{13}, {}^{(k)}a_{23}) \Big] \sin(p_1 x_1) \sin(p_2 x_2)
\end{aligned}
\tag{3-80}
$$

where the constants ${}^{(k)}A_1$, ${}^{(k)}A_2$, ${}^{(k)}B_1$, ${}^{(k)}B_2$, ${}^{(k)}D_1$ and ${}^{(k)}D_2$ are defined in Eq. (3-68). Normal and transverse shear stress components are derived from the equation above using constitutive and compatibility equations (3-49) and (3-56). Displacements and stresses are then collected in the following matrix form:

$$
\begin{bmatrix}
v_2(x_1,x_2,x_3) \\
v_1(x_1,x_2,x_3) \\
v_3(x_1,x_2,x_3) \\
\sigma_{33}(x_1,x_2,x_3) \\
\sigma_{23}(x_1,x_2,x_3) \\
\sigma_{13}(x_1,x_2,x_3)
\end{bmatrix}
= C(x_1,x_2)\,{}^{(k)}M(x_3)
\tag{3-81}
$$

where $C(x_1,x_2)$ and ${}^{(k)}M(x_3)$ are 6×6 and 6×1 matrices defined as follows:

$$C(x_2)=\begin{bmatrix} C_1 & 0 & 0 & 0 & 0 & 0 \\ 0 & C_2 & 0 & 0 & 0 & 0 \\ 0 & 0 & C_3 & 0 & 0 & 0 \\ 0 & 0 & 0 & C_4 & 0 & 0 \\ 0 & 0 & 0 & 0 & C_5 & 0 \\ 0 & 0 & 0 & 0 & 0 & C_6 \end{bmatrix} \tag{3-82}$$

$$C_1=\sin(p_1x_1)\cos(p_2x_2);C_2=\cos(p_1x_1)\sin(p_2x_2);C_3=\sin(p_1x_1)\sin(p_2x_2);$$
$$C_4=\sin(p_1x_1)\sin(p_2x_2);C_5=\sin(p_1x_1)\cos(p_2x_2);C_6=\cos(p_1x_1)\sin(p_2x_2);$$

$$^{(k)}M(x_3)=\,^{(k)}Q(x_3)+\,^{(k)}E(x_3)\begin{bmatrix} a_{11} \\ a_{21} \\ a_{12} \\ a_{22} \\ a_{13} \\ a_{23} \end{bmatrix}^{(k)} \tag{3-83}$$

The 6×1 matrix $^{(k)}Q(x_3)$ is independent of the unknowns and its elements are:

$$\begin{aligned}
&^{(k)}Q_1(x_3)=B_1e^{sx_3}+B_2e^{-sx_3}\\
&^{(k)}Q_2(x_3)=A_1e^{sx_3}+A_2e^{-sx_3}\\
&^{(k)}Q_3(x_3)=D_1e^{sx_3}+D_2e^{-sx_3}\\
&^{(k)}Q_4(x_3)=-p_2C_{23}\left(B_1e^{sx_3}+B_2e^{-sx_3}\right)-p_1C_{13}\left(A_1e^{sx_3}+A_2e^{-sx_3}\right)+\\
&+C_{33}s\left(D_1e^{sx_3}-D_2e^{-sx_3}\right)-\left(c_1e^{sx_3}+c_2e^{-sx_3}\right)\left(C_{23}\alpha_2+C_{13}\alpha_1+C_{33}\alpha_3\right)\\
&^{(k)}Q_5(x_3)=C_{55}\left[s\left(B_1e^{sx_3}-B_2e^{-sx_3}\right)+p_2\left(D_1e^{sx_3}+D_2e^{-sx_3}\right)\right]\\
&^{(k)}Q_6(x_3)=C_{44}\left[s\left(A_1e^{sx_3}-A_2e^{-sx_3}\right)+p_1\left(D_1e^{sx_3}+D_2e^{-sx_3}\right)\right]
\end{aligned} \tag{3-84}$$

The 6×6 matrix $^{(k)}E(x_3)$ relates to the complementary solution and depends on the sign of the discriminant. Expressions for $^{(k)}E(x_3)$ in different cases are given in the Appendix E.

Local transfer matrix of a generic layer

An expression for the unknown constants of the layer *k*, $^{(k)}\left[a_{11},a_{21},a_{12},a_{22},a_{13},a_{23}\right]^T$, is obtained by setting $x_3=x_3^{k-1}$ in Eq. (3-83). The local transfer matrix of the layer *k* is then derived by substituting the expression of the unknowns into Eq. (3-83) and setting $x_3=x_3^k$:

$$^{(k)}M(x_3^k)=\,^{(k)}E(x_3^k)\,^{(k)}E^{-1}(x_3^{k-1})\left[\,^{(k)}M(x_3^{k-1})-\,^{(k)}Q(x_3^{k-1})\right]+\,^{(k)}Q(x_3^k) \tag{3-85}$$

Eq. (3-85) establishes a relationship between the values of matrix ${}^{(k)}M$ at the top and bottom surfaces of the layer.

Continuity conditions and global transfer matrix

The continuity conditions between the layer *k* and *k*-1, Eq. (3-58), are written in matrix form:

$${}^{(k)}M(x_3^{k-1}) = \left(B^{k-1}\right)\ {}^{(k-1)}M(x_3^{k-1}) \tag{3-86}$$

with

$$B^{k-1} = \begin{bmatrix} 1 & 0 & 0 & 0 & 1/K_{S2}^{k-1} & 0 \\ 0 & 1 & 0 & 0 & 0 & 1/K_{S1}^{k-1} \\ 0 & 0 & 1 & 1/K_N^{k-1} & 0 & 0 \\ 0 & 0 & 0 & 1 & 0 & 0 \\ 0 & 0 & 0 & 0 & 1 & 0 \\ 0 & 0 & 0 & 0 & 0 & 1 \end{bmatrix} \tag{3-87}$$

The matrix B^{k-1} depends on the interfacial stiffnesses and for the case of perfect bonding, with $1/K_{S1}^{k-1} = 1/K_{S2}^{k-1} = 1/K_N^{k-1} = 0$, it becomes the identity matrix.

Starting from Eq. (3-85) and using the local and interfacial transfer matrices of the layers and interfaces below the layer *k* in equations (3-85) and (3-86), (see Figure 3-2), a relationship between ${}^{(k)}M(x_3^k)$ and ${}^{(1)}M(x_3^0)$ is derived:

$$\begin{aligned} {}^{(k)}M(x_3^k) = \left(B^k\right)^{-1} \Bigg\{ \prod_{i=k}^{1} \left\{ \left(B^i\right) {}^{(i)}E(x_3^i)\, {}^{(i)}E^{-1}(x_3^{i-1}) \right\} \left\{ {}^{(1)}M(x_3^0) - {}^{(1)}Q(x_3^0) \right\} + \\ + \sum_{i=2}^{k} \left(\prod_{j=k}^{i} \left\{ \left(B^j\right) {}^{(j)}E(x_3^j)\, {}^{(j)}E^{-1}(x_3^{j-1}) \right\} \left\{ \left(B^{i-1}\right) {}^{(i-1)}Q(x_3^{i-1}) - {}^{(i)}Q(x_3^{i-1}) \right\} \right) \Bigg\} + {}^{(k)}Q(x_3^k) \end{aligned} \tag{3-88}$$

The explicit expressions, relating the six unknown constants, ${}^{(k)}a_{11}$, ${}^{(k)}a_{21}$, ${}^{(k)}a_{12}$, ${}^{(k)}a_{22}$, ${}^{(k)}a_{13}$ and ${}^{(k)}a_{23}$, to those of the first layer are then derived by substituting ${}^{(k)}M(x_3^k)$ and ${}^{(1)}M(x_3^0)$ defined in Eq. (3-83), into Eq. (3-88):

$$
{}^{(k)}\begin{bmatrix} a_{11} \\ a_{21} \\ a_{12} \\ a_{22} \\ a_{13} \\ a_{23} \end{bmatrix} = {}^{(k)}E^{-1}(x_3^k)\left(B^k\right)^{-1}\left\{\prod_{i=k}^{1}\left\{\left(B^i\right){}^{(i)}E(x_3^i){}^{(i)}E^{-1}(x_3^{i-1})\right\}\right.{}^{(1)}E(x_3^0)\left.\begin{bmatrix} a_{11} \\ a_{21} \\ a_{12} \\ a_{22} \\ a_{13} \\ a_{23} \end{bmatrix}\right. +
$$

$$
+\sum_{i=2}^{k}\left(\prod_{j=k}^{i}\left\{\left(B^j\right){}^{(j)}E(x_3^j){}^{(j)}E^{-1}(x_3^{j-1})\right\}\left\{\left(B^{i-1}\right){}^{(i-1)}Q(x_3^{j-1}) - {}^{(i)}Q(x_3^{j-1})\right\}\right) \tag{3-89}
$$

for $k = 2, \ldots, n$. For fully bonded layers, the matrix $B = I$ in Eq. (3-89) can be omitted. The constants of the first layer may then be defined using six boundary conditions (3-59) at the top and bottom surfaces of the laminate and Eq. (3-89) for $k = n$, which lead to an algebraic system of six equations. A different approach, similar to that presented in Appendix D for the plane strain problem in Sect. 3.2, is followed to avoid the derivation of the constants; the approach yields the following explicit expressions for the displacements:

$$
{}^{(k)}v_2(x_1,x_2,x_3) =
$$

$$
\left\{{}^{(k)}Q_1(x_3)+\sum_{l=1}^{6}\left[\sum_{r=1}^{6}{}^{(k)}P_{1r}(x_3){}^{(k)}\Omega_{rl}\right]\left({}^{(1)}M_l(x_3^0)-{}^{(1)}Q_l(x_3^0)\right)+\sum_{t=1}^{6}{}^{(k)}P_{1t}(x_3){}^{(k)}S_t\right\}\times\sin(p_1x_1)\cos(p_2x_2)
$$

$$
{}^{(k)}v_1(x_1,x_2,x_3) =
$$

$$
\left\{{}^{(k)}Q_2(x_3)+\sum_{l=1}^{6}\left[\sum_{r=1}^{6}{}^{(k)}P_{2r}(x_3){}^{(k)}\Omega_{rl}\right]\left({}^{(1)}M_l(x_3^0)-{}^{(1)}Q_l(x_3^0)\right)+\sum_{t=1}^{6}{}^{(k)}P_{2t}(x_3){}^{(k)}S_t\right\}\times\cos(p_1x_1)\sin(p_2x_2)
$$

$$
{}^{(k)}v_3(x_1,x_2,x_3) =
$$

$$
\left\{{}^{(k)}Q_3(x_3)+\sum_{l=1}^{6}\left[\sum_{r=1}^{6}{}^{(k)}P_{3r}(x_3){}^{(k)}\Omega_{rl}\right]\left({}^{(1)}M_l(x_3^0)-{}^{(1)}Q_l(x_3^0)\right)+\sum_{t=1}^{6}{}^{(k)}P_{3t}(x_3){}^{(k)}S_t\right\}\times\sin(p_1x_1)\sin(p_2x_2)
\tag{3-90}
$$

and stresses:

$$
{}^{(k)}\sigma_{33}(x_1,x_2,x_3) =
$$

$$
\left\{{}^{(k)}Q_4(x_3)+\sum_{l=1}^{6}\left[\sum_{r=1}^{6}{}^{(k)}P_{4r}(x_3){}^{(k)}\Omega_{rl}\right]\left({}^{(1)}M_l(x_3^0)-{}^{(1)}Q_l(x_3^0)\right)+\sum_{t=1}^{6}{}^{(k)}P_{4t}(x_3){}^{(k)}S_t\right\}\times\sin(p_1x_1)\sin(p_2x_2)
$$

$$
\begin{aligned}
&{}^{(k)}\sigma_{23}(x_1,x_2,x_3) = \\
&\left\{ {}^{(k)}Q_5(x_3) + \sum_{l=1}^{6}\left[\sum_{r=1}^{6} {}^{(k)}P_{5r}(x_3)\,{}^{(k)}\Omega_{rl}\right]\left({}^{(1)}M_l(x_3^0) - {}^{(1)}Q_l(x_3^0)\right) + \sum_{t=1}^{6} {}^{(k)}P_{5t}(x_3)\,{}^{(k)}S_t \right\} \times \sin(p_1x_1)\cos(p_2x_2) \\
&{}^{(k)}\sigma_{13}(x_1,x_2,x_3) = \\
&\left\{ {}^{(k)}Q_6(x_3) + \sum_{l=1}^{6}\left[\sum_{r=1}^{6} {}^{(k)}P_{6r}(x_3)\,{}^{(k)}\Omega_{rl}\right]\left({}^{(1)}M_l(x_3^0) - {}^{(1)}Q_l(x_3^0)\right) + \sum_{t=1}^{6} {}^{(k)}P_{6t}(x_3)\,{}^{(k)}S_t \right\} \times \cos(p_1x_1)\sin(p_2x_2) \\
&{}^{(k)}\sigma_{22}(x_1,x_2,x_3) = \\
&\left\{ -p_1\,{}^{(k)}C_{12}\left[{}^{(k)}Q_2(x_3) + \sum_{l=1}^{6}\left[\sum_{r=1}^{6} {}^{(k)}P_{2r}(x_3)\,{}^{(k)}\Omega_{rl}\right]\left({}^{(1)}M_l(x_3^0) - {}^{(1)}Q_l(x_3^0)\right) + \sum_{t=1}^{6} {}^{(k)}P_{2t}(x_3)\,{}^{(k)}S_t \right] - \right. \\
&-p_2\,{}^{(k)}C_{22}\left[{}^{(k)}Q_1(x_3) + \sum_{l=1}^{6}\left[\sum_{r=1}^{6} {}^{(k)}P_{1r}(x_3)\,{}^{(k)}\Omega_{rl}\right]\left({}^{(1)}M_l(x_3^0) - {}^{(1)}Q_l(x_3^0)\right) + \sum_{t=1}^{6} {}^{(k)}P_{1t}(x_3)\,{}^{(k)}S_t \right] + \\
&\left. + {}^{(k)}C_{23}\left[{}^{(k)}Q_3(x_3),_3 + \sum_{l=1}^{6}\left[\sum_{r=1}^{6} {}^{(k)}P_{3r}(x_3),_3\,{}^{(k)}\Omega_{rl}\right]\left({}^{(1)}M_l(x_3^0) - {}^{(1)}Q_l(x_3^0)\right) + \sum_{t=1}^{6} {}^{(k)}P_{3t}(x_3),_3\,{}^{(k)}S_t \right] \right\} \times \\
&\qquad \times \sin(p_1x_1)\sin(p_2x_2) - {}^{(k)}\left(C_{12}\alpha_1 + C_{22}\alpha_2 + C_{23}\alpha_3\right){}^{(k)}T(x_1,x_2,x_3) \\
&{}^{(k)}\sigma_{11}(x_1,x_2,x_3) = \\
&\left\{ -p_1\,{}^{(k)}C_{11}\left[{}^{(k)}Q_2(x_3) + \sum_{l=1}^{6}\left[\sum_{r=1}^{6} {}^{(k)}P_{2r}(x_3)\,{}^{(k)}\Omega_{rl}\right]\left({}^{(1)}M_l(x_3^0) - {}^{(1)}Q_l(x_3^0)\right) + \sum_{t=1}^{6} {}^{(k)}P_{2t}(x_3)\,{}^{(k)}S_t \right] - \right. \\
&-p_2\,{}^{(k)}C_{12}\left[{}^{(k)}Q_1(x_3) + \sum_{l=1}^{6}\left[\sum_{r=1}^{6} {}^{(k)}P_{1r}(x_3)\,{}^{(k)}\Omega_{rl}\right]\left({}^{(1)}M_l(x_3^0) - {}^{(1)}Q_l(x_3^0)\right) + \sum_{t=1}^{6} {}^{(k)}P_{1t}(x_3)\,{}^{(k)}S_t \right] + \\
&\left. + {}^{(k)}C_{13}\left[{}^{(k)}Q_3(x_3),_3 + \sum_{l=1}^{6}\left[\sum_{r=1}^{6} {}^{(k)}P_{3r}(x_3),_3\,{}^{(k)}\Omega_{rl}\right]\left({}^{(1)}M_l(x_3^0) - {}^{(1)}Q_l(x_3^0)\right) + \sum_{t=1}^{6} {}^{(k)}P_{3t}(x_3),_3\,{}^{(k)}S_t \right] \right\} \times \\
&\qquad \times \sin(p_1x_1)\sin(p_2x_2) - {}^{(k)}\left(C_{11}\alpha_1 + C_{12}\alpha_2 + C_{13}\alpha_3\right){}^{(k)}T(x_1,x_2,x_3) \\
&{}^{(k)}\sigma_{12}(x_1,x_2,x_3) = \\
&{}^{(k)}C_{66}\left\{ p_2\left({}^{(k)}Q_2(x_3) + \sum_{l=1}^{6}\left[\sum_{r=1}^{6} {}^{(k)}P_{2r}(x_3)\,{}^{(k)}\Omega_{rl}\right]\left({}^{(1)}M_l(x_3^0) - {}^{(1)}Q_l(x_3^0)\right) + \sum_{t=1}^{6} {}^{(k)}P_{2t}(x_3)\,{}^{(k)}S_t \right) + \right. \\
&\left. p_1\left({}^{(k)}Q_1(x_3) + \sum_{l=1}^{6}\left[\sum_{r=1}^{6} {}^{(k)}P_{1r}(x_3)\,{}^{(k)}\Omega_{rl}\right]\left({}^{(1)}M_l(x_3^0) - {}^{(1)}Q_l(x_3^0)\right) + \sum_{t=1}^{6} {}^{(k)}P_{1t}(x_3)\,{}^{(k)}S_t \right) \right\} \times \\
&\qquad \times \cos(p_1x_1)\cos(p_2x_2)
\end{aligned}
\tag{3-91}
$$

with:

$$
{}^{(k)}P_{ir}(x_3) = \sum_{d=1}^{6}\left[\sum_{j=1}^{6} {}^{(k)}E_{ij}(x_3)\,{}^{(k)}E^{-1}{}_{jd}(x_3^k)\right]\left(B^k\right)^{-1}{}_{dr} \tag{3-92}
$$

The constants ${}^{(1)}M_l(x_3^0)$, ${}^{(k)}\Omega_{rl}$ and ${}^{(k)}S_t$ are given in Eqs. (F-1) and (F-2) in the Appendix F; ${}^{(k)}Q_l(x_3)$ and B^k in Eqs. (3-84) and (3-87); ${}^{(k)}E_{ij}(x_3)$ in Appendix E; ${}^{(k)}T(x_1,x_2,x_3)$ is defined in Sect. 3.3.2.

For fully bonded layers, Eq. (3-92) modifies as:

$${}^{(k)}P_{ir}(x_3)=\sum_{j=1}^{6}{}^{(k)}E_{ij}(x_3)\,{}^{(k)}E^{-1}{}_{jr}(x_3^k) \tag{3-93}$$

3.3.4 Application to simply supported plates subjected to mechanical loading

In this section, exact solutions for a simply supported anisotropic plate with three layers of equal thickness, symmetrically stacked and joined by two interfaces and subjected to bi-sinusoidal transverse loading are presented. The results are given in tables using at least four digits in order to generate benchmark solutions with enough precision for verification of approximate structural theories. The results are also presented in graph form, to highlight the important influence of the interfacial imperfections on the stress and displacement fields.

The thickness of the plate is *h* and the origin of the coordinate system is placed at mid-thickness of the left edge. Dimensionless stresses and displacements are given in Table 3-7 for plates with $a/h=4$ and different b/h and interfacial stiffnesses. The elastic constants of the layers are $E_L/E_T=25$, $G_{LT}/E_T=0.5$, $G_{TT}/E_T=0.2$, $\nu_{LT}=\nu_{TT}=0.25$ (subscripts *L* and *T* indicate in-plane principal material directions), and the stacking sequence is $(0,90,0)$ so that the *L* direction coincides with x_2 axis in the outer layers. The assumed ratios between the elastic constants of the layers could represent a graphite-epoxy laminate. The plate is subjected to normally applied tractions $f_3=f_u\sin(\pi x_1/b)\sin(\pi x_2/a)$ acting on its upper surface. The interfaces are identical with $K_{S1}=K_{S2}=K_S$ and the results are tabulated for perfectly bonded interfaces, $1/K_S=1/K_N=0$, sliding interfaces in constrained contact, $1/K_N=0$ and $K_S=0$, and partial bonding with dimensionless interfacial stiffnesses $K_Sh/E_T=0.2$ and $K_Nh/E_T=0.5$ (see Eq. (3-50) for the interfacial traction laws used in the model).

In order to avoid interpenetration between the layers, the results presented for the cases with $1/K_N\neq 0$, are valid only for positive applied surface tractions. The model presented in the previous section and the results are valid under the assumption of infinitesimal strains and displacements, which must be verified in each layer. The validity of this assumption and the range of values of the applied load for which the solutions in the tables are correct can be verified by using the maximum dimensionless transverse displacements and stresses given in the tables.

Table 3-7: Simply supported three-layer plate $(0,90,0)$, $a/h=4$: normal surface tractions $f_3 = f_u \sin(\pi x_1/b)\sin(\pi x_2/a)$ acting on upper surface. Elastic constants: $E_L/E_T = 25$, $G_{LT}/E_T = 0.5$, $G_{TT}/E_T = 0.2$ and $\nu_{LT} = \nu_{TT} = 0.25$. L direction coincides with x_2 axis in the outer layers. Subscripts l and u correspond to values below and above the interface. Identical interfaces with $K_{S1} = K_{S2} = K_S$.

T3-7-1: Perfect bonding: $1/K_S = 0$ **and** $1/K_N = 0$

$\frac{b}{h}$	x_3/h							
	-1/2	-1/3	$-1/6_l$	$-1/6_u$	$1/6_l$	$1/6_u$	1/3	1/2
	Dimensionless in-plane displacements: $v_1 E_T/(f_u h)$ *at* $x_1 = 0$ *and* $x_2 = a/2$							
4	1.459	0.900	0.458	0.458	-0.425	-0.425	-0.862	-1.460
10	0.983	0.649	0.354	0.354	-0.288	-0.288	-0.584	-0.935
20	0.540	0.366	0.211	0.211	-0.135	-0.135	-0.293	-0.476
	Dimensionless in-plane displacements: $v_2 E_T/(f_u h)$ *at* $x_1 = b/2$ *and* $x_2 = 0$							
4	0.599	0.145	-0.154	-0.154	0.203	0.203	-0.124	-0.620
10	0.876	0.231	-0.200	-0.200	0.250	0.250	-0.209	-0.897
20	0.910	0.244	-0.201	-0.201	0.252	0.252	-0.221	-0.930
	Dimensionless transverse displacements: $v_3 E_T/(f_u h)$ *at* $x_1 = b/2$ *and* $x_2 = a/2$							
4	4.962	5.020	5.070	5.070	5.226	5.226	5.333	5.431
10	6.992	7.030	7.069	7.069	7.227	7.227	7.345	7.463
20	7.209	7.240	7.275	7.275	7.433	7.433	7.555	7.679
	Dimensionless bending stresses: σ_{11}/f_u *at* $x_1 = b/2$ *and* $x_2 = a/2$							
4	-1.267	-0.713	-0.262	-8.900	8.546	0.476	0.932	1.525
10	-0.482	-0.222	0.005	-2.652	2.433	0.216	0.450	0.724
20	-0.264	-0.078	0.085	-0.692	0.696	0.145	0.314	0.511
	Dimensionless bending stresses: σ_{22}/f_u *at* $x_1 = b/2$ *and* $x_2 = a/2$							
4	-12.08	-3.011	3.040	0.100	0.106	-3.681	2.899	12.81
10	-17.33	-4.569	3.996	0.207	0.000	-4.674	4.440	18.05
20	-17.93	-4.778	4.053	0.229	-0.020	-4.744	4.640	18.64
	Dimensionless shear stresses: σ_{12}/f_u *at* $x_1 = 0$ *and* $x_2 = 0$							
4	0.808	0.410	0.119	0.119	-0.087	-0.087	-0.387	-0.817
10	0.524	0.291	0.108	0.108	-0.074	-0.074	-0.262	-0.508
20	0.283	0.163	0.067	0.067	-0.033	-0.033	-0.132	-0.260

$\frac{b}{h}$	x_3/h									
	-5/12	-1/3	-1/4	-1/6	-1/12	1/12	1/6	1/4	1/3	5/12
	Dimensionless transverse shear stresses: σ_{13}/f_u *at* $x_1 = 0$ *and* $x_2 = a/2$									
4	0.118	0.206	0.266	0.303	0.727	0.755	0.357	0.308	0.235	0.134
10	0.041	0.071	0.091	0.102	0.160	0.169	0.119	0.104	0.080	0.046
20	0.019	0.033	0.043	0.048	0.058	0.061	0.053	0.046	0.036	0.021
	Dimensionless transverse shear stresses: σ_{23}/f_u *at* $x_1 = b/2$ *and* $x_2 = 0$									
4	0.650	0.997	1.114	1.028	1.027	1.017	1.007	1.129	1.030	0.681
10	0.887	1.360	1.522	1.406	1.396	1.384	1.382	1.534	1.391	0.916
20	0.909	1.395	1.561	1.443	1.431	1.419	1.417	1.573	1.426	0.938
	Dimensionless transverse normal stresses: σ_{33}/f_u *at* $x_1 = b/2$ *and* $x_2 = a/2$									
4	0.027	0.093	0.179	0.269	0.372	0.614	0.718	0.811	0.901	0.971
10	0.032	0.109	0.207	0.307	0.402	0.593	0.688	0.788	0.887	0.967
20	0.033	0.110	0.209	0.310	0.404	0.592	0.686	0.786	0.886	0.966

T3-7-2: Partial bonding: $K_S h/E_T = 0.2$ **and** $K_N h/E_T = 0.5$ **(** $f_u > 0$ **)**

$\frac{b}{h}$	x_3/h							
	-1/2	-1/3	-1/6$_l$	-1/6$_u$	1/6$_l$	1/6$_u$	1/3	1/2
	Dimensionless in-plane displacements: $v_1 E_T/(f_u h)$ *at* $x_1 = 0$ *and* $x_2 = a/2$							
4	1.739	0.716	-0.221	0.900	-0.874	0.497	-0.669	-1.963
10	1.507	0.815	0.167	0.734	-0.678	-0.020	-0.764	-1.568
20	0.847	0.483	0.141	0.417	- 0.349	- 0.039	- 0.431	-0.852
	Dimensionless in-plane displacements: $v_2 E_T/(f_u h)$ *at* $x_1 = b/2$ *and* $x_2 = 0$							
4	0.899	0.039	-0.772	0.977	-0.769	1.001	-0.023	-1.115
10	1.511	0.089	-1.250	1.571	-1.326	1.487	-0.071	-1.729
20	1.591	0.100	-1.303	1.647	-1.394	1.541	-0.081	-1.809
	Dimensionless transverse displacements: $v_3 E_T/(f_u h)$ *at* $x_1 = b/2$ *and* $x_2 = a/2$							
4	8.600	8.666	8.693	9.257	9.411	10.72	10.85	10.94
10	14.11	14.16	14.19	14.95	15.11	16.25	16.37	16.47
20	14.77	14.82	14.85	15.62	15.78	16.91	17.04	17.14
	Dimensionless bending stresses: σ_{11}/f_u *at* $x_1 = b/2$ *and* $x_2 = a/2$							
4	-1.546	-0.540	0.398	-17.82	17.56	-0.423	0.746	2.018
10	-0.772	-0.231	0.290	-5.967	5.778	-0.142	0.458	1.087
20	-0.447	- 0.051	0.333	-1.843	1.824	-0.155	0.286	0.744
	Dimensionless bending stresses: σ_{22}/f_u *at* $x_1 = b/2$ *and* $x_2 = a/2$							
4	-18.05	-0.875	15.33	-0.875	0.944	-19.59	0.849	22.64
10	-29.85	-1.757	24.72	-1.198	1.242	-29.09	1.700	34.47
20	-31.35	-1.936	25.77	-1.215	1.253	-30.16	1.870	35.97
	Dimensionless shear stresses: σ_{12}/f_u *at* $x_1 = 0$ *and* $x_2 = 0$							
4	1.036	0.296	-0.390	0.737	-0.645	0.588	-0.272	-1.209
10	0.829	0.334	-0.131	0.535	-0.475	0.226	-0.311	-0.887
20	0.458	0.198	-0.047	0.293	- 0.246	0.106	- 0.176	-0.477

$\frac{b}{h}$	x_3/h									
	-5/12	-1/3	-1/4	-1/6	-1/12	1/12	1/6	1/4	1/3	5/12
	Dimensionless transverse shear stresses: σ_{13}/f_u *at* $x_1 = 0$ *and* $x_2 = a/2$									
4	0.138	0.219	0.248	0.224	1.093	1.119	0.274	0.306	0.272	0.172
10	0.062	0.101	0.118	0.113	0.256	0.266	0.132	0.137	0.117	0.072
20	0.030	0.049	0.057	0.055	0.088	0.091	0.062	0.065	0.055	0.034
	Dimensionless transverse shear stresses: σ_{23}/f_u *at* $x_1 = b/2$ *and* $x_2 = 0$									
4	0.907	1.238	1.065	0.350	0.428	0.430	0.354	1.280	1.522	1.126
10	1.436	1.963	1.962	0.564	0.633	0.632	0.563	1.899	2.238	1.650
20	1.496	2.045	1.764	0.590	0.652	0.651	0.587	1.969	2.319	1.709
	Dimensionless transverse normal stresses: σ_{33}/f_u *at* $x_1 = b/2$ *and* $x_2 = a/2$									
4	0.038	0.123	0.217	0.282	0.355	0.581	0.656	0.733	0.847	0.953
10	0.053	0.171	0.298	0.380	0.425	0.525	0.570	0.660	0.804	0.938
20	0.055	0.176	0.306	0.389	0.431	0.520	0.562	0.653	0.799	0.937

T3-7-3: Sliding interfaces in constrained contact: $K_S = 0$ **and** $1/K_N = 0$

$\frac{b}{h}$	x_3/h							
	-1/2	-1/3	$-1/6_l$	$-1/6_u$	$1/6_l$	$1/6_u$	1/3	1/2
	Dimensionless in-plane displacements: $v_1 E_T/(f_u h)$ *at* $x_1 = 0$ *and* $x_2 = a/2$							
4	1.646	0.035	-1.579	1.341	-1.338	1.821	0.177	-1.484
10	1.111	0.045	-1.023	1.057	-1.044	1.225	0.145	-0.942
20	0.582	0.028	-0.527	0.572	-0.551	0.648	0.087	-0.476
	Dimensionless in-plane displacements: $v_2 E_T/(f_u h)$ *at* $x_1 = b/2$ *and* $x_2 = 0$							
4	1.329	0.002	-1.328	1.726	-1.525	1.364	0.011	-1.359
10	2.172	0.004	-2.168	2.833	-2.549	2.209	0.013	-2.198
20	2.251	0.004	-2.247	2.947	-2.644	2.289	0.014	-2.275
	Dimensionless transverse displacements: $v_3 E_T/(f_u h)$ *at* $x_1 = b/2$ *and* $x_2 = a/2$							
4	13.01	13.07	13.06	13.06	13.22	13.22	13.39	13.49
10	21.07	21.13	21.14	21.14	21.31	21.31	21.45	21.55
20	21.81	21.87	21.88	21.88	22.05	22.05	22.19	22.28
	Dimensionless bending stresses: σ_{11}/f_u *at* $x_1 = b/2$ *and* $x_2 = a/2$							
4	-1.557	0.014	1.588	-26.63	26.85	-1.535	0.069	1.689
10	-0.778	0.045	0.869	-8.731	8.884	-0.689	0.144	0.982
20	-0.535	0.056	0.647	-2.680	2.851	-0.423	0.175	0.776
	Dimensionless bending stresses: σ_{22}/f_u *at* $x_1 = b/2$ *and* $x_2 = a/2$							
4	-26.48	0.004	26.55	-1.540	1.632	-26.99	0.018	27.36
10	-42.84	-0.007	42.91	-2.194	2.221	-43.41	-0.024	43.65
20	-44.33	-0.013	44.40	-2.221	2.233	-44.92	-0.039	45.12
	Dimensionless shear stresses: σ_{12}/f_u *at* $x_1 = 0$ *and* $x_2 = 0$							
4	1.168	0.015	-1.142	1.204	-1.124	1.251	0.074	-1.116
10	0.778	0.018	-0.743	0.860	-0.810	0.828	0.059	-0.715
20	0.405	0.011	-0.383	0.456	-0.424	0.434	0.035	-0.366

$\frac{b}{h}$	x_3/h									
	-5/12	-1/3	-1/4	-1/6	-1/12	1/12	1/6	1/4	1/3	5/12
	Dimensionless transverse shear stresses: σ_{13}/f_u *at* $x_1 = 0$ *and* $x_2 = a/2$									
4	0.131	0.174	0.131	0	1.299	1.302	0	0.134	0.178	0.135
10	0.052	0.069	0.052	0	0.212	0.212	0	0.053	0.070	0.053
20	0.025	0.032	0.025	0	0.048	0.049	0	0.025	0.033	0.025
	Dimensionless transverse shear stresses: σ_{23}/f_u *at* $x_1 = b/2$ *and* $x_2 = 0$									
4	1.289	1.690	1.291	0	0.132	0.132	0	1.319	1.732	1.325
10	2.014	2.641	2.015	0	0.124	0.124	0	2.043	2.681	2.048
20	2.073	2.719	2.075	0	0.113	0.113	0	2.102	2.759	2.107
	Dimensionless transverse normal stresses: σ_{33}/f_u *at* $x_1 = b/2$ *and* $x_2 = a/2$									
4	0.052	0.165	0.277	0.330	0.382	0.609	0.662	0.716	0.831	0.946
10	0.075	0.236	0.397	0.472	0.480	0.513	0.521	0.597	0.760	0.924
20	0.077	0.241	0.405	0.482	0.487	0.506	0.511	0.588	0.755	0.922

Figure 3-12 and Figure 3-13 highlight the influence of the interfacial imperfections on the field variables: in-plane and transverse displacements may become discontinuous at the interfaces and the stress distributions are substantially modified with changes in position and value of the maxima.

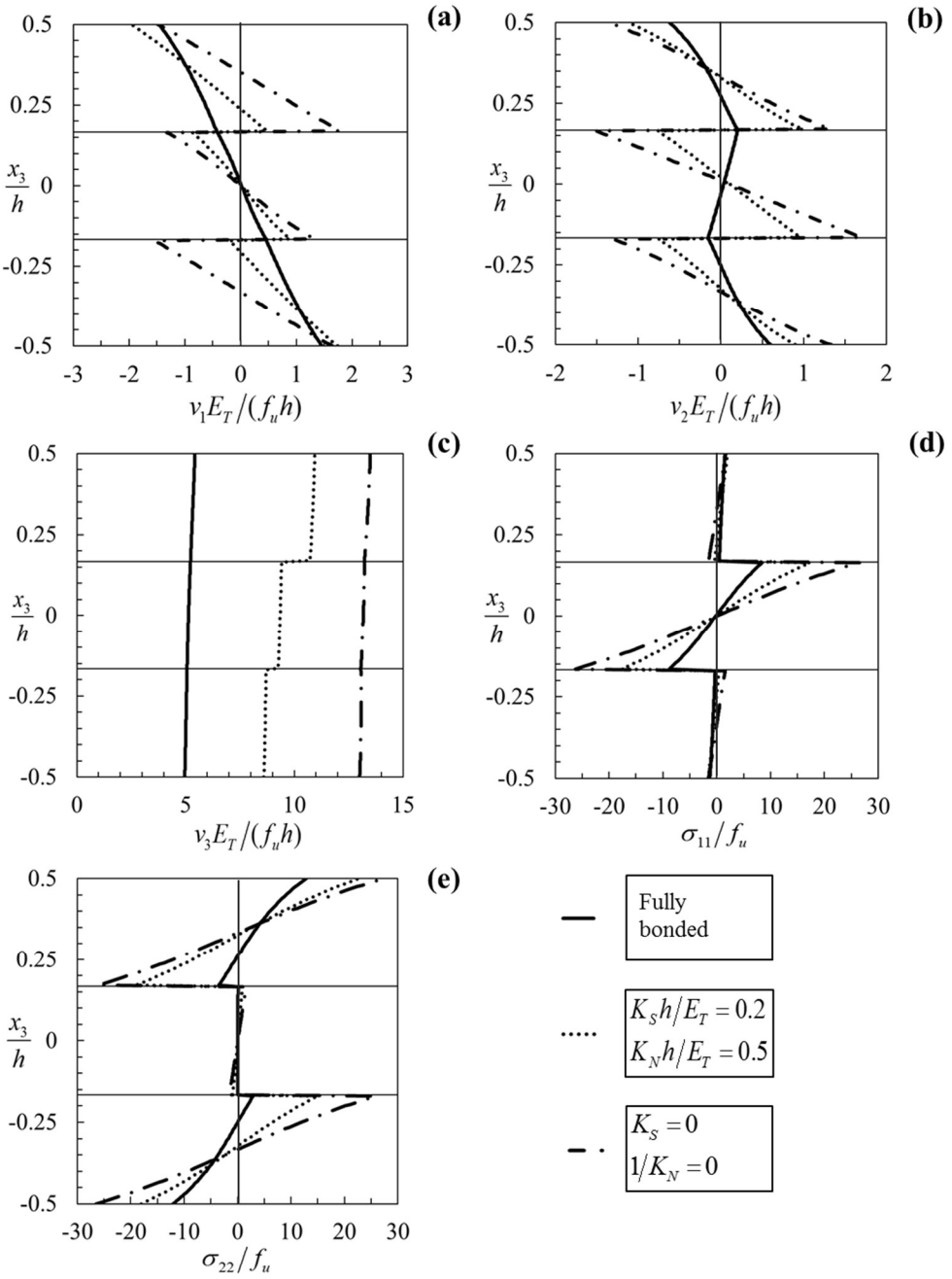

Figure 3-12: Through thickness variation of (a) displacements in x_1 direction at $(x_1 = 0, x_2 = a/2)$, (b) displacements in x_2 direction at $(x_1 = b/2, x_2 = 0)$, (c) transverse displacements at $(x_1 = b/2, x_2 = a/2)$, (d) bending stresses in x_1 direction at $(x_1 = b/2, x_2 = a/2)$ and (e) bending stresses in x_2 direction at $(x_1 = b/2, x_2 = a/2)$ in a simply supported three-layer square plate $(0,90,0)$, $a/h = b/h = 4$, normal surface tractions $f_3 = f_u \sin(\pi x_1/b)\sin(\pi x_2/a)$ acting on upper surface. Elastic constants: $E_L/E_T = 25$, $G_{LT}/E_T = 0.5$, $G_{TT}/E_T = 0.2$ and $\nu_{LT} = \nu_{TT} = 0.25$. L direction coincides with x_2 axis in the outer layers. Identical interfaces with $K_{S1} = K_{S2} = K_S$.

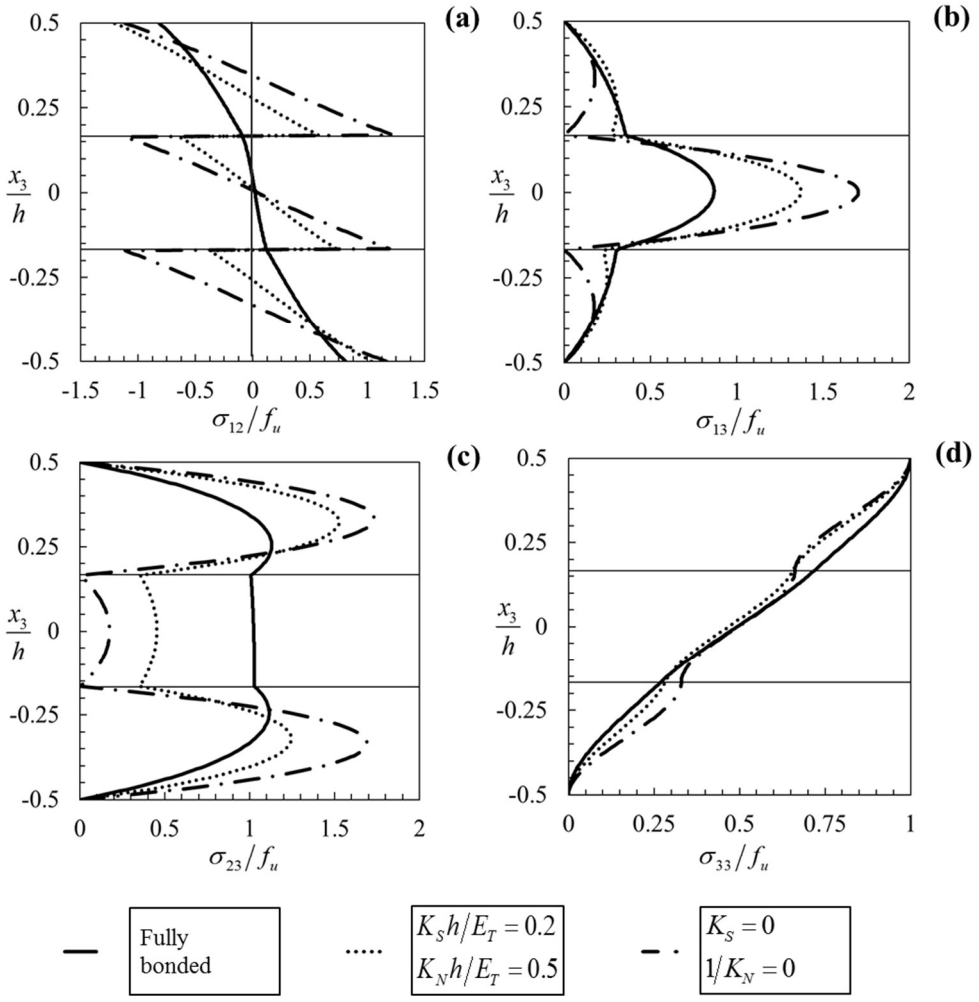

Figure 3-13: Through thickness variation of (a) in-plane shear stresses at $(x_1 = 0, x_2 = 0)$, (b) transverse shear stresses σ_{13} at $(x_1 = 0, x_2 = a/2)$, (c) transverse shear stresses σ_{23} at $(x_1 = b/2, x_2 = 0)$ and (d) transverse normal stresses at $(x_1 = b/2, x_2 = a/2)$ in a simply supported three-layer square plate $(0,90,0)$, $a/h = b/h = 4$, normal surface tractions $f_3 = f_u \sin(\pi x_1/b)\sin(\pi x_2/a)$ acting on upper surface. Elastic constants: $E_L/E_T = 25$, $G_{LT}/E_T = 0.5$, $G_{TT}/E_T = 0.2$ and $\nu_{LT} = \nu_{TT} = 0.25$. L direction coincides with x_2 axis in the outer layers. Identical interfaces with $K_{S1} = K_{S2} = K_S$.

3.3.5 Application to simply supported plates subjected to thermal loading

This section presents exact solutions of temperature, displacements and stresses in a simply supported symmetrically laminated plate subjected to bi-sinusoidal thermal loading. The plate is composed of three layers of equal thickness, joined by two identical interfaces with $K_{S1} = K_{S2} = K_S$. The origin of the coordinate system is at the mid-thickness. The thermo-elastic constants of the layers are $E_L/E_T = 25$, $G_{LT}/E_T = 0.5$, $G_{TT}/E_T = 0.2$, $\nu_{LT} = \nu_{TT} = 0.25$, $\alpha_T/\alpha_L = 62$ and $K_L/K_T = 38$ (subscripts L and T indicate in-plane principal material directions). The stacking sequence is $(0,90,0)$ so that the L direction coincides with x_2 axis in the outer layers.

Results in Table 3-8 and Table 3-9 correspond to plates with $a/h = 4$ and subjected to thermal loading $T = T_u \sin(\pi x_1/b)\sin(\pi x_2/a)$ on the upper surface of the plate; the temperature increment at the lower surface of the plate is zero. Results in Table 3-8 correspond to layers in perfect thermal contact, $R = 0$, and those in Table 3-9 to layers with interfacial thermal resistance, $RK_L/h = 15$. Dimensionless stresses and displacements are presented for three b/h equal to 4, 10, 20 and for three cases of perfect bonding, $1/K_S = 1/K_N = 0$, partial bonding with dimensionless interfacial stiffnesses equal to $K_S h/E_T = 0.2$ and $1/K_N = 0$, and sliding interfaces in constrained contact, $K_S = 0$ and $1/K_N = 0$.

Table 3-8: Simply supported three-layer plate $(0,90,0)$, $a/h=4$: applied temperature $T=T_u\sin(\pi x_1/b)\sin(\pi x_2/a)$ on upper surface. Thermo-elastic constants: $E_L/E_T=25$, $G_{LT}/E_T=0.5$, $G_{TT}/E_T=0.2$, $\nu_{LT}=\nu_{TT}=0.25$, $\alpha_T/\alpha_L=62$ and $K_L/K_T=38$. L direction coincides with x_2 axis in the outer layers. Perfect thermal contact, $R=0$. Subscripts *l* and *u* correspond to values below and above the interface. Identical interfaces with $K_{S1}=K_{S2}=K_S$.

T3-8-1: Perfect bonding: $1/K_S=0$ **and** $1/K_N=0$; **Perfect thermal contact:** $R=0$

$\frac{b}{h}$	x_3/h							
	-1/2	-1/3	-1/6$_l$	-1/6$_u$	1/6$_l$	1/6$_u$	1/3	1/2
	Dimensionless in-plane displacements: $v_1/(\alpha_L T_u h)$ *at* $x_1=0$ *and* $x_2=a/2$							
4	1.543	0.669	-0.044	-0.044	-3.188	-3.188	-8.604	-12.77
10	-2.515	-2.613	-2.795	-2.795	-3.980	-3.980	-6.168	-7.720
20	-3.453	-3.494	-3.661	-3.661	-4.207	-4.207	-5.182	-5.900
	Dimensionless in-plane displacements: $v_2/(\alpha_L T_u h)$ *at* $x_1=b/2$ *and* $x_2=0$							
4	0.853	0.141	-0.429	-0.429	-0.182	-0.182	-1.008	-2.942
10	-0.010	-0.130	-0.390	-0.390	-0.660	-0.660	-1.150	-2.713
20	-0.294	-0.236	-0.407	-0.407	-0.800	-0.800	-1.182	-2.631
	Dimensionless transverse displacements: $v_3/(\alpha_L T_u h)$ *at* $x_1=b/2$ *and* $x_2=a/2$							
4	7.470	7.616	7.966	7.966	10.46	10.46	14.20	22.66
10	0.688	0.837	1.473	1.473	5.492	5.492	9.834	18.71
20	-1.329	-1.149	-0.405	-0.405	4.078	4.078	8.579	17.55
	Dimensionless bending stresses: $\sigma_{11}/(\alpha_L T_u E_T)$ *at* $x_1=b/2$ *and* $x_2=a/2$							
4	-1.383	-1.366	-2.075	-0.417	55.03	-9.494	-20.54	-51.78
10	0.794	-1.039	-4.130	18.77	21.05	-14.60	-26.97	-59.44
20	0.602	-1.595	-5.245	10.63	5.653	-16.15	-28.48	-60.96
	Dimensionless bending stresses: $\sigma_{22}/(\alpha_L T_u E_T)$ *at* $x_1=b/2$ *and* $x_2=a/2$							
4	-17.10	-3.410	7.071	-1.848	-11.27	-3.554	3.650	19.83
10	0.403	1.534	4.578	-4.560	-15.15	2.896	4.151	13.41
20	5.925	3.359	4.294	-5.437	-16.17	4.845	4.251	11.43
	Dimensionless shear stresses: $\sigma_{12}/(\alpha_L T_u E_T)$ *at* $x_1=0$ *and* $x_2=0$							
4	0.941	0.318	-0.186	-0.186	-1.324	-1.324	-3.774	-6.169
10	-0.989	-1.047	-1.159	-1.159	-1.667	-1.667	-2.603	-3.458
20	-1.379	-1.391	-1.470	-1.470	-1.715	-1.715	-2.128	-2.523

$\frac{b}{h}$	x_3/h									
	-5/12	-1/3	-1/4	-1/6	-1/12	1/12	1/6	1/4	1/3	5/12
	Dimensionless transverse shear stresses: $\sigma_{13}/(\alpha_L T_u E_T)$ *at* $x_1=0$ *and* $x_2=a/2$									
4	0.138	0.255	0.363	0.477	0.216	-2.356	-5.253	-4.644	-3.761	-2.344
10	-0.075	-0.129	-0.155	-0.146	-0.708	-1.859	-2.490	-2.180	-1.741	-1.066
20	-0.091	-0.169	-0.230	-0.271	-0.499	-0.915	-1.107	-0.989	-0.805	-0.501
	Dimensionless transverse shear stresses: $\sigma_{23}/(\alpha_L T_u E_T)$ *at* $x_1=b/2$ *and* $x_2=0$									
4	0.895	1.331	1.401	1.117	1.252	1.796	2.320	2.323	2.015	1.306
10	-0.065	-0.168	-0.331	-0.593	-0.260	0.857	1.695	1.463	1.180	0.743
20	-0.342	-0.601	-0.836	-1.101	-0.690	0.619	1.551	1.252	0.970	0.600
	Dimensionless transverse normal stresses: $\sigma_{33}/(\alpha_L T_u E_T)$ *at* $x_1=b/2$ *and* $x_2=a/2$									
4	0.037	0.125	0.236	0.348	0.451	0.541	0.433	0.262	0.129	0.036
10	-0.003	-0.013	-0.033	-0.066	-0.106	-0.141	-0.116	-0.074	-0.038	-0.012
20	-0.012	-0.045	-0.095	-0.161	-0.226	-0.257	-0.200	-0.122	-0.061	-0.018

T3-8-2: Partial bonding: $K_S h/E_T = 0.2$ **and** $1/K_N = 0$; **Perfect thermal contact:** $R = 0$

$\frac{b}{h}$	x_3/h							
	-1/2	-1/3	$-1/6_l$	$-1/6_u$	$1/6_l$	$1/6_u$	1/3	1/2
	Dimensionless in-plane displacements: $v_1/(\alpha_L T_u h)$ *at* $x_1 = 0$ *and* $x_2 = a/2$							
4	1.038	0.061	-0.842	0.439	-2.089	-14.18	-17.89	-21.48
10	-1.434	-1.588	-1.769	-1.804	-2.824	-10.91	-12.63	-14.08
20	-2.071	-2.107	-2.205	-2.778	-3.220	-7.196	-8.000	-8.674
	Dimensionless in-plane displacements: $v_2/(\alpha_L T_u h)$ *at* $x_1 = b/2$ *and* $x_2 = 0$							
4	0.793	-0.032	-0.888	-1.047	-3.081	0.699	-0.479	-2.484
10	0.148	-0.143	-0.578	-3.585	-4.876	-0.150	-0.947	-2.692
20	-0.161	-0.196	-0.417	-4.492	-5.362	-0.481	-1.068	-2.632
	Dimensionless transverse displacements: $v_3/(\alpha_L T_u h)$ *at* $x_1 = b/2$ *and* $x_2 = a/2$							
4	7.988	8.110	8.414	8.414	10.78	10.78	14.20	22.38
10	2.346	2.513	3.164	3.164	6.988	6.988	11.25	20.05
20	-0.285	-0.092	0.668	0.668	4.907	4.907	9.399	18.36
	Dimensionless bending stresses: $\sigma_{11}/(\alpha_L T_u E_T)$ *at* $x_1 = b/2$ *and* $x_2 = a/2$							
4	-0.974	-0.859	-1.390	-9.852	33.90	-1.061	-13.35	-45.00
10	0.422	-1.355	-4.405	11.60	12.77	-12.52	-24.98	-57.44
20	0.358	-1.817	-5.458	7.975	2.673	-15.73	-28.05	-60.52
	Dimensionless bending stresses: $\sigma_{22}/(\alpha_L T_u E_T)$ *at* $x_1 = b/2$ *and* $x_2 = a/2$							
4	-15.82	0.101	16.23	-1.490	-9.252	-18.80	-4.952	12.53
10	-2.804	1.717	8.213	-2.111	-11.92	-6.606	0.675	13.51
20	3.248	2.513	4.440	-2.241	-12.61	-1.308	2.123	11.55
	Dimensionless shear stresses: $\sigma_{12}/(\alpha_L T_u E_T)$ *at* $x_1 = 0$ *and* $x_2 = 0$							
4	0.719	0.011	-0.679	-0.239	-2.030	-5.294	-7.214	-9.412
10	-0.540	-0.646	-0.786	-1.272	-1.875	-4.308	-5.110	-5.952
20	-0.826	-0.843	-0.898	-1.444	-1.685	-2.864	-3.225	-3.613

$\frac{b}{h}$	x_3/h									
	-5/12	-1/3	-1/4	-1/6	-1/12	1/12	1/6	1/4	1/3	5/12
	Dimensionless transverse shear stresses: $\sigma_{13}/(\alpha_L T_u E_T)$ *at* $x_1 = 0$ *and* $x_2 = a/2$									
4	0.094	0.162	0.212	0.256	0.578	-0.619	-2.418	-2.586	-2.422	-1.685
10	-0.037	-0.055	-0.049	-0.007	-0.391	-1.181	-1.617	-1.532	-1.311	-0.851
20	-0.052	-0.091	-0.114	-0.115	-0.305	-0.644	-0.795	-0.757	-0.651	-0.424
	Dimensionless transverse shear stresses: $\sigma_{23}/(\alpha_L T_u E_T)$ *at* $x_1 = b/2$ *and* $x_2 = 0$									
4	0.770	1.005	0.757	-0.032	0.057	0.392	0.756	1.358	1.453	1.042
10	0.092	0.038	-0.176	-0.601	-0.435	0.315	0.945	1.143	1.097	0.759
20	-0.198	-0.372	-0.563	-0.815	-0.612	0.270	0.976	0.981	0.874	0.589
	Dimensionless transverse normal stresses: $\sigma_{33}/(\alpha_L T_u E_T)$ *at* $x_1 = b/2$ *and* $x_2 = a/2$									
4	0.032	0.101	0.174	0.216	0.247	0.299	0.242	0.149	0.077	0.023
10	0.003	0.007	0.002	-0.023	-0.063	-0.118	-0.114	-0.086	-0.049	-0.015
20	-0.007	-0.027	-0.058	-0.105	-0.155	-0.197	-0.167	-0.112	-0.060	-0.018

T3-8-3: Sliding interfaces in constrained contact: $K_S = 0$ **and** $1/K_N = 0$; **Perfect thermal contact:** $R = 0$

$\frac{b}{h}$	x_3/h							
	-1/2	-1/3	$-1/6_l$	$-1/6_u$	$1/6_l$	$1/6_u$	1/3	1/2
	Dimensionless in-plane displacements: $v_1/(\alpha_L T_u h)$ *at* $x_1 = 0$ *and* $x_2 = a/2$							
4	-0.254	-0.780	-1.333	0.462	-0.640	-24.06	-25.75	-28.29
10	-1.513	-1.589	-1.691	0.187	-0.147	-23.95	-24.58	-25.59
20	-1.107	-1.121	-1.150	0.211	0.077	-14.87	-15.17	-15.67
	Dimensionless in-plane displacements: $v_2/(\alpha_L T_u h)$ *at* $x_1 = b/2$ *and* $x_2 = 0$							
4	0.407	-0.003	-0.435	-4.256	-5.838	0.768	-0.124	-1.694
10	0.062	-0.042	-0.196	-11.42	-12.556	0.147	-0.647	-2.224
20	-0.068	-0.064	-0.120	-13.622	-14.578	-0.114	-0.861	-2.427
	Dimensionless transverse displacements: $v_3/(\alpha_L T_u h)$ *at* $x_1 = b/2$ *and* $x_2 = a/2$							
4	3.954	4.031	4.307	4.307	6.485	6.485	9.615	17.57
10	0.832	0.998	1.660	1.660	5.077	5.077	9.197	17.86
20	-0.247	-0.042	0.740	0.740	4.477	4.477	8.939	17.86
	Dimensionless bending stresses: $\sigma_{11}/(\alpha_L T_u E_T)$ *at* $x_1 = b/2$ *and* $x_2 = a/2$							
4	0.119	-0.218	-1.126	-9.706	5.889	6.675	-7.228	-39.80
10	0.464	-1.375	-4.497	-2.523	-6.767	-8.456	-21.27	-53.91
20	0.188	-1.993	-5.660	-1.967	-8.463	-14.57	-26.96	-59.46
	Dimensionless bending stresses: $\sigma_{22}/(\alpha_L T_u E_T)$ *at* $x_1 = b/2$ *and* $x_2 = a/2$							
4	-7.964	-0.317	7.372	1.000	-7.393	-18.24	-10.39	-1.694
10	-1.096	-0.278	0.695	3.905	-6.073	-11.412	-4.291	5.189
20	1.376	-0.123	-1.408	4.852	-5.459	-8.199	-1.675	7.790
	Dimensionless shear stresses: $\sigma_{12}/(\alpha_L T_u E_T)$ *at* $x_1 = 0$ *and* $x_2 = 0$							
4	0.060	-0.307	-0.694	-1.490	-2.544	-9.146	-10.16	-11.78
10	-0.584	-0.631	-0.695	-1.720	-2.030	-9.383	-9.754	-10.40
20	-0.440	-0.445	-0.461	-0.987	-1.115	-5.848	-6.024	-6.344

$\frac{b}{h}$	x_3/h									
	-5/12	-1/3	-1/4	-1/6	-1/12	1/12	1/6	1/4	1/3	5/12
	Dimensionless transverse shear stresses: $\sigma_{13}/(\alpha_L T_u E_T)$ *at* $x_1 = 0$ *and* $x_2 = a/2$									
4	-0.006	-0.013	-0.015	0.000	0.385	0.390	0.000	-0.878	-1.342	-1.169
10	-0.040	-0.058	-0.048	0.000	-0.034	-0.033	0.000	-0.342	-0.530	-0.465
20	-0.025	-0.036	-0.029	0.000	-0.029	-0.028	0.000	-0.168	-0.262	-0.231
	Dimensionless transverse shear stresses: $\sigma_{23}/(\alpha_L T_u E_T)$ *at* $x_1 = b/2$ *and* $x_2 = 0$									
4	0.374	0.491	0.375	0.000	-0.142	-0.199	0.000	0.431	0.578	0.454
10	0.041	0.055	0.043	0.000	-0.231	-0.247	0.000	0.371	0.509	0.410
20	-0.067	-0.087	-0.064	0.000	-0.249	-0.253	0.000	0.345	0.480	0.392
	Dimensionless transverse normal stresses: $\sigma_{33}/(\alpha_L T_u E_T)$ *at* $x_1 = b/2$ *and* $x_2 = a/2$									
4	0.014	0.043	0.071	0.085	0.094	0.128	0.135	0.120	0.079	0.028
10	0.001	0.003	0.005	0.006	-0.003	-0.043	-0.053	-0.044	-0.026	-0.008
20	-0.003	-0.008	-0.014	-0.017	-0.026	-0.067	-0.076	-0.065	-0.040	-0.013

Table 3-9: Simply supported three-layer plate $(0,90,0)$, $a/h=4$: applied temperature $T=T_u\sin(\pi x_1/b)\sin(\pi x_2/a)$ on upper surface. Thermo-elastic constants: $E_L/E_T=25$, $G_{LT}/E_T=0.5$, $G_{TT}/E_T=0.2$, $\nu_{LT}=\nu_{TT}=0.25$, $\alpha_T/\alpha_L=62$ and $K_L/K_T=38$. L direction coincides with x_2 axis in the outer layers. Imperfect thermal contact with $RK_L/h=15$. Subscripts *l* and *u* correspond to values below and above the interface, Identical interfaces with $K_{S1}=K_{S2}=K_S$.

T3-9-1: Perfect bonding: $1/K_S=0$ and $1/K_N=0$; **Imperfect thermal contact:** $RK_L/h=15$

$\frac{b}{h}$	x_3/h							
	-1/2	-1/3	$-1/6_l$	$-1/6_u$	$1/6_l$	$1/6_u$	1/3	1/2
	Dimensionless in-plane displacements: $v_1/(\alpha_L T_u h)$ *at* $x_1=0$ *and* $x_2=a/2$							
4	1.926	0.927	0.068	0.068	-3.295	-3.295	-8.945	-13.20
10	-2.277	-2.418	-2.671	-2.671	-3.931	-3.931	-6.181	-7.748
20	-3.334	-3.390	-3.589	-3.589	-4.170	-4.170	-5.176	-5.902
	Dimensionless in-plane displacements: $v_2/(\alpha_L T_u h)$ *at* $x_1=b/2$ *and* $x_2=0$							
4	1.006	0.204	-0.390	-0.390	-0.115	-0.115	-1.007	-3.012
10	0.117	-0.070	-0.343	-0.343	-0.609	-0.609	-1.134	-2.719
20	-0.206	-0.197	-0.381	-0.381	-0.775	-0.775	-1.181	-2.654
	Dimensionless transverse displacements: $v_3/(\alpha_L T_u h)$ *at* $x_1=b/2$ *and* $x_2=a/2$							
4	8.555	8.654	8.788	8.788	10.213	10.21	14.72	23.37
10	1.533	1.574	1.791	1.791	5.008	5.008	9.855	18.87
20	-0.739	-0.678	-0.381	-0.381	3.704	3.704	8.671	17.77
	Dimensionless bending stresses: $\sigma_{11}/(\alpha_L T_u E_T)$ *at* $x_1=b/2$ *and* $x_2=a/2$							
4	-1.715	-0.944	-0.447	-2.282	60.97	-15.13	-22.39	-51.42
10	0.694	0.063	-1.017	17.26	23.88	-18.32	-28.34	-59.43
20	0.566	-0.378	-1.928	9.102	8.049	-19.58	-29.75	-60.95
	Dimensionless bending stresses: $\sigma_{22}/(\alpha_L T_u E_T)$ *at* $x_1=b/2$ *and* $x_2=a/2$							
4	-20.18	-4.298	7.409	-1.373	-5.375	-8.575	2.319	21.29
10	-2.126	1.108	5.709	-5.419	-10.25	-0.519	2.960	13.53
20	4.189	3.385	5.951	-7.367	-12.279	2.122	3.411	11.86
	Dimensionless shear stresses: $\sigma_{12}/(\alpha_L T_u E_T)$ *at* $x_1=0$ *and* $x_2=0$							
4	1.151	0.444	-0.126	-0.126	-1.339	-1.339	-3.908	-6.367
10	-0.876	-0.960	-1.103	-1.103	-1.639	-1.639	-2.606	-3.470
20	-1.325	-1.347	-1.439	-1.439	-1.698	-1.698	-2.125	-2.526

$\frac{b}{h}$	x_3/h									
	-5/12	-1/3	-1/4	-1/6	-1/12	1/12	1/6	1/4	1/3	5/12
	Dimensionless transverse shear stresses: $\sigma_{13}/(\alpha_L T_u E_T)$ *at* $x_1=0$ *and* $x_2=a/2$									
4	0.160	0.272	0.344	0.381	0.189	-2.575	-5.771	-4.875	-3.830	-2.342
10	-0.073	-0.140	-0.201	-0.253	-0.785	-1.962	-2.650	-2.261	-1.774	-1.074
20	-0.091	-0.177	-0.257	-0.331	-0.543	-0.967	-1.182	-1.027	-0.821	-0.504
	Dimensionless transverse shear stresses: $\sigma_{23}/(\alpha_L T_u E_T)$ *at* $x_1=b/2$ *and* $x_2=0$									
4	1.063	1.593	1.706	1.424	1.508	1.751	1.966	2.220	2.043	1.365
10	0.061	0.017	-0.141	-0.450	-0.102	0.773	1.344	1.291	1.114	0.731
20	-0.261	-0.496	-0.757	-1.100	-0.610	0.577	1.305	1.146	0.945	0.608
	Dimensionless transverse normal stresses: $\sigma_{33}/(\alpha_L T_u E_T)$ *at* $x_1=b/2$ *and* $x_2=a/2$									
4	0.044	0.148	0.278	0.407	0.525	0.621	0.478	0.269	0.124	0.034
10	0.002	0.002	-0.006	-0.030	-0.062	-0.092	-0.084	-0.062	-0.035	-0.011
20	-0.009	-0.036	-0.080	-0.144	-0.206	-0.231	-0.184	-0.118	-0.061	-0.018

T3-9-2: Partial bonding: $K_S h/E_T = 0.2$ and $1/K_N = 0$; **Imperfect thermal contact:** $RK_L/h = 15$

$\frac{b}{h}$	x_3/h							
	-1/2	-1/3	-1/6$_l$	-1/6$_u$	1/6$_l$	1/6$_u$	1/3	1/2
	Dimensionless in-plane displacements: $v_1/(\alpha_L T_u h)$ *at* $x_1 = 0$ *and* $x_2 = a/2$							
4	1.421	0.429	-0.496	0.458	-2.043	-15.39	-19.08	-22.61
10	-1.002	-1.153	-1.347	-1.753	-2.747	-11.35	-13.06	-14.47
20	-1.829	-1.858	-1.957	-2.746	-3.170	-7.403	-8.203	-8.863
	Dimensionless in-plane displacements: $v_2/(\alpha_L T_u h)$ *at* $x_1 = b/2$ *and* $x_2 = 0$							
4	0.839	0.004	-0.822	-0.183	-2.000	0.661	-0.475	-2.458
10	0.191	-0.091	-0.466	-2.894	-3.900	-0.221	-0.951	-2.635
20	-0.150	-0.152	-0.301	-4.222	-4.783	-0.574	-1.085	-2.588
	Dimensionless transverse displacements: $v_3/(\alpha_L T_u h)$ *at* $x_1 = b/2$ *and* $x_2 = a/2$							
4	8.227	8.300	8.390	8.390	9.734	9.734	13.89	22.23
10	2.422	2.481	2.716	2.716	5.783	5.783	10.55	19.48
20	-0.469	-0.395	-0.082	-0.082	3.782	3.782	8.737	17.82
	Dimensionless bending stresses: $\sigma_{11}/(\alpha_L T_u E_T)$ *at* $x_1 = b/2$ *and* $x_2 = a/2$							
4	-1.284	-0.522	0.041	-10.06	36.62	-5.815	-14.53	-44.12
10	0.278	-0.328	-1.403	10.54	15.20	-16.06	-26.21	-57.33
20	0.318	-0.626	-2.190	6.554	4.914	-19.10	-29.29	-60.50
	Dimensionless bending stresses: $\sigma_{22}/(\alpha_L T_u E_T)$ *at* $x_1 = b/2$ *and* $x_2 = a/2$							
4	-16.80	-0.265	15.97	-1.654	-4.193	-21.523	-6.179	12.23
10	-3.672	1.420	8.029	-3.477	-7.749	-7.568	-0.110	12.40
20	3.027	2.451	4.314	-4.365	-9.153	-1.693	1.638	10.69
	Dimensionless shear stresses: $\sigma_{12}/(\alpha_L T_u E_T)$ *at* $x_1 = 0$ *and* $x_2 = 0$							
4	0.887	0.170	-0.518	0.108	-1.587	-5.786	-7.679	-9.844
10	-0.363	-0.467	-0.602	-1.143	-1.691	-4.490	-5.278	-6.097
20	-0.730	-0.741	-0.792	-1.410	-1.621	-2.952	-3.307	-3.684

$\frac{b}{h}$	x_3/h									
	-5/12	-1/3	-1/4	-1/6	-1/12	1/12	1/6	1/4	1/3	5/12
	Dimensionless transverse shear stresses: $\sigma_{13}/(\alpha_L T_u E_T)$ *at* $x_1 = 0$ *and* $x_2 = a/2$									
4	0.116	0.183	0.207	0.191	0.529	-0.754	-2.670	-2.632	-2.377	-1.629
10	-0.029	-0.054	-0.072	-0.081	-0.440	-1.244	-1.720	-1.572	-1.319	-0.847
20	-0.049	-0.092	-0.129	-0.158	-0.334	-0.676	-0.847	-0.778	-0.656	-0.423
	Dimensionless transverse shear stresses: $\sigma_{23}/(\alpha_L T_u E_T)$ *at* $x_1 = b/2$ *and* $x_2 = 0$									
4	0.831	1.108	0.890	0.128	0.226	0.398	0.532	1.250	1.415	1.037
10	0.141	0.118	-0.077	-0.486	-0.269	0.323	0.736	0.986	0.988	0.699
20	-0.186	-0.353	-0.539	-0.784	-0.487	0.314	0.842	0.872	0.793	0.542
	Dimensionless transverse normal stresses: $\sigma_{33}/(\alpha_L T_u E_T)$ *at* $x_1 = b/2$ *and* $x_2 = a/2$									
4	0.035	0.111	0.192	0.242	0.281	0.337	0.261	0.148	0.073	0.021
10	0.005	0.013	0.014	-0.005	-0.037	-0.079	-0.084	-0.069	-0.042	-0.014
20	-0.007	-0.025	-0.056	-0.100	-0.145	-0.173	-0.146	-0.100	-0.054	-0.017

T3-9-3: Sliding interfaces in constrained contact: $K_S = 0$ and $1/K_N = 0$; **Imperfect thermal contact:** $RK_L/h = 15$

$\frac{b}{h}$	x_3/h							
	-1/2	-1/3	$-1/6_l$	$-1/6_u$	$1/6_l$	$1/6_u$	1/3	1/2
	Dimensionless in-plane displacements: $v_1/(\alpha_L T_u h)$ *at* $x_1 = 0$ *and* $x_2 = a/2$							
4	0.194	-0.190	-0.581	0.332	-0.430	-26.35	-27.73	-30.02
10	-0.587	-0.602	-0.626	0.101	-0.069	-25.22	-25.74	-26.65
20	-0.504	-0.486	-0.473	0.158	0.105	-15.57	-15.82	-16.28
	Dimensionless in-plane displacements: $v_2/(\alpha_L T_u h)$ *at* $x_1 = b/2$ *and* $x_2 = 0$							
4	0.310	0.000	-0.317	-2.273	-3.309	0.557	-0.134	-1.554
10	-0.006	-0.016	-0.045	-9.352	-9.921	-0.075	-0.677	-2.099
20	-0.130	-0.028	0.049	-12.66	-13.07	-0.317	-0.898	-2.333
	Dimensionless transverse displacements: $v_3/(\alpha_L T_u h)$ *at* $x_1 = b/2$ *and* $x_2 = a/2$							
4	3.027	3.056	3.124	3.124	4.344	4.344	8.173	16.28
10	0.030	0.092	0.342	0.342	3.089	3.089	7.693	16.48
20	-1.084	-0.998	-0.661	-0.661	2.748	2.748	7.667	16.71
	Dimensionless bending stresses: $\sigma_{11}/(\alpha_L T_u E_T)$ *at* $x_1 = b/2$ *and* $x_2 = a/2$							
4	-0.214	-0.053	-0.034	-7.208	5.108	2.799	-7.783	-38.46
10	0.186	-0.521	-1.713	-2.790	-4.679	-11.71	-22.27	-53.60
20	0.105	-0.864	-2.474	-3.196	-6.320	-17.84	-28.12	-59.38
	Dimensionless bending stresses: $\sigma_{22}/(\alpha_L T_u E_T)$ *at* $x_1 = b/2$ *and* $x_2 = a/2$							
4	-6.141	-0.079	6.003	-0.026	-3.512	-17.36	-11.18	-4.107
10	0.165	-0.105	-0.318	1.462	-3.205	-9.331	-4.494	2.818
20	2.582	-0.053	-2.599	2.184	-2.738	-6.390	-1.747	5.967
	Dimensionless shear stresses: $\sigma_{12}/(\alpha_L T_u E_T)$ *at* $x_1 = 0$ *and* $x_2 = 0$							
4	0.198	-0.075	-0.353	-0.763	-1.469	-10.13	-10.94	-12.40
10	-0.232	-0.239	-0.253	-1.429	-1.586	-9.918	-10.21	-10.80
20	-0.208	-0.193	-0.182	-0.932	-0.985	-6.140	-6.284	-6.577

$\frac{b}{h}$	x_3/h									
	-5/12	-1/3	-1/4	-1/6	-1/12	1/12	1/6	1/4	1/3	5/12
	Dimensionless transverse shear stresses: $\sigma_{13}/(\alpha_L T_u E_T)$ *at* $x_1 = 0$ *and* $x_2 = a/2$									
4	0.019	0.024	0.017	0.000	0.302	0.305	0.000	-0.754	-1.194	-1.067
10	-0.016	-0.023	-0.019	0.000	-0.015	-0.014	0.000	-0.308	-0.490	-0.438
20	-0.012	-0.017	-0.014	0.000	-0.014	-0.014	0.000	-0.152	-0.243	-0.218
	Dimensionless transverse shear stresses: $\sigma_{23}/(\alpha_L T_u E_T)$ *at* $x_1 = b/2$ *and* $x_2 = 0$									
4	0.296	0.388	0.296	0.000	-0.049	-0.080	0.000	0.346	0.468	0.370
10	-0.012	-0.015	-0.011	0.000	-0.105	-0.118	0.000	0.265	0.372	0.306
20	-0.122	-0.159	-0.121	0.000	-0.118	-0.122	0.000	0.260	0.370	0.309
	Dimensionless transverse normal stresses: $\sigma_{33}/(\alpha_L T_u E_T)$ *at* $x_1 = b/2$ *and* $x_2 = a/2$									
4	0.012	0.036	0.061	0.073	0.082	0.120	0.128	0.115	0.077	0.027
10	-0.001	-0.002	-0.004	-0.004	-0.008	-0.027	-0.032	-0.026	-0.015	-0.005
20	-0.005	-0.014	-0.024	-0.029	-0.033	-0.053	-0.057	-0.049	-0.030	-0.010

Figure 3-14, Figure 3-15 and Figure 3-16 depict through thickness variations of temperature, displacements and stresses in a three-layer simply supported square plate with two identical interfaces and $a/h = b/h = 8$. The plate is subjected to temperature $T_0 \sin(\pi x_1/b)\sin(\pi x_2/a)$ and $-T_0 \sin(\pi x_1/b)\sin(\pi x_2/a)$ on its upper and lower surfaces, respectively. The material properties and the stacking sequence are given in the caption of the figures. To illustrate the effect of the interfacial thermal

imperfections on the field variables, results for three cases of thermally perfect interfaces, interfaces with intermediate thermal resistance $RK_L/h = 15$ and impermeable interfaces are presented; the interfaces are assumed to be mechanically perfect. A non-zero interfacial thermal resistance induces temperature jumps at the layer interfaces (Figure 3-14) and modifies displacement and stress distributions.

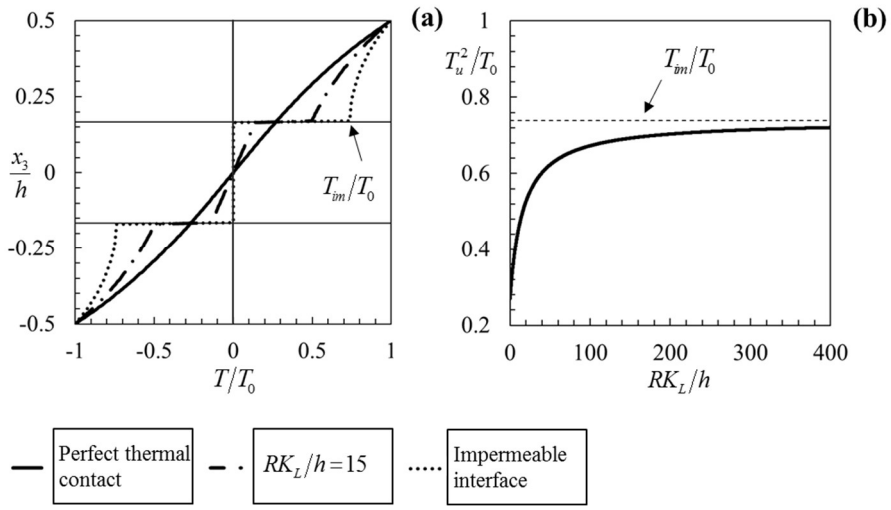

Figure 3-14: (a) Through-thickness temperature distribution at $(x_1 = b/2, x_2 = a/2)$ in a three-layer plate $(0,90,0)$, $a/h = b/h = 8$, applied temperature $T_0 \sin(\pi x_1/b)\sin(\pi x_2/a)$ on upper and $-T_0 \sin(\pi x_1/b)\sin(\pi x_2/a)$ on lower surfaces, and (b) normalized temperature in the upper layer at the interface at $(x_1 = b/2, x_2 = a/2)$ on increasing RK_L/h ($RK_L/h = 0$ perfect contact; $h/(RK_L) = 0$ impermeable interface). The thermal conductivities of the layers are $K_L/K_T = 38$. L direction coincides with x_2 axis in the outer layers.

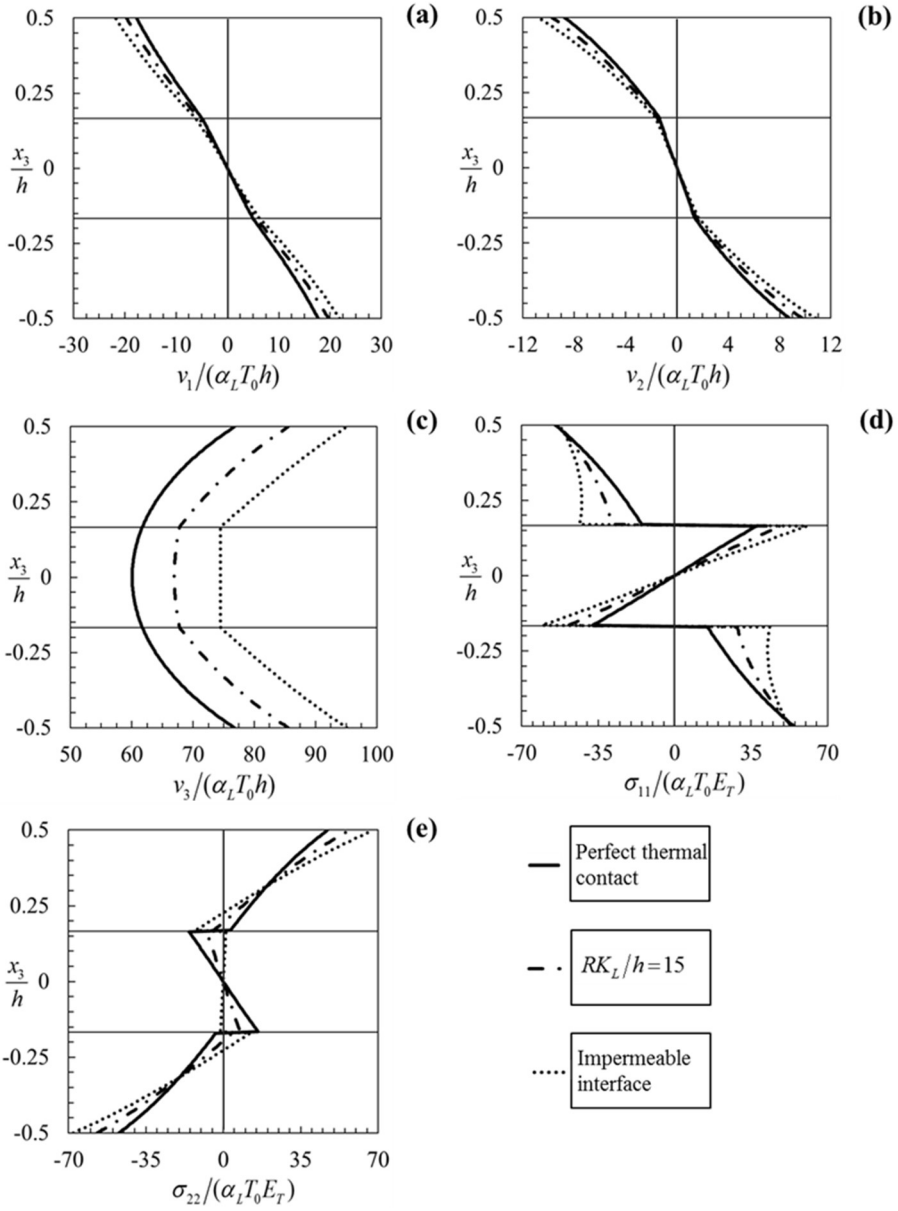

Figure 3-15: Through thickness variation of (a) displacements in x_1 direction at $(x_1 = 0, x_2 = a/2)$, (b) displacements in x_2 direction at $(x_1 = b/2, x_2 = 0)$, (c) transverse displacements at $(x_1 = b/2, x_2 = a/2)$, (d) bending stresses in x_1 direction at $(x_1 = b/2, x_2 = a/2)$ and (e) bending stresses in x_2 direction at $(x_1 = b/2, x_2 = a/2)$ in a simply supported three-layer plate $(0,90,0)$, $a/h = b/h = 8$, applied temperature $T_0 \sin(\pi x_1/b)\sin(\pi x_2/a)$ on upper and $-T_0 \sin(\pi x_1/b)\sin(\pi x_2/a)$ on lower surfaces. Thermo-elastic constants: $E_L/E_T = 25$, $G_{LT}/E_T = 0.5$, $G_{TT}/E_T = 0.2$, $\nu_{LT} = \nu_{TT} = 0.25$, $\alpha_T/\alpha_L = 62$ and $K_L/K_T = 38$. L direction coincides with x_2 axis in the outer layers. Interfaces are mechanically perfect.

Figure 3-16(b) and (c) show that even in the absence of mechanical loading, shear forces are generated at the plate edges to maintain the equilibrium of the structure. For the plates under the plane-strain conditions and subjected to pure thermal loading, distribution of the shear stresses at the plate edges are self-equilibrating so that the resultant shear forces are zero, e.g., Figure 3-10(b).

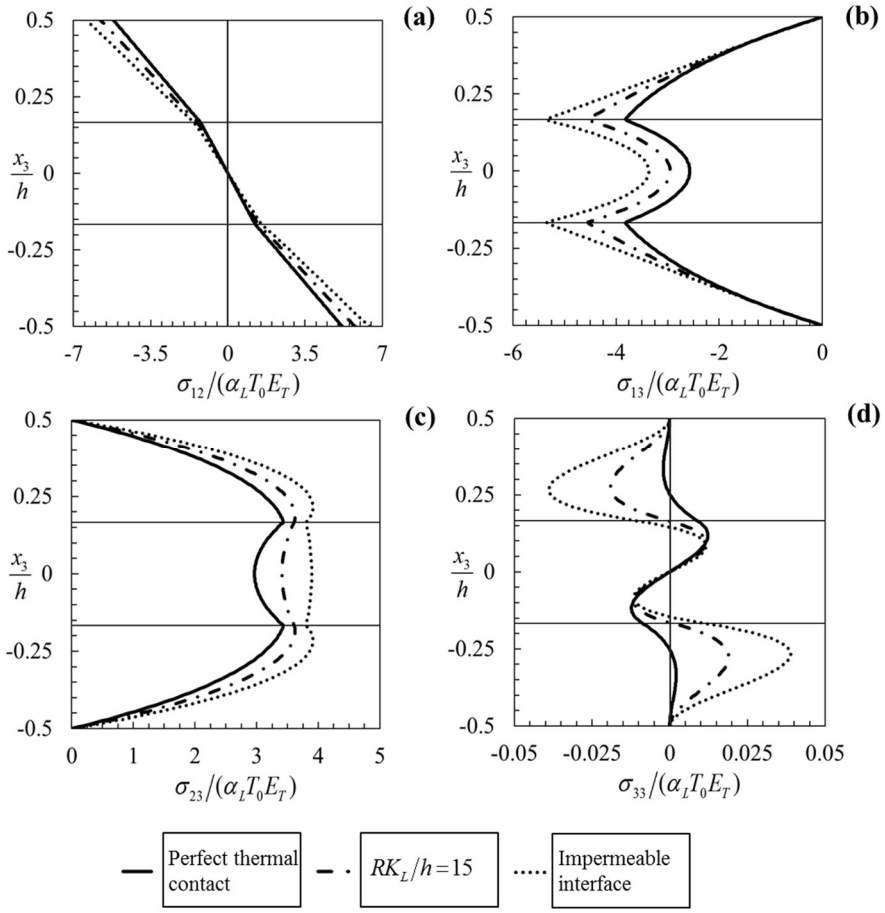

Figure 3-16: Through thickness variation of (a) in-plane shear stresses at $(x_1 = 0, x_2 = 0)$, (b) transverse shear stresses σ_{13} at $(x_1 = 0, x_2 = a/2)$, (c) transverse shear stresses σ_{23} at $(x_1 = b/2, x_2 = 0)$ and (d) transverse normal stresses at $(x_1 = b/2, x_2 = a/2)$ in a simply supported three-layer plate $(0,90,0)$, $a/h = b/h = 8$, applied temperature $T_0 \sin(\pi x_1/b)\sin(\pi x_2/a)$ on upper and $-T_0 \sin(\pi x_1/b)\sin(\pi x_2/a)$ on lower surfaces. Thermo-elastic constants: $E_L/E_T = 25$, $G_{LT}/E_T = 0.5$, $G_{TT}/E_T = 0.2$, $\nu_{LT} = \nu_{TT} = 0.25$, $\alpha_T/\alpha_L = 62$ and $K_L/K_T = 38$. L direction coincides with x_2 axis in the outer layers. Interfaces are mechanically perfect.

3.4 CONCLUSIONS

A matrix technique, based on the transfer matrix method in [51] and the thermo-elasticity models in [6, 7], has been formulated to efficiently solve stationary two- and three-dimensional thermo-elasticity problems in rectangular simply supported multilayered plates, with an arbitrary number of layers, which may be in imperfect mechanical and thermal contact, subjected to sinusoidally varying transverse loads and thermal gradients. The matrix technique systematizes the analysis and facilitates the solution of the system of algebraic equations resulting from the imposition of continuity and boundary conditions. The method uses local transfer matrices and continuity conditions at the interfaces to establish explicit matrix relationships between the unknown integration constants in the solution of a generic layer and those of the first layer. Novel explicit expressions are derived for temperature, displacements and stresses which are valid for an arbitrary number of layers and arbitrary layups and interfacial thermal and mechanical imperfections. The expressions simplify in the case of perfect thermal or mechanical contact. The expressions are in

dimensionless form to facilitate parametric analyses of the problem. The solutions can be applied to solve problems with different load distributions via Fourier's series approximations.

Some benchmark solutions are presented in tabular and graph forms for laminates and sandwiches with different layups, length-to-thickness ratios and interfacial stiffnesses and resistances, to highlight the efficacy of the method and the important effect of the imperfections on the field variables.

A HOMOGENIZED APPROACH FOR DELAMINATION FRACTURE OF LAMINATED WIDE PLATES AND BEAMS

4.1 INTRODUCTION

Delamination fracture is one of the dominant failure mechanisms of layered structures. Because of the high level of interlaminar stresses caused by the inhomogeneous material structure, delaminations may then propagate and cause stiffness degradation or final failure of the component.

The aim of this chapter is to formulate a homogenized fracture model based on the multiscale structural theory formulated in [25] for laminated wide plates with an arbitrary number of layers and cohesive or traction-free interfaces. The multiscale structural theory [25], which was recalled in Sect. 2.3.4 of Chapter 2, is particularized to a bi-material wide plate with a single delamination, Figure 4-1. A fracture model is then formulated to study mode II dominant problems using a homogenized approach. The conditions for which the mode II dominant assumption is applicable, will be discussed later in the chapter.

The homogenized fracture model is applied to the model system in Figure 4-3, which has been extensively studied in the literature and for which accurate Linear Elastic Fracture Mechanics solutions have been derived and are available for verification [93-97]. The model is then used to analyze delamination growth and investigate the structural response of End Notched Flexural (ENF) specimens; the results are compared with the solutions of other structural models to shed light on the advantages and limitations of the homogenized approach.

The homogenized fracture model for bi-material wide plates and beams with a single traction-free delamination is presented in Sect. 4.2. In Sect. 4.3, the quantities which are needed for the calculation of the energy release rate in a bi-material edge-cracked element through an application of the J-integral, are derived. An explicit expression of the energy release rate is derived in Sect. 4.4 in terms of force and moment sub-resultants and rotations of the layer arms; the expression is then particularized to a homogeneous material. In Sect. 4.5, a bi-material ENF specimen is considered and the predictive capabilities of the proposed homogenized fracture model are investigated. Conclusions are given in Sect. 4.6.

4.2 HOMOGENIZED STRUCTURAL THEORY FOR BI-MATERIAL WIDE PLATES AND BEAMS

4.2.1 Model assumptions

Figure 4-1(a) illustrates a portion of a bi-material wide plate with a single delamination, subjected to arbitrary transverse loads, and deforming in cylindrical bending. The plate is studied using the homogenized description of the actual problem shown in Figure 4-1(b) and the multiscale structural theory presented in Sect. 2.3.4 of Chapter 2 [25].

A system of Cartesian coordinates $x_1 - x_2 - x_3$ is introduced, whose origin is arbitrarily placed. The layers are linearly elastic, homogenous and orthotropic with principal material axes parallel to the geometrical axes. The layer *k*, with *k* = 1, 2 numbered from bottom to top, is defined by x_3^{k-1} and x_3^k, the coordinates of its lower and upper surfaces, and has thickness ${}^{(k)}h$ (the superscript (*k*) on the left of a quantity, for *k* = 1, 2, shows association with the layer *k*).

It is assumed that the delamination is under mode II dominant conditions. This assumption significantly simplifies the analysis, allowing to provide new insight into the capabilities of the homogenized structural theory for calculating fracture parameters. The assumption is exact when the crack surface opening displacement is zero, e.g. a plate with a symmetric layup subjected to anti-symmetric loading about the interface, for instance a homogenous ENF specimen with two layers of equal thickness. The assumption is acceptable when the crack surfaces are in frictionless contact, e.g. a homogenous ENF specimen with a thicker lower layer or a bi-material ENF specimen with a stiffer lower layer.

The layers are assumed to be incompressible in the thickness direction and the transverse normal stresses ${}^{(k)}\sigma_{33}$ to be negligible compared to the other stress components. Under this assumption, the 3D constitutive equations for the layer *k* particularized to plane-strain conditions are:

$$\begin{aligned} {}^{(k)}\sigma_{22} &= {}^{(k)}\overline{C}_{22}\,{}^{(k)}\varepsilon_{22} \\ {}^{(k)}\sigma_{23} &= {}^{(k)}C_{44}\,2\,{}^{(k)}\varepsilon_{23} \end{aligned} \tag{4-1}$$

with ${}^{(k)}\sigma_{ij}$ and ${}^{(k)}\varepsilon_{ij}$ for *i*, *j* = 2, 3 the stress and strain components, and ${}^{(k)}\overline{C}_{22} = {}^{(k)}\left(C_{22} - C_{23}C_{32}/C_{33}\right)$, where ${}^{(k)}C_{ij}$ are the coefficients of the stiffness matrix in engineering notation. The model presented in this chapter is also applicable to bi-material beams with longitudinal axis x_2, provided that ${}^{(k)}\overline{C}_{22}$ is replaced by the Young's modulus of the layers in x_2 direction.

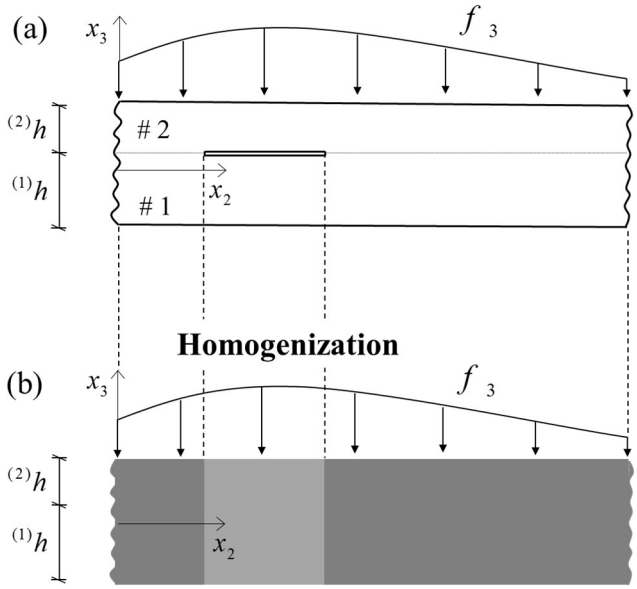

Figure 4-1: A bi-material element extracted from a wide plate subjected to transverse loads, and (b) its homogenized description obtained through the multiscale structural theory.

Under these assumptions, the displacement components in the layer k, ${}^{(k)}v_i$ for i = 1, 2, 3 simplify as ${}^{(k)}v_1 = 0$, ${}^{(k)}v_2 = {}^{(k)}v_2(x_2, x_3)$ and ${}^{(k)}v_3 = w_0(x_2)$, and the infinitesimal strain components are:

$$\begin{aligned} {}^{(k)}\varepsilon_{22}(x_2, x_3) &= {}^{(k)}v_{2,2}(x_2, x_3) \\ 2\,{}^{(k)}\varepsilon_{23}(x_2, x_3) &= {}^{(k)}v_{2,3}(x_2, x_3) + {}^{(k)}v_{3,2}(x_2, x_3) \end{aligned} \tag{4-2}$$

Here and throughout the derivation, a comma followed by a subscript denotes a derivative with respect to the corresponding coordinate.

A cohesive interface, which is a zero-thickness mathematical surface where the material properties and displacements are discontinuous while the interfacial tractions are continuous, is introduced along the delamination line in the schematic in Figure 4-1. The mechanical behavior of the interface is governed by a cohesive traction law which relates the relative sliding displacement of the layers at the interface, $\hat{v}_2$:

$$\hat{v}_2(x_2) = {}^{(2)}v_2(x_2, x_3 = x_3^1) - {}^{(1)}v_2(x_2, x_3 = x_3^1) \tag{4-3}$$

to the interfacial cohesive traction $\hat{\sigma}_S(x_2)$. In [25], piecewise linear traction laws were introduced to approximate general nonlinear cohesive traction laws, and to represent all nonlinear mechanisms taking place at the interfaces, e.g. brittle, cohesive and bridging fracture and contact. Here, in order to study the model system in Figure 4-3 and compare the solutions of the homogenized model with accurate LEFM solutions derived in [94, 95], the following piecewise linear interfacial traction law is considered, Figure 4-2(a):

$$\hat{\sigma}_S(x_2) = \begin{cases} K_S \hat{v}_2(x_2) & \text{for } \hat{v}_2(x_2) \le \hat{v}_{2c} \\ 0 & \text{for } \hat{v}_2(x_2) \ge \hat{v}_{2c} \end{cases} \tag{4-4}$$

with $\hat{v}_{2c}$ a critical sliding displacement for which $\hat{\sigma}_S(x_2)$ vanishes. This law approximates linear elastic fracture mechanics [21-23], by imposing a very stiff initial branch, which approximates the perfect bonding of the two sub-layers in the intact region, and a second branch with zero interfacial stiffness, to model the traction-free delamination. In order to simplify the treatment of the problem, the interfacial traction law in Eq. (4-4) and Figure 4-2(a), is approximated in the solution by the following law (Figure 4-2(b)):

$$\hat{\sigma}_S(x_2) = \begin{cases} K_S \hat{v}_2(x_2) & \text{for } \hat{v}_2(x_2) \le \hat{v}_{2c} \\ K_S \hat{v}_2(x_2) & \text{for } \hat{v}_2(x_2) \ge \hat{v}_{2c} \ \text{ with } K_S \to 0 \end{cases} \tag{4-5}$$

where the interfacial shear tractions in both intact and delaminated portions of the plate are assumed to be proportional to the interfacial relative sliding displacements; the interfacial stiffness of the initial branch is very high to model the perfect bonding of the two sub-layers in the intact region, while the interfacial stiffness of the second branch is very low to model the traction-free delamination. The numerical values for the interfacial stiffnesses in the intact/delaminated portion should be chosen as large/small as possible, considering that numerical problems do not arise in calculations. The advantage of the interfacial traction

law (4-5) used to approximate (4-4) is that it allows to formulate the multiscale model and derive the solutions for a generic linear interfacial traction law with interfacial stiffness K_S and then use the solutions to describe the different portions of the plate. Different portions of the plate could also be modeled with the asymptotic limits of the multiscale theory, which is derived in [7] and correspond to the fully bonded limit, to describe the intact portion, and to the fully debonded limit, to describe the delaminated portion.

The interfacial tractions are related to the transverse shear stresses in the adjacent layers through, e.g., $\hat{\sigma}_S(x_2) = \left[{}^{(1)}\sigma_{23}(x_2, x_3 = x_3^1) \right] n_3$, with n_3 the component of the unit outward normal to the upper surface of the first layer.

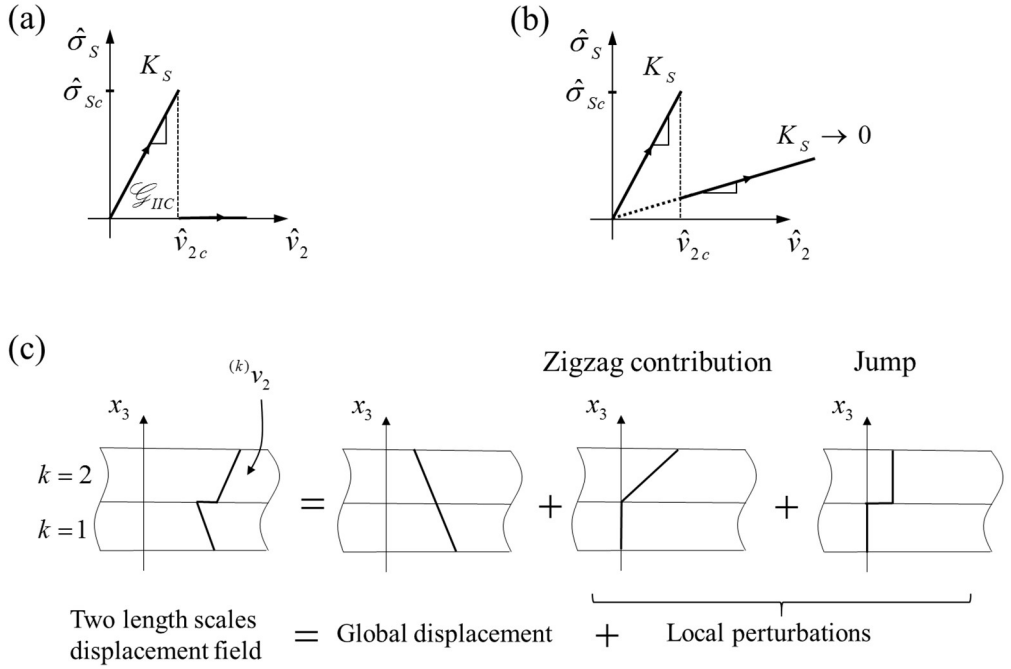

Figure 4-2: (a) Interfacial traction law used to approximate linear elastic fracture mechanics. (b) The interfacial traction law used in the solution of the problem through the multiscale model. (c) Schematic description of the assumed two length scales displacement field: global displacement and local perturbations.

4.2.2 Multiscale treatment and homogenization

The two length scales displacement field introduced in Eq. (2-30), which is described by global variables and local perturbations, is particularized to two-layer wide plate in Figure 4-1; the displacement field in the layer *k* for *k* = 1 and 2, is (see Figure 4-2(c)):

$$
\begin{aligned}
&{}^{(1)}v_2(x_2,x_3) = v_{02}(x_2) + x_3\varphi_2(x_2)\\
&{}^{(2)}v_2(x_2,x_3) = v_{02}(x_2) + x_3\varphi_2(x_2) + \Omega_2\ (x_2)(x_3 - x_3^1) + \hat{v}_2(x_2)\\
&{}^{(k)}v_3(x_2) = w_0(x_2)
\end{aligned}
\tag{4-6}
$$

The global variables, $v_{02}(x_2)$, $\varphi_2(x_2)$ and $w_0(x_2)$, define the displacement field of the first order shear deformation theory, which is continuous with continuous first derivative in the thickness direction; when the reference surface $x_3 = 0$ is placed at the mid-thickness of the first layer, the global variables then define the displacement components of points on the reference surface and the rotations of its normal axes. The local variables account for the zigzag contribution due to the inhomogeneous material structure, through the zigzag function $\Omega_2(x_2)(x_3 - x_3^1)$, and the interfacial sliding jumps, due to the presence of the cohesive interface, through $\hat{v}_2(x_2)$. The variables, Ω_2 and $\hat{v}_2$ are derived in terms of the global variables by imposing continuity of the interfacial shear tractions, which yield ${}^{(2)}\sigma_{23}(x_3 = x_3^1) = {}^{(1)}\sigma_{23}(x_3 = x_3^1)$, and the assumed interfacial traction law, Eq. (4-5) [25]. This yields:

$$
\begin{aligned}
&\Omega_2 = \left(w_{0,2} + \varphi_2\right)\Lambda_{22}\\
&\hat{v}_2 = \left(w_{0,2} + \varphi_2\right)\Psi_{22}
\end{aligned}
\tag{4-7}
$$

with

$$
\begin{aligned}
&\Lambda_{22} = {}^{(1)}C_{44}\left(\frac{1}{{}^{(2)}C_{44}} - \frac{1}{{}^{(1)}C_{44}}\right)\\
&\Psi_{22} = \frac{{}^{(2)}C_{44}\left(1 + \Lambda_{22}\right)}{K_S}
\end{aligned}
\tag{4-8}
$$

In a plate with two layers having the same elastic properties, Λ_{22} is zero since ${}^{(1)}C_{44} = {}^{(2)}C_{44}$ and the zigzag contribution Ω_2 vanishes from the displacement field (4-6). Moreover, the relative displacement of the layers at the interface, $\hat{v}_2$, and Ψ_{22} given in Eqs. (4-7) and (4-8), vanish in the intact portion of the plate, where K_S is a large number, and the displacement field would then coincide with that of the global first order model if the two layers have the same elastic constants.

Substituting the small-scale variables from Eq. (4-7) into Eq. (4-6) yields the macro-scale displacement field, which is defined only in terms of the global variables, $v_{02}(x_2)$, $\varphi_2(x_2)$ and $w_0(x_2)$, and is a particularization of that derived in [25] and given in Eq. (2-31), to a two-layer wide plate with the interfacial traction law in Eq. (4-5). The macro-scale displacement field is written as:

$$
\begin{aligned}
&{}^{(k)}v_2(x_2,x_3) = v_{02}(x_2) + x_3\varphi_2(x_2) + \left[w_{0,2}(x_2) + \varphi_2(x_2)\right]R^k_{S22}(x_3)\\
&{}^{(k)}v_3(x_2) = w_0(x_2)
\end{aligned}
\tag{4-9}
$$

for k = 1, 2 and

$$R^1_{S22}(x_3) = 0$$
$$R^2_{S22}(x_3) = \Lambda_{22}\left(x_3 - x^1_3\right) + \Psi_{22} \tag{4-10}$$

The strain components in the layer k for $k = 1, 2$ are derived through the macro-scale displacement field in Eq. (4-9) and the compatibility equations (4-2):

$$^{(k)}\varepsilon_{22}(x_2, x_3) = v_{02},_2(x_2) + x_3\varphi_2,_2(x_2) + \left[w_0,_{22}(x_2) + \varphi_2,_2(x_2)\right]R^k_{S22}$$
$$2\,^{(k)}\varepsilon_{23}(x_2, x_3) = \left[w_0,_2(x_2) + \varphi_2(x_2)\right]\left(1 + R^k_{S22},_3\right) \tag{4-11}$$

The stress components in the layer k for $k = 1, 2$ are derived through the strain components in Eq. (4-11) and the constitutive equations (4-1):

$$^{(k)}\sigma_{22}(x_2, x_3) = {}^{(k)}\overline{C}_{22}\left(v_{02},_2(x_2) + x_3\varphi_2,_2(x_2) + \left[w_0,_{22}(x_2) + \varphi_2,_2(x_2)\right]R^k_{S22}\right)$$
$$^{(k)}\sigma_{23}(x_2) = {}^{(k)}C_{44}\left[w_0,_2(x_2) + \varphi_2(x_2)\right]\left(1 + R^k_{S22},_3\right) \tag{4-12}$$

Eqs. (4-8) and (4-10) show that the transverse shear stresses, Eq. (4-12), are constant through the thickness since $^{(1)}C_{44} = {}^{(2)}C_{44}\left(1 + R^2_{S22},_3\right)$ and $^{(1)}\sigma_{23} = {}^{(2)}\sigma_{23} = {}^{(2)}C_{44}\left(1 + \Lambda_{22}\right)\left(w_0,_2 + \varphi_2\right)$. This is a consequence of the a priori imposition of the continuity of the shear tractions at the interface and the assumption of a first order global displacement field. Following the approach which is commonly used in the structural low order theories, accurate predictions of the transverse shear stresses and strains, in both delaminated and intact regions, can however be made a posteriori from the bending stresses in Eq. (4-12), through the imposition of local equilibrium:

$$^{(k)}\sigma_{22},_2 + {}^{(k)}\sigma^{post}_{23},_3 = 0$$
$$2\,^{(k)}\varepsilon^{post}_{23} = \frac{^{(k)}\sigma^{post}_{23}}{^{(k)}C_{44}} \tag{4-13}$$

In [7, 11, 25] the shear stresses calculated a posteriori have been observed to accurately describe the fields in plates with continuous interfacial imperfections subjected to thermo-mechanical loading.

The interfacial tractions in terms of the global variables are:

$$\hat{\sigma}_S = {}^{(2)}C_{44}\left(1 + \Lambda_{22}\right)\left(w_0,_2 + \varphi_2\right) \tag{4-14}$$

Since the interfacial tractions vanish in the delaminated portion of the plate, Eq. (4-14) shows that $w_0,_2 + \varphi_2$ vanishes, and as a consequence, transverse shear strains and stresses , Eqs. (4-11) and (4-12), also vanish. Vanishing transverse shear strains and stresses in the delaminated portion of the plate, which is a consequence of the homogenized procedure, limits the accuracy of the solutions for the compliance of the plate and the energy release rate. In Sect. 4.4, it will be shown that by using a posteriori calculated quantities deduced from the a posteriori stresses in Eq. (4-13), such as transverse shear forces and generalized shear

strains energetically associated to the transverse shear forces, the energy terms due to the shear deformations can be accurately taken into account in the derivation of the energy release rate. The effects that neglecting the shear deformations has on the solution of the problem will be discussed in Sect. 4.3.

4.2.3 Homogenized field equations

The homogenized equilibrium equations, boundary and continuity conditions in the delaminated and intact regions of the plate, are derived using the Principle of Virtual Work and following what done in [25]. The equilibrium equations in terms of force and moment resultants are:

$$\begin{aligned} &N_{22},_2 = 0 \\ &M^b_{22},_2 - Q_{2g} = 0 \\ &Q_{2g},_2 + f_3 = 0 \end{aligned} \tag{4-15}$$

where f_3 are the transverse distributed forces acting on the top and bottom surfaces of the plate. The force and moment resultants and loading terms in Eq. (4-15) are:

- normal force and bending moment:

$$\left(N_{22}, M^b_{22}\right) = \sum_{k=1}^{2} \int_{x_3^{k-1}}^{x_3^k} {}^{(k)}\sigma_{22}\left(1, x_3\right) dx_3 \tag{4-16}$$

- generalized transverse shear force:

$$Q_{2g} = Q_2^b + Q_2^z - M^{zS}_{22},_2 - \hat{\sigma}_2 \tag{4-17}$$

- transverse shear force:

$$Q_2^b = \sum_{k=1}^{2} \int_{x_3^{k-1}}^{x_3^k} {}^{(k)}\sigma_{23} dx_3 \tag{4-18}$$

- force and moment resultants associated to the multilayered structure and cohesive interface:

$$\begin{aligned} &M^{zS}_{22} = \sum_{k=1}^{2} \int_{x_3^{k-1}}^{x_3^k} {}^{(k)}\sigma_{22} R^k_{S22} dx_3 \\ &Q_2^z = \sum_{k=1}^{2} \int_{x_3^{k-1}}^{x_3^k} {}^{(k)}\sigma_{23} R^k_{S22},_3 dx_3 \\ &\hat{\sigma}_2 = -{}^{(2)}C_{44}\left(1 + \Lambda_{22}\right)\hat{v}_2 \end{aligned} \tag{4-19}$$

The first equilibrium equation in (4-15) describes equilibrium in the longitudinal direction, and coincides with that of the equivalent single layer theory. The second equation relates the first derivative of the bending moment and the generalized transverse shear force; the equation is similar to that of the equivalent single layer theory, but for the presence of the generalized shear force which substitutes the classical transverse shear force, Q_2^b, of the equivalent single layer theory. The generalized transverse shear force, Q_{2g} in Eq.

(4-17), was introduced in [11] for the general case of a plate with *n* layers, and has additional contributions compared to Q_2^b, which are due to the inhomogeneous material structures, M_{22}^{zS}, Q_2^z, and displacement at the interface, M_{22}^{zS}, $\hat{\sigma}_2$. The introduction of Q_{2g} is physically important since it is statically equivalent at any arbitrary section of the plate with outward normal $\boldsymbol{n} = \{0,1,0\}^T$, to the vertical equilibrant of the external forces acting on the portion of the plate to the right of the section. In addition, the generalized transverse shear force is the resultant of the a posteriori calculated transverse shear stresses, Eq. (4-13), over the thickness of the plate:

$$Q_{2g} = \sum_{k=1}^{2} \int_{x_3^{k-1}}^{x_3^k} {}^{(k)}\sigma_{23}^{post} dx_3 \tag{4-20}$$

In the intact portion of the bi-material wide plate, the term $\hat{\sigma}_2$ defined in Eq. (4-19) vanishes, since $\hat{v}_2 = 0$, and the equilibrium equations (4-15) coincide with those of the original first order zigzag theory developed in [62] for fully bonded plates. In the intact portion of a homogenous plate, M_{22}^{zS}, Q_2^z and $\hat{\sigma}_2$ defined in Eq. (4-19) vanish since $\Lambda_{22} = R_{S22}^k = \hat{v}_2 = 0$, and therefore Q_{2g} equals the transverse shear force Q_2^b, and the equilibrium equations (4-15) simplify to those of the first order shear deformation theory.

The homogenized boundary conditions at the plate edges are derived as:

$$\begin{array}{lll} N_{22}n_2 = \tilde{N}_2 & \text{or} & v_{02} = \tilde{v}_{02} \\ M_{22}^b n_2 = \tilde{M}_2^b & \text{or} & \varphi_2 = \tilde{\varphi}_2 \\ Q_{2g}n_2 = \tilde{N}_3 & \text{or} & w_0 = \tilde{w}_0 \\ M_{22}^{zS}n_2 = \tilde{M}_2^{zS} & \text{or} & w_{0,2} = \tilde{w}_{0,2} \end{array} \tag{4-21}$$

with n_2 the component of the outward normal. The terms with the tilde define prescribed values of displacements, forces and couples at the plate edges, and are given in Eq. (G-1) in Appendix G.

The homogenized boundary conditions (4-21) cannot be used to describe the edge-cracked specimen in Figure 4-3(a), if ${}^{(1)}N$ and ${}^{(2)}N$, or ${}^{(1)}M$ and ${}^{(2)}M$, or ${}^{(1)}Q$ and ${}^{(2)}Q$ are applied to the delaminated arms in opposite directions. For instance, in a Double Cantilever Beam specimen, the homogenized boundary condition on Q_{2g}, which is the net value of the applied shear forces through the whole thickness of the specimen, would be zero. However, these boundary conditions are limited to laboratory test specimens and are unlikely to occur in practical cases, where the delamination arise between the internal layers and the loads are applied on the outer surfaces of the structure; in such cases, the edge-cracked specimen in Figure 4-3(a) represents and element extracted from a delaminated plate and the end forces are the force and moment resultants.

Along a clamped support, where $\varphi_2 = w_{0,2} = 0$, the transverse shear strain in Eq. (4-11), transverse shear stress in Eq. (4-12), Q_2^b in Eq. (4-18) and Q_2^z in Eq. (4-19) vanish. The effect of vanishing transverse shear strain and stress at a clamped boundary on the solution of the multiscale model was studied in [26] by

considering a symmetric cantilevered wide plate with two layers bonded by a linear elastic interface and subjected to a concentrated load at the free end. It was shown that vanishing transverse shear strain and stress at the clamped boundary only affects the solutions within a localized region near the boundary and the solution of the model out of the boundary layer is accurate; the size of the boundary layer depends on the interfacial stiffness and is negligibly small for very stiff and very compliant interfaces [26]. The generalized transverse shear force, Q_{2g} in Eq. (4-17), which is related to the first derivative of the bending moment through the second equilibrium equation (4-15), accurately describe the shear force at any cross section including clamped supports [26].

The constitutive equations of the multiscale structural theory are derived by substituting the stresses and interfacial relative sliding displacement from Eqs. (4-12) and (4-7) into Eqs. (4-16)-(4-19):

$$\begin{Bmatrix} N_{22} \\ M_{22}^{b} \\ M_{22}^{zS} \end{Bmatrix} = \begin{bmatrix} C_{22}^{0} & C_{22}^{1} & C_{22}^{0S} \\ C_{22}^{1} & C_{22}^{2} & C_{22}^{1S} \\ C_{22}^{0S} & C_{22}^{1S} & C_{22}^{S2} \end{bmatrix} \begin{Bmatrix} v_{02},_{2} \\ \varphi_{2},_{2} \\ \varphi_{2},_{2}+w_{0},_{22} \end{Bmatrix}$$

$$Q_{2g} = \left(k_{44}C_{44}^{P}+C_{22}^{S}\right)\left(\varphi_{2}+w_{0},_{2}\right) - \begin{bmatrix} C_{22}^{0S} & C_{22}^{1S} & C_{22}^{S2} \end{bmatrix} \begin{Bmatrix} v_{02},_{22} \\ \varphi_{2},_{22} \\ \varphi_{2},_{22}+w_{0},_{222} \end{Bmatrix} \tag{4-22}$$

where the coefficients, C_{22}^{r}, C_{22}^{rS}, C_{22}^{S2}, C_{44}^{P} and C_{22}^{S} for $r = 0, 1, 2$, can be calculated a priori, depend on the geometry, the layup and the status of the interface and are defined in Eq. (G-2) in Appendix G. M_{22}^{zS}, which is a moment resultant due to the inhomogeneous material structure and the interface, contributes into the equilibrium equations (4-15) only through Q_{2g}, and appears in one of the boundary conditions of the homogenized model in Eq. (4-21).

Unlike the original zigzag theory [62, 63] and the refined zigzag theory [27] for fully bonded plates , a shear correction factor, k_{44}, has been introduced [25] in Eq. (4-22) to improve the approximate description of the shear, following the approach used for the low order structural theories. The correction factor is defined following the classical approach used in the first order theories, [58, 98], as $k_{44} = \left(Q_{2}^{b}+Q_{2}^{z}\right)\Big/\left[C_{44}^{p}\left(\varphi_{2}+w_{0},_{2}\right)\right]$. The introduction of the shear correction factor has some advantages. It allows to recover the constitutive equations of the equivalent single layer first order shear deformation theory in the limiting case of a fully bonded and homogeneous plate, for which $k_{44} = 5/6$ is required. Also, in a plate with imperfect interfaces, where the transverse shear strains and stresses in the layers will progressively reduce on decreasing the interfacial stiffness, as it can be understood from Eqs. (4-5), (4-11), (4-12) and (4-14), the shear correction factor may be used to account for the missing contribution of the shear deformations in the equilibrium equations of the model, as suggested in [25]. In general, the shear correction factor is a problem dependent parameter and depends on the stacking sequence, geometry, material and interfacial properties and loading conditions. Therefore, introduction of the shear correction factor keeps the constitutive equations of the homogenized model, Eq. (4-22), general enough to be used for different problems, e.g. dynamic problems; if the shear correction factor is not needed, for instance in

bending problem of fully bonded multilayered plates subjected to static loadings, the shear correction factor should be equal to 1.

The coefficient C_{22}^0, C_{22}^1 and C_{22}^2 are the so-called plate extensional, coupling and bending stiffnesses, depend on the material properties and thicknesses of the layers and have the same values in the intact and delaminated portions of the plate. When the reference surface $x_3 = 0$ is placed along the neutral axis of the intact portion of the plate, C_{22}^1 is zero. The coefficients with superscript *S* depend on the interfacial stiffnesses, Λ_{22} and the thickness of the layers, and have different values in the intact and delaminated portions of the plate. The coefficient C_{22}^S vanishes in the intact portion of the plate, and the constitutive equations (4-22) coincide with those of the original first order zigzag theory for fully bonded plates and $k_{44} = 1$ [62]; in addition, in the intact portion of a homogenous plate all the terms with superscript *S* vanish and the constitutive equations (4-22) simplify to those of the first order shear deformation theory; $k_{44} = 5/6$ is then needed for static problems to get the constitutive equations of the first order shear deformation theory.

Substitution of the plate constitutive equations (4-22) into the equilibrium equations (4-15) yields the equilibrium equations in terms of displacements:

$$
\begin{aligned}
&C_{22}^0 v_{02,22} + (C_{22}^1 + C_{22}^{0S})\varphi_{2,22} + C_{22}^{0S} w_{0,222} = 0 \\
&(C_{22}^1 + C_{22}^{0S}) v_{02,22} + (C_{22}^2 + 2C_{22}^{1S} + C_{22}^{S2})\varphi_{2,22} + (C_{22}^{1S} + C_{22}^{S2}) w_{0,222} \\
&-[k_{44} C_{44}^P + C_{22}^S](w_{0,2} + \varphi_2) = 0 \\
&C_{22}^{0S} v_{02,222} + (C_{22}^{1S} + C_{22}^{S2})\varphi_{2,222} + C_{22}^{S2} w_{0,2222} - [k_{44} C_{44}^P + C_{22}^S](w_{0,22} + \varphi_{2,2}) - f_3 = 0
\end{aligned}
\tag{4-23}
$$

Similarly, the boundary conditions in terms of displacements can be obtained by substitution of the plate constitutive equations (4-22) into the boundary conditions (4-21). The boundary conditions in terms of the displacements are presented in Appendix G.

The system (4-23) has order VIII. The equations are decoupled by subsequent derivations/substitutions and eliminating φ_2 through the introduction of a variable γ given by $\gamma = \varphi_2 + w_{0,2}$, which represents the transverse shear strain of the first layer, $2\,{}^{(1)}\varepsilon_{23}$ given in Eq. (4-11), since $R_{S22}^1 = 0$. The system of decoupled equations, which has the same order of the original system is:

$$
\begin{aligned}
&\gamma_{,222} - \bar{B}\gamma_{,2} + \bar{C} f_3 = 0 \\
&w_{0,222} = \bar{D}\gamma_{,22} + \bar{E}\gamma \\
&v_{02,22} = \frac{C_{22}^1}{C_{22}^0} w_{0,222} - \frac{C_{22}^1 + C_{22}^{0S}}{C_{22}^0}\gamma_{,22} \\
&\varphi_2 = \gamma - w_{0,2}
\end{aligned}
\tag{4-24}
$$

where

$$
\begin{aligned}
\bar{A} &= \frac{C_{22}^{0S}C_{22}^{1} - C_{22}^{1S}C_{22}^{0}}{\left(C_{22}^{1}+C_{22}^{0S}\right)C_{22}^{1} - \left(C_{22}^{2}+C_{22}^{1S}\right)C_{22}^{0}} \\
\bar{B} &= \frac{C_{22}^{0}\left(1-\bar{A}\right)\left(k_{44}C_{44}^{P}+C_{22}^{S}\right)}{\bar{A}\left[\left(C_{22}^{1}+C_{22}^{0S}\right)^{2} - \left(C_{22}^{2}+2C_{22}^{1S}+C_{22}^{S2}\right)C_{22}^{0}\right] - \left(C_{22}^{1}+C_{22}^{0S}\right)C_{22}^{0S} + \left(C_{22}^{1S}+C_{22}^{S2}\right)C_{22}^{0}} \\
\bar{C} &= \frac{\bar{B}}{\left(k_{44}C_{44}^{P}+C_{22}^{S}\right)\left(\bar{A}-1\right)}; \quad \bar{D} = \frac{\left(C_{22}^{1}+C_{22}^{0S}\right)^{2} - \left(C_{22}^{2}+2C_{22}^{1S}+C_{22}^{S2}\right)C_{22}^{0}}{\left(C_{22}^{1}+C_{22}^{0S}\right)C_{22}^{1} - \left(C_{22}^{2}+C_{22}^{1S}\right)C_{22}^{0}} \\
\bar{E} &= \frac{\left(k_{44}C_{44}^{P}+C_{22}^{S}\right)C_{22}^{0}}{\left(C_{22}^{1}+C_{22}^{0S}\right)C_{22}^{1} - \left(C_{22}^{2}+C_{22}^{1S}\right)C_{22}^{0}}
\end{aligned}
\tag{4-25}
$$

The constants $\bar{A}$, $\bar{B}$, $\bar{C}$, $\bar{D}$ and $\bar{E}$ depend on the C_{22}^{r}, C_{22}^{rS}, C_{22}^{S2}, C_{44}^{P}, C_{22}^{S} and the shear correction factor. The first equation (4-24) is a third order differential equation in γ whose solution allows cascading solutions for w_0 and v_{02} through the solutions of a third order and a second order equation, respectively. The last equation (4-24) then defines φ_2.

The system of decoupled equations (4-24) has different coefficients in the intact and delaminated portions of the plate and the solution of the bi-material plate in Figure 4-1(b) needs the imposition of the continuity conditions on the global variables, v_{02}, φ_2, w_0, $w_{0,2}$, N_{22}, M_{22}^{b}, Q_{2g} and M_{22}^{zS} at the cross sections separating the two portions. The global displacement variables v_{02}, φ_2, w_0 are obtained by solving the system of decoupled equations (4-24) for the different regions, imposing the boundary conditions (4-21) and continuity conditions at the cross sections of the traction-free delamination tips.

In the special case of a plate with traction-free external surfaces, the closed form solution of the system of decoupled equations (4-24) with $f_3 = 0$ is:

$$
\begin{aligned}
\gamma &= \varphi_2 + w_{0,2} = c_1 e^{\sqrt{\bar{B}}x_2} + c_2 e^{-\sqrt{\bar{B}}x_2} + c_3 \\
w_0 &= \frac{\bar{D}\bar{B}+\bar{E}}{\bar{B}\sqrt{\bar{B}}}\left[c_1 e^{\sqrt{\bar{B}}x_2} - c_2 e^{-\sqrt{\bar{B}}x_2}\right] + \frac{\bar{E}c_3}{6}\left(x_2\right)^3 + c_4\left(x_2\right)^2 + c_5 x_2 + c_6 \\
\varphi_2 &= \left(1 - \frac{\bar{D}\bar{B}+\bar{E}}{\bar{B}}\right)\left[c_1 e^{\sqrt{\bar{B}}x_2} + c_2 e^{-\sqrt{\bar{B}}x_2}\right] - \frac{\bar{E}c_3}{2}\left(x_2\right)^2 - 2c_4 x_2 + c_3 - c_5 \\
v_{02} &= \frac{\bar{B}\left(C_{22}^{1}\bar{D} - C_{22}^{1} - C_{22}^{0S}\right) + C_{22}^{1}\bar{E}}{C_{22}^{0}\bar{B}}\left[c_1 e^{\sqrt{\bar{B}}x_2} + c_2 e^{-\sqrt{\bar{B}}x_2}\right] + \frac{c_3 C_{22}^{1}\bar{E}}{2C_{22}^{0}}\left(x_2\right)^2 + c_7 x_2 + c_8
\end{aligned}
\tag{4-26}
$$

where c_i for i = 1, …, 8, are integration constants to be determined by the imposition of the boundary and continuity conditions. These solutions will be applied later for the calculation of the energy release rate.

In Appendix H, perturbation analysis is used to derive asymptotic limits of the displacement variables in Eq. (4-26). The perturbation analysis investigates the solution for small values of a perturbation parameter, δ; the perturbation parameter is chosen as $\delta = 1/K_S \to 0$ to investigate the fully bonded limit and describes

the intact region of the plate, and as $\delta = \overline{B} \to 0$, where $\overline{B}$, which is defined in Eq. (4-25), goes to zero with the same order as K_S, is used to investigate the fully debonded limit which describes the delaminated region of the plate. The displacement variables and integration constants c_i for i = 1, 2 and 3, which depend on the interfacial stiffness, are expanded into power series of the perturbation parameter, δ, and taking the limit as $\delta \to 0$ yields the zero-order solutions (see Appendix H).

When $\delta = 1/K_S \to 0$, Ψ_{22} in Eq. (4-8), $\hat{v}_2$ in Eq. (4-7) and C_{22}^S in Appendix G Eq. (G-2) vanish and R_{S22}^2 in Eq. (4-10) modifies in $R_{S22}^2 = \Lambda_{22}\left(x_3 - x_3^1\right)$. The constants C_{22}^{rS} and C_{22}^{S2} in Appendix G Eq. (G-2), and $\overline{A}$, $\overline{B}$, $\overline{C}$, $\overline{D}$ and $\overline{E}$ in Eq. (4-25) simplify by substituting $R_{S22}^2 = \Lambda_{22}\left(x_3 - x_3^1\right)$ into Eqs. (G-2) and (4-25).

When $\delta = \overline{B} \to 0$, the finite coefficients in Eq. (4-26) are $\overline{A} \to 1$, C_{22}^r, $\overline{E}$, $\overline{D}\overline{B}$, $C_{22}^{0s}\overline{B}$; R_{S22}^2 in Eq. (4-10) modifies in $R_{S22}^2 = {}^{(2)}C_{44}\left(1 + \Lambda_{22}\right)/K_S$ and the coefficients C_{22}^{rS}, C_{22}^S and C_{22}^{S2} simplify by substituting $R_{S22}^2 = {}^{(2)}C_{44}\left(1 + \Lambda_{22}\right)/K_S$ into Eq. (G-2) in Appendix G. The coefficients C_{22}^{rS}, C_{22}^S, $\overline{D}$, Ψ_{22} and R_{S22}^2 go to infinity with the order $O(1/\delta)$, and C_{22}^{S2} goes to infinity with the order $O\left(1/\delta^2\right)$ (see Table H-1 in Appendix H).

4.3 DERIVATION OF LOCAL FIELDS

In order to verify the model capability to analyze brittle fracture, the model system in Figure 4-3(a) will be examined. Accurate LEFM solutions are available for this problem [93-97]. The model system is an edge-cracked bi-material element subjected to end forces applied per unit width. The element has upper and lower traction-free surfaces and the lengths of the crack and the ligament ahead of the crack tip, *a* and *c,* are assumed to be sufficiently long to ensure that the stress fields at the traction-free delamination tip depend only on the value of the force and moment resultants and the stress distributions at the ends of the element are unaffected by the delamination tip stress field. The minimum lengths *a* and *c* then depend on the material properties mismatch of the layers, the loading and geometry conditions [95, 99]. The element could represent a fracture mechanics specimen or an element extracted from a delaminated plate subjected to arbitrary loading conditions; in this latter case, the end forces are the force and moment resultants at the sections, which can be derived through accurate, e.g. FEM, or approximate, e.g. plate theories, solutions of the problem.

The model system in Figure 4-3(a) could represent an element including the crack tip taken from the plate in Figure 4-1(a). Using the homogenized description of Figure 4-1(b), the homogenized crack tip element in Figure 4-3(b), is then used to demonstrate, in a homogenized description, the model system in Figure 4-3(a).

The analysis of the macro-scale displacement field and the stress/strain field derived in Sect. 4.2, allows to investigate the local fields in the layers of the model system in Figure 4-3(b), and the local fields will be used in the next section to calculate the energy release rate.

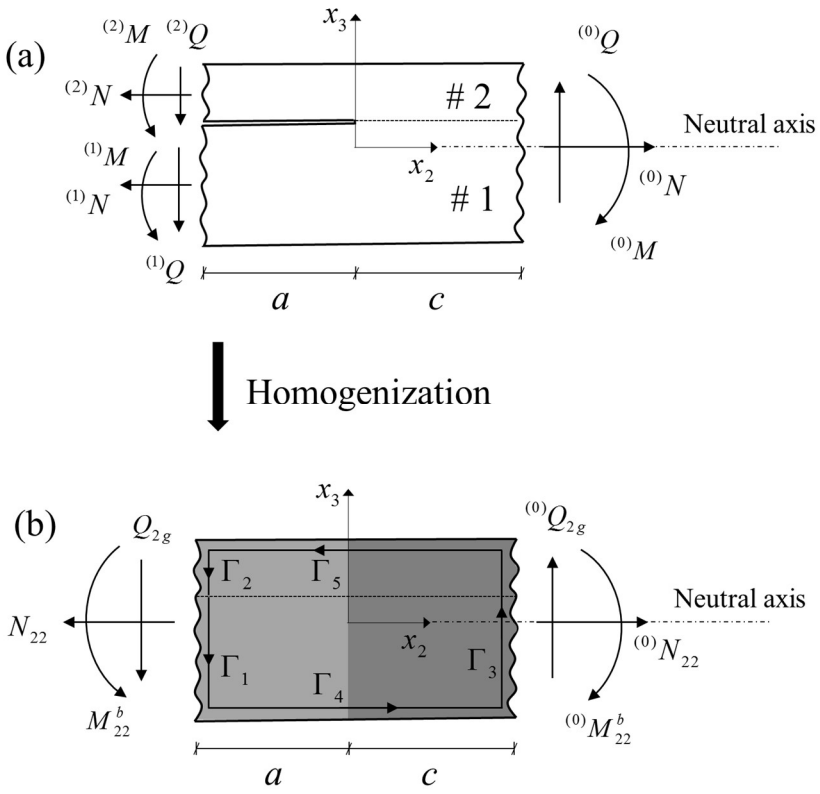

Figure 4-3: (a) a bi-material cracked element subjected to end forces. The element is extracted from a loaded plate, e.g. Figure 4-1(a). (b) The homogenized representation of the cracked element, showing the path Γ used for the calculation of the J-integral.

In order to define the local fields, it is convenient to use as the origin of the system of Cartesian coordinates $x_1 - x_2 - x_3$ the delamination crack tip cross section and assume the x_2 axis along the neutral axis of the intact portion of the element. In the derivation that follows it is assumed that the neutral axis falls into the lower layer. This assumption simplifies the derivation and the conclusions will be applicable also to problems where the neutral axis is in the upper layer. The distances between the reference plane $x_3 = 0$ and the geometrical mid-thickness of the first and second layers are $^{(1)}e$ and $^{(2)}e$ (see Figure 4-4). Local coordinates are introduced at the mid-thickness of the first layer, $^{(1)}X_3 = x_3 + {}^{(1)}e$, and at that the second layer, $^{(2)}X_3 = x_3 - {}^{(2)}e$. The local coordinates coincide with the neutral axes of the layers in the delaminated portion of the model. The superscript (0) on the left of a global quantity, e.g. $^{(0)}M_{22}^b$ in Figure 4-3(b), shows association with the intact portion of the element.

Local rotations of the layers, shown in Figure 4-4, can be introduced which define the rotations of the lines perpendicular to the neutral axes of the layers, and correspond to the slope with respect to x_3 of the longitudinal displacement of the layers in Eq. (4-9). Using Eq. (4-9) they are given by:

$$
\begin{aligned}
&{}^{(1)}\varphi_2\left(x_2\right)=\varphi_2\left(x_2\right)\\
&{}^{(2)}\varphi_2\left(x_2\right)=\varphi_2\left(x_2\right)+\left[\varphi_2\left(x_2\right)+w_0\left(x_2\right),_2\right]\Lambda_{22}
\end{aligned}
\tag{4-27}
$$

Equation (4-27) defines the local rotations of the layers both in the delaminated and in the intact portions of the plate, which depend on the global rotation $\varphi_2\left(x_2\right)$ and on the terms accounting for the multilayer structure, given in Eq. (4-7).

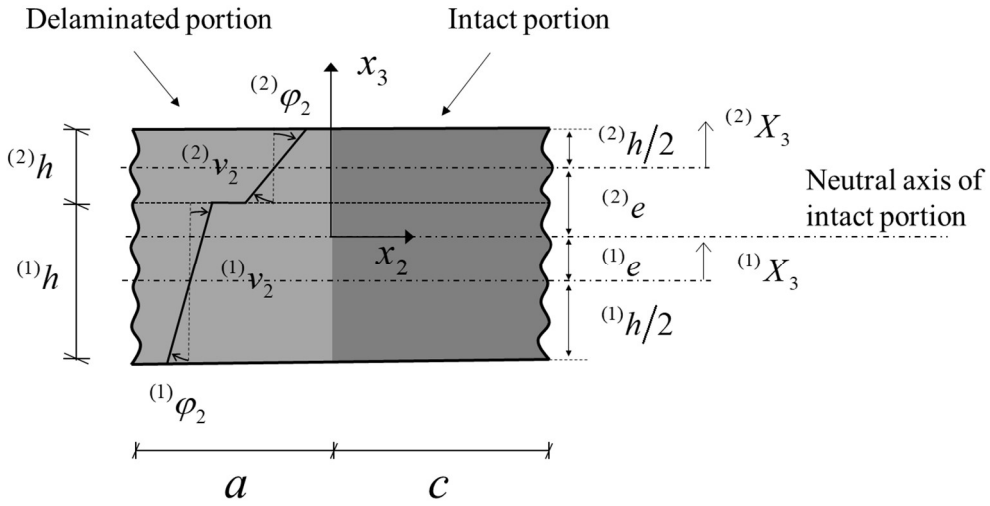

Figure 4-4: Local coordinates and rotations of the layers in the homogenized element.

If the edge-cracked specimen in Figure 4-4 is homogeneous, $\Lambda_{22}=0$ and the rotations of the layers in the intact portion of the element coincide with the global rotation, ${}^{(1)}\varphi_2={}^{(2)}\varphi_2=\varphi_2$. If the specimen is not homogeneous, the local rotations of the layers in the intact region, far from the traction-free delamination tip, would be different, as it is expected due to the inhomogeneous material structure and the enforcement of the continuity condition on the transverse shear tractions at the layer interface.

In Appendix H, the zero-order solutions of the displacement variables for the fully debonded limit which describe the delaminated portion of the plate, are presented; it is shown that the zero-order solution of $\varphi_2+w_0,_2$ is zero in this limit. Therefore, the rotations of the layers in the delaminated portion of the element defined in Eq. (4-27), coincide with the global rotation, ${}^{(1)}\varphi_2={}^{(2)}\varphi_2=\varphi_2$. Moreover, imposing the continuity conditions at the delamination tip cross section on φ_2 and $w_0,_2$, as part of the solution of the homogenized structural model, forces the solution of $\varphi_2+w_0,_2$ to be zero also in the intact portion of the element at the traction-free delamination tip cross section. Therefore, Eq. (4-27) shows that the model also predicts the same rotations for the upper and lower layers in the intact region at the traction-free delamination tip cross section. As a consequence, the rotations of the layers at the delamination tip cross section in the intact and delaminated regions are all equal, and this reduces the accuracy of the predicted energy release rates of the model system, as explained below.

The structural concept of root-rotations, which are defined as the relative rotations of the layers at the delamination tip cross section, have been frequently used in the literature, e.g. [95], to account for the primary effect of the elastic near tip deformations on the fracture parameters. In the light of Eq. (4-27), the root-rotations for the model system in Figure 4-3 are $\Delta\varphi_i = {}^{(i)}\varphi\left(x_2 = 0^+\right) - {}^{(i)}\varphi\left(x_2 = 0^-\right)$ for i = 1, 2, where ${}^{(i)}\varphi\left(x_2 = 0^+\right)$ and ${}^{(i)}\varphi\left(x_2 = 0^-\right)$ are the local rotation of the layer i at the traction-free delamination tip in the intact and delaminated portions, respectively. As explained in the previous paragraph, the multiscale structural model predicts the same rotations for the layers at the delamination tip cross section, and therefore the model neglects the root-rotations. In sect. 4.4, the effect of neglecting the root-rotations on the energy release rate of the model system will be discussed.

The transverse shear strains of the layers in Eq. (4-11) can be rewritten in terms of the rotations of the layers in Eq. (4-27), and this yields an expression which is similar to that of the first order shear deformation theory:

$$2\,{}^{(k)}\varepsilon_{23} = w_{0,2} + {}^{(k)}\varphi_2 \tag{4-28}$$

Again, Eq. (4-28) is valid both in the intact and in the delaminated portions of the specimen.

The force and moment sub-resultants acting in the first and second layers in the delaminated and intact portions of the element in Figure 4-3(b) are defined using the local coordinates as:

$$\begin{aligned}
&\left[{}^{(i)}N_{22}\left(x_2\right), {}^{(i)}M^b_{22}\left(x_2\right)\right] = \int_{-{}^{(i)}h/2}^{{}^{(i)}h/2} {}^{(i)}\sigma_{22}\left(x_2, {}^{(i)}X_3\right)\left[1, {}^{(i)}X_3\right] d\,{}^{(i)}X_3 \\
&{}^{(i)}Q_{2g}\left(x_2\right) = \int_{-{}^{(i)}h/2}^{{}^{(i)}h/2} {}^{(i)}\sigma^{post}_{23}\left(x_2, {}^{(i)}X_3\right) d\,{}^{(i)}X_3
\end{aligned} \tag{4-29}$$

for i = 1 and 2 where the superscript (i) shows association with the layer i. Since the upper and lower surfaces of the model system in Figure 4-3 are traction-free, $f_3 = 0$ and the equilibrium equations of the homogenized model in Eq. (4-15) show that ${}^{(i)}N_{22}$ and ${}^{(i)}Q_{2g}$ are independent of x_2 in the delaminated and intact regions, and have different values in different portions of the element, while the bending moment varies linearly in x_2. The global forces and moments in the intact region, ${}^{(0)}N_{22}$, ${}^{(0)}M^b_{22}$ and ${}^{(0)}Q_{2g}$ are:

$$\begin{aligned}
&{}^{(0)}N_{22}\left(x_2\right) = {}^{(1)}N_{22}\left(x_2\right) + {}^{(2)}N_{22}\left(x_2\right) = N_{22} \\
&{}^{(0)}M^b_{22}\left(x_2\right) = {}^{(1)}M^b_{22}\left(x_2\right) + {}^{(2)}M^b_{22}\left(x_2\right) = M^b_{22}\left(x_2\right) \\
&{}^{(0)}Q_{2g}\left(x_2\right) = {}^{(1)}Q_{2g}\left(x_2\right) + {}^{(2)}Q_{2g}\left(x_2\right) = Q_{2g}
\end{aligned} \tag{4-30}$$

In Eq. (4-29), the bending stresses and the transverse shear stresses calculated a posteriori through local equilibrium are defined by Eqs. (4-12) and (4-13).

Generalized shear strains energetically associated to the transverse shear forces, ${}^{(0)}Q_{2g}$, ${}^{(1)}Q_{2g}$ and ${}^{(2)}Q_{2g}$, are calculated a posteriori as follows, which accurately describe the shear deformations through the thickness of the layers and the whole cross section in the intact region [7]. The generalized shear strains through the thickness of the layers are:

$$2\,{}^{(i)}\varepsilon_{23g} = \frac{{}^{(i)}Q_{2g}}{{}^{(i)}k_{44}\,{}^{(i)}C_{44}\,{}^{(i)}h} \tag{4-31}$$

for $i = 1$ and 2. ${}^{(i)}k_{44}$ are shear correction factors, which are different from $k_{44} = \left(Q_2^b + Q_2^z\right)\Big/\left[C_{44}^p\left(\varphi_2 + w_{0,2}\right)\right]$ introduced in Sect. 4.2.3 to improve approximate description of the shear of the homogenized structural theory. When Eq. (4-31) is used for the delaminated portion of the element, where the layers deform independently as two homogeneous layers, the value of ${}^{(i)}k_{44} = 5/6$ is needed for accurate prediction of the generalized shear strains.

The generalized shear strain through the thickness of the model system in the intact region is:

$$2\,{}^{(0)}\varepsilon_{23g} = \frac{{}^{(0)}Q_{2g}}{{}^{(0)}k_{44}C_{44}^p} \tag{4-32}$$

where ${}^{(0)}k_{44}$ is a shear correction factor, which is generally different than $k_{44} = \left(Q_2^b + Q_2^z\right)\Big/\left[C_{44}^p\left(\varphi_2 + w_{0,2}\right)\right]$ in definition, but for a homogeneous element where ${}^{(0)}Q_{2g} = Q_2^b$, since M_{22}^{zS}, Q_2^z and $\hat{\sigma}_2$ defined in Eq. (4-19) vanish because $\Lambda_{22} = R_{S22}^k = \hat{v}_2 = 0$. Similar to ${}^{(1)}k_{44}$ and ${}^{(2)}k_{44}$ introduced above, ${}^{(0)}k_{44}$ relates the generalized shear force and strain in the intact portion of the element and allows to improve the accuracy of the generalized shear strain calculated from Eq. (4-32).

In the remaining part of this section, the normal strains and stresses of the layers in the intact and delaminated portions of the element will be defined in terms of ${}^{(i)}N_{22}$ and ${}^{(i)}M_{22}^b$ for $i = 0$, 1 and 2.

The normal strains and stresses, Eqs. (4-11) and (4-12), in the first layer of the delaminated region are expressed using the local coordinate, ${}^{(1)}X_3 = x_3 + {}^{(1)}e$ as:

$$\begin{aligned}
{}^{(1)}\varepsilon_{22}\left(x_2, {}^{(1)}X_3\right) &= \left[v_{02,2}\left(x_2\right) - {}^{(1)}e\ \varphi_{2,2}\left(x_2\right)\right] + {}^{(1)}X_3\ \varphi_{2,2}\left(x_2\right) \\
{}^{(1)}\sigma_{22}\left(x_2, {}^{(1)}X_3\right) &= {}^{(1)}\bar{C}_{22}\left(\left[v_{02,2}\left(x_2\right) - {}^{(1)}e\ \varphi_{2,2}\left(x_2\right)\right] + {}^{(1)}X_3\ \varphi_{2,2}\left(x_2\right)\right)
\end{aligned} \tag{4-33}$$

Substituting ${}^{(1)}\sigma_{22}\left(x_2, {}^{(1)}X_3\right)$ from Eq. (4-33) into the first equation (4-29) and performing the integration yields:

$$\begin{aligned}
v_{02,2}\left(x_2\right) - {}^{(1)}e\ \varphi_{2,2}\left(x_2\right) &= \frac{{}^{(1)}N_{22}}{{}^{(1)}\bar{C}_{22}\,{}^{(1)}h} \\
\varphi_{2,2}\left(x_2\right) &= \frac{12\,{}^{(1)}M_{22}^b\left(x_2\right)}{{}^{(1)}\bar{C}_{22}\left({}^{(1)}h\right)^3}
\end{aligned} \tag{4-34}$$

Substitution of the displacement variables from Eq. (4-34) into Eq. (4-33) gives the normal strain and bending stress of the first layer in the delaminated region, in terms of the normal force and bending moment sub-resultants:

$$
\begin{aligned}
{}^{(1)}\varepsilon_{22}\left(x_2, {}^{(1)}X_3\right) &= \frac{{}^{(1)}N_{22}}{{}^{(1)}\overline{C}_{22}\,{}^{(1)}h} + {}^{(1)}X_3\ \frac{12\,{}^{(1)}M^b_{22}\left(x_2\right)}{{}^{(1)}\overline{C}_{22}\left({}^{(1)}h\right)^3} \\
{}^{(1)}\sigma_{22}\left(x_2, {}^{(1)}X_3\right) &= \frac{{}^{(1)}N_{22}}{{}^{(1)}h} + {}^{(1)}X_3\ \frac{12\,{}^{(1)}M^b_{22}\left(x_2\right)}{\left({}^{(1)}h\right)^3}
\end{aligned}
\tag{4-35}
$$

Equation (4-35) has the same form as that of the equivalent single layer theory for a homogeneous layer. The equation shows the high efficacy of the multiscale structural theory to capture local strains and stresses in such highly discontinuous structural system with only three kinematic variables.

The longitudinal displacements in the second layer, Eq. (4-9) for $k = 2$, can be simplified and expressed in terms of the displacement jump using Eqs. (4-7), (4-8) and (4-10) and noting that $\varphi_2 + w_{0,2}$ vanishes in the delaminated portion of the element. This yields:

$$
{}^{(2)}v_2\left(x_2, x_3\right) = \left[v_{02}\left(x_2\right) + \hat{v}_2\left(x_2\right)\right] + x_3\varphi_2\left(x_2\right) \tag{4-36}
$$

The normal strain and bending stress in the second layer, Eqs. (4-11) and (4-12) with $k = 2$, in the delaminated region are defined using the local coordinate ${}^{(2)}X_3 = x_3 - {}^{(2)}e$ and Eqs. (4-1), (4-2) and (4-36):

$$
\begin{aligned}
{}^{(2)}\varepsilon_{22}\left(x_2, {}^{(2)}X_3\right) &= \left(v_{02,2}\left(x_2\right) + \hat{v}_{2,2}\left(x_2\right) + \varphi_{2,2}\left(x_2\right){}^{(2)}e\right) + {}^{(2)}X_3\ \varphi_{2,2}\left(x_2\right) \\
{}^{(2)}\sigma_{22}\left(x_2, {}^{(2)}X_3\right) &= {}^{(2)}\overline{C}_{22}\left[\left(v_{02,2}\left(x_2\right) + \hat{v}_{2,2}\left(x_2\right) + \varphi_{2,2}\left(x_2\right){}^{(2)}e\right) + {}^{(2)}X_3\ \varphi_{2,2}\left(x_2\right)\right]
\end{aligned}
\tag{4-37}
$$

Substituting ${}^{(2)}\sigma_{22}\left(x_2, {}^{(2)}X_3\right)$ from Eq. (4-37) into the first equation of (4-29) and performing the integration yield:

$$
\begin{aligned}
v_{02,2}\left(x_2\right) + \hat{v}_{2,2}\left(x_2\right) + \varphi_{2,2}\left(x_2\right){}^{(2)}e &= \frac{{}^{(2)}N_{22}}{{}^{(2)}\overline{C}_{22}\,{}^{(2)}h} \\
\varphi_{2,2}\left(x_2\right) &= \frac{12\,{}^{(2)}M^b_{22}\left(x_2\right)}{{}^{(2)}\overline{C}_{22}\left({}^{(2)}h\right)^3}
\end{aligned}
\tag{4-38}
$$

Substitution of the displacement variables from Eq. (4-38) into Eq. (4-37) gives the normal strain and bending stress of the second layer in the delaminated region, in terms of the normal force and bending moment sub-resultants:

$$
\begin{aligned}
{}^{(2)}\varepsilon_{22}\left(x_2, {}^{(2)}X_3\right) &= \frac{{}^{(2)}N_{22}}{{}^{(2)}\bar{C}_{22}\,{}^{(2)}h} + {}^{(2)}X_3\ \frac{12\,{}^{(2)}M^b_{22}\left(x_2\right)}{{}^{(2)}\bar{C}_{22}\left({}^{(2)}h\right)^3} \\
{}^{(2)}\sigma_{22}\left(x_2, {}^{(2)}X_3\right) &= \frac{{}^{(2)}N_{22}}{{}^{(2)}h} + {}^{(2)}X_3\ \frac{12\,{}^{(2)}M^b_{22}\left(x_2\right)}{\left({}^{(2)}h\right)^3}
\end{aligned}
\tag{4-39}
$$

As for the first layer, Eq. (4-35), Eq. (4-39) has the same form as that of the equivalent single layer theory for a homogeneous layer. Defining the normal strains and bending stresses of the layers with the same forms as those of the equivalent single layer theory, will allow later in Sect. 4.4 to derive an explicit expression for the energy release rate of the model system in Figure 4-3(a), which coincides with the classical solution of the problem.

If the shear forces in the model system in Figure 4-3(a) are absent, ${}^{(i)}Q = 0$ for i = 0, 1 and 2, the transverse shear stresses in Eq. (4-12) become zero, and this implies that $w_{0},_2 + \varphi_2$ is zero. As a consequence, the local variables of the homogenized model, Ω_2 and $\hat{v}_2$ defined in Eq. (4-7) are also zero and the displacement field, Eq. (4-9), coincides with that of the classical plate theory. The model is then unable to describe the response of delaminated portion. Therefore, equations (4-35) and (4-39) are valid for problems in the presence of the shear forces, e.g. plates subjected to transverse loads.

For the intact portion of the layer in Figure 4-3(b), an approach similar to that used above can be followed. The constitutive equations of the model, given in Eq. (4-22), are:

$$
\begin{aligned}
N_{22} &= C^0_{22} v_{02},_2\left(x_2\right) + C^{0S}_{22}\left[\varphi_2,_2\left(x_2\right) + w_0,_{22}\left(x_2\right)\right] \\
M^b_{22}\left(x_2\right) &= C^2_{22}\varphi_2,_2\left(x_2\right) + C^{1S}_{22}\left[\varphi_2,_2\left(x_2\right) + w_0,_{22}\left(x_2\right)\right]
\end{aligned}
\tag{4-40}
$$

where $C^1_{22} = 0$ has been set equal to zero since the reference surface $x_3 = 0$ is placed along the neutral axis of the intact portion. The second terms on the right hand side of the equation vanish for a homogenous element, since $R^2_{S\,22}$ and therefore C^{0S}_{22} and C^{1S}_{22} defined in Eq. (G-2) in Appendix G vanish, and the equations then coincide with those of the first order shear deformation theory. The term in the square bracket is $\gamma,_2$, where $\gamma = \varphi_2 + w_0,_2$ has been derived in closed form in Eq. (4-26). The exponential terms in the solution of γ, Eq. (4-26), decrease exponentially moving from the traction-free delamination tip. If the distance c is sufficiently long, the exponential terms then become negligible and γ becomes constant with respect to x_2; this implies that $\gamma,_2$ becomes zero. As a consequence, the constitutive equation (4-40) simplifies as:

$$
\begin{aligned}
N_{22} &= C^0_{22} v_{02},_2 \\
M^b_{22}\left(x_2\right) &= C^2_{22}\varphi_2,_2\left(x_2\right)
\end{aligned}
\tag{4-41}
$$

The normal strain and bending stress in the intact region at a sufficient distance from the crack tip are then defined in terms of the global normal force and bending moment resultants using Eqs. (4-11), (4-12), (4-30) and (4-41):

$$
\begin{aligned}
{}^{(k)}\varepsilon_{22}(x_2,x_3) &= \frac{{}^{(0)}N_{22}}{C_{22}^0} + x_3\frac{{}^{(0)}M_{22}^b(x_2)}{C_{22}^2} \\
{}^{(k)}\sigma_{22}(x_2,x_3) &= {}^{(k)}\bar{C}_{22}\left[\frac{{}^{(0)}N_{22}}{C_{22}^0} + x_3\frac{{}^{(0)}M_{22}^b(x_2)}{C_{22}^2}\right]
\end{aligned}
\tag{4-42}
$$

As for the first and second layers in the delaminated portion of the specimen, Eqs. (4-35) and (4-39), Eq. (4-42) has the same form as that of the equivalent single layer theory.

The local fields defined in this section, Eqs. (4-27), (4-28), (4-31), (4-32), (4-35), (4-39) and (4-42), will be used in the next section to derive an explicit expression for the energy release rate of the model system in Figure 4-3(a), and to compare the results of the homogenized structural theory with accurate 2D LEFM solutions.

4.4 ENERGY RELEASE RATE

In this section the local fields defined in Sect. 4.3 are used to derive in closed-form an explicit expression for the energy release rate of the homogenized model system in Figure 4-3(b), through an application of the J-integral. The accurate derivation of the fracture parameters in the system in Figure 4-3(a) has been presented in [94] based on 2D elasticity, dimensional analysis, interfacial fracture mechanics and finite element simulations; the energy release rate and mode mixity angle have been defined in terms of the end forces and rotations of the different arms. In [95] another expression has been derived for homogeneous and orthotropic layers which explains the physical and mechanical significance of the terms in [94].

The solution of the homogenized structural theory is limited to problems in the presence of shear forces where the crack is under mode II dominant conditions. Problems characterized by mixed-mode conditions could similarly be studied through the extended version of the multiscale model in [25] which accounts also for interfacial opening displacements. In addition, the homogenized structural theory cannot be applied to the edge-cracked specimen in Figure 4-3(a), if ${}^{(1)}N$ and ${}^{(2)}N$, or ${}^{(1)}M$ and ${}^{(2)}M$, or ${}^{(1)}Q$ and ${}^{(2)}Q$ are applied to the delaminated arms in the opposite directions. For instance, in a Double Cantilever Beam specimen, the homogenized boundary condition (4-21) on Q_{2g}, which is the net value of the applied shear forces through the whole thickness of the specimen, would be zero. However, this problem is limited to laboratory test specimens and are unlikely to occur in practical cases, where the delamination arise between the internal layers and the loads are applied on the outer surfaces of the structure; in such cases, the edge-cracked specimen in Figure 4-3(a) represents and element extracted from a delaminated plate and the end forces are the force and moment resultants.

4.4.1 J-integral along the external boundaries of the element

The energy release rate of the homogenized element in Figure 4-3(b) is calculated through an application of the J-integral, $\mathcal{G}_{II} = J = \int_{\Gamma} (W dx_3 - \sigma_{ij} n_j v_{i,2}\, d\Gamma)$ for $i, j = 2, 3$, with $\Gamma = \sum_{i=1}^{5} \Gamma_i$ a path surrounding the crack tip which follows the external boundaries of the element in Figure 4-3(b); $W = \left(\sigma_{22}\varepsilon_{22} + 2\sigma_{23}\varepsilon_{23}\right)/2$ is the strain energy density, n_j is the component of the unit outward vector normal to the path, $\sigma_{ij} n_j$ are the tractions along the contour. The components of the J-integral along the paths Γ_4 and Γ_5 are $J_4 = J_5 = 0$, since the upper and lower surfaces are traction-free. In the calculations of the components of the J-integral along the paths Γ_1, Γ_2 and Γ_3, the a posteriori calculated transverse shear stresses, Eq. (4-13), and the generalized transverse shear strains, Eqs. (4-31) and (4-32), are used.

Upon substitution of W and the tractions, ${}^{(1)}\sigma_{22} n_2$ and ${}^{(1)}\sigma_{23}^{post} n_2$ with $n_2 = -1$, into the definition of the J-integral along the path Γ_1 and some manipulations, $J_1\left(x_2 = -a\right)$ can be written as:

$$J_1\left(x_2 = -a\right) = \frac{1}{2}\int_{-\frac{{}^{(1)}h}{2}}^{\frac{{}^{(1)}h}{2}} {}^{(1)}\sigma_{22}\, {}^{(1)}\varepsilon_{22} d\,{}^{(1)}X_3 - \frac{1}{2}\int_{-\frac{{}^{(1)}h}{2}}^{\frac{{}^{(1)}h}{2}} 2\,{}^{(1)}\sigma_{23}^{post}\, {}^{(1)}\varepsilon_{23g} d\,{}^{(1)}X_3 + \\ + \int_{-\frac{{}^{(1)}h}{2}}^{\frac{{}^{(1)}h}{2}} {}^{(1)}\sigma_{23}^{post}\, {}^{(1)}v_{3,2}\, d\,{}^{(1)}X_3 \tag{4-43}$$

Using the generalized transverse shear strain $2\,{}^{(1)}\varepsilon_{23g}$ and Eq. (4-28), ${}^{(1)}v_{3,2}$ in the third term on the right hand side of Eq. (4-43) is substituted by $2\,{}^{(1)}\varepsilon_{23g} - {}^{(1)}\varphi_2$, since ${}^{(1)}v_3 = w_0$. Equation (4-43) then becomes:

$$J_1\left(x_2 = -a\right) = \frac{1}{2}\int_{-\frac{{}^{(1)}h}{2}}^{\frac{{}^{(1)}h}{2}} {}^{(1)}\sigma_{22}\, {}^{(1)}\varepsilon_{22} d\,{}^{(1)}X_3 + \frac{1}{2}\int_{-\frac{{}^{(1)}h}{2}}^{\frac{{}^{(1)}h}{2}} 2\,{}^{(1)}\sigma_{23}^{post}\, {}^{(1)}\varepsilon_{23g} d\,{}^{(1)}X_3 - \\ - {}^{(1)}\varphi_2 \int_{-\frac{{}^{(1)}h}{2}}^{\frac{{}^{(1)}h}{2}} {}^{(1)}\sigma_{23}^{post} d\,{}^{(1)}X_3 \tag{4-44}$$

The second term on the right hand side of Eq. (4-44), can be written as follows, by substituting the generalized transverse shear strain, $2\,{}^{(1)}\varepsilon_{23g}$, from Eq. (4-31) and using the definition of ${}^{(1)}Q_{2g}$ given in Eq. (4-29):

$$\frac{1}{2}\int_{-\frac{{}^{(1)}h}{2}}^{\frac{{}^{(1)}h}{2}} 2\,{}^{(1)}\sigma_{23}^{post}\, {}^{(1)}\varepsilon_{23g} d\,{}^{(1)}X_3 = \frac{1}{2}\frac{{}^{(1)}Q_{2g}}{{}^{(1)}k_{44}\, {}^{(1)}C_{44}\, {}^{(1)}h}\int_{-\frac{{}^{(1)}h}{2}}^{\frac{{}^{(1)}h}{2}} {}^{(1)}\sigma_{23}^{post} d\,{}^{(1)}X_3 = \frac{1}{2}\frac{\left[{}^{(1)}Q_{2g}\right]^2}{{}^{(1)}k_{44}\, {}^{(1)}C_{44}\, {}^{(1)}h} \tag{4-45}$$

The integration of the a posteriori calculated transverse shear stresses through the thickness of the first layer in the third term on the right hand side of Eq. (4-44), is equal to ${}^{(1)}Q_{2g}$ (Eq. (4-29)). The first term on the right hand side of Eq. (4-44) is calculated in terms of the normal and moment sub-resultants, ${}^{(1)}N_{22}$ and

${}^{(1)}M_{22}^{b}$, using the bending stresses and normal strains given in Eq. (4-35). This yields the following expression for the component of the J-integral along the path Γ_1:

$$J_1\left(x_2=-a\right)=\frac{1}{2}\left(\frac{\left[{}^{(1)}N_{22}\right]^2}{{}^{(1)}\overline{C}_{22}\,{}^{(1)}h}+\frac{12\left[{}^{(1)}M_{22}^{b}\right]^2}{{}^{(1)}\overline{C}_{22}\left({}^{(1)}h\right)^3}+\frac{\left[{}^{(1)}Q_{2g}\right]^2}{{}^{(1)}k_{44}\,{}^{(1)}C_{44}\,{}^{(1)}h}-2\,{}^{(1)}\varphi_2\,{}^{(1)}Q_{2g}\right) \tag{4-46}$$

The component of the J-integral along the path Γ_2 can be calculated following the same procedure explained above for the calculation of $J_1\left(x_2=-a\right)$. Upon substitution of W and the tractions, ${}^{(2)}\sigma_{22}n_2$ and ${}^{(2)}\sigma_{23}^{post}n_2$ with $n_2=-1$, into the definition of the J-integral along the path Γ_2 and some manipulations, $J_2\left(x_2=-a\right)$ can be written as:

$$\begin{aligned}J_2\left(x_2=-a\right)=&\frac{1}{2}\int_{-\frac{{}^{(2)}h}{2}}^{\frac{{}^{(2)}h}{2}}{}^{(2)}\sigma_{22}\,{}^{(2)}\varepsilon_{22}d\,{}^{(2)}X_3-\frac{1}{2}\int_{-\frac{{}^{(2)}h}{2}}^{\frac{{}^{(2)}h}{2}}2\,{}^{(2)}\sigma_{23}^{post}\,{}^{(2)}\varepsilon_{23g}d\,{}^{(2)}X_3+\\&+\int_{-\frac{{}^{(2)}h}{2}}^{\frac{{}^{(2)}h}{2}}{}^{(2)}\sigma_{23}^{post}\,{}^{(2)}v_{3,2}\,d\,{}^{(2)}X_3\end{aligned} \tag{4-47}$$

Using the generalized transverse shear strain $2\,{}^{(2)}\varepsilon_{23g}$ and Eq. (4-28), ${}^{(2)}v_{3,2}$ in the third term on the right hand side of Eq. (4-47) is substituted by $2\,{}^{(2)}\varepsilon_{23g}-{}^{(2)}\varphi_2$, since ${}^{(2)}v_3=w_0$. Equation (4-47) then becomes:

$$\begin{aligned}J_2\left(x_2=-a\right)=&\frac{1}{2}\int_{-\frac{{}^{(2)}h}{2}}^{\frac{{}^{(2)}h}{2}}{}^{(2)}\sigma_{22}\,{}^{(2)}\varepsilon_{22}d\,{}^{(2)}X_3+\frac{1}{2}\int_{-\frac{{}^{(2)}h}{2}}^{\frac{{}^{(2)}h}{2}}2\,{}^{(2)}\sigma_{23}^{post}\,{}^{(2)}\varepsilon_{23g}d\,{}^{(2)}X_3-\\&-{}^{(2)}\varphi_2\int_{-\frac{{}^{(2)}h}{2}}^{\frac{{}^{(2)}h}{2}}{}^{(2)}\sigma_{23}^{post}d\,{}^{(2)}X_3\end{aligned} \tag{4-48}$$

The second term on the right hand side of Eq. (4-48), is calculated, by substituting the generalized transverse shear strain, $2\,{}^{(2)}\varepsilon_{23g}$, from Eq. (4-31) and using the definition of ${}^{(2)}Q_{2g}$ given in Eq. (4-29). The integration of the a posteriori calculated transverse shear stresses through the thickness of the second layer in the third term on the right hand side of Eq. (4-48), is equal to ${}^{(2)}Q_{2g}$ (Eq. (4-29)). The first term on the right hand side of Eq. (4-48) is also calculated in terms of the normal and moment sub-resultants, ${}^{(2)}N_{22}$ and ${}^{(2)}M_{22}^{b}$, using the bending stresses and normal strains given in Eq. (4-39). This yields the following expression for the component of the J-integral along the path Γ_2:

$$J_2\left(x_2=-a\right)=\frac{1}{2}\left(\frac{\left[{}^{(2)}N_{22}\right]^2}{{}^{(2)}\bar{C}_{22}\,{}^{(2)}h}+\frac{12\left[{}^{(2)}M_{22}^{b}\right]^2}{{}^{(2)}\bar{C}_{22}\left({}^{(2)}h\right)^3}+\frac{\left[{}^{(2)}Q_{2g}\right]^2}{{}^{(2)}k_{44}\,{}^{(2)}C_{44}\,{}^{(2)}h}-2\,{}^{(2)}\varphi_2\,{}^{(2)}Q_{2g}\right) \tag{4-49}$$

To calculate the component of the J-integral along the path Γ_3, W and the tractions, ${}^{(i)}\sigma_{22}n_2$ and ${}^{(i)}\sigma_{23}^{post}n_2$ with $n_2=1$, are substituted into the definition of J-integral:

$$\begin{aligned}J_3\left(x_2=c\right)=&-\frac{1}{2}\sum_{i=1}^{2}\int_{x_3^{i-1}}^{x_3^i}{}^{(i)}\sigma_{22}\,{}^{(i)}\varepsilon_{22}dx_3+\frac{1}{2}\sum_{i=1}^{2}\int_{x_3^{i-1}}^{x_3^i}2\,{}^{(i)}\sigma_{23}^{post}\,{}^{(i)}\varepsilon_{23g}dx_3-\\&-\sum_{i=1}^{2}\int_{x_3^{i-1}}^{x_3^i}{}^{(i)}\sigma_{23}^{post}\,{}^{(i)}v_{3,2}\,dx_3\end{aligned} \tag{4-50}$$

Equation (4-50) can be further simplified by substituting ${}^{(i)}v_{3,2}=2\,{}^{(i)}\varepsilon_{23g}-{}^{(i)}\varphi_2$, obtained from Eq. (4-28) and using the generalized transverse shear strains and ${}^{(i)}v_3=w_0$:

$$\begin{aligned}J_3\left(x_2=c\right)=&-\frac{1}{2}\sum_{i=1}^{2}\int_{x_3^{i-1}}^{x_3^i}{}^{(i)}\sigma_{22}\,{}^{(i)}\varepsilon_{22}dx_3-\frac{1}{2}\sum_{i=1}^{2}\int_{x_3^{i-1}}^{x_3^i}2\,{}^{(i)}\sigma_{23}^{post}\,{}^{(i)}\varepsilon_{23g}dx_3+\\&+\sum_{i=1}^{2}{}^{(i)}\varphi_2\int_{x_3^{i-1}}^{x_3^i}{}^{(i)}\sigma_{23}^{post}dx_3\end{aligned} \tag{4-51}$$

The first term on the right hand side of Eq. (4-51) is calculated by substituting the bending stresses and normal strains from Eq. (4-42), performing the integration and using the definitions given in Eq. (G-2) in Appendix G for the coefficients C_{22}^0 and C_{22}^2:

$$-\frac{1}{2}\sum_{i=1}^{2}\int_{x_3^{i-1}}^{x_3^i}{}^{(i)}\sigma_{22}\,{}^{(i)}\varepsilon_{22}dx_3=-\frac{1}{2}\left(\frac{\left[{}^{(0)}N_{22}\right]^2}{C_{22}^0}+\frac{\left[{}^{(0)}M_{22}^{b}\right]^2}{C_{22}^2}\right) \tag{4-52}$$

The second term on the right hand side of Eq. (4-51), is an energy term due to the shear deformations and can be expressed accurately as the work done by the generalized transverse shear force, ${}^{(0)}Q_{2g}$ defined in Eq. (4-30), on the generalized transverse shear strain energetically associated to the generalized transverse shear force in Eq. (4-32):

$$-\frac{1}{2}\sum_{i=1}^{2}\int_{x_3^{i-1}}^{x_3^i}2\,{}^{(i)}\sigma_{23}^{post}\,{}^{(i)}\varepsilon_{23g}dx_3=-\frac{1}{2}\frac{\left[{}^{(0)}Q_{2g}\right]^2}{{}^{(0)}k_{44}C_{44}^{p}} \tag{4-53}$$

The integration of the a posteriori calculated transverse shear stresses through the thickness of the layers in the third term on the right hand side of Eq. (4-51), is equal to ${}^{(i)}Q_{2g}$ for i = 1 and 2 (Eq. (4-29)).

Substituting Eqs. (4-52) and (4-53) into Eq. (4-51) and noting that the integration of the a posteriori calculated transverse shear stresses through the thickness of the layers in the third term on the right hand side of Eq. (4-51), is equal to ${}^{(i)}Q_{2g}$ for i = 1 and 2 (Eq. (4-29)), the following expression for the component of the J-integral along the path Γ_3 is derived:

$$J_3\left(x_2=c\right)=-\frac{1}{2}\left(\frac{\left[{}^{(0)}N_{22}\right]^2}{C_{22}^0}+\frac{\left[{}^{(0)}M_{22}^b\right]^2}{C_{22}^2}+\frac{\left[{}^{(0)}Q_{2g}\right]^2}{{}^{(0)}k_{44}C_{44}^p}\right)+{}^{(1)}\varphi_2\,{}^{(1)}Q_{2g}+{}^{(2)}\varphi_2\,{}^{(2)}Q_{2g} \tag{4-54}$$

The energy release rate of the homogenized element in Figure 4-3(b) is then derived by summing Eqs. (4-46), (4-49) and (4-54):

$$\begin{aligned}\mathscr{G}_{II}=&\frac{1}{2}\left[\sum_{i=1}^{2}\left(\frac{\left[{}^{(i)}N_{22}\right]^2}{{}^{(i)}\bar{C}_{22}\,{}^{(i)}h}+\frac{12\left[{}^{(i)}M_{22}^b\right]^2}{{}^{(i)}\bar{C}_{22}\left({}^{(i)}h\right)^3}+\frac{\left[{}^{(i)}Q_{2g}\right]^2}{{}^{(i)}k_{44}\,{}^{(i)}C_{44}\,{}^{(i)}h}-2\,{}^{(i)}\varphi_2\left(x_2=-a\right){}^{(i)}Q_{2g}\left(x_2=-a\right)\right)-\right.\\&\left.\left(\frac{\left[{}^{(0)}N_{22}\right]^2}{C_{22}^0}+\frac{\left[{}^{(0)}M_{22}^b\right]^2}{C_{22}^2}+\frac{\left[{}^{(0)}Q_{2g}\right]^2}{{}^{(0)}k_{44}C_{44}^p}-2\,{}^{(1)}\varphi_2\left(x_2=c\right){}^{(1)}Q_{2g}\left(x_2=c\right)-2\,{}^{(2)}\varphi_2\left(x_2=c\right){}^{(2)}Q_{2g}\left(x_2=c\right)\right)\right]\end{aligned} \tag{4-55}$$

where ${}^{(i)}N_{22}$, ${}^{(i)}M_{22}^b$ and ${}^{(i)}Q_{2g}$ for i = 0, 1 and 2, are the force and moment sub-resultants acting on the different arms and are given in Eqs. (4-29) and (4-30), ${}^{(1)}\varphi_2=\varphi_2$ and ${}^{(2)}\varphi_2$ are the rotations of the first and second layers at the edges of the homogenized element, and are given in Eq. (4-27).

Equation (4-55) defines the energy release rate in terms of the force and moment sub-resultants on the different arms and end rotations which should be calculated through the multiscale structural theory. As it will be demonstrated in Sect. 4.5, the multiscale model is able to well predict the force and moment sub-resultants. The rotations of the layers at the edges of the element depend on two contributions: (i) the end rotations of arms rigidly clamped at the crack tip cross section and subjected to the end force and moment sub-resultants and (ii) the elastic near tip deformations. The structural concept of root-rotations, which are defined as the relative rotations of the layers at the delamination tip cross section, have been frequently used in the literature, e.g. [95], to account for the contribution of the elastic near tip deformations into the end rotations. As it was explained in Sect. 4.3 after Eq. (4-27), the multiscale structural theory neglects the root-rotations and predicts the rotations of the layers at the edges of the element as they are rigidly clamped at the crack tip. This fact will be demonstrated in Sect. 4.4.2, by particularizing Eq. (4-55) to the case of homogeneous layers and expressing the energy release rate in terms of the crack tip force and moment resultants. The contribution of the root-rotations into the energy release rate can be important even in the presence of long cracks and/or thin plates [95]. The missing contribution of the root-rotations in the solution of the multiscale model, can be accurately accounted for through the expression in [94, 95], once the force and moment sub-resultants are obtained by the multiscale structural model.

Except for the root-rotations contribution, the expression for the energy release rate in Eq. (4-55) is the same as that obtained in [95] for a homogeneous layer, and is the same as that which can be derived using

the results in [94] for a bi-material edge-cracked element. In Sect. 4.5, the accuracy of the multiscale structural theory in predicting the energy release rates through Eq. (4-55) will be investigated by comparing the results with 2D solutions obtained in [94].

4.4.2 Energy release rate in a homogeneous layer

When the edge-cracked element in Figure 4-3 is homogeneous, i.e. the first and second layers have the same material properties, the neutral axis of the intact section coincides with the mid-thickness axis of the element and the following relationships hold: $\Lambda_{22}=0$, ${}^{(1)}\varphi_2={}^{(2)}\varphi_2=\varphi_2$, ${}^{(1)}e={}^{(2)}h/2$ and ${}^{(2)}e={}^{(1)}h/2$. Therefore, the expression given in Eq. (4-55) for the energy release rate simplifies as:

$$\mathcal{G}_{II}=\frac{1}{2}\left[\sum_{i=1}^{2}\left(\frac{\left[{}^{(i)}N_{22}\right]^2}{\bar{C}_{22}{}^{(i)}h}+\frac{12\left[{}^{(i)}M_{22}^{b}\right]^2}{\bar{C}_{22}\left({}^{(i)}h\right)^3}+\frac{\left[{}^{(i)}Q_{2g}\right]^2}{{}^{(i)}k_{44}C_{44}{}^{(i)}h}-2\varphi_2\left(x_2=-a\right){}^{(i)}Q_{2g}\right)-\right.$$
$$\left.-\left(\frac{\left[{}^{(0)}N_{22}\right]^2}{\bar{C}_{22}\left({}^{(1)}h+{}^{(2)}h\right)}+\frac{12\left[{}^{(0)}M_{22}^{b}\right]^2}{\bar{C}_{22}\left({}^{(1)}h+{}^{(2)}h\right)^3}+\frac{\left[{}^{(0)}Q_{2g}\right]^2}{{}^{(3)}k_{44}C_{44}\left({}^{(1)}h+{}^{(2)}h\right)}-2\varphi_2\left(x_2=c\right){}^{(0)}Q_{2g}\right)\right] \tag{4-56}$$

In order to demonstrate the limitation of the homogenized structural theory with respect to exact LEFM solutions, i.e. neglecting root-rotations, Eq. (4-56) is redefined in terms of crack tip force and moment resultants, which are related to the values at the edges by the following relations:

$$\begin{aligned}
&{}^{(i)}N_{22}\left(x_2=0\right)={}^{(i)}N_{22}\left(x_2=-a\right);\ {}^{(0)}N_{22}\left(x_2=0\right)={}^{(0)}N_{22}\left(x_2=c\right)\\
&{}^{(i)}Q_{2g}\left(x_2=0\right)={}^{(i)}Q_{2g}\left(x_2=-a\right);\ {}^{(0)}Q_{2g}\left(x_2=0\right)={}^{(0)}Q_{2g}\left(x_2=c\right)\\
&{}^{(i)}M_{22}^{b}\left(x_2=0\right)={}^{(i)}M_{22}^{b}\left(x_2=-a\right)+{}^{(i)}Q_{2g}\left(x_2=-a\right)a\\
&{}^{(0)}M_{22}^{b}\left(x_2=0\right)={}^{(0)}M_{22}^{b}\left(x_2=c\right)-{}^{(0)}Q_{2g}\left(x_2=c\right)c
\end{aligned} \tag{4-57}$$

The rotations of the end sections of the layer in Figure 4-3 are calculated as functions of the rotations of the crack tip cross sections and the force and moment sub-resultants, by integrating the second equations in Eqs. (4-34) and (4-38) from $x_2=-a$ to $x_2=0$, and Eq. (4-41) from $x_2=0$ to $x_2=c$:

$$\begin{aligned}
\varphi_2\left(x_2=-a\right)&={}^{(i)}\varphi_2\left(x_2=0\right)-\left[\frac{12\,{}^{(i)}M_{22}^{b}\left(x_2=-a\right)a}{\bar{C}_{22}\left({}^{(i)}h\right)^3}+\frac{6\,{}^{(i)}Q_{2g}\left(x_2=-a\right)a^2}{\bar{C}_{22}\left({}^{(i)}h\right)^3}\right]\\
\varphi_2\left(x_2=c\right)&={}^{(0)}\varphi_2\left(x_2=0\right)+\frac{12\,{}^{(0)}M_{22}^{b}\left(x_2=c\right)c}{\bar{C}_{22}\left({}^{(1)}h+{}^{(2)}h\right)^3}-\frac{6\,{}^{(0)}Q_{2g}\left(x_2=c\right)c^2}{\bar{C}_{22}\left({}^{(1)}h+{}^{(2)}h\right)^3}
\end{aligned} \tag{4-58}$$

for i = 1, 2. Substituting Eqs. (4-57) and (4-58) into Eq. (4-56) yields:

$$\mathcal{G}_{II} = \frac{1}{2}\left[\sum_{i=1}^{2}\left(\frac{\left[{}^{(i)}N_{22}\right]^2}{\bar{C}_{22}\,{}^{(i)}h} + \frac{12\left[{}^{(i)}M_{22}^{b}\right]^2}{\bar{C}_{22}\left({}^{(i)}h\right)^3} + \frac{\left[{}^{(i)}Q_{2g}\right]^2}{{}^{(i)}k_{44}C_{44}\,{}^{(i)}h} + 2\,{}^{(i)}Q_{2g}\Delta\varphi_i\right) - \left(\frac{\left[{}^{(0)}N_{22}\right]^2}{\bar{C}_{22}\left({}^{(1)}h + {}^{(2)}h\right)} + \frac{12\left[{}^{(0)}M_{22}^{b}\right]^2}{\bar{C}_{22}\left({}^{(1)}h + {}^{(2)}h\right)^3} + \frac{\left[{}^{(0)}Q_{2g}\right]^2}{{}^{(3)}k_{44}C_{44}\left({}^{(1)}h + {}^{(2)}h\right)}\right)\right] \tag{4-59}$$

where ${}^{(i)}N_{22}$, ${}^{(i)}M_{22}^{b}$ and ${}^{(i)}Q_{2g}$ for $i = 0, 1, 2$, are calculated at the delamination tip cross section through Eq. (4-57), and $\Delta\varphi_i = {}^{(0)}\varphi\left(x_2 = 0\right) - {}^{(i)}\varphi\left(x_2 = 0\right)$ for $i = 1, 2$ are the root-rotations. Since the homogenized structural theory does not account for the root-rotations, due to the imposition of the continuity condition on the global bending rotation variable at the traction-free delamination tip cross section as part of the solution of the model, ${}^{(0)}\varphi\left(x_2 = 0\right) = {}^{(1)}\varphi\left(x_2 = 0\right) = {}^{(2)}\varphi\left(x_2 = 0\right) = \varphi\left(x_2 = 0\right)$, $\Delta\varphi_i$ in Eq. (4-59) is zero and the energy release rate predicted by the model is:

$$\mathcal{G}_{II} = \frac{1}{2}\left[\sum_{i=1}^{2}\left(\frac{\left[{}^{(i)}N_{22}\right]^2}{\bar{C}_{22}\,{}^{(i)}h} + \frac{12\left[{}^{(i)}M_{22}^{b}\right]^2}{\bar{C}_{22}\left({}^{(i)}h\right)^3} + \frac{\left[{}^{(i)}Q_{2g}\right]^2}{{}^{(i)}k_{44}C_{44}\,{}^{(i)}h}\right) - \left(\frac{\left[{}^{(0)}N_{22}\right]^2}{\bar{C}_{22}\left({}^{(1)}h + {}^{(2)}h\right)} + \frac{12\left[{}^{(0)}M_{22}^{b}\right]^2}{\bar{C}_{22}\left({}^{(1)}h + {}^{(2)}h\right)^3} + \frac{\left[{}^{(0)}Q_{2g}\right]^2}{{}^{(3)}k_{44}C_{44}\left({}^{(1)}h + {}^{(2)}h\right)}\right)\right] \tag{4-60}$$

Except for the root-rotations contribution, the expression for the energy release rate in Eq. (4-60) is the same as that obtained in [95], Eq. (4-59), for a homogeneous layer. Similar to Eq. (4-55), the missing contribution of the root-rotations in the solution of the multiscale model, Eq. (4-60), can be accurately accounted for through the expression in [95], once the force and moment sub-resultants are obtained by the multiscale structural model. In [95], the root-rotations are defined in a tabular form for edge-cracked homogeneous and orthotropic layers subjected to arbitrary end forces. The expressions for the root-rotations in [95] depend linearly on the crack tip stress resultants through compliance coefficients, which are derived numerically using rigorous finite element simulations.

In Sect. 4.5, the accuracy of the multiscale structural theory in predicting the energy release rates through Eq. (4-60) will be investigated by comparing the results with 2D solutions in [95].

4.4.3 Energy release rate in terms of local measures

An expression for the energy release rate of the edge-cracked element in Figure 4-3(a) is derived in terms of the crack surface relative displacements through the application of the J-integral along the path Γ, shown in Figure 4-5(a), which follows the delamination surfaces. The expression is then presented in terms of the variables of the multiscale structural theory, which yields the energy release rate of the homogenized edge-cracked element in Figure 4-3(b) in terms of the crack surface relative displacements.

The calculation can be conveniently performed using Bueckner's superposition principle, Figure 4-5 and the procedure presented in [100, 101]. The edge-cracked element, shown in Figure 4-5(a), is considered as superposition of an intact element subjected to the end forces, Figure 4-5(b), and an edge-cracked element subjected to applied shear and normal tractions, $\tau(x_2)$ and $\sigma(x_2)$, along the crack surfaces, Figure 4-5(c). The applied shear and normal tractions in the cracked element are equal but opposite in sign to the shear and normal tractions generated by the end forces, at the distance ${}^{(1)}h$ from the bottom surface of the intact element.

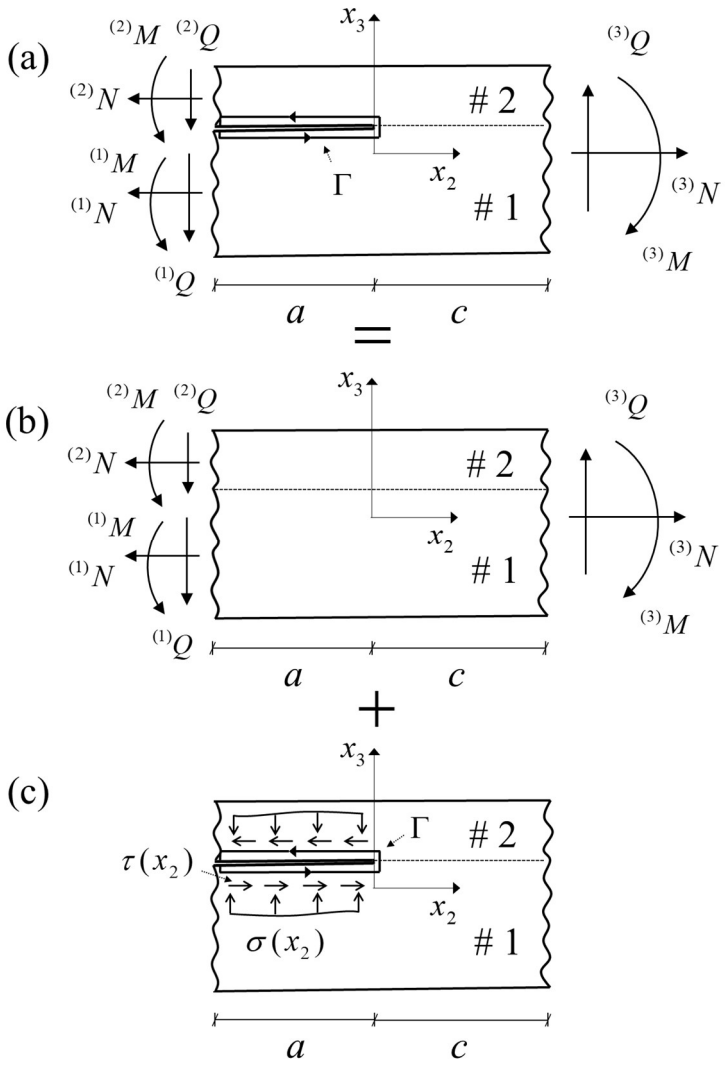

Figure 4-5: (a) the edge-cracked element under mode II dominant assumption, which is created by superposing intact (b), and cracked (c) problems.

An application of the J-integral along a path around the crack surfaces in Figure 4-5(c) yields:

$$\mathcal{G}_{II} = -\int_{x_2=-a}^{x_2=0} \tau(x_2)\,{}^{(1)}v_{2,2}\,dx_2 - \int_{x_2=-a}^{x_2=0} \sigma(x_2)\,{}^{(1)}v_{3,2}\,dx_2 - \int_{x_2=0}^{x_2=-a} \tau(x_2)\,{}^{(2)}v_{2,2}\,dx_2 - \int_{x_2=0}^{x_2=-a} \sigma(x_2)\,{}^{(2)}v_{3,2}\,dx_2 \tag{4-61}$$

where the first two terms on the right hand side of Eq. (4-61) account for the component of the J-integral along the lower crack surface and the remaining terms account for the component of the J-integral along the upper crack surface. Collecting the terms in Eq. (4-61) multiplying $\tau(x_2)$ and $\sigma(x_2)$, yields:

$$\mathcal{G}_{II} = \int_{x_2=-a}^{x_2=0} \tau(x_2)\hat{v}_{2,2}\, dx_2 + \int_{x_2=-a}^{x_2=0} \sigma(x_2)\left({}^{(2)}v_3 - {}^{(1)}v_3\right)_{,2}\, dx_2 \tag{4-62}$$

The second term on the right hand side of Eq. (4-62) is zero, since ${}^{(2)}v_3 = {}^{(1)}v_3$ in a mode II dominant problem. The first term on the right hand side of Eq. (4-62) is defined in terms of the variables of the multiscale structural theory to derive and expression for the energy release rate of the homogenized edge-cracked element in Figure 4-3(b) in terms of the crack surface relative displacements:

$$\mathcal{G}_{II} = {}^{(1)}\sigma_{23}^{post}\left(x_2, x_3 = x_3^1\right)\left[\hat{v}_2\left(x_2 = -a\right) - \hat{v}_2\left(x_2 = 0\right)\right] \tag{4-63}$$

where ${}^{(1)}\sigma_{23}^{post}\left(x_2, x_3 = x_3^1\right) = -\tau(x_2)$ is the shear stress calculated a posteriori through the multiscale structural theory in the intact problem in Figure 4-5(b), and the crack surface relative displacement is obtained through Eq. (4-7) from the homogenized description of the problem in Figure 4-5(a), since the relative sliding displacement of the problem in Figure 4-5(c) is equal to that of the specimen in Figure 4-5(a).

The expression in Eq. (4-63) defines the energy release rate of the model system in Figure 4-3, as function of the crack surface relative displacement. The relative displacement of the crack surfaces is a local measure, which is used in cohesive crack modeling to study propagation of delaminations. In cohesive crack models, this local measure is usually calculated by through the thickness discretization of the domain. In the homogenized model, however, the relative sliding displacement is predicted without through thickness discretization, through the homogenized description of the problem, with the same number of variables as that needed for modeling a single intact homogenous layer. The accuracy of Eq. (4-63), which reflects the accuracy of the multiscale structural theory in predicting relative crack sliding displacements, will be investigated in Sect. 4.5 by comparing the results with two-dimensional solutions.

4.4.4 Energy release rate through total potential energy

The energy release rate of the homogenized edge-cracked element in Figure 4-3(b) can be derived as total potential energy decrease during unit crack extension:

$$\mathcal{G}_{II} = -\frac{d\prod}{da} = -\frac{d\left(U+V\right)}{da} \tag{4-64}$$

where $\prod$, U and V are, respectively, the total potential energy, total strain energy and the potential of external forces. The expression in Eq. (4-64) is equivalent to the J-integral and is based on the principle of energy conservation, which states that the energy added to and dissipated from the system during the crack extension must be the same.

Application of Eq. (4-64) to the End Notched Flexural (ENF) specimen in Figure 4-6, yields the following well-known expression for the energy release rate:

$$\mathcal{G}_{II} = \frac{P^2}{2}\frac{dC}{da} \tag{4-65}$$

where P is the applied concentrated load and $C = w_0\left(x_2 = L\right)/P$ the compliance of the specimen.

As it was explained after Eq. (4-14), the multiscale structural theory neglects the shear deformations in the delaminated portion, and therefore, the model underestimates the compliance of the specimen. This problem then affects the accuracy of the predicted energy release rates through the compliance method, Eq. (4-65). In Sect. 4.5.4, the multiscale structural theory is used to define the compliance of a homogeneous ENF specimen and calculate the energy release rate through Eq. (4-65); the results are discussed and compared with two-dimensional solutions.

4.5 MODEL APPLICATIONS AND DISCUSSION

In this section the fracture model formulated in the previous sections is applied to calculate the energy release rate of an ENF specimen, Figure 4-6(a). This is an experimental fracture specimen where, for some combinations of material properties and layer thicknesses, the delamination is in pure mode II conditions or mode II dominant conditions. For example, when the layers of the specimen have the same material properties, the delamination is in pure mode II conditions for ${}^{(1)}h = {}^{(2)}h$, and in mode II dominant conditions when the upper layer is thinner ${}^{(2)}h < {}^{(1)}h$, due to localized contact at the crack tip [102]. The problem may also be dominated by mode II deformations for incompressible isotropic layers when ${}^{(2)}h = {}^{(1)}h$ and the first layer is stiffer than the second layer [103], ${}^{(2)}E/{}^{(1)}E \le 1$ with ${}^{(k)}E$ the Young's modulus of the layer k, again due to localized contact at the crack tip.

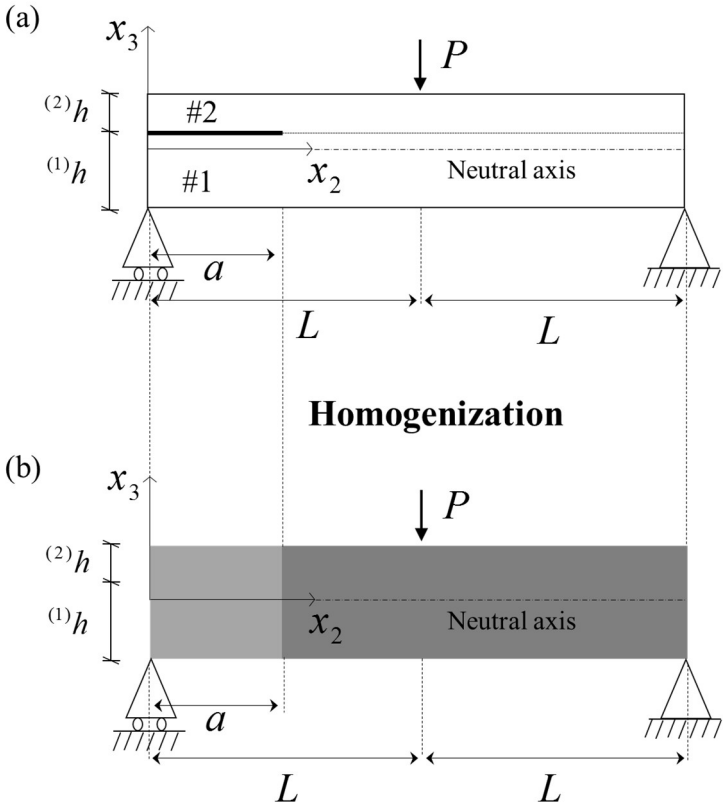

Figure 4-6: (a) The ENF specimen under mode II dominant conditions and (b) the homogenized description of the problem.

Force and moment resultants and sub-resultants in the ENF specimen, Figure 4-6, are derived in closed-form; the force and moment resultants for $0 \le x_2 \le L$ are obtained through simple equilibrium considerations:

$$^{(0)}N_{22} = 0; \qquad ^{(0)}M^b_{22} = -\frac{P}{2}x_2; \qquad ^{(0)}Q_{2g} = -\frac{P}{2} \tag{4-66}$$

Comparing the second equations in Eqs. (4-34) and (4-38) shows that the layers in the delaminated region have the same curvature, $\varphi_{2,2}$. This yields:

$$\frac{^{(2)}M^b_{22}}{^{(1)}M^b_{22}} = \frac{^{(2)}Q_{2g}}{^{(1)}Q_{2g}} = \frac{^{(2)}\bar{C}_{22}}{^{(1)}\bar{C}_{22}}\left(\frac{^{(2)}h}{^{(1)}h}\right)^3 \tag{4-67}$$

Using Eqs. (4-66) and (4-67), and noting that the shear force and moment resultants in (4-66) are the summation of the shear force and moment sub-resultants, $^{(0)}M^b_{22} = {}^{(1)}M^b_{22} + {}^{(2)}M^b_{22}$ and $^{(0)}Q_{2g} = {}^{(1)}Q_{2g} + {}^{(2)}Q_{2g}$, the force and moment sub-resultants in the layers are derived as:

$$
\begin{aligned}
&{}^{(1)}Q_{2g} = -\frac{1}{1+\dfrac{{}^{(2)}\bar{C}_{22}}{{}^{(1)}\bar{C}_{22}}\left(\dfrac{{}^{(2)}h}{{}^{(1)}h}\right)^3}\frac{P}{2}; \qquad {}^{(2)}Q_{2g} = -\frac{\dfrac{{}^{(2)}\bar{C}_{22}}{{}^{(1)}\bar{C}_{22}}\left(\dfrac{{}^{(2)}h}{{}^{(1)}h}\right)^3}{1+\dfrac{{}^{(2)}\bar{C}_{22}}{{}^{(1)}\bar{C}_{22}}\left(\dfrac{{}^{(2)}h}{{}^{(1)}h}\right)^3}\frac{P}{2} \\
&{}^{(1)}M_{22}^{b} = {}^{(1)}Q_{2g}x_2; \qquad {}^{(2)}M_{22}^{b} = {}^{(2)}Q_{2g}x_2 \\
&{}^{(1)}N_{22} = {}^{(2)}N_{22} = 0
\end{aligned}
\tag{4-68}
$$

Note that the normal force resultants and sub-resultants are zero for the ENF specimen, due to the absence of axial forces.

In the following, the force and moment resultants and sub-resultants derived in Eqs. (4-66) and (4-68) will be used along with Eqs. (4-55) and (4-60) to derived, in closed-form, the energy release rates of some ENF specimens.

4.5.1 Energy release rate in a homogeneous ENF specimen with equal thickness layers

Here, a homogeneous ENF specimen with ${}^{(2)}h = {}^{(1)}h = h$ is considered. The material properties of the layers are: $E_T/E_L = 0.071$, $G_{LT}/E_L = 0.033$, $\nu_{LT} = 0.32$ and $\nu_{TT} = 0.45$ (subscripts L and T indicate in-plane principal material directions and the L direction coincides with x_2 axis in the layers). The assumed ratios between the elastic constants of the layers could represent a graphite-epoxy composite, and provide a challenging case, in which the effects of the root-rotations are pronounced. The delamination is under pure mode II conditions due to the symmetric layup and the anti-symmetric loading about the delamination line.

The crack tip force and moment resultants and sub-resultants are obtained through Eqs. (4-66) and (4-68), and are substituted into Eq. (4-60) with ${}^{(i)}k_{44} = 5/6$ for $i = 0, 1, 2$, to calculate the energy release rate of the specimen. The normal forces are zero for this problem, and the terms in Eq. (4-60) which depend on the shear forces, give a zero contribution, due to the symmetry of the geometry about the delamination line. The energy release rate is then defined only by the terms accounting for the contributions of the crack tip bending moments:

$$
\frac{\mathcal{G}_{II}\bar{C}_{22}h}{P^2} = \frac{9}{16}\left(\frac{a}{h}\right)^2 \tag{4-69}
$$

The 2D Linear Elastic Fracture Mechanics solution for the energy release rate has been derived in [95]:

$$
\frac{\mathcal{G}_{II}\bar{C}_{22}h}{P^2} = \frac{9}{16}\left(\frac{a}{h}\right)^2\left[1+0.728\left(\frac{h}{a}\right)-0.529\left(\frac{h}{a}\right)^2\right] \tag{4-70}
$$

The summation of the second and third terms in the square bracket account for the root-rotations produced by the bending moments and by the shear forces.

4.5.2 Homogeneous ENF specimen with unequal thickness layers

A homogeneous ENF specimen with ${}^{(1)}h = 4h/3$ and ${}^{(2)}h = 2h/3$ is considered, in this section. In this case since ${}^{(1)}h > {}^{(2)}h$, the interface between the layers is under compression and the delamination under mode II dominant conditions, due to localized contact at the crack tip [102]. The material properties of the layers are: $E_T/E_L = 0.071$, $G_{LT}/E_L = 0.033$, $\nu_{LT} = 0.32$ and $\nu_{TT} = 0.45$ (subscripts L and T indicate in-plane principal material directions and the L direction coincides with x_2 axis in the layers).

The crack tip force and moment resultants and sub-resultants are obtained through Eqs. (4-66) and (4-68), and are substituted into Eq. (4-60) with ${}^{(i)}k_{44} = 5/6$ for $i = 0, 1, 2$, to calculate the energy release rate of the specimen:

$$\frac{\mathcal{G}_{II}\bar{C}_{22}h}{P^2} = \frac{3}{8}\left(\frac{a}{h}\right)^2\left[1+1.357\left(\frac{h}{a}\right)^2\right] \tag{4-71}$$

Unlike the previous example, the geometry is not symmetric about the delamination plane and both shear forces and bending moments contribute into the energy release rate. The first term on the right hand side of Eq. (4-71), defines the contribution of the crack tip bending moments and the second term, which is independent of the delamination length, defines the contribution of the crack tip shear forces.

The accurate 2D LEFM solution for the energy release rate is obtained in [95]:

$$\frac{\mathcal{G}_{II}\bar{C}_{22}h}{P^2} = \frac{3}{8}\left(\frac{a}{h}\right)^2\left[1+1.357\left(\frac{h}{a}\right)^2+2.141\left(\frac{h}{a}\right)+0.101\left(\frac{h}{a}\right)^2\right] \tag{4-72}$$

where the summation of the third and fourth terms account for the effect of the shear forces on the crack tip root-rotations generated by the bending moments and the shear forces. The second term, which becomes independent of the delamination length after expanding the expression, accounts for the contribution of shear deformations along the beam arms. This contribution is captured through the homogenized model, thanks to the a posteriori treatment of the shear stresses, which was presented in Sect. 4.3 and allows to account for the shear deformations along the delaminated arms where the interfacial tractions vanish. The contribution of the root-rotations is instead missing in Eq. (4-71). This example also provides a challenging case, in which the contribution of the root-rotations is significant. For instance, for a dimensionless crack length equal to 10, the contribution of the root-rotations, is about 18% of the whole energy release rate and it remains large also for very long crack lengths.

4.5.3 Bi-material ENF specimen with equal thickness layers

A bi-material ENF specimen made of two incompressible isotropic layers with ${}^{(1)}h = {}^{(2)}h = h$ and ${}^{(2)}E/{}^{(1)}E = 2/3$ is considered. For this geometry and material properties, the interface between the layers is under compression and the delamination under mode II dominant conditions.

An expression for the energy release rate of the bi-material element in terms of the crack tip force and moment resultants and sub-resultants can be obtained by removing the terms multiplying the end rotations

in Eq. (4-55); using the resulting expression together with the crack tip force and moment resultants and sub-resultants in Eqs. (4-66) and (4-68), ${}^{(i)}k_{44} = 5/6$ for i = 1, 2, and ${}^{(0)}k_{44} = 1$, the following equation is obtained for the energy release rate of this example:

$$\frac{\mathscr{G}_{II}{}^{(2)}Eh}{P^2} = 0.334\left(\frac{a}{h}\right)^2\left[1 + 0.240\left(\frac{h}{a}\right)^2\right] \tag{4-73}$$

The first term on the right hand side of Eq. (4-73), defines the contribution of the bending moments and the second term, which is independent of the delamination length, defines the contribution of the shear forces.

The accurate 2D elasticity solution is obtained in [103]:

$$\frac{\mathscr{G}_{II}{}^{(2)}Eh}{P^2} = 0.334\left(\frac{a}{h}\right)^2\left[1 + 0.446\left(\frac{h}{a}\right) + 0.060\left(\frac{h}{a}\right)^2\right] \tag{4-74}$$

where the first term defines the contribution of the bending moments, and the remaining terms account for the contributions of the shear forces due to the work done on the transverse shear deformations and on the root-rotations.

4.5.4 Numerical results and discussion

In Sects. 4.5.1, 4.5.2 and 4.5.3, the energy release rates of different ENF specimens were calculated using the local fields derived in Sect. 4.3, assuming that the lengths of the crack and the ligament ahead of the crack tip, *a* and *c,* are sufficiently long. This assumption ensures that the stress fields at the traction-free delamination tip depend only on the value of the force and moment resultants and the stress distributions at the ends of the element are unaffected by the delamination tip stress field. In order to verify this assumption, the multiscale structural theory in [25] is applied here to analyze the ENF specimen in Figure 4-6, and the crack tip force and moment resultants and sub-resultants are calculated numerically by introducing a cohesive interface governed by the interfacial traction law (4-5), and the solution of the displacement variables of the multiscale model. This analysis also allows to investigate the capability of the multiscale structural theory to predict the displacements, stresses and interfacial tractions in a specimen with finite length delamination.

The material and interfacial properties are given for each example considered in the following. The numerical values for the interfacial stiffnesses in the intact/delaminated portion are chosen as large/small as possible, considering that numerical problems do not arise in calculations. The specimen is discretized into three portions separated at the coordinates $x_2 = a$ and $x_2 = L$. The global variables in three different regions are defined in Eq. (4-26), where the shear correction factor is assumed to be $k_{44} = 5/6$ for homogeneous specimens and $k_{44} = 1$ for bi-material specimens. The twenty-four integration constants in the solution of the global variables are calculated by imposing boundary and continuity conditions. The boundary conditions are given in Eq. (4-21), with $\tilde{w}_0 = \tilde{M}_2^b = \tilde{M}_2^{zS} = 0$ at $x_2 = 0$ and $2L$, $\tilde{N}_2 = 0$ at $x_2 = 0$ and $\tilde{v}_{02} = 0$ at $x_2 = 2L$. The continuity conditions are imposed at $x_2 = a$ and $x_2 = L$ on the global variables

v_{02}, φ_2, w_0, $w_{0,2}$, N_{22}, M_{22}^b, Q_{2g} and M_{22}^{zS}. Displacements, strains and stresses in the layers and the relative crack sliding displacement along with the force and moment resultants and sub-resultants are calculated from the global variables using Eqs. (4-7), (4-9), (4-11), (4-12) and (4-29). The energy release rate is then calculated using Eqs. (4-55), (4-60), (4-63) and (4-65).

It was observed that the crack tip force and moment resultants and sub-resultants calculated numerically through the solution of the displacement variables of the multiscale model virtually coincide with those derived from equilibrium considerations and given in Eqs. (4-66) and (4-68). Consequently, the energy release rates obtained numerically also virtually coincide with the closed-form solutions in Eqs. (4-69), (4-71) and (4-73).

As an alternative, the intact and delaminated portions of the specimen in Figure 4-6 could be described by the zero-order solution of the homogenized theory, derived in Appendix H through a perturbation expansion of the exact solution of the equilibrium equations of the model, Eq. (4-26). The perturbation parameter, δ, is chosen as $\delta = 1/K_S \to 0$ to investigate the fully bonded limit (intact region), and as $\delta = \overline{B} \to 0$, where $\overline{B}$ defined in Eq. (4-25) goes to zero with the same order as K_S, to investigate the fully debonded limit (delaminated region). The procedure for obtaining zero-order solutions are explained after Eq. (4-26) and in Appendix H.

In the fully bonded limit, $\delta = 1/K_S \to 0$, and the coefficients C_{22}^{0S} defined in Eq. (G-2) in Appendix G, and $\overline{A}$, $\overline{B}$, $\overline{C}$, $\overline{D}$ and $\overline{E}$ in Eq. (4-25) simplify by substituting $R_{S22}^2 = \Lambda_{22}\left(x_3 - x_3^1\right)$. The zero-order solution of the model are then obtained by substituting the simplified coefficients into Eq. (4-26). The zero-order equilibrium equations of the model (4-24) has order VIII, and the zero-order solution coincides with the solution of the original first order zigzag theory developed in [62] for fully bonded plates.

In the fully debonded limit, $\delta = \overline{B} \to 0$, and the finite coefficients in Eq. (4-26) are $\overline{A} \to 1$, C_{22}^r, $\overline{E}$, $\overline{D}\overline{B}$, $C_{22}^{0s}\overline{B}$; the coefficients C_{22}^{0S} and $\overline{D}$ are instead unbounded. The zero-order equilibrium equations of the model (4-24) has order VIII, and the zero-order solution is derived in Appendix H.

If the specimen in Figure 4-6 is homogeneous, the last boundary condition in Eq. (4-21) becomes an identity, in the intact region, and the order of the system of equilibrium equations in the intact region reduces to VI, which is lower than the order VIII of the equilibrium equations in the delaminated region, Eq. (4-24) [7]. Therefore, the higher order moment M_{22}^{zS} which appears in the last boundary condition in Eq. (4-21), $M_2^{zS} n_2 = \tilde{M}_2^{zS}$, should be zero at the delamination tip cross section. The solution of the global variables in ENF specimen, which have now twenty integration constants, are derived by imposing boundary conditions, $\tilde{N}_2 = \tilde{w}_0 = \tilde{M}_2^b = \tilde{M}_2^{zS} = 0$ at $x_2 = 0$, $\tilde{v}_{02} = \tilde{w}_0 = \tilde{M}_2^b = 0$ at $2L$, and continuity conditions at $x_2 = a$ and $x_2 = L$ on v_{02}, φ_2, w_0, N_{22}, M_{22}^b, Q_{2g} together with $\tilde{M}_2^{zS} = 0$ in the delaminated region at $x_2 = a$.

The difference between the orders of the governing field equations in the fully bonded and fully debonded limits in a homogeneous specimen, as explained above, indicates a singularity in the model, as demonstrated in [7], and singular behaviors such as boundary layer are expected to form near the regions where the

kinematic constraints are imposed. Indeed, boundary layer is found in the solution of the homogenized model for the ENF specimen (see Sect. 4.5.6).

Figure 4-7, Figure 4-8 and Figure 4-9 refer to the examples considered in Sects. 4.5.1, 4.5.2 and 4.5.3. The figures present the relative percent error between the energy release rates obtained through the proposed homogenized model, Eqs. (4-55), (4-60), (4-63) and (4-65), and the accurate 2D solutions, Eqs. (4-70), (4-72) and (4-74).

In the solution of the homogenized model, the dimensionless interfacial stiffnesses $K_S h/E_L$ for the intact and delaminated portions of the specimen are set to be 10^3 and 10^{-10}, respectively. For instance for the example in Sect. 4.5.1, percentage change in the energy release rate obtained through Eq. (4-60) by increasing the dimensionless interfacial stiffness of the intact region to 10^4 and decreasing that of the delaminated portion to 10^{-11} is less than 10^{-5} %.

Figure 4-7 refers to the homogeneous ENF specimen with the layers with equal thickness considered in Sect. 4.5.1, and presents the relative percent error between the energy release rate obtained through the proposed homogenized model, Eqs. (4-60), (4-63) and (4-65), and the accurate 2D solution in Eq. (4-70). The results of Eq. (4-63), which defines the energy release rate in terms of the crack surface relative displacements, virtually coincide with those of Eq. (4-60), which uses sub-resultants. Both solutions are in agreement with the accurate 2D solutions and the relative error, caused by the root-rotations contribution, is below 6.4% already for $a/h = 10$.

The predictions of the model through the compliance method, Eq. (4-65), have less accuracy compared to those made through Eqs. (4-60) and (4-63), as explained in the following. The multiscale structural theory underestimates the compliance of the ENF specimen, due to neglecting the shear deformations in the delaminated portion of the plate. In this example, the part of the compliance of the specimen associated with the shear deformations, or the transverse shear compliance, is independent of the delamination length. This is due to the symmetry of the geometry with respect to the crack line. In other words, when the delamination grows, the reduction in the transverse shear compliance of the intact region, is the same as the increase in that of the delaminated region. This explains why the shear deformations/forces do not contribute into the energy release rate for this ENF specimen. However, since the shear deformations of the delaminated region are neglected, the homogenized structural model only accounts for the reduction of the transverse shear compliance of the intact region, and this gives an incorrect contribution into the energy release rates calculated through the compliance method, Eq. (4-65).

The macro-structural behavior of the specimen will be presented in Sect. 4.5.5.

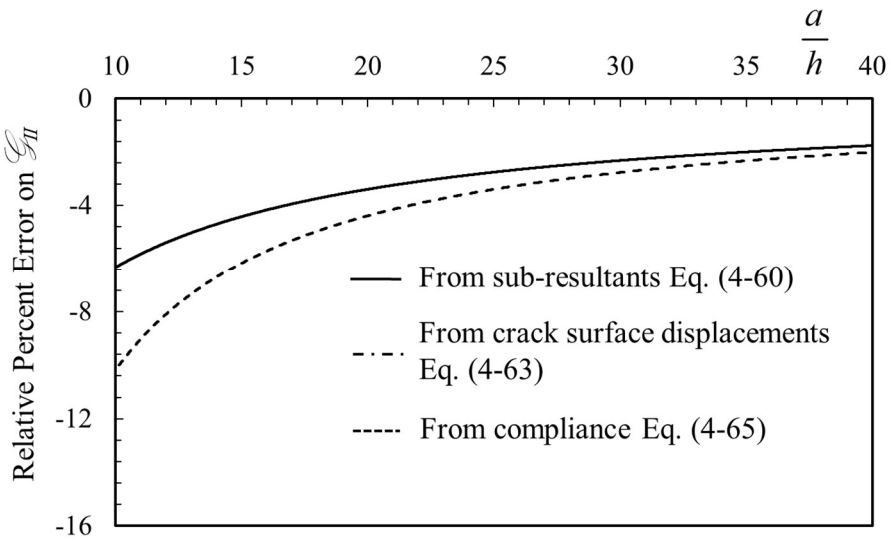

Figure 4-7: Relative percent error between the energy release rates of the homogenized model and 2D solution [95] in homogeneous ENF specimen with ${}^{(2)}h = {}^{(1)}h = h$. Material: $E_T/E_L = 0.071$, $G_{LT}/E_L = 0.033$, $\nu_{LT} = 0.32$ and $\nu_{TT} = 0.45$ (L and T indicate in-plane principal material directions with L = x_2). "From sub-resultants Eq. (4-60)", "From crack surface displacements Eq. (4-63)" and "from compliance Eq. (4-65)" refer to relative percent errors of energy release rates in Eqs. (4-60), (4-63) and (4-65), and Eq. (4-70).

Figure 4-8 refers to the homogeneous ENF specimen with the layers with unequal thickness considered in Sect. 4.5.2, and presents the relative percent error between the energy release rate obtained through the proposed homogenized model, Eqs. (4-60) in terms of the crack tip force and moment sub-resultants and (4-63) in terms of the crack surface relative displacements, and the accurate 2D solution in Eq. (4-72). The solutions obtained through Eq. (4-60) are more accurate than those obtained by Eq. (4-63), since Eq. (4-60) accounts for the contribution of shear deformations into the energy release rate; Eq. (4-63) accounts only for the contribution of the bending moments into the energy release rate.

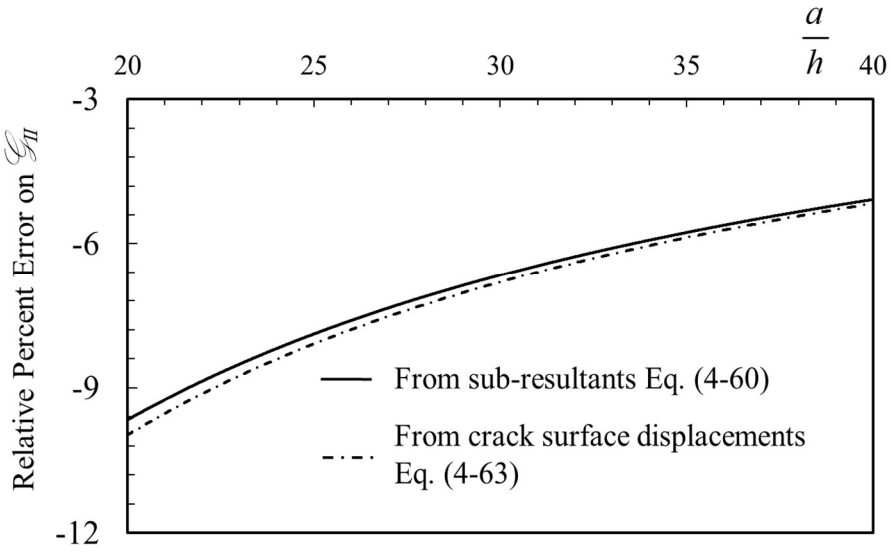

Figure 4-8: Relative percent error between the energy release rates of the homogenized model and 2D solution [95] in homogeneous ENF specimen with ${}^{(1)}h = 4h/3$ *and* ${}^{(2)}h = 2h/3$. Material: $E_T/E_L = 0.071$, $G_{LT}/E_L = 0.033$, $\nu_{LT} = 0.32$ and $\nu_{TT} = 0.45$ (L and T indicate in-plane principal material directions with L = x_2). "From sub-

resultants Eq. (4-60)" and "From crack surface displacements Eq. (4-63)" refer to relative percent errors of energy release rates in Eqs. (4-60) and (4-63), and Eq. (4-72).

Figure 4-9 refers to the bi-material ENF specimen with the layers with equal thickness considered in Sect. 4.5.3, and presents the relative percent error between the energy release rate obtained through the proposed homogenized model, Eqs. (4-55) in terms of the force and moment sub-resultants and (4-63) in terms of the crack surface relative displacements, and the accurate 2D solution in Eq. (4-74).

The predictions of the homogenized model through Eqs. (4-55) and (4-63) are in good agreement with accurate solution, Eq. (4-74), and tend to the same values for long delaminations, for which the bending moment contribution into the energy release rate dominates those of the shear deformations and root-rotations. Also for this bi-material example, the results obtained through Eq. (4-63) accounts only for the contribution of the bending moments into the energy release rate.

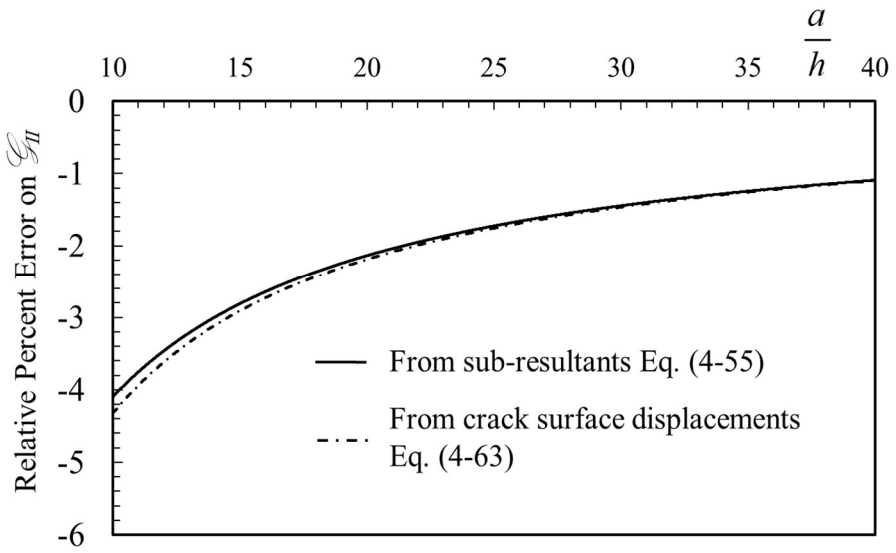

Figure 4-9: Relative percent error between the energy release rates of the homogenized model and 2D solution [103] in bi-material ENF specimen made of two incompressible isotropic layers with ${}^{(1)}h = {}^{(2)}h = h$ and ${}^{(2)}E/{}^{(1)}E = 2/3$. "From sub-resultants Eq. (4-55)" and "From crack surface displacements Eq. (4-63)" refer to relative percent errors of energy release rates in Eqs. (4-55) and (4-63), and Eq. (4-74).

4.5.5 Macro-structural behavior of a homogeneous ENF specimen

The macro-structural response of the specimen studied in Sect. 4.5.1, is presented here. The specimen is homogeneous with ${}^{(2)}h = {}^{(1)}h = h$, $2L = 200h/3$ and an initial delamination of length $a_0 = 20h$. The material properties of the layers are: $E_T/\overline{C}_{22} = 0.071$ and $G_{LT}/\overline{C}_{22} = 0.033$ (subscripts L and T indicate in-plane principal material directions and the L direction coincides with x_2 axis in the layers). In the solution of the homogenized model, the dimensionless interfacial stiffnesses $K_S h/\overline{C}_{22}$ for the intact and delaminated portions of the specimen are set to be 10^3 and 10^{-10}, respectively. Once the global kinematic variables in different portions of the specimen are defined, as explained after Figure 4-6, displacements, strains and stresses in the layers are calculated through Eqs. (4-7), (4-9), (4-11) and (4-12).

The macro-structural response of the specimen is shown in Figure 4-10. The critical load for the propagation of the delamination, P_C, is obtained from Eq. (4-69) and the delamination is assumed to propagate when its energy release rate equals the fracture energy, $\mathcal{G}_{IIC}$:

$$\frac{P_C}{\sqrt{\mathcal{G}_{IIC} h \bar{C}_{22}}} = \frac{4}{3}\left(\frac{h}{a_0}\right) \tag{4-75}$$

The nonlinear portion of the macro-structural behavior corresponding to the post-peak response, after $P_C \Big/ \sqrt{\mathcal{G}_{IIC} h \bar{C}_{22}}$ has been reached, is obtained by controlling the crack length from the initial value $a_0/h = 20$ to mid-span $a_0/h = 100/3$; the corresponding critical loads are calculated from Eq. (4-75) and the load point displacements from the solution of the global variable, $w_0(x_2 = L)$, Eq. (4-26). The homogenized model captures the snap-back instability in the post-peak response, which is inherently a discrete fracture event. The crack length control procedure does not require numerical techniques such as arc-length procedures to capture the snap-back behavior. The crack length monotonically increases during the process.

The solution of the multiscale model is valid until the delamination reaches the mid-span, where the concentrated load is applied; the solution for crack lengths higher than the mid-span is presented in Figure 4-10 by dots, and is given only to show the limit of the solution which tends to that of a fully delaminated specimen, the dash-dot line in Figure 4-10.

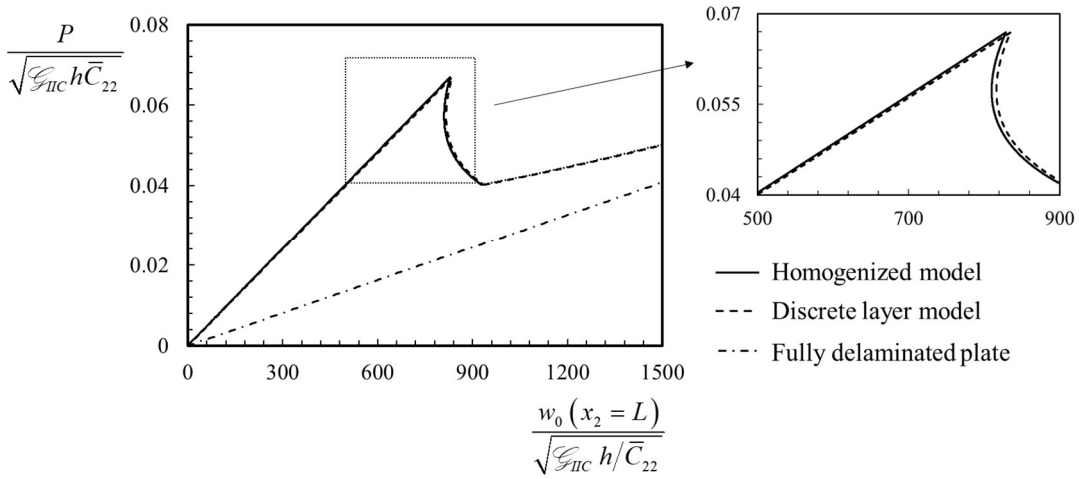

Figure 4-10: Dimensionless critical load versus load point displacement of homogeneous ENF specimen with ${}^{(2)}h = {}^{(1)}h = h$, $2L = 200h/3$ and $a_0 = 20h$. Material: $E_T/\bar{C}_{22} = 0.071$, $G_{LT}/\bar{C}_{22} = 0.033$ (L and T indicate in-plane principal material directions with L = x_2). Shear correction factor, $k_{44} = 5/6$.

The dimensionless load-deflection response is compared in the figure with that obtained through a discrete layer model [102]. In this approach, the layers in the delaminated region are modeled separately by the first order shear deformation theory and are allowed to freely slide along each other, while they remain in contact. The intact portion of the specimen is also modeled by the first order shear deformation

theory. The equilibrium equations of the layers are then solved and the boundary and continuity conditions are imposed to obtain the solution. This approach, as the multiscale model, neglect the crack tip root-rotations, which can be accounted for a posteriori for the calculation of the fracture parameters [95].

The critical load obtained through the homogenized model coincides with that of the discrete layer model, while the deflections are slightly underestimated due to neglecting the shear deformations in the delaminated region, which is expected (see Figure 4-10).

4.5.6 Displacements, stresses and interfacial tractions in a homogeneous ENF specimen

In this section the capability of the multiscale structural model to predict the displacements, stresses and cohesive interfacial tractions in a specimen with a finite length delamination is investigated. A homogeneous ENF specimen with material properties, $E_T/E_L = 0.071$, $G_{LT}/E_L = 0.033$, $\nu_{LT} = 0.32$ and $\nu_{TT} = 0.45$ (subscripts L and T indicate in-plane principal material directions and the L direction coincides with x_2 axis in the layer) is considered. The thicknesses of the layers, the specimen and traction-free delamination lengths are ${}^{(1)}h = {}^{(2)}h = h$, $2L/h = 100$ and $a/h = 30$. The delamination is under pure mode II conditions due to the symmetric layup and the anti-symmetric loading about the delamination line. In the solution of the homogenized model, the dimensionless interfacial stiffnesses $K_S h/E_L$ for the intact and delaminated portions of the specimen are set to be 10^3 and 10^{-10}, respectively. Once the global kinematic variables in different portions of the specimen are defined, as explained after Figure 4-6, displacements, strains and stresses in the layers are calculated through Eqs. (4-7), (4-9), (4-11) and (4-12).

Predictions of the homogenized structural theory are compared with those of a discrete layer interface model [20, 104, 105]. In this approach, an interface is introduced along the delamination line; the domain is discretized both through the length and thickness directions, at coordinates $x_2 = a$, $x_2 = L$ and $x_3 = 0$, into six sub-layers, which are modeled separately by the first order shear deformation theory. The interfacial constitutive law defined in Eq. (4-4) is used with $K_S h/E_L = 10^3$; the two sub-layers within the delaminated portion are allowed to freely slide along each other. The same transverse displacements are assumed for the sub-layers at each cross sections. In the bonded portion of the specimen, the interfacial shear tractions are related to the interfacial relative displacements, through the interfacial constitutive law in Eq. (4-4), and act as surface tractions on the upper surface of the first layer and the lower surface of the second layer. The coupled equilibrium equations of the layers are then solved and the boundary and continuity conditions are imposed to obtain the solution of the discrete problem.

The transverse displacements obtained through the homogenized model slightly differ from those of the discrete model due to neglecting shear deformations in the delaminated portion of the specimen (not shown). The longitudinal displacements, bending and transverse shear stresses predicted by the homogenized structural theory, coincide with those of the discrete model, but for a very small region ahead of the traction-free delamination tip. A comparison between the bending stresses at the lower surface of the specimen, predicted by the homogenize model, Eq. (4-12) for k =1 and $x_3 = x_3^0$, and the discrete layer interface model are shown in Figure 4-11 through the length. The figure shows that the bending stresses predicted by the homogenized model coincide with those of the discrete model, except for a very small

region at the vicinity and ahead of the traction-free delamination tip; the bending stress predicted by the homogenized model is not continuous at the traction-free delamination tip cross-section (see the inset in the figure).

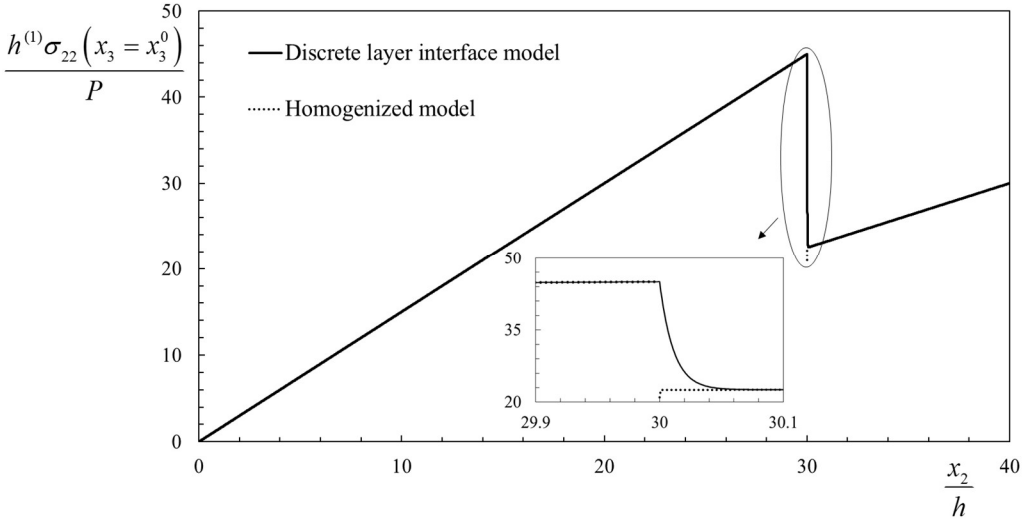

Figure 4-11: Comparison of the bending stresses at the lower surface of the plate through the length, calculated by the homogenized model and the discrete layer interface model.

The different predictions of the homogenized structural model in a localized area near the traction-free delamination tip, in Figure 4-11, was expected because of the imposition of the continuity conditions on the global variables only, which results in satisfying the equilibrium at the delamination tip cross-section, only in a global sense. The length of this region decreases by increasing the interfacial stiffness.

The through the thickness distributions of the bending stresses at the traction-free delamination tip, $\sigma_{22}\left(x_2 = a\right)$, in the cracked and intact regions calculated by two models are shown in Figure 4-12. The bending stresses in the cracked region predicted by the discrete model are the same as those calculated for the intact region and local equilibrium is satisfied in both sub-layers. On the other hand, the bending stresses in the delaminated region predicted by the homogenized model, which coincide with those obtained by the discrete model, differ from those calculated for the intact region. This behavior is a consequence of the imposition of continuity on the global quantities, namely the bending moment, which result in the violation of the local equilibrium of the sub-layers. It is interesting to note that, in addition to a correct description of the global force and moment resultants at the crack tip sections, which is due to the imposition of the continuity conditions, the force and moment sub-resultants in the single layers are correctly predicted and it is only at the stress level and in a region very close to the crack tip that the solution of the homogenized approach differs from that of the discrete layer interface model.

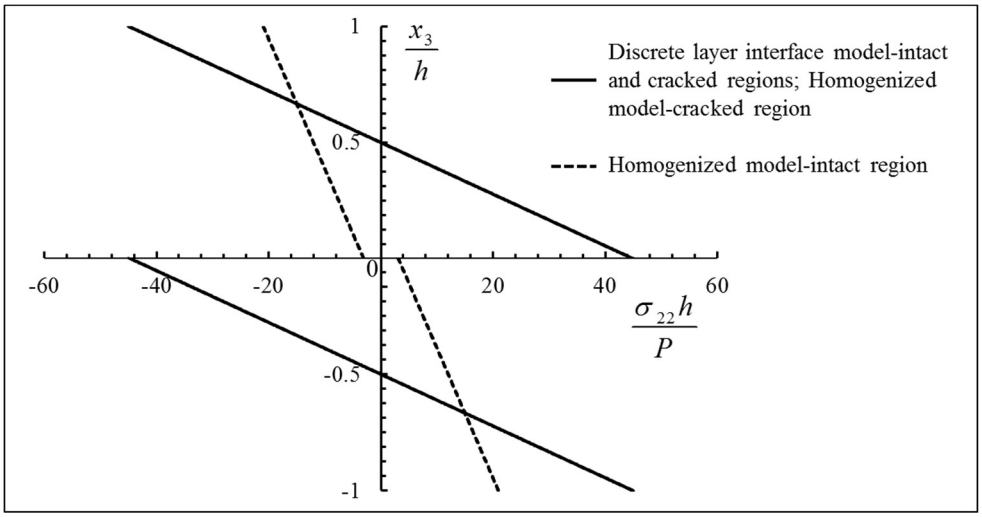

Figure 4-12: Distributions of bending stresses at the traction-free delamination tip in the cracked and intact regions.

A comparison between the interfacial shear tractions calculated a posteriori by the homogenized model and those obtained through the discrete model is shown in Figure 4-13, which refers to a very small region near the traction-free delamination tip at $x_2/h = 30$. Different predictions of the bending stresses in the crack tip region (see Figure 4-11 and Figure 4-12), correspond to different predictions for the interfacial shear tractions. The interfacial tractions predicted by the homogenized structural theory differ from those obtained by the discrete model within the small crack tip region. The solutions of both models out of the boundary region coincide and tend to the constant value -3/8, which is the transverse shear stress of the layers at the interface.

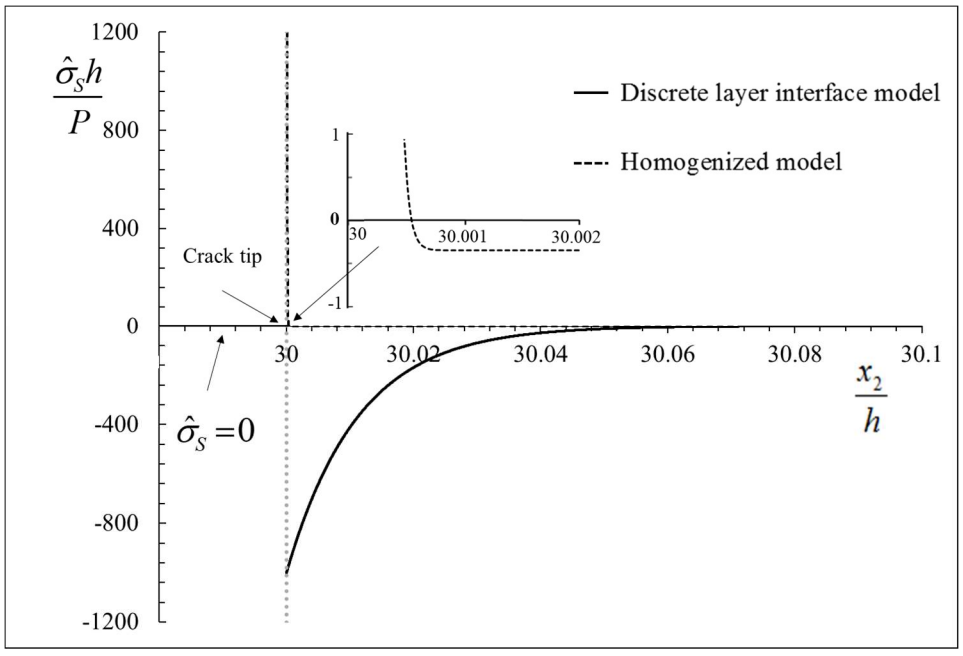

Figure 4-13: Comparison between the interfacial tractions calculated a posteriori by the homogenized model and those obtained through discrete layer interface model. The dimensionless interfacial shear tractions tend to the

constant value -3/8, which is the maximum transverse shear stress of the layers far from the traction-free delamination tip.

A boundary layer similar to that observed in Figure 4-13 at the traction-free delamination tip, was observed [26] in the solution of the multiscale model in a region near the clamped end of a symmetric cantilevered wide plate with two layers bonded by a linear elastic interface and subjected to a concentrated load at the free end. The kinematic boundary conditions of the homogenized model at a clamped end, $\varphi_2 = w_{0},_2 = 0$, yield zero transverse shear strain in Eq. (4-11), transverse shear stress in Eq. (4-12) and Q_2^b in Eq. (4-18) at the support; it was demonstrated in [26] that vanishing transverse shear strain and stress at the clamped boundary only affects the solutions within a localized region near the boundary and the solution of the model out of the boundary layer is accurate; the size of the boundary layer depends on the interfacial stiffness and is negligibly small for very stiff and very compliant interfaces [26]. The generalized transverse shear force, Q_{2g} in Eq. (4-17), which is related to the first derivative of the bending moment through the second equilibrium equation (4-15), accurately describes the shear force at any cross section including clamped supports [26].

The same phenomenon occurs in the problem considered in this section as a consequence of imposing the continuity of φ_2 and $w_{0},_2$ at the traction-free delamination tip cross-section, which yields a vanishing $\varphi_2 = w_{0},_2 = 0$ in the intact region at the delamination tip, while Q_{2g} correctly describes the distribution of the transverse shear force at any cross section of the ENF specimen including the traction-free delamination tip cross section.

4.6 CONCLUSIONS

A homogenized fracture model has been formulated by particularizing the multiscale structural theory developed in [25] for laminated wide plates with an arbitrary number of layers and cohesive or traction-free interfaces, to a bi-material plate with a single delamination under mode II dominant conditions. The model has then been used to study a fundamental fracture mechanics model system, an edge-cracked bi-material element subjected to generalized end forces, for which accurate Linear Elastic Fracture Mechanics solutions are available in the literature.

The energy release rate has been derived through an application of the J-integral in the homogenized problem using the local fields calculated through the multiscale model. The derived expression is similar to that derived from 2D analysis but does not account for the contributions of the crack tip root-rotations, which however can be calculated a posteriori using the equations derived in [94, 95] once the crack tip force and moment sub-resultants have been calculated through the homogenized approach. The energy release rate of the model system has been derived also in terms of the relative crack sliding displacements, through an application of the J-integral along a path which follows the delamination surfaces.

The formulated fracture model has been applied to calculate the fracture parameters of different ENF specimens. Numerical results have been presented and compared with accurate LEFM solutions to highlight the capabilities of the multiscale model to predict the energy release rate and the relative crack sliding displacements. It has been shown that the homogenized model captures the load-displacement response of the ENF specimen including the snap-back instability, which is a discrete fracture event.

A homogenous ENF specimen under pure mode II conditions has been considered to investigate the capability of the homogenized model to predict displacements, stresses and interfacial tractions in the crack tip region in plates with finite length delaminations. It has been shown that the multiscale structural theory is able to accurately predict the global measures, the energy release rate and the local measures everywhere but a localized area ahead of the traction-free delamination tip, where a boundary layer forms as a consequence of the imposition of the continuity conditions on the global variables only, which results in satisfying the equilibrium at the delamination tip cross-section, only in a global sense. It is then expected that the extended version of the model [25], which uses a similar kinematic assumptions and accounts for the interfacial opening displacements, can adequately model problems characterized by mixed-mode conditions.

Within the framework of Linear Elastic Fracture Mechanics, accurate predictions of the stress sub-resultants at the delaminations tips in plates with multiple delaminations, enable calculating the energy release rates, e.g. through Eq. (4-59). Based on the work presented in this chapter, it is foreseen that the homogenized structural model is able to accurately predict the force and moment resultants and sub-resultants and capture macro-structural response of plates with many layers and delaminations, through the homogenized description of the problem, with the same number of variables as that needed for modeling a single intact homogenous layer. However, the homogenized structural model underestimates the compliances of plates with multiple delaminations and this affects the accuracy of the predicted force and moment resultants in statically indeterminate structures.

A HOMOGENIZED STRUCTURAL THEORY BASED ON THE REFINED ZIGZAG THEORY FOR WIDE PLATES AND BEAMS WITH IMPERFECT INTERFACES AND DELAMINATIONS

5.1 INTRODUCTION

To try and overcome the limitation of the homogenized model [25], i.e. neglecting the shear deformations in fully debonded laminates, this chapter aims at formulating a homogenized structural model based on the refined zigzag theory (RZT) [27] and on the multiscale approach proposed in [11, 25], for multilayered wide plates and beams with an arbitrary number of layers and imperfect interfaces and delaminations. The interfaces are assumed to be rigid against relative opening displacements, and governed by a linear elastic interfacial constitutive law. The refined theory uses four kinematic variables and allows to accurately model all boundary conditions including clamped supports, has enough kinematic flexibility to adequately describe the shear deformations through the thickness of an imperfectly bonded laminate with continuous interfaces, and requires only C^0-continuous shape functions for finite element implementation.

In Sect. 5.2, the model assumptions are presented. In Sect. 5.3, the displacement field of the first order shear deformation theory is enriched by piecewise linear and discontinuous zigzag functions, which account for the zigzag patterns in the longitudinal displacement of the layers, due to the inhomogeneous material structure, and the interfacial jumps due to the imperfect interfaces. The homogenized equilibrium equations and boundary conditions are then derived through the Principle of Virtual Works. In Sec. 5.4, the model is applied to solve simply supported and cantilevered plates with different layups and state of the interfacial imperfections, and results are compared with the exact 2D elasticity solutions obtained in Chapter 3, and with the solutions of the discrete layer interface model introduced in Sect. 4.5.6 in Chapter 4. A preliminary application to delamination fracture problems in Section 5.5 reveals a drawback of the model for studying laminates with finite length interfaces. Conclusions are given in Sect. 5.6.

5.2 MODEL ASSUMPTIONS

A rectangular multilayered plate with global thickness h, in-plane dimensions L_1 and $L_2 = L$ with $L_1 >> L_2$, and $x_1 - x_2 - x_3$ a system of Cartesian coordinates with origin at the left edge is demonstrated in Figure 5-1. The plane $x_3 = 0$ defines the reference surface of the plate, S. The plate is composed of n linearly elastic, homogenous and orthotropic layers with principal material axes parallel to the geometrical axes. The layers are joined by $n-1$ interfaces, which are zero-thickness mathematical surfaces where material properties and displacements may be discontinuous. The plate is subjected to distributed static loads acting on the upper, lower and lateral bounding surfaces, S^+, S^- and B, and deforms in cylindrical bending

parallel to the plane $x_2 - x_3$. The layer *k*, with $k = 1, \ldots n$ numbered from bottom to top, is defined by x_3^{k-1} and x_3^k, the coordinates of its lower and upper surfaces, ${}^{(k)}S^-$ and ${}^{(k)}S^+$, and has thickness ${}^{(k)}h$ (the superscript (*k*) on the left of a quantity shows association with the layer *k*, while the superscript *k* on the right identifies the interface between layers *k* and $k+1$). The layers are assumed to be incompressible in the thickness direction and the interfaces to be rigid against relative opening displacements. Under these assumptions, the displacement components in each layer can be written as ${}^{(k)}v_1 = 0$, ${}^{(k)}v_2 = {}^{(k)}v_2(x_2, x_3)$ and ${}^{(k)}v_3 = w_0(x_2)$ where ${}^{(k)}v_i$ is the displacement component in the layer *k* in x_i direction and *i* = 1, 2, 3.

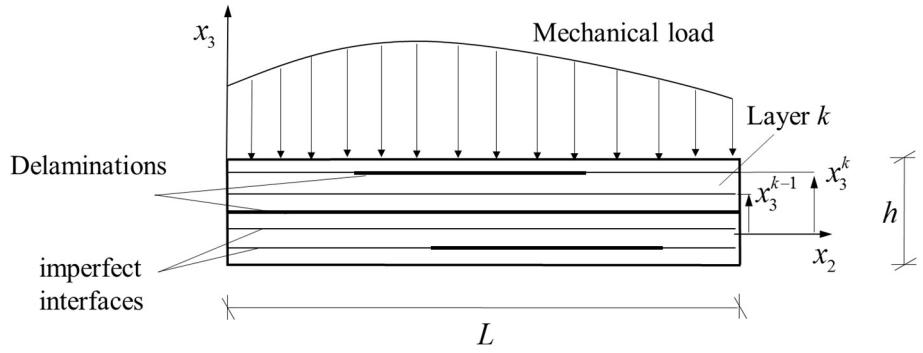

Figure 5-1: Multilayered wide plate/beam with imperfect interfaces and delaminations.

The transverse normal stresses of the layers, ${}^{(k)}\sigma_{33}$, are assumed to be negligible compared with the other stress components. Under this assumption, the 3D constitutive equations for the layer *k* particularized to plane-strain conditions are:

$$\begin{aligned} {}^{(k)}\sigma_{22} &= {}^{(k)}\overline{C}_{22}\,{}^{(k)}\varepsilon_{22} \\ {}^{(k)}\sigma_{23} &= {}^{(k)}C_{44}2\,{}^{(k)}\varepsilon_{23} \end{aligned} \tag{5-1}$$

with ${}^{(k)}\sigma_{ij}$ and ${}^{(k)}\varepsilon_{ij}$ the stress and strain components, and ${}^{(k)}\overline{C}_{22} = {}^{(k)}\left(C_{22} - C_{23}C_{32}/C_{33}\right)$, where ${}^{(k)}C_{ij}$ are the coefficients of the stiffness matrix. The model presented in this chapter is also applicable to beams with longitudinal axis x_2, provided that ${}^{(k)}\overline{C}_{22}$ is replaced by the Young's modulus of the layers in x_2 direction.

The mechanical behavior of the interfaces is described through a linear elastic interfacial traction law, which relates the interfacial shear tractions, $\hat{\sigma}_S^k(x_2)$, to the interfacial sliding jumps:

$$\hat{v}_2^k(x_2, x_3 = x_3^k) = {}^{(k+1)}v_2(x_2, x_3 = x_3^k) - {}^{(k)}v_2(x_2, x_3 = x_3^k) \tag{5-2}$$

through:

$$\hat{\sigma}_S^k(x_2) = K_S^k \hat{v}_2^k(x_2) \tag{5-3}$$

with K_S^k the interfacial tangential stiffness. The interfacial shear traction, $\hat{\sigma}_S^k(x_2)$, is the traction generated at the interface due to the applied loads and is assumed to be different than that acting along the upper

surface of the layer *k*. This assumption, as it will be shown in Sect. 5.4 through applications of the model to simply supported and cantilevered wide plates, allows to adequately account for the shear deformations within the layers of a fully debonded plate.

The interfacial traction law (5-3) well describes the response of thin elastic layers, for which the interfacial stiffness will depend on the shear rigidity and thickness of the layer. The law with $K_S^k = 0$ which results in $\hat{\sigma}_S^k = 0$, describes fully debonded layers, and with $1/K_S^k = 0$ which results in $\hat{v}_2^k = 0$, represents fully bonded layers.

5.3 HOMOGENIZED STRUCTURAL THEORY

A homogenized structural theory, based on the RZT [27] and on the multiscale approach proposed in [11, 25], is formulated in this section for solving the problem in Figure 5-1. The following displacement field is assumed in the layer *k* (Figure 5-2):

$$\begin{aligned} {}^{(k)}v_2(x_2,x_3) &= v_{02}(x_2) + x_3\varphi_2(x_2) + \theta_2(x_2)\,{}^{(k)}\phi(x_3) \\ {}^{(k)}v_3(x_2,x_3) &= w_0(x_2) \end{aligned} \tag{5-4}$$

The global variables $v_{02}(x_2)$, $\varphi_2(x_2)$ and $w_0(x_2)$ define the displacement field of a first order shear deformation theory. The third term on the right hand side of Eq. (5-4), $\theta_2(x_2)\,{}^{(k)}\phi(x_3)$, are local perturbations or enrichments, and account for the zigzag contributions due to the inhomogeneous material structure, already presented in the theory in [27], and the interfacial jumps due to the imperfect interfaces; ${}^{(k)}\phi(x_3)$ for $k = 1, \ldots n$ are assumed to be piecewise linear zigzag functions of x_3 with discontinuities at the interfaces (see Figure 5-2), and $\theta_2(x_2)$, which is a global variable, is the amplitude of the zigzag functions. The zigzag functions in Eq. (5-4) are assumed to be discontinuous at the interfaces, ${}^{(k)}\phi(x_3^k) \neq {}^{(k+1)}\phi(x_3^k)$, to account for the interfacial jumps. The displacement field (5-4) has four kinematic variable, $v_{02}(x_2)$, $\varphi_2(x_2)$, $\theta_2(x_2)$ and $w_0(x_2)$, which is one variable more than that used in Chapter 4, Eq. (4-9) [25].

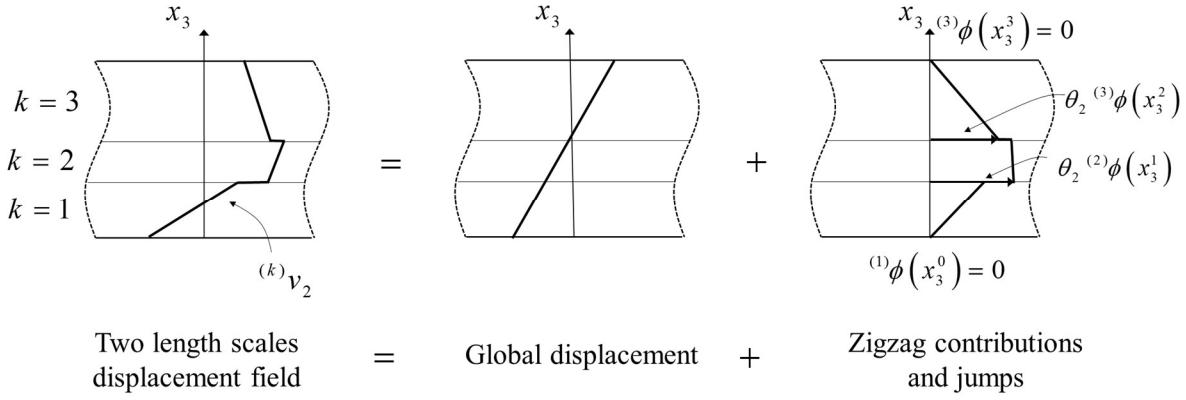

Figure 5-2: Schematic description of the assumed displacement field in a three layers laminate: global displacement and local perturbations.

The zigzag function in the layer k for $k = 1, \ldots n$ is given as:

$$^{(k)}\phi(x_3) = {}^{(k)}\beta\left(x_3 - x_3^{k-1}\right) + {}^{(k)}\phi(x_3^{k-1}) \tag{5-5}$$

where $^{(k)}\beta = {}^{(k)}\phi(x_3),_3$ is the slope, which is one of the unknowns, and $^{(k)}\phi(x_3^{k-1})$ is the value of the function at the lower surface of the layer k, and is another unknown. The zigzag functions in Eq. (5-5) are fully defined through $2\times n$ unknown functions $^{(k)}\beta$ and $^{(k)}\phi(x_3^{k-1})$ for $k = 1, \ldots n$. The difference between the values of the zigzag function at the upper surface of the layer k, $^{(k)}\phi(x_3^k)$, and at the lower surface, $\Delta^{(k)}\phi = {}^{(k)}\phi(x_3^k) - {}^{(k)}\phi(x_3^{k-1})$, is defined by substituting $x_3 = x_3^k$ into Eq. (5-5):

$$\Delta^{(k)}\phi = {}^{(k)}\beta\,{}^{(k)}h \tag{5-6}$$

where $^{(k)}h$ is the thickness of the layer. $\Delta^{(k)}\phi$ defined in Eq. (5-6) will be used later in the derivation of the zigzag functions.

The interfacial sliding jumps are defined in terms of the zigzag functions and the kinematic variable θ_2, using Eqs. (5-2) and (5-4):

$$\hat{v}_2^k(x_2) = \theta_2(x_2)\left[{}^{(k+1)}\phi(x_3^k) - {}^{(k)}\phi(x_3^k)\right] \tag{5-7}$$

Once the zigzag functions have been derived, the interfacial sliding jumps are defined by Eq. (5-7).

5.3.1 Derivation of the zigzag functions

In order to derive the unknown zigzag functions, the interfaces at the coordinates $x_3 = x_3^k$ for $k = 1, \ldots n-1$ are considered as thin layers $\bar{k}$ for $\bar{k} = 1, \ldots n-1$, with thickness $\bar{h}$, which are assumed to be perfectly bonded to their lower and upper layers, k and $k + 1$ (see Figure 5-3). The thin layers are then considered as regular layers of the model. In the new representation of the problem, the lower and upper surfaces of the layer k for $k = 2, \ldots n$, are at the coordinates $x_3^{k-1} + \bar{h}$ and x_3^k, respectively; the lower and upper surfaces of the first layer are at the coordinates x_3^0 and x_3^1. In the limiting case of $\bar{h} \to 0$, the thin layers represent the zero-thickness imperfect interfaces.

The zigzag functions are first derived for the system of perfectly bonded layers and thin layers in Figure 5-3(b), following the RZT for perfectly bonded laminates [27], and then by taking the limit as $\bar{h} \to 0$, the zigzag functions for the problem in Figure 5-3(a) are obtained in terms of the thickness and transverse shear stiffness of the layers, and the interfacial stiffness of the interfaces.

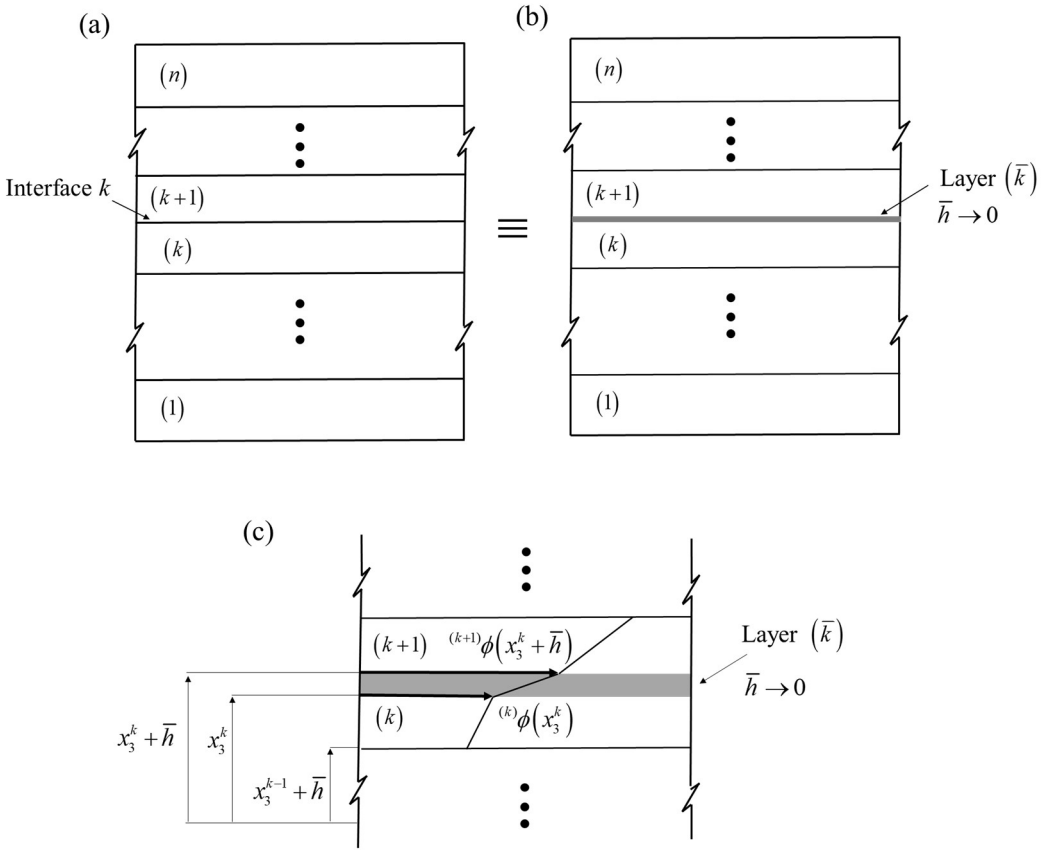

Figure 5-3: (a) Layers joined by imperfect interfaces. (b) Representing imperfect interfaces as thin layers. (c) Values of the zigzag functions below and above the thin layer $\bar{k}$, perfectly bonded to layers k and k+1.

The transverse shear strains within the layers in Figure 5-3(b) are derived by substituting Eq. (5-5) into the displacement field in Eq. (5-4), and using linear compatibility:

$$\begin{aligned} 2\,{}^{(k)}\varepsilon_{23} &= {}^{(k)}v_{2,3} + {}^{(k)}v_{3,2} = \left(\varphi_2 + w_{0,2}\right) + \theta_2\,{}^{(k)}\beta \\ 2\,{}^{(\bar{k})}\varepsilon_{23} &= {}^{(\bar{k})}v_{2,3} + {}^{(\bar{k})}v_{3,2} = \left(\varphi_2 + w_{0,2}\right) + \theta_2\,{}^{(\bar{k})}\beta \end{aligned} \tag{5-8}$$

where the superscript $\left(\bar{k}\right)$ on the left of a quantity shows association with the thin layer $\bar{k}$. Following [27], a difference function is defined:

$$\eta = \left(\varphi_2 + w_{0,2}\right) - \theta_2 \tag{5-9}$$

Using Eqs. (5-1), (5-8) and (5-9), the transverse shear stresses in the layers in Figure 5-3(b) are written in terms of $\varphi_2 + w_{0,2}$, $^{(k)}\beta$ and η:

$$
\begin{aligned}
{}^{(k)}\sigma_{23} &= {}^{(k)}C_{44}\left[\left(\varphi_2 + w_{0,2}\right)\left(1+{}^{(k)}\beta\right) - \eta\,{}^{(k)}\beta\right] \\
{}^{(\bar{k})}\sigma_{23} &= {}^{(\bar{k})}C_{44}\left[\left(\varphi_2 + w_{0,2}\right)\left(1+{}^{(\bar{k})}\beta\right) - \eta\,{}^{(\bar{k})}\beta\right]
\end{aligned}
\tag{5-10}
$$

To define the slopes of the zigzag functions, ${}^{(k)}\beta$ and ${}^{(\bar{k})}\beta$, the shear coefficients which multiply $\varphi_2 + w_{0,2}$ term in Eq. (5-10), which is the well-known shear strain in the first order shear deformation theory, are assumed to be the same for each layer:

$$
\bar{G} = {}^{(k+1)}C_{44}\left(1+{}^{(k+1)}\beta\right) = {}^{(\bar{k})}C_{44}\left(1+{}^{(\bar{k})}\beta\right) = {}^{(k)}C_{44}\left(1+{}^{(k)}\beta\right)
\tag{5-11}
$$

for k and $\bar{k} = 1, \ldots, n-1$. As mentioned in [106], the constraints in Eq. (5-11) can be also derived based on the minimization of the shear strain energy. The constraints in Eq. (5-11) allow to relate the slops of the zigzag functions in the layers to $\bar{G}$:

$$
\begin{aligned}
{}^{(k)}\beta &= \frac{\bar{G}}{{}^{(k)}C_{44}} - 1 \\
{}^{(\bar{k})}\beta &= \frac{\bar{G}}{{}^{(\bar{k})}C_{44}} - 1
\end{aligned}
\tag{5-12}
$$

for $k = 1, \ldots, n$, and $\bar{k} = 1, \ldots, n-1$.

In the following, we first derive the value of the zigzag function at the lower surface of the layer $k + 1$, ${}^{(k+1)}\phi\left(x_3^k + \bar{h}\right)$ in Figure 5-3(b), in terms of the slopes of the zigzag functions in the layers below the layer $k + 1$ and assuming a zero value for the zigzag function at the lower surface of the plate ${}^{(1)}\phi\left(x_3^0\right) = 0$, and use the derived expression to determine ${}^{(n)}\phi\left(x_3^n\right)$; $\bar{G}$ is then derived by imposing the value of the zigzag function at the upper surface of the plate to be zero ${}^{(n)}\phi\left(x_3^n\right) = 0$ [27]. Imposing ${}^{(1)}\phi\left(x_3^0\right) = {}^{(n)}\phi\left(x_3^n\right) = 0$ results in zigzag functions with desirable properties, which will be discussed later (after Eq. (5-16)) [27].

Since the layers and thin layers are assumed to be perfectly bonded, the following relationships exist between the values of the zigzag functions in layers k, $k + 1$ and $\bar{k}$ (see Figure 5-3(c)):

$$
\begin{aligned}
{}^{(k+1)}\phi\left(x_3^k + \bar{h}\right) &= {}^{(\bar{k})}\phi\left(x_3^k + \bar{h}\right) \\
{}^{(k)}\phi\left(x_3^k\right) &= {}^{(\bar{k})}\phi\left(x_3^k\right)
\end{aligned}
\tag{5-13}
$$

Subtracting the second equation from the first equation in Eq. (5-13) and using Eq. (5-6) to define the difference between the values of the zigzag function of the thin layer $\bar{k}$ at its upper and lower surfaces, $\Delta^{(\bar{k})}\phi = {}^{(\bar{k})}\phi(x_3^k + \bar{h}) - {}^{(\bar{k})}\phi(x_3^k) = {}^{(\bar{k})}\beta\bar{h}$, yield:

$$^{(k+1)}\phi\left(x_3^k+\bar{h}\right)=\,^{(\bar{k})}\beta\bar{h}+\,^{(k)}\phi\left(x_3^k\right) \tag{5-14}$$

Equations (5-6) and (5-14) can be used to further relate $^{(k+1)}\phi\left(x_3^k+\bar{h}\right)$ to the value of the zigzag function of the layer *k* at its lower surface, $^{(k)}\phi\left(x_3^{k-1}+\bar{h}\right)$. Repeating this procedure and imposing $^{(1)}\phi\left(x_3^0\right)=0$ result in the following expression:

$$^{(k+1)}\phi\left(x_3^k+\bar{h}\right)=\sum_{i=1}^{k}\left[\,^{(i)}\beta\,^{(i)}h+\,^{(\bar{i})}\beta\bar{h}\right] \tag{5-15}$$

for $k=1,\ldots,n-1$. The value of the zigzag function at the top of the plate in Figure 5-3(b), $^{(n)}\phi\left(x_3^n\right)$, can be defined by substituting $k=n-1$ in Eq. (5-15) and using Eq. (5-6) for $k=n$. $\bar{G}$ is then derived by imposing $^{(n)}\phi\left(x_3^n\right)=0$ and using Eq. (5-12):

$$\bar{G}=\frac{h+(n-1)\bar{h}}{\sum_{i=1}^{n}\dfrac{^{(i)}h}{^{(i)}C_{44}}+\sum_{i=1}^{n-1}\dfrac{\bar{h}}{^{(\bar{i})}C_{44}}} \tag{5-16}$$

where $h+(n-1)\bar{h}$ is the total thickness of the plate in Figure 5-3(b).

Substituting $\bar{G}$ from Eq. (5-16) into the expressions for the slops of the zigzag functions $^{(k)}\beta$ and $^{(\bar{k})}\beta$ in Eq. (5-12) and integrating the slopes over the whole thickness of the plate, yield zero [27]. This desirable property allows to define the integration of the transverse shear strains in the layers and thin layers in Figure 5-3(b), Eq. (5-8), through the whole thickness of the plate as $\left(h+(n-1)\bar{h}\right)\left(\varphi_2+w_{0,2}\right)$, where $\varphi_2+w_{0,2}$, the well-known shear strain in the first order shear deformation theory, represents the average shear strain of the cross section [27].

The transverse shear strain within the thin layers can be written as:

$$2\,^{(\bar{k})}\varepsilon_{23}=\frac{^{(\bar{k})}\bar{\hat{v}}_2}{\bar{h}} \tag{5-17}$$

where $^{(\bar{k})}\bar{\hat{v}}_2$ is the relative sliding displacement across the thin layer $\bar{k}$. Therefore, the transverse shear stress within the thin layers is:

$$^{(\bar{k})}\sigma_{23}=\frac{^{(\bar{k})}C_{44}\;^{(\bar{k})}\bar{\hat{v}}_2}{\bar{h}} \tag{5-18}$$

Comparing Eq. (5-18) with the interfacial constitutive law in Eq. (5-3) and noting that when $\bar{h} \to 0$, ${}^{(\bar{k})}\sigma_{23}$ and ${}^{(\bar{k})}\bar{\hat{v}}_2$ represent the interfacial traction and jump, yield $K_S^k = {}^{(\bar{k})}C_{44}/\bar{h}$. Therefore, Eq. (5-16) when $\bar{h} \to 0$ becomes:

$$G = \lim_{\bar{h}\to 0} \bar{G} = \frac{h}{\sum_{i=1}^{n} \frac{{}^{(i)}h}{{}^{(i)}C_{44}} + \sum_{i=1}^{n-1} \frac{1}{K_S^i}} \tag{5-19}$$

Substituting $1/K_S^i = 0$ in Eq. (5-19) yields G for a perfectly bonded laminate, which coincides with that derived in [27].

The ${}^{(k)}\beta$ for k = 1, …, n in the plate in Figure 5-3(a) is calculated through Eqs. (5-12), (5-16) and (5-19), and taking the limit as $\bar{h} \to 0$:

$${}^{(k)}\beta = G/{}^{(k)}C_{44} - 1 \tag{5-20}$$

Substitution of ${}^{(\bar{k})}\beta$ from Eq. (5-12) into Eq. (5-15) and taking the limit as $\bar{h} \to 0$, yield:

$${}^{(k+1)}\phi\left(x_3^k\right) = \sum_{i=1}^{k} \left[{}^{(i)}\beta\, {}^{(i)}h + \frac{G}{K_S^i} \right] \tag{5-21}$$

for k = 1, …, $n-1$. The zigzag functions in the layers of the plate in Figure 5-3(a) are defined by Eqs. (5-5) and (5-21):

$$\begin{aligned} {}^{(k)}\phi\left(x_3\right) &= {}^{(k)}\beta\left(x_3 - x_3^{k-1}\right) + \sum_{i=1}^{k-1} \left[{}^{(i)}\beta\, {}^{(i)}h + \frac{G}{K_S^i} \right] \\ {}^{(k)}\beta &= \left(\frac{G}{{}^{(k)}C_{44}} - 1 \right) \end{aligned} \tag{5-22}$$

Substituting $1/K_S^i = 0$ in Eq. (5-22) yields the zigzag functions of a perfectly bonded laminate, which coincides with those derived in [27]. The interfacial displacement jumps are then derived through Eqs. (5-7) and (5-22):

$$\hat{v}_2^k = \frac{G\theta_2}{K_S^k} \tag{5-23}$$

The interfacial traction at the interface $x_3 = x_3^k$, $\hat{\sigma}_S^k$, are derived from the interfacial constitutive equation (5-3) and Eq. (5-23):

$$\hat{\sigma}_S^k = G\theta_2(x_2) \tag{5-24}$$

Substitution of the derived zigzag functions in Eq. (5-22) into Eq. (5-4) yields the displacement field in terms of four kinematic variables, $v_{02}(x_2)$, $\varphi_2(x_2)$, $w_0(x_2)$ and $\theta_2(x_2)$:

$$\begin{aligned} {}^{(k)}v_2(x_2,x_3) &= \left[v_{02}(x_2) + \theta_2(x_2)\left(\sum_{i=1}^{k-1}\left[{}^{(i)}\beta^{(i)}h + \frac{G}{K_S^i} \right] - {}^{(k)}\beta x_3^{k-1} \right) \right] + \left[\varphi_2(x_2) + \theta_2(x_2)\,{}^{(k)}\beta \right] x_3 \\ {}^{(k)}v_3(x_2,x_3) &= w_0(x_2) \end{aligned} \tag{5-25}$$

where ${}^{(k)}\beta = G \big/ {}^{(k)}C_{44} - 1$ and G is defined in Eq. (5-19).

The local rotations of the layers, ${}^{(k)}\Phi$, which are defined as the rotations of the lines perpendicular to the reference surface, and correspond to the slope with respect to x_3 of the longitudinal displacement of the layers, are:

$${}^{(k)}\Phi = \varphi_2(x_2) + \theta_2(x_2)\,{}^{(k)}\beta \tag{5-26}$$

Equation (5-26) shows that at a cross section, where two homogenized domains characterized by different interfacial stiffness, e.g. plates with finite length delaminations, are joined, the local rotations of the layers at the left and right of the joining cross section are different due to different ${}^{(k)}\beta$ defined in Eq. (5-20) (the global variables φ_2 and θ_2 are continuous at the joining cross section because of the continuity conditions, see Eq. (5-34)). The model would also predict different local rotations in layers at the left and right of a cross section, where two domains with the same interfacial stiffness and different shear moduli, C_{44}, are joined.

The strain components in the layer k are derived through the displacement field in Eq. (5-4) with ${}^{(k)}\phi$ defined in Eq. (5-22) and the linear compatibility equations:

$$\begin{aligned} {}^{(k)}\varepsilon_{22}(x_2,x_3) &= {}^{(k)}v_{2,2}(x_2,x_3) = v_{02,2} + x_3\varphi_{2,2} + \theta_{2,2}\,{}^{(k)}\phi \\ 2\,{}^{(k)}\varepsilon_{23}(x_2,x_3) &= {}^{(k)}v_{2,3}(x_2,x_3) + {}^{(k)}v_{3,2}(x_2,x_3) = \left(\varphi_2 + w_{0,2}\right) + \theta_2\,{}^{(k)}\beta \end{aligned} \tag{5-27}$$

where ${}^{(k)}\beta$ is defined in Eq. (5-20). The normal strain, ${}^{(k)}\varepsilon_{22}$, is piecewise linear through the thickness of the plate and discontinuous at the interfaces, while the transverse shear strain, $2\,{}^{(k)}\varepsilon_{23}$, is piecewise constant through the thickness of the plate, and becomes constant through the thickness of fully debonded laminates, since ${}^{(k)}\beta = -1$ from Eq. (5-20), and homogenous plates, since ${}^{(k)}\beta$ is constant through the thickness, due to the same material properties of the layers. The transverse shear strains of the layers in Eq. (5-27) can be rewritten in a form similar to that of the equivalent single layer first order shear deformation theory by using the local rotations of the layers defined in Eq. (5-26), $2\,{}^{(k)}\varepsilon_{23} = {}^{(k)}\Phi + w_{0,2}$.

The stress components in the layer k are derived through the strain components in Eq. (5-27) and the constitutive equations (5-1):

$$\begin{aligned} {}^{(k)}\sigma_{22}(x_2,x_3) &= {}^{(k)}\overline{C}_{22}\left[v_{02},_2 + x_3\varphi_2,_2 + \theta_2,_2\ {}^{(k)}\phi\right] \\ {}^{(k)}\sigma_{23}(x_2,x_3) &= {}^{(k)}C_{44}\left[\left(\varphi_2 + w_0,_2\right) + \theta_2\ {}^{(k)}\beta\right] \end{aligned} \tag{5-28}$$

The bending stress, ${}^{(k)}\sigma_{22}$, is piecewise linear through the thickness of the plate and discontinuous at the interfaces, due to the contribution of the zigzag function, while the transverse shear stress, ${}^{(k)}\sigma_{23}$, is piecewise constant through the thickness of the plate, due to different ${}^{(k)}\beta$ for each layer, and becomes constant through the thickness of homogenous plates, since ${}^{(k)}\beta$ is constant through the thickness. The transverse shear stress of the layers in Eq. (5-28) can be rewritten in a form similar to that of the equivalent single layer first order shear deformation theory by using the local rotations of the layers defined in Eq. (5-26), ${}^{(k)}\sigma_{23} = {}^{(k)}C_{44}\left[{}^{(k)}\Phi + w_0,_2\right]$. Accurate prediction of the transverse shear stresses can be made a posteriori from the bending stresses in Eq. (5-28) by using local equilibrium ${}^{(k)}\sigma_{22},_2 + {}^{(k)}\sigma_{23,3}^{post} = 0$.

The current structural theory has the ability to account for the shear deformations/stresses within the layers even at the presence of fully debonded interfaces and traction-free delaminations. In this limit, the term G defined in Eq. (5-19) vanishes since $K_S \to 0$, and therefore ${}^{(k)}\beta = -1$ for $k = 1, \ldots, n$; this does not result in vanishing transverse shear strains, Eq. (5-27), and transverse shear stresses, Eq. (5-28). This feature of the present model especially improves the accuracy of the predicted transverse displacements, which is important in the modeling of statically indeterminate plate, in which the solution depends on the compliance of the plate.

5.3.2 Homogenized field equations

The homogenized equilibrium equations and boundary conditions are derived through the Principle of Virtual Works:

$$\begin{aligned} &\sum_{k=1}^{n}\int_S\int_{x_3^{k-1}}^{x_3^k}\left({}^{(k)}\sigma_{22}\delta\,{}^{(k)}\varepsilon_{22} + 2\,{}^{(k)}\sigma_{23}\delta\,{}^{(k)}\varepsilon_{23}\right)dx_3dS + \sum_{k=1}^{n-1}\int_{{}^{(k)}S^+}\hat{\sigma}_S^k\delta\hat{v}_2^k dS \\ &-\int_{S^+}F_i^{S^+}\delta\,{}^{(n)}v_i dS - \int_{S^-}F_i^{S^-}\delta\,{}^{(1)}v_i dS - \int_B F_i^B\delta v_i dB = 0 \end{aligned} \tag{5-29}$$

with i = 2, 3 and $F_i^{S^+}$, $F_i^{S^-}$ and F_i^B the components of the external forces acting along the boundary surfaces of the plate, S^+, S^- and B. The symbol δ is the variational operator and the virtual displacements are independent and arbitrary. The equilibrium equations and boundary conditions are derived by substituting strain and displacement components and interfacial displacement jumps from Eqs. (5-4), (5-23), and (5-27) into Eq. (5-29) and using Green's theorem whenever necessary:

$$\begin{aligned} &\delta v_{02}: \quad N_{22},_2 + f_2 = 0 \\ &\delta\varphi_2: \quad M_{22},_2 - Q_2 + f_{2m} = 0 \end{aligned} \tag{5-30}$$

$$\begin{aligned}
&\delta w_0: \quad Q_{2,2} + f_3 = 0 \\
&\delta\theta_2: \quad M_{22}^{zS},_2 - Q_2^z - \hat{\sigma}_2 = 0
\end{aligned}$$

where the force and moment resultants and loading terms are:

- normal force and bending moment, and moment resultant associated to the zigzag functions

$$\left(N_{22}, M_{22}, M_{22}^{zS}\right) = \sum_{k=1}^{n} \int_{x_3^{k-1}}^{x_3^k} {}^{(k)}\sigma_{22}\left(1, x_3, {}^{(k)}\phi\right) dx_3 \tag{5-31}$$

- shear force and shear force associated to the zigzag functions

$$\begin{aligned}
&\left(Q_2, Q_2^z\right) = \sum_{k=1}^{n} \int_{x_3^{k-1}}^{x_3^k} {}^{(k)}\sigma_{23}\left(1, {}^{(k)}\beta\right) dx_3 \\
&\hat{\sigma}_2 = G \sum_{k=1}^{n-1} \frac{\hat{\sigma}_S^k}{K_S^k}
\end{aligned} \tag{5-32}$$

- distributed tangential and transverse loads and couples

$$\begin{aligned}
&f_2 = F_2^{S+} + F_2^{S-} \\
&f_{2m} = F_2^{S+} x_3^n + F_2^{S-} x_3^0 \\
&f_3 = F_3^{S+} + F_3^{S-}
\end{aligned} \tag{5-33}$$

The first three equilibrium equations in Eq. (5-30) are the same as those of the first order shear deformation theory, while the fourth equilibrium equation defines the equilibrium of bending moment and shear force associated to the zigzag functions.

There are two differences between the equilibrium equations (5-30) and those of the refined zigzag theory developed in [27] for fully bonded plates. First, the zigzag functions and ${}^{(k)}\beta$ defined in this chapter, Eq. (5-22), which appear in the definitions of the stress resultants in Eqs. (5-31) and (5-32), are different from those derived in [27] due to the presence of imperfect interfaces. The second difference is the term $\hat{\sigma}_2$, which appears in the fourth equilibrium equation (5-30) again due to the presence of the imperfect interfaces.

The boundary conditions at the plate edges, $x_2 = 0,\ L$, with $\boldsymbol{n} = \{0, \pm 1, 0\}^T$ the outward normal, are:

$$\begin{aligned}
&\delta v_{02}: \quad N_{22} n_2 = \tilde{N}_2 \quad \text{or} \quad v_{02} = \tilde{v}_{02} \\
&\delta\varphi_2: \quad M_{22} n_2 = \tilde{M}_2 \quad \text{or} \quad \varphi_2 = \tilde{\varphi}_2 \\
&\delta w_0: \quad Q_2 n_2 = \tilde{N}_3 \quad \text{or} \quad w_0 = \tilde{w}_0 \\
&\delta\theta_2: \quad M_{22}^{zS} n_2 = \tilde{M}_2^{zS} \quad \text{or} \quad \theta_2 = \tilde{\theta}_2
\end{aligned} \tag{5-34}$$

where the terms with the tilde define prescribed values of displacements, forces and couples at the plate edges:

$$\begin{aligned}
\tilde{N}_i &= \sum_{k=1}^{n} \int_{x_3^{k-1}}^{x_3^k} {}^{(k)}F_i^B \, dx_3 \\
\tilde{M}_2 &= \sum_{k=1}^{n} \int_{x_3^{k-1}}^{x_3^k} {}^{(k)}F_2^B \, x_3 \, dx_3 \\
\tilde{M}_2^{zS} &= \sum_{k=1}^{n} \int_{x_3^{k-1}}^{x_3^k} {}^{(k)}F_2^B \, {}^{(k)}\phi \, dx_3
\end{aligned} \tag{5-35}$$

for $i = 2$ and 3.

The constitutive equations of the structural theory are derived by substituting the stress components from Eq. (5-28), into Eqs. (5-31) and (5-32):

$$\begin{aligned}
\begin{Bmatrix} N_{22} \\ M_{22} \\ M_{22}^{zS} \end{Bmatrix} &= \begin{bmatrix} C_{22}^0 & C_{22}^1 & C_{22}^{0S} \\ C_{22}^1 & C_{22}^2 & C_{22}^{1S} \\ C_{22}^{0S} & C_{22}^{1S} & C_{22}^{S2} \end{bmatrix} \begin{Bmatrix} v_{02,2} \\ \varphi_{2,2} \\ \theta_{2,2} \end{Bmatrix} \\
\begin{Bmatrix} Q_2 \\ Q_2^z \end{Bmatrix} &= k_{44} \begin{bmatrix} C_{44}^0 & C_{44}^1 \\ C_{44}^1 & C_{44}^2 \end{bmatrix} \begin{Bmatrix} \varphi_2 + w_{0,2} \\ \theta_2 \end{Bmatrix}
\end{aligned} \tag{5-36}$$

where

$$\begin{aligned}
\left[C_{22}^r, C_{22}^{rS}, C_{22}^{S2} \right] &= \sum_{k=1}^{n} {}^{(k)}\overline{C}_{22} \int_{x_3^{k-1}}^{x_3^k} \left[(x_3)^r, (x_3)^r \, {}^{(k)}\phi, ({}^{(k)}\phi)^2 \right] dx_3 \\
C_{44}^r &= \sum_{k=1}^{n} {}^{(k)}C_{44} \int_{x_3^{k-1}}^{x_3^k} \left({}^{(k)}\beta \right)^r dx_3
\end{aligned} \tag{5-37}$$

The term $\hat{\sigma}_2$ in Eq. (5-32) can be also written in terms of the kinematic variable of the model, θ_2, by substituting the interfacial tractions from Eq. (5-24) into Eq. (5-32):

$$\begin{aligned}
\hat{\sigma}_2 &= C_{22}^S \theta_2 \\
C_{22}^S &= G^2 \sum_{k=1}^{n-1} \frac{1}{K_S^k}
\end{aligned} \tag{5-38}$$

A shear correction factor, k_{44}, is introduced in Eq. (5-36) to improve the approximate description of the shear strain of the global model. The introduction of the shear correction factor has some advantages. It allows to recover the constitutive equations of the equivalent single layer first order shear deformation theory in the limiting case of a fully bonded and homogeneous plate, for which $k_{44} = 5/6$ is required. If the shear correction factor is not needed, for instance in bending problem of fully bonded multilayered plates

subjected to static loadings, the shear correction factor should be equal to 1. In this work, $k_{44}=1$ is assumed for multilayered and $k_{44}=5/6$ for homogenous plates.

The definition of the transverse shear force, Q_2, in Eq. (5-36) and the boundary conditions in Eq. (5-34) highlight a drawback of the proposed theory for solving problems, in which the solution requires the imposition of the continuity conditions between domains characterized by different interfacial stiffness, e.g. plates with finite length delaminations; in such problems, the solution of the present theory does not enforce the continuity condition on the slope of the transverse displacement, $w_{0},_{2}$, as explained in the following. Using Eq. (5-36), the continuity condition of the transverse shear force at the coordinate $x_2=a$, where the interfacial stiffness of domains at the left, $x_2=a^-$, and right, $x_2=a^+$, of the coordinate $x_2=a$ is different, yields:

$$\left[C_{44}^{0}\left(\varphi_2+w_{0},_{2}\right)+C_{44}^{1}\theta_2\right]_{x_2=a^-}=\left[C_{44}^{0}\left(\varphi_2+w_{0},_{2}\right)+C_{44}^{1}\theta_2\right]_{x_2=a^+} \tag{5-39}$$

The coefficient C_{44}^{0} defined in Eq. (5-37) is independent of the interfacial stiffness and is the same at the left and right of the coordinate $x_2=a$, while C_{44}^{1}, defined in Eq. (5-37), depends on the interfacial stiffness and is different for the regions at the left and right of the coordinate $x_2=a$. Since φ_2 and θ_2 are imposed to be continuous at $x_2=a$, as continuity conditions of the global kinematic variables of the model, Eq. (5-39) yields the following relationship for the difference between the slopes of the transverse displacement of the domains at $x_2=a$, $\Delta w_{0},_{2}\left(x_2=a\right)=\left[w_{0},_{2}\left(x_2=a^-\right)-w_{0},_{2}\left(x_2=a^+\right)\right]$:

$$\Delta w_{0},_{2}\left(x_2=a\right)=\frac{\left(G\right)_{x_2=a^+}-\left(G\right)_{x_2=a^-}}{C_{44}^{0}}h\theta_2\left(x_2=a\right) \tag{5-40}$$

and G is defined in Eq. (5-19). The continuity condition on $w_{0},_{2}$ at $x_2=a$, which results $\Delta w_{0},_{2}\left(x_2=a\right)=0$, would be enforced only if the G of the domains at the left and right of the coordinate $x_2=a$, are the same; this happens when the interfacial stiffnesses of two regions are the same. Equation (5-40) also shows that if the shear moduli of the domains at the left and right of the joining cross section at $x_2=a$, are different, $\Delta w_{0},_{2}\left(x_2=a\right)\neq 0$ even if the interfacial stiffness of the domains are the same; this is because G defined in Eq. (5-19) depends not only to the interfacial stiffness, but also to the shear modulus of the layers. The influence of the violation of the continuity condition of $w_{0},_{2}$, on the solution of the model for plates with finite length delaminations will be investigated in Sect. 5.5.

Substitutions of the force and moment resultants from Eqs. (5-36), and Eq. (5-38) into the equilibrium equations (5-30) yield the equilibrium equations in terms of the kinematic variables:

$$\delta v_{02}: \quad C_{22}^{0}v_{02},_{22}+C_{22}^{1}\varphi_2,_{22}+C_{22}^{0S}\theta_2,_{22}+f_2=0 \tag{5-41}$$

$$\delta\varphi_2: \quad C_{22}^{1}v_{02},_{22}+C_{22}^{2}\varphi_2,_{22}+C_{22}^{1S}\theta_2,_{22}-k_{44}C_{44}^{0}\left(\varphi_2+w_0,_2\right)-k_{44}C_{44}^{1}\theta_2+f_{2m}=0$$

$$\delta w_0: \quad k_{44}C_{44}^{0}\left(\varphi_2,_2+w_0,_{22}\right)+k_{44}C_{44}^{1}\theta_2,_2+f_3=0$$

$$\delta\theta_2: \quad C_{22}^{0S}v_{02},_{22}+C_{22}^{1S}\varphi_2,_{22}+C_{22}^{S2}\theta_2,_{22}-k_{44}C_{44}^{1}\left(\varphi_2+w_0,_2\right)-\left(k_{44}C_{44}^{2}+C_{22}^{S}\right)\theta_2=0$$

Substitutions of the force and moment resultants from Eqs. (5-36), and Eq. (5-38) into the boundary conditions (5-34) yield the boundary conditions in terms of the kinematic variables:

$$\begin{aligned}
&\delta v_{02}: && \left(C_{22}^{0}v_{02},_2+C_{22}^{1}\varphi_2,_2+C_{22}^{0S}\theta_2,_2\right)n_2=\tilde{N}_2 && \text{or} && v_{02}=\tilde{v}_{02}\\
&\delta\varphi_2: && \left(C_{22}^{1}v_{02},_2+C_{22}^{2}\varphi_2,_2+C_{22}^{1S}\theta_2,_2\right)n_2=\tilde{M}_2 && \text{or} && \varphi_2=\tilde{\varphi}_2\\
&\delta w_0: && k_{44}\left(C_{44}^{0}\left(\varphi_2+w_0,_2\right)+C_{44}^{1}\theta_2\right)n_2=\tilde{N}_3 && \text{or} && w_0=\tilde{w}_0\\
&\delta\theta_2: && \left(C_{22}^{0S}v_{02},_2+C_{22}^{1S}\varphi_2,_2+C_{22}^{S2}\theta_2,_2\right)n_2=\tilde{M}_2^{zS} && \text{or} && \theta_2=\tilde{\theta}_2
\end{aligned} \tag{5-42}$$

Solution of the boundary value problem is defined by the equilibrium equations (5-41) and boundary conditions (5-42).

The asymptotic limit of the equilibrium equations (5-41) and boundary conditions (5-42) corresponding to perfectly bonded layers, can be obtained by setting $1/K_S^i=0$ in the equilibrium equations (5-41) and boundary conditions (5-42). This yields $C_{22}^{S}=\hat{\sigma}_2=0$ in Eq. (5-38), and modifies the zigzag functions ${}^{(k)}\phi$ and ${}^{(k)}\beta$ defined in Eq. (5-22); the equations of the model then coincide with those of the refined zigzag theory developed in [27] for fully bonded laminates.

The system (5-41) has order VIII. The equations are decoupled by subsequent derivations/substitutions and eliminating $w_0,_2$ through the introduction of a variable γ given by $\gamma=\varphi_2+w_0,_2$. The system of decoupled equations, which has the same order of the original system is:

$$\begin{aligned}
&\theta_2,_{222}+\frac{C_{44}^{0}B_1+C_{44}^{1}}{C_{44}^{0}A_1}\theta_2,_2+\frac{f_3+k_{44}C_{44}^{0}D_1\left(x_2\right),_2}{k_{44}C_{44}^{0}A_1}=0\\
&\gamma=A_1\theta_2,_{22}+B_1\theta_2+D_1\left(x_2\right)\\
&v_{02},_{22}=\frac{C_{22}^{1}C_{22}^{S2}-C_{22}^{1S}C_{22}^{0S}}{C_{22}^{0}C_{22}^{1S}-C_{22}^{1}C_{22}^{0S}}\theta_2,_{22}-\frac{C_{22}^{1}\left(k_{44}C_{44}^{2}+C_{22}^{S}\right)}{C_{22}^{0}C_{22}^{1S}-C_{22}^{1}C_{22}^{0S}}\theta_2-\frac{k_{44}C_{44}^{1}C_{22}^{1}}{C_{22}^{0}C_{22}^{1S}-C_{22}^{1}C_{22}^{0S}}\gamma-\frac{C_{22}^{1S}}{C_{22}^{0}C_{22}^{1S}-C_{22}^{1}C_{22}^{0S}}f_2\\
&\varphi_2,_{22}=\frac{\left(C_{22}^{0S}\right)^2-C_{22}^{0}C_{22}^{S2}}{C_{22}^{0}C_{22}^{1S}-C_{22}^{1}C_{22}^{0S}}\theta_2,_{22}+\frac{C_{22}^{0}\left(k_{44}C_{44}^{2}+C_{22}^{S}\right)}{C_{22}^{0}C_{22}^{1S}-C_{22}^{1}C_{22}^{0S}}\theta_2+\frac{k_{44}C_{44}^{1}C_{22}^{0}}{C_{22}^{0}C_{22}^{1S}-C_{22}^{1}C_{22}^{0S}}\gamma+\frac{C_{22}^{0S}}{C_{22}^{0}C_{22}^{1S}-C_{22}^{1}C_{22}^{0S}}f_2\\
&w_0,_2=\gamma-\varphi_2
\end{aligned} \tag{5-43}$$

where:

$$A_1 = \frac{C_{22}^1\left[C_{22}^1C_{22}^{S2} - C_{22}^{1S}C_{22}^{0S}\right] + C_{22}^2\left[\left(C_{22}^{0S}\right)^2 - C_{22}^0C_{22}^{S2}\right] + C_{22}^{1S}\left[C_{22}^0C_{22}^{1S} - C_{22}^1C_{22}^{0S}\right]}{k_{44}C_{44}^0\left(C_{22}^0C_{22}^{1S} - C_{22}^1C_{22}^{0S}\right) + k_{44}C_{44}^1\left[\left(C_{22}^1\right)^2 - C_{22}^0C_{22}^2\right]}$$

$$B_1 = \frac{\left[C_{22}^2C_{22}^0 - \left(C_{22}^1\right)^2\right]\left[k_{44}C_{44}^2 + C_{22}^S\right] - k_{44}C_{44}^1\left[C_{22}^0C_{22}^{1S} - C_{22}^1C_{22}^{0S}\right]}{k_{44}C_{44}^0\left[C_{22}^0C_{22}^{1S} - C_{22}^1C_{22}^{0S}\right] + k_{44}C_{44}^1\left[\left(C_{22}^1\right)^2 - C_{22}^0C_{22}^2\right]} \tag{5-44}$$

$$D_1\left(x_2\right) = \frac{f_{2m}\left[C_{22}^0C_{22}^{1S} - C_{22}^1C_{22}^{0S}\right] + f_2\left[C_{22}^2C_{22}^{0S} - C_{22}^1C_{22}^{1S}\right]}{k_{44}C_{44}^0\left[C_{22}^0C_{22}^{1S} - C_{22}^1C_{22}^{0S}\right] + k_{44}C_{44}^1\left[\left(C_{22}^1\right)^2 - C_{22}^0C_{22}^2\right]}$$

The first equation (5-43) is a third order differential equation in θ_2 whose solution allows cascading solutions for γ through an algebraic equation, and v_{02} and φ_2 through solutions of two second order differential equations. The last equation (5-43), which is a first order differential equation, defines w_0.

5.4 MODEL VERIFICATION AND APPLICATIONS

In this section, the accuracy of the homogenized structural theory will be verified against exact 2D elasticity solutions derived in Chapter 3 for simply supported unidirectional and multilayered plates deforming in cylindrical bending and subjected to sinusoidal transverse loading, $F_3^{S^+} = F_3^{S^-} = f_0/2\left[\sin(\pi x_2/L)\right]$, Figure 5-4. The examples in this section are those considered in [25], to investigate the capabilities of the multiscale structural theory. In the examples, the layers are connected by linear elastic interfaces, which have the same interfacial stiffnesses. Three cases of perfect bonding, full debonding and partial bonding are examined. The plate has three layers and length-to-thickness ratio is $L/h = 4$. The origin of the coordinate system is placed at the mid-thickness. The elastic constants of the layers are $E_L/E_T = 25$, $G_{LT}/E_T = 0.5$, $G_{TT}/E_T = 0.2$ and $\nu_{LT} = \nu_{TT} = 0.25$ (subscripts L and T indicate in-plane principal material directions). The assumed ratios between the elastic constants of the layers could represent a graphite-epoxy laminate.

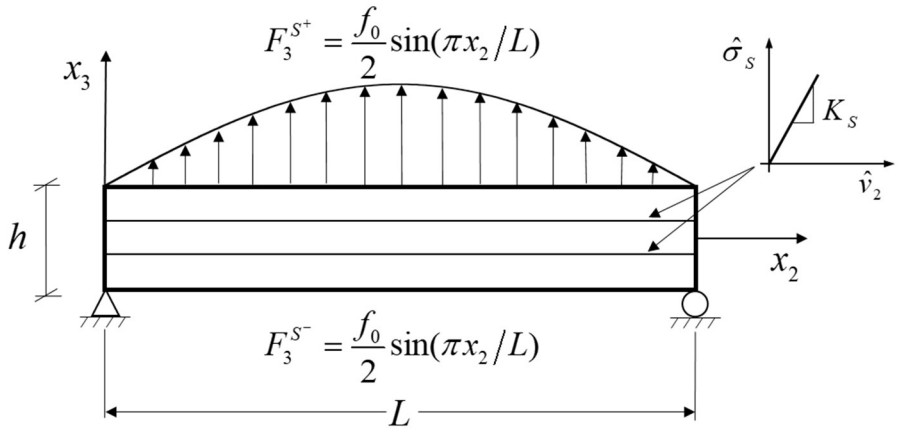

Figure 5-4: Three-layered plate with linear elastic interfaces subjected to sinusoidal transverse loading.

The following boundary conditions are imposed at the edges of the simply supported plate (Eq. (5-34)):

$$\begin{aligned} &x_2 = 0: \quad \tilde{w}_0 = \tilde{v}_{02} = \tilde{M}_2 = \tilde{M}_2^{zS} = 0 \\ &x_2 = L: \quad \tilde{w}_0 = \tilde{N}_2 = \tilde{M}_2 = \tilde{M}_2^{zS} = 0 \end{aligned} \tag{5-45}$$

The solutions of the displacement variables are then obtained by solving the equilibrium equations (5-41) and imposing the boundary conditions (5-45) for the simply supported plate. Once the global variables $v_{02}(x_2)$, $\varphi_2(x_2), w_0(x_2)$ and $\theta_2(x_2)$ are obtained, the displacements, the bending stresses, the interfacial tractions and jumps are defined through Eqs. (5-25), (5-28), (5-24) and (5-23). The transverse shear stresses of the layers are derived from the bending stresses by using equilibrium equation ${}^{(k)}\sigma_{22,2} + {}^{(k)}\sigma_{23,3}^{post} = 0$.

For fully bonded case, the asymptotic limit of the equilibrium equations (5-41), which is obtained by setting $1/K_S^i = 0$ is solved. Results for plates with fully debonded layers, are obtained by assuming a very small value for the interfacial stiffness, by which the solutions converge.

Unidirectional plate with imperfect interfaces

Here, the plate is assumed to be homogenous with stacking sequence $(0,0,0)$. Figure 5-5 shows the through thickness variation of the longitudinal displacements at $x_2 = 0$ and of the transverse displacements at $x_2 = L/2$. Results for the bending stresses at $x_2 = L/2$, and a posteriori calculated transverse shear stresses at $x_2 = 0$ are shown through the thickness of the plate in Figure 5-6. Three different cases of perfectly bonded interfaces, interfaces with intermediate imperfection with dimensionless interfacial stiffness $K_S h/E_T = 0.25$ and fully debonded interfaces are considered. Results of the present model and those predicted by the homogenized structural model used in Chapter 4 [25] are compared with the exact 2D elasticity solutions derived in Chapter 3.

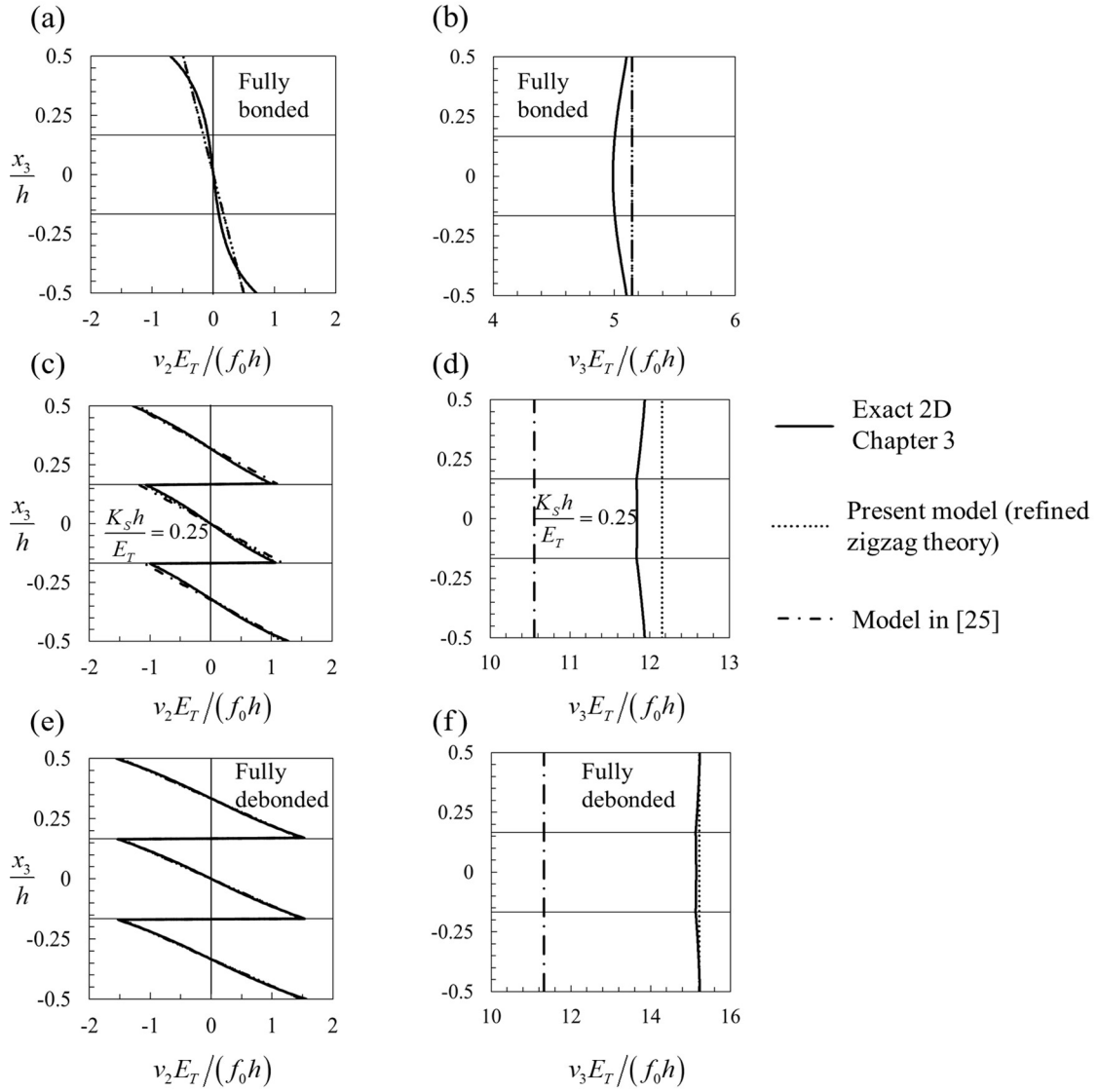

Figure 5-5: Longitudinal at $x_2 = 0$ and transverse at $x_2 = L/2$ displacements through the thickness in a simply supported three-layer wide plate $(0,0,0)$, $L/h = 4$, transverse loading $F_3^{S^+} = F_3^{S^-} = f_0/2\left[\sin(\pi x_2/L)\right]$. Elastic constants: $E_L/E_T = 25$, $G_{LT}/E_T = 0.5$, $G_{TT}/E_T = 0.2$ and $\nu_{LT} = \nu_{TT} = 0.25$. Shear correction factor $k_{44} = 5/6$.

The displacement and the stress fields in the layers are strongly affected by the presence of the imperfect interfaces; the longitudinal displacements and the bending stresses of the layers become discontinuous and the maximum deflection and transverse shear stress of the plate increase. The structural theory formulated in this chapter and the one used in Chapter 4 [25] accurately capture the interfacial displacement jumps due to the imperfect interfaces. The longitudinal displacements, and the bending and transverse shear stresses predicted by the models are similar and very accurate for all cases examined.

Figure 5-5(b) shows the transverse displacements at the mid-span of the perfectly bonded plate; both models, which coincide with the equivalent single layer first order shear deformation theory, overestimate the exact solutions. At the presence of imperfect interfaces, the present model predicts more accurate transverse displacements compared to those predicted by the model used in Chapter 4 [25], Figure 5-5(d)

and (f), due to a better description of the shear deformations in the layers of the imperfectly bonded plates. The present model adequately predicts the transverse displacements when the plate is fully debonded (Figure 5-5(f)). In this case, the layers deform independently as a thinner structure. For thinner plates, e.g. $L/h=10$, the solutions of both models significantly improve and are in excellent agreement with the exact solution for all interfacial stiffness values (not shown).

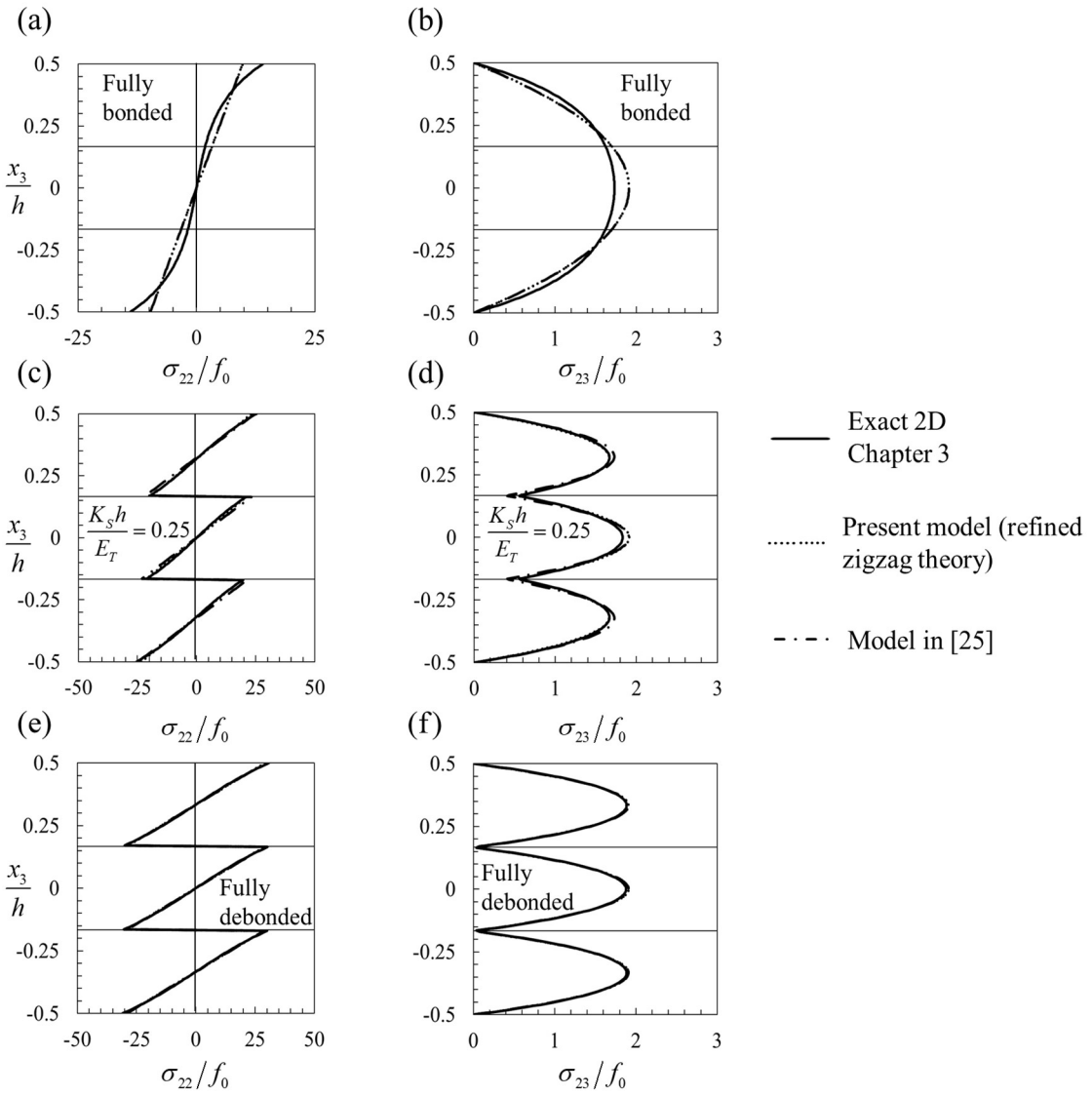

Figure 5-6: Bending at $x_2=L/2$ and transverse shear at $x_2=0$ stresses through the thickness in a simply supported three-layer wide plate $(0,0,0)$, $L/h=4$, transverse loading $F_3^{S^+}=F_3^{S^-}=f_0/2\left[\sin(\pi x_2/L)\right]$. Elastic constants: $E_L/E_T=25$, $G_{LT}/E_T=0.5$, $G_{TT}/E_T=0.2$ and $\nu_{LT}=\nu_{TT}=0.25$. Transverse shear stresses are calculated a posteriori from bending stresses. Shear correction factor $k_{44}=5/6$.

To further demonstrate the capability of the present model to accurately predict transverse displacements for plates with imperfectly bonded layers, a simply supported homogenous plate deforming in cylindrical bending, with two identical layers and length-to-thickness ratio $L/h=4$, is considered. This example was

considered in [25], to investigate the capabilities of the multiscale structural theory. The laminate is subjected to transverse loading $F_3^{S^+} = f_0 \sin(\pi x_2/L)$ on its upper surface, while the lower surface of the plate is traction-free. The elastic constants of the layers are $E_L/E_T = 25$, $G_{LT}/E_T = 0.5$, $G_{TT}/E_T = 0.2$ and $\nu_{LT} = \nu_{TT} = 0.25$ (subscripts L and T indicate in-plane principal material directions) and stacking sequence $(0,0)$. Figure 5-7 illustrates the transverse displacements at $x_2 = L/2$ on the top of the plate, normalized to exact 2D elasticity solutions of a fully debonded plate, $(v_3)_{2D,\lim}$, on varying the interfacial stiffness (decreasing interfacial stiffness from left to right). The transverse displacements predicted by the present model are in good agreement with the exact solutions for any value of the interfacial stiffness. As noted and explained in [25], the predictions of the model used in Chapter 4 [25] are accurate for large values of the interfacial stiffness and deviate from the exact solutions for smaller values; the deviation occurs because the transverse shear strains/stresses in the model used in Chapter 4 [25] decrease/vanish on decreasing/vanishing the interfacial stiffness, as it can be understood from Eqs. (4-5), (4-11), (4-12) and (4-14) [25]. This was discussed in [25] that this behavior is a consequence of the a priori imposition of the continuity of the shear tractions at the interfaces and the assumption of a first order global displacement field. For small values of the interfacial stiffness, the solution of the homogenized structural model [25] tends to the solution corresponding to two layers free to slide over each other and modeled separately by the kinematic assumptions of the classical plate theory, in which the shear deformations in the layer are neglected [25]. The solution of the model in [25] significantly improves for thinner plates or for plates with more layers and interfaces [25]. In [25], it was suggested to modify the shear correction factor of fully bonded plates and define a shear correction factor, which depends on the stiffness of the interfaces, to account for the missing contribution of the shear deformations to the displacement field.

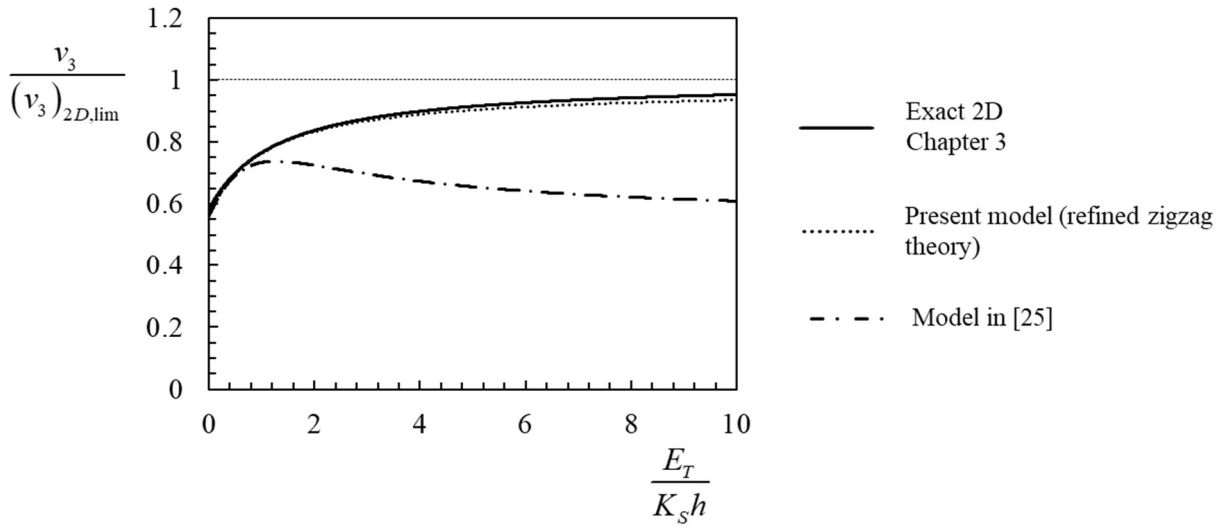

Figure 5-7: Transverse displacements at $x_2 = L/2$ at the top of a simply supported two-layer wide plate $(0,0)$, $L/h = 4$; layers connected by a linear elastic interface at the mid-thickness, transverse loading $F_3^{S^+} = f_0 \sin(\pi x_2/L)$ on its upper surface, while the lower surface of the plate is traction-free [25]. The results are normalized to those of a fully debonded plate, $(v_3)_{2D,\lim}$, and shown on varying the interfacial stiffness (decreasing

interfacial stiffness from left to right). Elastic constants: $E_L/E_T = 25$, $G_{LT}/E_T = 0.5$, $G_{TT}/E_T = 0.2$ and $\nu_{LT} = \nu_{TT} = 0.25$. Shear correction factor $k_{44} = 5/6$.

Multilayered plate with imperfect interfaces

Here, the plate in Figure 5-4 is considered with a stacking sequence of $(0,90,0)$. The plate is highly anisotropic and provides a challenging case to assess the predictive capabilities of the model [25]. This example also was considered in [25]. Figure 5-8 and Figure 5-9 illustrate the through thickness variation of the longitudinal and transverse displacements, and bending and transverse shear stresses at different cross-sections of the plate. Results are presented on varying the interfacial stiffness.

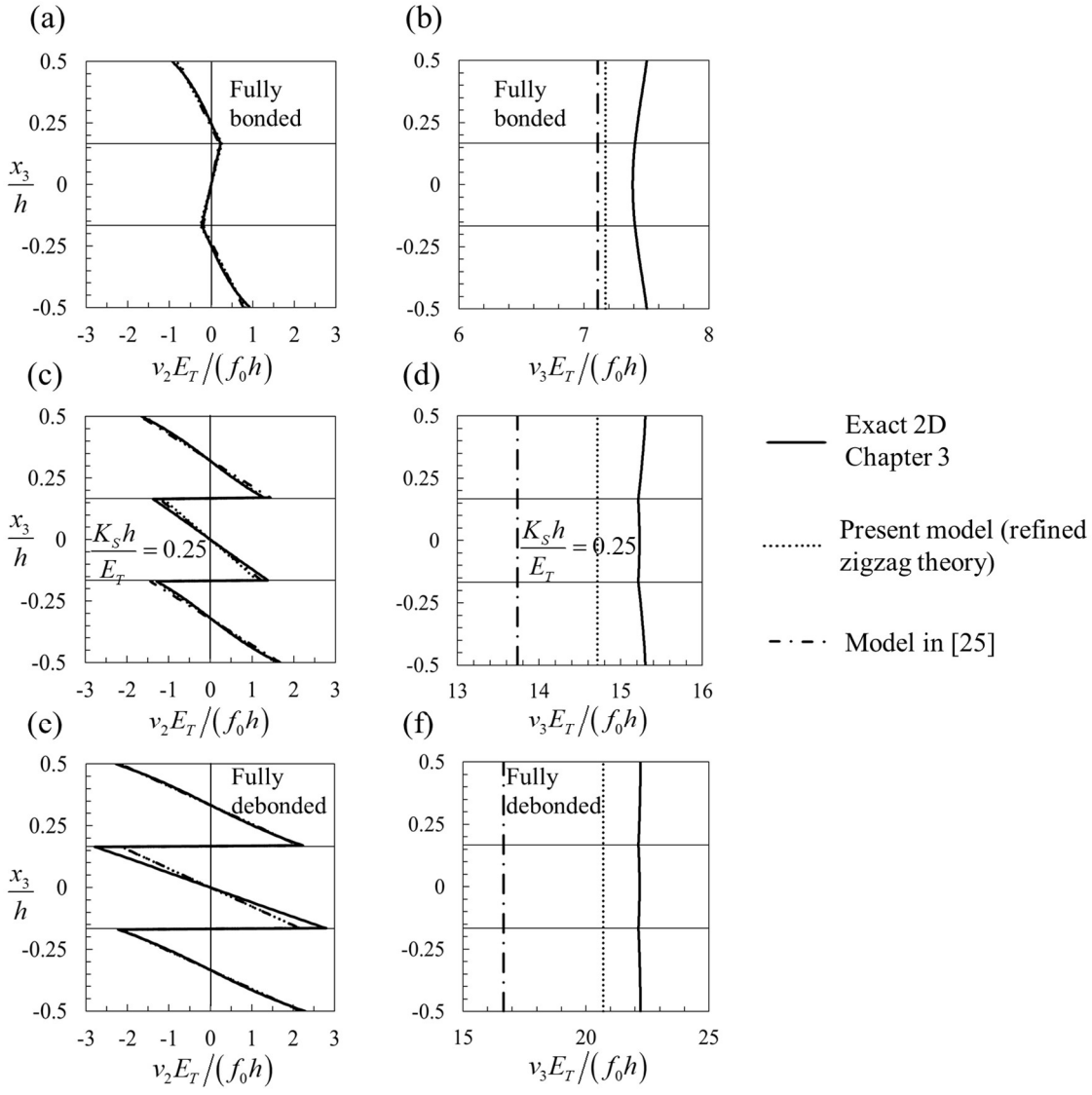

Figure 5-8: Longitudinal at $x_2 = 0$ and transverse at $x_2 = L/2$ displacements through the thickness in a simply supported three-layer wide plate $(0,90,0)$, $L/h = 4$, transverse loading $F_3^{S^+} = F_3^{S^-} = f_0/2[\sin(\pi x_2/L)]$. Elastic constants: $E_L/E_T = 25$, $G_{LT}/E_T = 0.5$, $G_{TT}/E_T = 0.2$ and $\nu_{LT} = \nu_{TT} = 0.25$. Shear correction factor $k_{44} = 1$.

The diagrams in Figure 5-8 refer to the longitudinal and transverse displacements at $x_2 = 0$ and $x_2 = L/2$; the refined theory and the model used in Chapter 4 [25] capture the zigzag pattern in the longitudinal displacements of the layers and the interfacial displacement jumps. The present model predicts the transverse displacements more accurately than the model used in Chapter 4 [25].

The bending and transverse shear stresses at $x_2 = L/2$ and $x_2 = 0$ are shown in Figure 5-9. The bending and the transverse shear stresses predicted by the models are in good agreement with the exact 2D elasticity solution. Through the thickness distribution of the bending stresses, which are characterized by jumps at the interfaces, are well captured by both models. For the plate with partially bonded layers, the present model predicts the transverse shear stresses with high accuracy, also at the interfaces. For thinner plates, e.g. $L/h = 10$, the solutions of both models significantly improve and are in excellent agreement with the exact solution for all interfacial stiffness values (not shown).

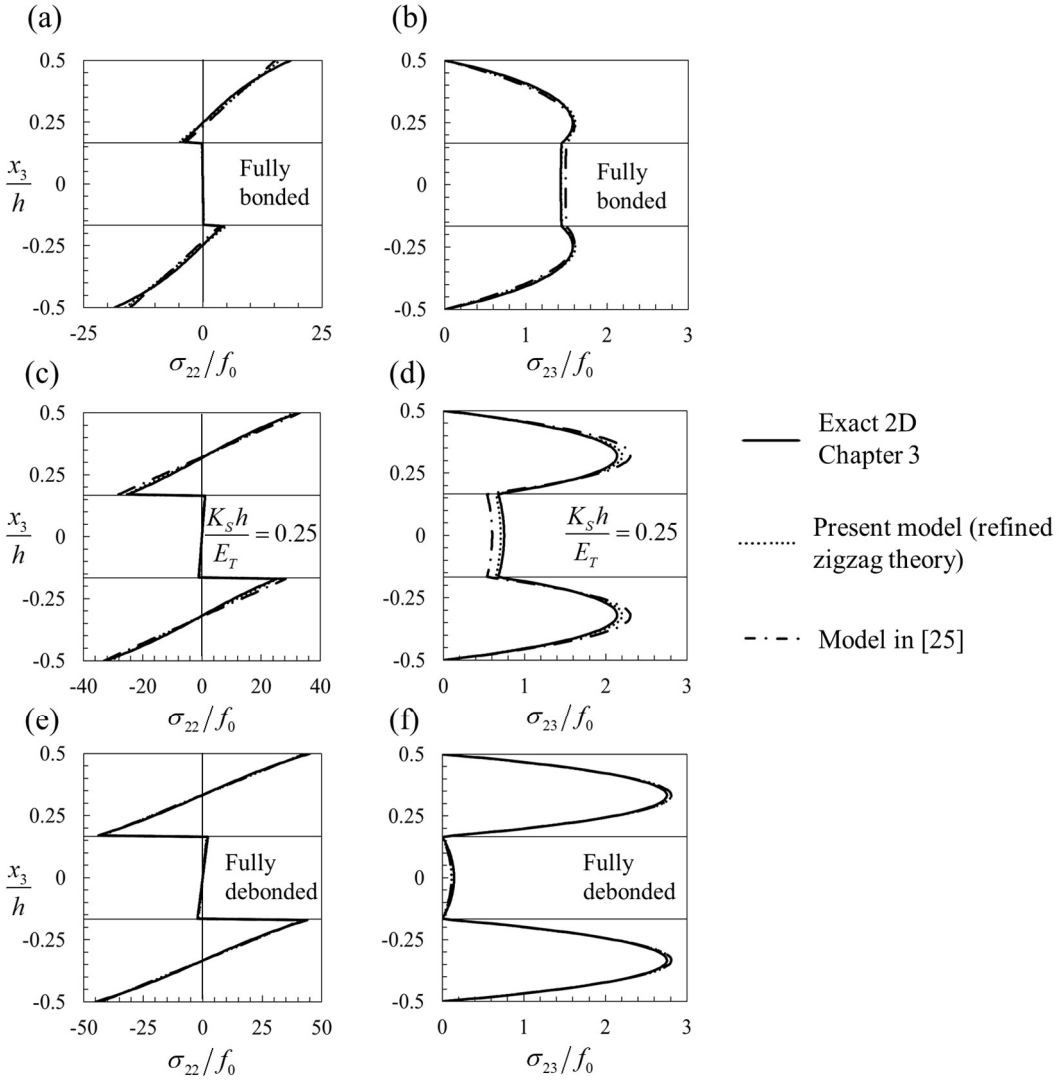

Figure 5-9: Bending at $x_2 = L/2$ and transverse shear at $x_2 = 0$ stresses through the thickness in a simply supported three-layer wide plate $(0,90,0)$, $L/h = 4$, transverse loading $F_3^{S^+} = F_3^{S^-} = f_0/2\left[\sin(\pi x_2/L)\right]$. Elastic

constants: $E_L/E_T = 25$, $G_{LT}/E_T = 0.5$, $G_{TT}/E_T = 0.2$ and $\nu_{LT} = \nu_{TT} = 0.25$. Transverse shear stresses are calculated a posteriori from bending stresses. Shear correction factor $k_{44} = 1$.

Cantilevered Plate

To demonstrate the predictive capabilities of the formulated model along the clamped supports, the example considered in [26] is used here: a cantilevered plate deforming in cylindrical bending with $L/h = 10$ and two layers connected by a linear elastic interface and subjected to a concentrated transverse force at the free end, Figure 5-10. The origin of the coordinate system is placed at the mid-thickness. The two identical layers of the plate are connected by a linear elastic interface at the mid-thickness, $x_3 = 0$. The elastic constants of the layers are: $E_L/E_T = 25$, $G_{LT}/E_T = 0.5$, $G_{TT}/E_T = 0.2$ and $\nu_{LT} = \nu_{TT} = 0.25$ (subscripts *L* and *T* indicate in-plane principal material directions) and stacking sequence $(0,0)$.

The boundary conditions at the edges of the cantilevered plate in Figure 5-10, Eq. (5-34), are:

$$\begin{aligned} &x_2 = 0: \quad \tilde{w}_0 = \tilde{v}_{02} = \tilde{\varphi}_2 = \tilde{\theta}_2 = 0 \\ &x_2 = L: \begin{cases} \tilde{N}_2 = \tilde{M}_2 = \tilde{M}_2^{zS} = 0 \\ Q_2 = F \end{cases} \end{aligned} \tag{5-46}$$

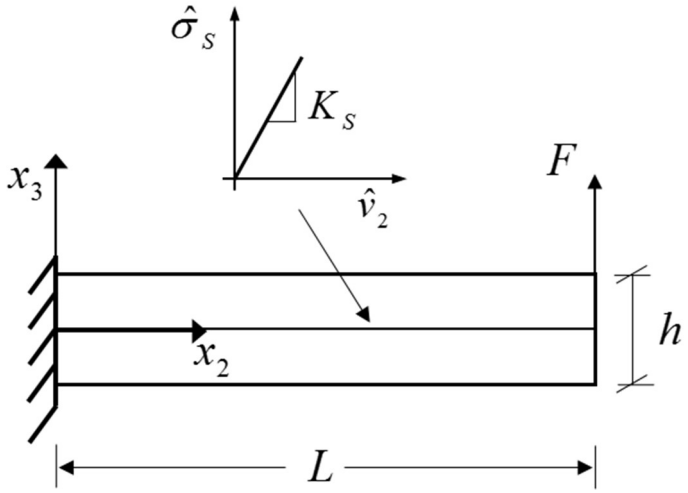

Figure 5-10: A cantilevered plate composed of two layers joined by a linear elastic interface at the mid-thickness and subjected to transverse load F at the free end [26].

The boundary conditions at $x_2 = 0$ satisfy the conditions at the clamped end, i.e. zero displacements. The solutions of the displacement variables are then obtained by solving the equilibrium equations (5-41) and imposing the boundary conditions (5-46).

Figure 5-11 illustrates the variations of the interfacial shear tractions, Eq. (5-24), along the plate length for three different values of the interfacial stiffness; the interfacial tractions calculated through Eq. (5-24), $\hat{\sigma}_S$, coincide with those obtained a posteriori, ${}^{(1)}\sigma_{23}^{post}(x_3 = 0) = {}^{(2)}\sigma_{23}^{post}(x_3 = 0)$. The results of the present

model are compared with those of the model used in Chapter 4 [25], and the discrete layer interface model presented in Sect. 4.5.6 in Chapter 4 with the interfacial constitutive equation (5-3).

The interfacial shear tractions predicted by the present structural model coincide with those obtained by the discrete layer interface model, for any value of the interfacial stiffness. As noted and explained in [26], the interfacial shear tractions predicted through the structural theory used in Chapter 4 [25], have different behaviour within a region near the clamped edge, and coincide with the solutions of the discrete layer model out of the region; the size of this region depends on the interfacial stiffness and is negligible for very stiff and compliant interfaces [26].

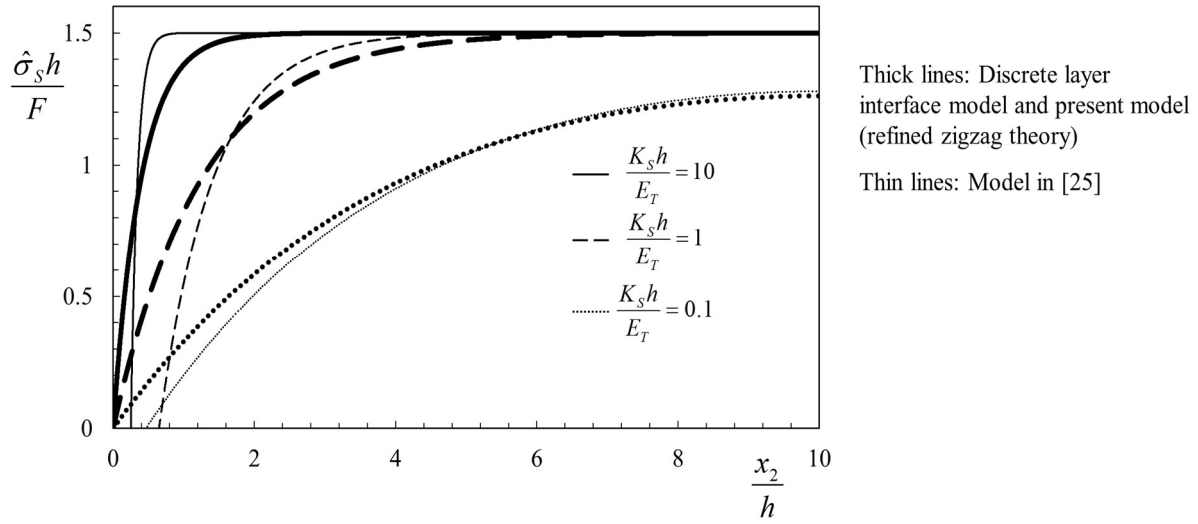

Figure 5-11: Interfacial tractions along the length of a cantilever two-layer with plate $(0,0)$, $L/h=10$, subjected to a concentrated transverse force *F* at the free end (Figure 5-10) [26]. Two identical layers connected by a linear elastic interface at the mid-thickness. The elastic constants: $E_L/E_T=25$, $G_{LT}/E_T=0.5$, $G_{TT}/E_T=0.2$ and $\nu_{LT}=\nu_{TT}=0.25$. Interfacial tractions predicted by the model used in Chapter 4 [25] are calculated a posteriori from the bending stresses.

5.5 PRELIMINARY APPLICATIONS TO DELAMINATION PROBLEMS

To preliminarily investigate the applicability of the formulated model to fracture problems, the model is applied to analyze the specimen shown in Figure 5-12 with $2L/h=100$ and $a/h=30$. The origin of the coordinate system is placed at the mid-thickness. The specimen deforms in cylindrical bending, and is made of two layers with the same thickness *h* and material properties $E_T/E_L=0.071$, $G_{LT}/E_L=0.033$, $\nu_{LT}=0.32$ and $\nu_{TT}=0.45$ (subscripts *L* and *T* indicate in-plane principal material directions and the *L* direction coincides with x_2 axis in the layers), and is subjected to a concentrated load *P* at the mid-span. The layers are bonded with two linear elastic interfaces with different interfacial stiffness for $0\le x_2\le a$ and $a\le x_2\le 2L$. The dimensionless interfacial stiffnesses $K_S h/E_L$ for the portion of the specimen within $a\le x_2\le 2L$, is set to be 10^4 to approximate the perfect bonding of two layers in the intact region. Different values of the interfacial stiffness are assumed for the portion of the specimen within $0\le x_2\le a$ to investigate the solutions of the formulated model. The terms G and β defined in Eqs. (5-19) and (5-22)

are simplified for this example as $G = 2hK_S G_{LT} / (2hK_S + G_{LT})$ and $\beta = -G_{LT} / (2hK_S + G_{LT})$; substituting G and β into Eq. (5-25), the longitudinal displacements of the layers are:

$$
\begin{aligned}
{}^{(1)}v_2 &= \left(v_{02} - \theta_2 \frac{G_{LT} h}{2hK_S + G_{LT}} \right) + x_3 \left(\varphi_2 - \theta_2 \frac{G_{LT}}{2hK_S + G_{LT}} \right) \\
{}^{(2)}v_2 &= \left(v_{02} + \theta_2 \frac{G_{LT} h}{2hK_S + G_{LT}} \right) + x_3 \left(\varphi_2 - \theta_2 \frac{G_{LT}}{2hK_S + G_{LT}} \right)
\end{aligned}
\tag{5-47}
$$

where the terms multiply x_3, $\varphi_2 - \theta_2 G_{LT} / (2hK_S + G_{LT})$ define the local rotations of the layers.

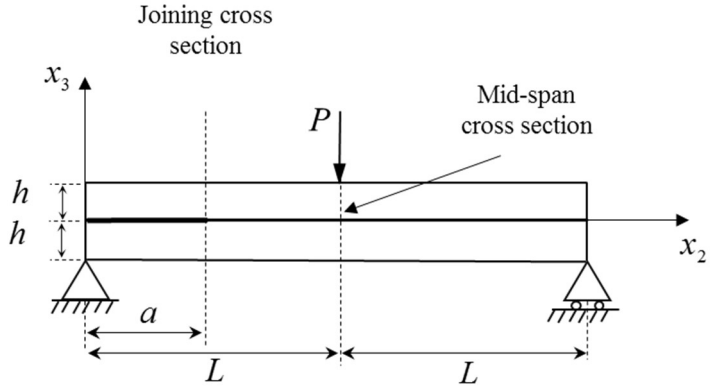

Figure 5-12: ENF specimen with two layers of equal thickness, bonded by two linear elastic interfaces with different interfacial stiffness for $0 \le x_2 \le a$ and $a \le x_2 \le 2L$.

The specimen is discretized into three portions separated at the coordinates $x_2 = a$ and $x_2 = L$. The solutions of the displacement variables, v_{02}, φ_2, w_0 and θ_2 in three different regions, are obtained by solving the equilibrium equations (5-41) and imposing the boundary conditions at $x_2 = 0$ and $x_2 = 2L$, and continuity conditions at $x_2 = a$ and $x_2 = L$. The following boundary conditions are imposed at the plate edges (Eq. (5-34)):

$$
\begin{aligned}
&x_2 = 0: \quad \tilde{w}_0 = \tilde{v}_{02} = \tilde{M}_2 = \tilde{M}_2^{zS} = 0 \\
&x_2 = 2L: \quad \tilde{w}_0 = \tilde{N}_2 = \tilde{M}_2 = \tilde{M}_2^{zS} = 0
\end{aligned}
\tag{5-48}
$$

The continuity conditions are imposed at $x_2 = a$ and $x_2 = L$ on the global variables v_{02}, φ_2, w_0, θ_2, N_{22}, M_{22}, Q_2 and M_{22}^{zS}, which yield:

$$\text{at } x_2 = a \begin{cases} v_{02}\left(x_2 = a^-\right) = v_{02}\left(x_2 = a^+\right) & N_{22}\left(x_2 = a^-\right) = N_{22}\left(x_2 = a^+\right) \\ \varphi_2\left(x_2 = a^-\right) = \varphi_2\left(x_2 = a^+\right) & M_{22}\left(x_2 = a^-\right) = M_{22}\left(x_2 = a^+\right) \\ \theta_2\left(x_2 = a^-\right) = \theta_2\left(x_2 = a^+\right) & Q_2\left(x_2 = a^-\right) = Q_2\left(x_2 = a^+\right) \\ w_0\left(x_2 = a^-\right) = w_0\left(x_2 = a^+\right) & M_{22}^{zS}\left(x_2 = a^-\right) = M_{22}^{zS}\left(x_2 = a^+\right) \end{cases}$$

$$\text{at } x_2 = L \begin{cases} v_{02}\left(x_2 = L^-\right) = v_{02}\left(x_2 = L^+\right) & N_{22}\left(x_2 = L^-\right) = N_{22}\left(x_2 = L^+\right) \\ \varphi_2\left(x_2 = L^-\right) = \varphi_2\left(x_2 = L^+\right) & M_{22}\left(x_2 = L^-\right) = M_{22}\left(x_2 = L^+\right) \\ \theta_2\left(x_2 = L^-\right) = \theta_2\left(x_2 = L^+\right) & Q_2\left(x_2 = L^-\right) = Q_2\left(x_2 = L^+\right) \\ w_0\left(x_2 = L^-\right) = w_0\left(x_2 = L^+\right) & M_{22}^{zS}\left(x_2 = L^-\right) = M_{22}^{zS}\left(x_2 = L^+\right) \end{cases} \tag{5-49}$$

where the superscript – and + on the right of a coordinate show association of the global variables with the domains at the left and right of that coordinate, respectively. Once the global variables are obtained, the displacements, the bending stresses, the interfacial tractions and jumps are defined through Eqs. (5-47), (5-28), (5-24) and (5-23). The transverse shear stresses of the layers are derived from the bending stresses by using equilibrium ${}^{(k)}\sigma_{22,2} + {}^{(k)}\sigma_{23,3}^{post} = 0$.

As already explained after Eq. (5-26), Eq. (5-47) shows that at $x_2 = a$, where two domains characterized by different interfacial stiffness are joined, the imposition of the continuity of the global kinematic variables does not enforce the continuity of the longitudinal displacements. The local rotations of the layers at the left and right of the coordinate, $\varphi_2 - \theta_2\, G_{LT} / \left(2hK_S + G_{LT}\right)$, are also different.

The mid-span deflection predicted by the formulated model for two sets of the interfacial stiffnesses, and those predicted by the discrete layer interface model presented in Sect. 4.5.6 in Chapter 4, are shown in Figure 5-13. The interfacial stiffnesses are given in the caption of the figure. The trasnverse displacements predicted by the present model are in agreement with those obtained through the discrete layer model.

Diagrams in Figure 5-14 show the distributions of the interfacial tractions and jumps in the specimen with $K_S h / E_L = 10$ and $K_S h / E_L = 10^4$ within $0 \le x_2 \le a$ and $a \le x_2 \le 2L$, respectively. The results are presented for the left side of the plate from $x_2 = 0$ to $x_2 = L$. The interfacial tractions and jumps obtained through the present model coincide with those calculated by the discrete model, except in a region in the vicinity of the crack tip at $x_2 = a$, which is the cross section where the continuity conditions are imposed; a similar boundary region was also observed in Sect. 4.5.6 in the solution of the homogenized model used in Chapter 4. The solutions of the present theory coincide with those of the discrete layer interface model also near the mid-span cross section; this was expected since the conditions at the mid-span are similar to a clamped end, and it was shown previously that the formulated theory is able to accurately model clamped boundaries.

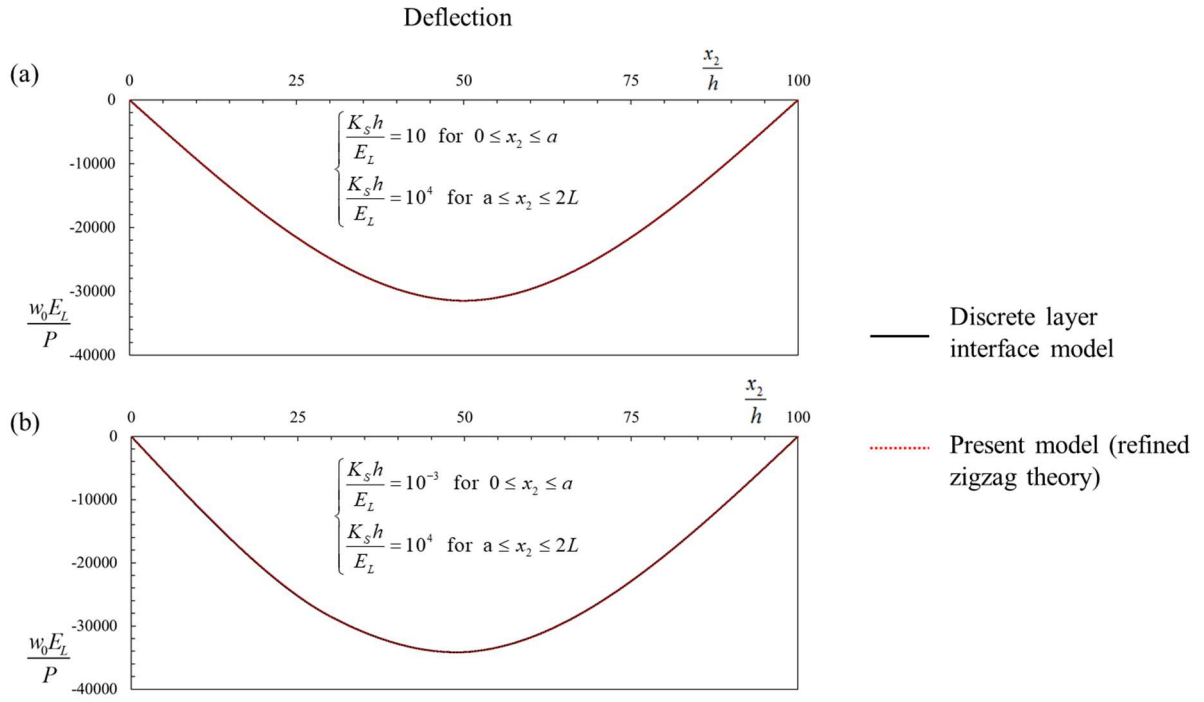

Figure 5-13: Deflection of the specimen in Figure 5-12 with $2L/h = 100$ and $a/h = 30$ made of $E_T/E_L = 0.071$, $G_{LT}/E_L = 0.033$, $\nu_{LT} = 0.32$ and $\nu_{TT} = 0.45$. (a) $K_S h/E_L = 10$ for $0 \le x_2 \le a$ and $K_S h/E_L = 10^4$ for $a \le x_2 \le 2L$ (fully bonded), and (b) $K_S h/E_L = 10^{-3}$ for $0 \le x_2 \le a$ and $K_S h/E_L = 10^4$ for $a \le x_2 \le 2L$. Correction factor $k_{44} = 5/6$.

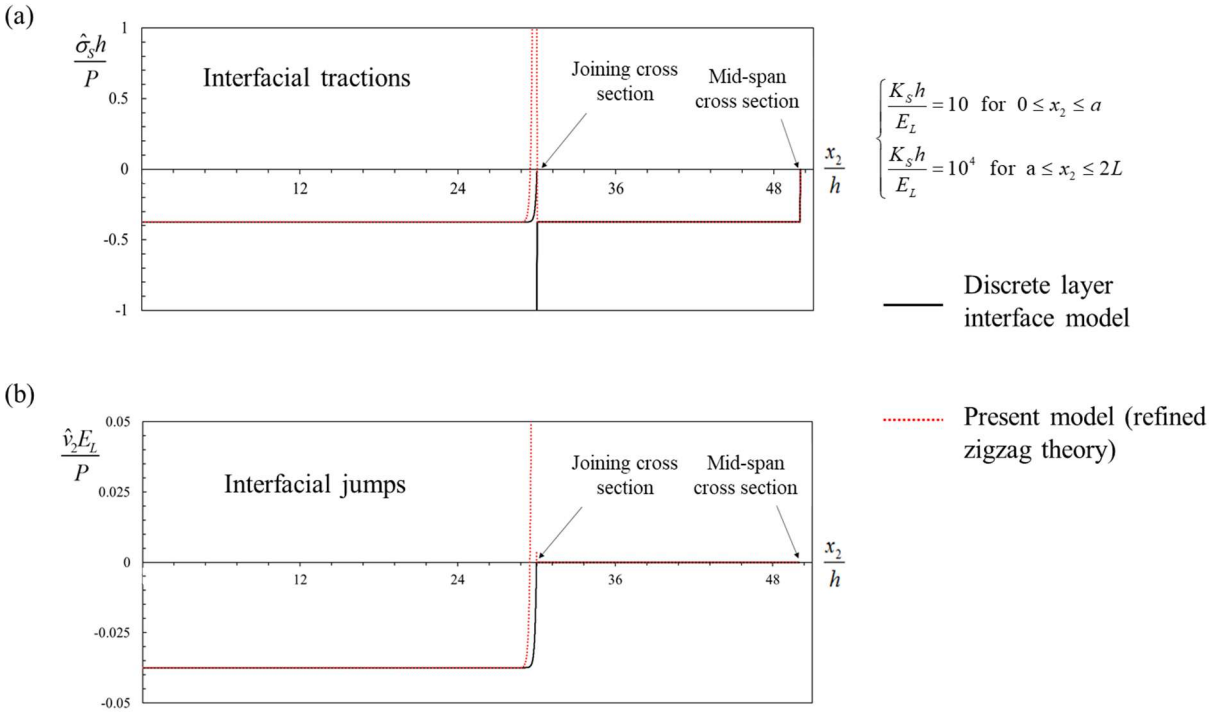

Figure 5-14: (a) Interfacial tractions and (b) interfacial jumps from $x_2 = 0$ to $x_2 = L$ in the specimen in Figure 5-12 with $2L/h = 100$ and $a/h = 30$ made of $E_T/E_L = 0.071$, $G_{LT}/E_L = 0.033$, $\nu_{LT} = 0.32$ and $\nu_{TT} = 0.45$. $K_S h/E_L = 10$ for $0 \le x_2 \le a$ and $K_S h/E_L = 10^4$ for $a \le x_2 \le 2L$ (fully bonded). Correction factor $k_{44} = 5/6$.

Diagrams in Figure 5-15 refer to the specimen in Figure 5-12 with $K_S h/E_L = 10^{-3}$ and $K_S h/E_L = 10^4$ within $0 \le x_2 \le a$ and $a \le x_2 \le 2L$, respectively. The interfacial tractions and jumps calculated by the present model for $0 \le x_2 \le a$ are in agreement with the solutions of the discrete model. The discontinuity in the interfacial jumps predicted by the present model at $x_2 = a$, is due to the imposition of the continuity conditions on the global variables only. The solutions of both models coincide in the intact part of the specimen, except for the interfacial tractions within a very small region ahead of joining cross section at $x_2 = a$.

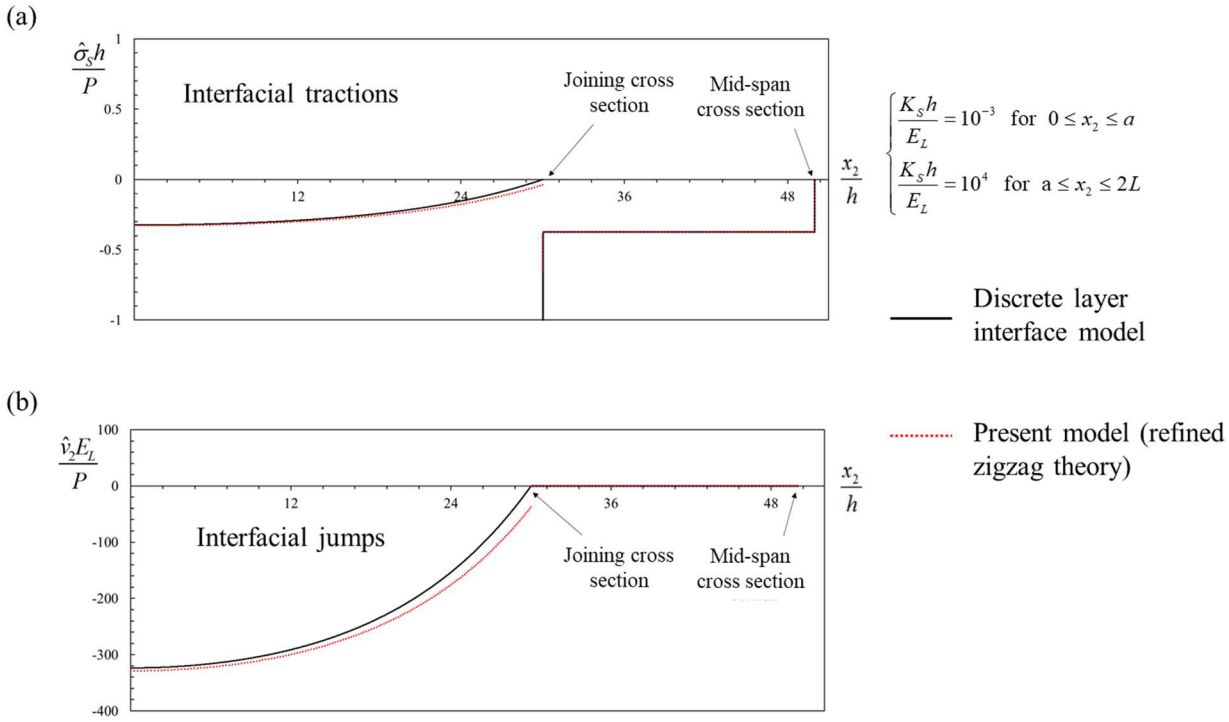

Figure 5-15: (a) Interfacial tractions and (b) interfacial jumps from $x_2 = 0$ to $x_2 = L$ in the specimen in Figure 5-12 with $2L/h = 100$ and $a/h = 30$ made of $E_T/E_L = 0.071$, $G_{LT}/E_L = 0.033$, $\nu_{LT} = 0.32$ and $\nu_{TT} = 0.45$. $K_S h/E_L = 10^{-3}$ for $0 \le x_2 \le a$ and $K_S h/E_L = 10^4$ for $a \le x_2 \le 2L$ (fully bonded). Correction factor $k_{44} = 5/6$.

To model a traction-free delamination, the interfacial stiffness of the region between $x_2 = 0$ and $x_2 = a$ should be reduced to a very small number. Figure 5-16(a) refers to the deflection of the specimen with $K_S h/E_L = 10^{-4}$ and $K_S h/E_L = 10^4$ within $0 \le x_2 \le a$ and $a \le x_2 \le 2L$, respectively. The transverse displacements predicted by the present model differ from those obtained through the discrete layer model. This discrepancy is due to the absence of the continuity condition on the slope of the transverse displacement variable, $w_{0,2}$, in the solution of the present model, as already explained by Eq. (5-40). The continuity condition on $w_{0,2}$ at $x_2 = a$ would be enforced through the continuity of the transverse shear force Q_2 defined in Eq. (5-32), only if the G defined in Eq. (5-19), of the homogenized domains at the left and right of the coordinate $x_2 = a$, are the same; this happens when the interfacial stiffnesses of two regions are the same. The violation of the continuity condition on $w_{0,2}$ has negligible effect on the predicted transverse displacements in Figure 5-13; the difference between the transverse displacements predicted by

two models then becomes noticeable when the interfacial stiffness of the portion of the plate within $0 \le x_2 \le a$ is reduced to $K_S h/E_L = 10^{-4}$.

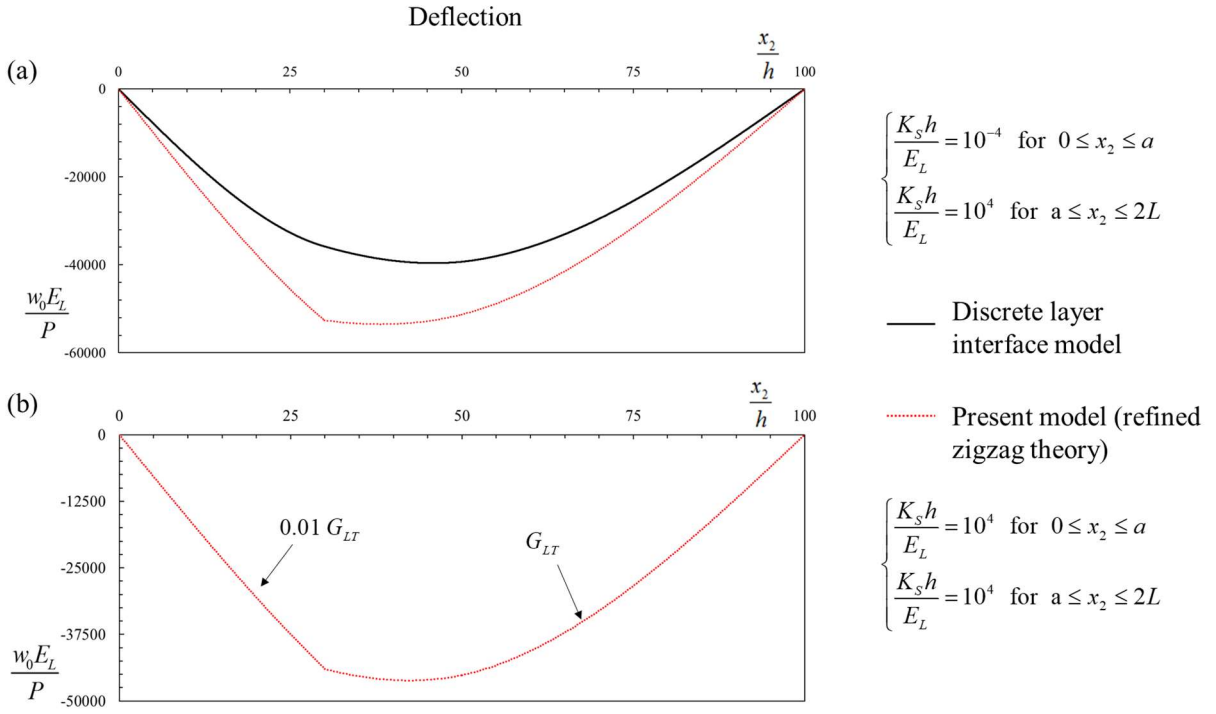

Figure 5-16: (a) Deflection of the specimen in Figure 5-12 with $2L/h = 100$ and $a/h = 30$ made of $E_T/E_L = 0.071$, $G_{LT}/E_L = 0.033$, $\nu_{LT} = 0.32$ and $\nu_{TT} = 0.45$. $K_S h/E_L = 10^{-4}$ for $0 \le x_2 \le a$ and $K_S h/E_L = 10^{4}$ for $a \le x_2 \le 2L$ (fully bonded). (b) Deflection of a perfectly bonded specimen in Figure 5-12 with $2L/h = 100$ and $a/h = 30$ made of $E_T/E_L = 0.071$, $G_{LT}/E_L = 0.033$, $\nu_{LT} = 0.32$ and $\nu_{TT} = 0.45$. The shear modulus in the portion of the specimen within $0 \le x_2 \le a$ is reduced to $0.01G_{LT}$. Correction factor $k_{44} = 5/6$.

Equation (5-19) shows that if the shear moduli of the materials within $0 \le x_2 \le a$ and $a \le x_2 \le 2L$ are different, the G would be different in different portions of the specimen. In this case, if the difference is large enough, the discontinuity in the first derivative of the transverse displacements would become noticeable also in plates with no delamination, Eq. (5-40). Figure 5-16(b) refers to the specimen in Figure 5-12 with $K_S h/E_L = 10^4$ everywhere through the length, namely a fully bonded plate; the shear modulus of the portion of the specimen within $0 \le x_2 \le a$ is reduced to be 1% of that of the portion of the plate within $a \le x_2 \le 2L$, $0.01G_{LT}$. Similar to Figure 5-16(a), the deflection of the specimen is characterized by different $w_{0,2}$ at $x_2 = a$.

The above mentioned problem does not arise in applications of the homogenized structural theory used in Chapter 4 [25], since one of the global continuity conditions of that model is on $w_{0,2}$ (see Eq. (4-21)). The drawback then limits the applications of the present model to Linear Elastic Fracture Mechanics problems, in which the difference between the G defined in Eq. (5-19), of the homogenized domains ahead and behind the traction-free delamination tip is maximal, due to the very large/small values of the interfacial

stiffness in the intact/delaminated regions. However, the model may be applicable to cohesive crack modeling, by approximating nonlinear cohesive traction laws by piecewise linear branches [25].

5.6 CONCLUSIONS

In this chapter, a new multiscale structural theory, based on the refined zigzag theory [27] and on the multiscale approach proposed in [11, 25] to analyze multilayered plates with imperfect interfaces and delaminations, has been formulated for laminated composite wide plates and beams with an arbitrary number of layers and imperfect interfaces and delaminations, to overcome the limitation of the homogenized model [25], i.e. neglecting the shear deformations in fully debonded laminates. The interfaces are assumed to be rigid against relative opening displacements and their mechanical behaviour are described through the linear elastic interfacial constitutive law. A homogenization technique has been used to derive the local variables in terms of the global ones; the number of kinematic variables in this model is independent of the number of layers and imperfect interfaces, as those of the original models in [11, 25, 27]. Piecewise linear and discontinuous zigzag functions are derived by modeling the imperfect interfaces as thin layers with vanishing thickness. The model allows to account for the shear deformations through the thickness of laminates with continuous imperfect or fully debonded interfaces, enables accurate modeling of all boundary conditions including clamped ends, and needs only C^0-continuous shape functions for finite element implementation. It has been proved that the model runs into difficulties when applied to problems, whose solutions require the imposition of the continuity conditions between regions characterized by different transverse shear moduli or interfacial stiffness, e.g. a plate with finite length imperfect interface or delamination. The problem is just a consequence of the fact that the model cannot deal with continuity conditions.

Applications of the formulated model have been presented for simply supported plates with continuous linear elastic imperfect interfaces. Comparisons with the exact elasticity solutions obtained in Chapter 3, highlight the accuracy of the proposed model to account for the shear deformations in imperfectly bonded laminates. This feature of the new model allows to also accurately predict the transverse displacements independent of the status of the interfaces.

Results have been also presented for a homogeneous cantilevered plate with two layers connected by a linear elastic interface and subjected to end concentrated force. It has been shown that the interfacial shear tractions predicted by the new homogenized model coincide with those obtained by the discrete layer interface model, for any values of the interfacial stiffness.

To preliminarily investigate the applicability of the formulated model to fracture problems, a simply supported plate with two layers and a mid-thickness delamination, subjected to a concentrated force at the mid-span, has been studied. The layers are connected by two different interfaces in different portions of the specimen, to reproduce a fully bonded portion (on the right of the crack tip) and a partially/fully debonded portion (on the left of the crack tip). The transverse displacements, interfacial tractions and jumps have been calculated on varying the interfacial stiffness, and compared with those obtained through the discrete layer interface model. It has been found that, since the continuity conditions of the formulated model do not results in the continuity of $w_{0,2}$, the accuracy of the obtained results depends on the difference between

the interfacial stiffnesses of the interfaces. This limitation strongly affects the applications of the model to Linear Elastic Fracture Mechanics problems.

CONCLUSIONS

Current applications of laminated composite and sandwich structures require withstanding severe mechanical loadings and surviving aggressive environments, characterized for instance by very high or very low temperatures. To design layered structures and define their load-bearing capacity and life, accurate understanding of their mechanical behavior in the elastic and post-elastic regimes is needed. The focus of this PhD thesis has been on formulating accurate and efficient methods for modeling the elastic and delamination response of layered composite structures subjected to stationary thermo-mechanical loading. In the following, the content and the main achievements of the work are summarized.

A brief introduction has been presented in Chapter 2 on two approaches for studying the mechanical behavior of multilayered structures subjected to thermo-mechanical loading. In the first part, some of two- and three-dimensional thermo-elasticity models for laminated and sandwich structures with thermally and mechanically perfect and imperfect interfaces were introduced. Thermo-elasticity models based on matrix methods were also discussed. In the second part of the chapter, two types of structural theories, namely the equivalent single layer and the zigzag theories, have been introduced with focus on new multiscale and refined models.

In Chapter 3, a matrix technique has been formulated based on the transfer matrix method [51] and the 2D/3D thermo-elasticity models in [6, 7], to derive novel explicit expressions for the field variables of rectangular simply supported laminated and sandwich plates with thermally and mechanically imperfect interfaces subjected to stationary thermo-mechanical loading. The matrix technique systematizes the analysis by relating the integration constants in the solution of a generic layer to those of the first layer, through local transfer matrices and continuity conditions at the interfaces. In this manner, the thermo-elasticity problem of a plate with many layers and imperfect interfaces has been reduced to that of a single-layer plate whose solution has been obtained by the imposition of the boundary conditions. The expressions are valid for plates with any numbers of imperfectly bonded layers in imperfect thermal contact, are applicable to limiting cases of fully bonded layers in perfect thermal contact, and fully debonded layers or impermeable interfaces. They can be easily applied to generate benchmark solutions and used for the verification of numerical models and approximate theories, with no need to solve algebraic systems, as in the classical approaches, or to perform extensive matrix multiplications, as in other matrix formulations in the literature; the expressions have been used for verification of the structural model formulated in Chapter 5. Some benchmark solutions have been presented in tabular and graph forms for plates with different layups, length-to-thickness ratios, interfacial stiffnesses and thermal resistances, to highlight the efficacy of the method and the important effect of the imperfections on the field variables.

In Chapter 4, a fracture model has been formulated based on the multiscale homogenized structural theory [25], which allows to study delamination fracture in layered structures without the through thickness discretization which is required and used in discrete-layer cohesive-interface approaches. The multiscale

structural theory has been particularized to a bi-material plate with a single delamination under mode II dominant conditions and subjected to transverse loading. The model has then been applied to analyze an edge-cracked bi-material element subjected to generalized end forces, for which accurate LEFM solutions are available in the literature. The energy release rate of the model system has been derived in closed-form in terms of the stress sub-resultants and rotations of the delamination arms, through an application of the J-integral in the homogenized problem using the local fields calculated through the multiscale model. The derived expression for the energy release rate neglects the contribution of the crack tip root-rotations, which can be calculated a posteriori through the equations and tables given in [94, 95] and the crack tip stress resultants predicted by the multiscale model. Apart from the contribution of the root-rotations, the expression derived for the energy release rate is the same as those obtained in [94, 95], for bi-material and homogeneous plates. The J-integral has been calculated also along a path which follows the delamination surfaces, and the energy release rate of the model system has been derived in terms of the relative crack sliding displacements, which are local measures and important for cohesive crack modeling.

The formulated fracture model has been applied to study delamination growth and investigate the structural response of different homogeneous and bi-material ENF specimens. The energy release rate has been calculated in terms of the crack tip stress sub-resultants and the relative crack sliding displacements predicted by the homogenized structural theory, and compared with accurate 2D solutions. It has been observed that the energy release rates calculated using the relative crack sliding displacements can account only for the contribution of the bending moments due to a limitation of the model in treating shear. Furthermore, it has been proved that the multiscale model is able to accurately capture the macro-structural response of the ENF specimen, bending and transverse shear stresses and interfacial shear tractions except for a very small region localized ahead of the traction-free delamination tip, where a boundary layer forms as a consequence of the imposition of the continuity conditions on the global variables only, which results in satisfying the equilibrium at the delamination tip cross-section, only in a global sense. Based on the study conducted in Chapter 4, it has been concluded that, within the framework of Linear Elastic Fracture Mechanics, the multiscale structural theory is expected to be able to accurately predict the energy release rates and the structural response of plates with many layers and delaminations; the limitation of the theory is its inability to account for the shear deformations in the delaminated portions of the structures, which is a consequence of the imposition of continuity between the interfacial tractions and the tractions at the layer surfaces.

In chapter 5, a homogenized structural theory has been formulated which is based on the refined zigzag theory [27] and the homogenized structural theory already used in Chapter 4 [25]. The model is formulated for plates deforming in cylindrical bending, with an arbitrary number of layers and imperfect interfaces. A linear elastic interfacial constitutive law has been used to describe the mechanical behavior of the interfaces, which are assumed to be able to slide only. The number of the kinematic variables of the model is independent of the number of layers and imperfect interfaces. Homogenized equilibrium equations and boundary conditions have been derived using the Principle of Virtual Works. The formulated model is able to accurately account for the shear deformations in plates with continuous imperfect interfaces, and model all boundary conditions including clamped supports; the theory needs only C^0-continuous shape functions for finite element implementation. It has been proved that the model runs into difficulties when applied to

problems, whose solutions require the imposition of the continuity conditions between regions characterized by different transverse shear moduli or interfacial stiffness, e.g. a plate with finite length imperfect interface or delamination. The problem is just a consequence of the fact that the model cannot deal with continuity conditions.

The model has been applied to three different cases to reveal its advantages and limitations. In the first case, the model has been used to study simply supported plates with continuous imperfect and fully debonded interfaces subject to sinusoidal transverse load. Highly anisotropic plates with small length-to-thickness ratio have been considered; comparisons with the exact elasticity solutions obtained in Chapter 3 prove the accuracy of the solutions. In the second case, the model has been applied to a cantilever wide plate with two layers connected by a linear elastic interface and subjected to an end concentrated force. It has been observed that the interfacial shear tractions predicted by the proposed model coincide with those obtained through the discrete layer interface model, for any value of the interfacial stiffness.

In the third case, a simply supported plate with two layers connected by two different interfaces in different portions of the specimen, and subjected to a concentrated force at the mid-span has been studied. The predicted transverse displacements, interfacial tractions and jumps have been compared with those obtained through discrete layer interface model, on varying the interfacial stiffness. It has been found that, since the continuity conditions of the formulated model do not result in the continuity of the slope of the transverse displacement variable, the accuracy of the obtained results depends on the difference between the interfacial stiffnesses of the interfaces; for cases in which the interfacial stiffness of the delaminated portion of the specimen is set to be a very small number to model a traction-free delamination, the transverse displacements in the specimen are incorrectly predicted. This limitation strongly affects the applications of the model to Linear Elastic Fracture Mechanics problems and has effects in cohesive crack modeling.

6.1 FUTURE DEVELOPMENTS

Some aspects of the work presented in the thesis need further investigation in order to achieve more generality. The following are some relevant topics which deserve considerations:

- The transfer matrix method is an efficient technique which can be applied to derive explicit expressions for the field variables of layered shell structures with imperfect interfaces subjected to thermo-mechanical loads. The technique can be applied also to time-dependent elasticity problems.
- The homogenized structural model used in Chapter 4, has been formulated in [25] for plates with many layers and mixed-mode interfaces. The theory may be applied to problems characterized by mixed-mode conditions.
- The structural model formulated in chapter 5 is able to accurately predict the field variables of wide plates with continuous imperfect interfaces and delaminations subjected to static loading. The model can be easily extended to plates subjected to dynamically applied loads; it can be also extended to plates subjected to thermal loadings. Moreover, through thickness compressibility/extensibility of layers may be accounted for to extend the range of applicability of the model, e.g. to sandwich structures with soft core and imperfect bonding at the core-face sheets interface.

APPENDIX A

DERIVATION OF THE UNKNOWN CONSTANTS OF THE HEAT CONDUCTION PROBLEM IN CHAPTER 3

Equation (3-23) is expanded as:

$$\begin{aligned} {}^{(k)}c_1 &= {}^{(k)}F_{11}\,{}^{(1)}c_1 + {}^{(k)}F_{12}\,{}^{(1)}c_2 \\ {}^{(k)}c_2 &= {}^{(k)}F_{21}\,{}^{(1)}c_1 + {}^{(k)}F_{22}\,{}^{(1)}c_2 \end{aligned} \tag{A-1}$$

where:

$${}^{(k)}F_{ij} = \sum_{t=1}^{2}\left\{\sum_{r=1}^{2} {}^{(k)}Z_{ir}\,{}^{(k)}N_{rt}\right\}{}^{(1)}D_{tj}\left(x_3^0\right) \tag{A-2}$$

The terms ${}^{(k)}Z_{ir}$, for $i, r = 1, 2$ are:

$$\begin{aligned} {}^{(k)}Z_{11} &= \frac{e^{-{}^{(k)}sx_3^k}}{2},\quad {}^{(k)}Z_{21} = \frac{e^{{}^{(k)}sx_3^k}}{2} \\ {}^{(k)}Z_{12} &= \frac{{}^{(k+1)}K_3 e^{-{}^{(k)}sx_3^k}}{2}\left[\frac{1}{{}^{(k)}K_3\,{}^{(k)}s} - R^k\right] \\ {}^{(k)}Z_{22} &= -\frac{{}^{(k+1)}K_3 e^{{}^{(k)}sx_3^k}}{2}\left[\frac{1}{{}^{(k)}K_3\,{}^{(k)}s} + R^k\right] \end{aligned} \tag{A-3}$$

and ${}^{(1)}D_{tj}\left(x_3^0\right)$ are given in Eq. (3-18) and the ${}^{(k)}N_{rt}$, for $r, t = 1, 2$, are defined by the recursive formula:

$$\begin{aligned} {}^{(k)}N_{rt} &= \sum_{l=1}^{2} {}^{(k)}A_{rl}\,{}^{(k-1)}N_{lt} \quad \text{for } k = 2, \ldots, n \\ {}^{(1)}N_{rt} &= {}^{(1)}A_{rt} \end{aligned} \tag{A-4}$$

where:

$$
\begin{aligned}
{}^{(k)}A_{11} &= \frac{\left(1+{}^{(k)}K_3\,{}^{(k)}sR^k\right)\left(1+e^{2\,{}^{(k)}s\,{}^{(k)}h}\right)-2\,{}^{(k)}K_3\,{}^{(k)}sR^k}{2e^{\,{}^{(k)}s\,{}^{(k)}h}} \\
{}^{(k)}A_{12} &= \frac{\left(1+{}^{(k)}K_3\,{}^{(k)}sR^k\right)\left(1+e^{2\,{}^{(k)}s\,{}^{(k)}h}\right)-2}{2\,{}^{(k)}se^{\,{}^{(k)}s\,{}^{(k)}h}} \\
{}^{(k)}A_{21} &= \frac{{}^{(k)}K_3}{{}^{(k+1)}K_3}\frac{{}^{(k)}s\left(e^{2\,{}^{(k)}s\,{}^{(k)}h}-1\right)}{2e^{\,{}^{(k)}s\,{}^{(k)}h}} \\
{}^{(k)}A_{22} &= \frac{{}^{(k)}K_3}{{}^{(k+1)}K_3}\frac{e^{2\,{}^{(k)}s\,{}^{(k)}h}+1}{2e^{\,{}^{(k)}s\,{}^{(k)}h}}
\end{aligned}
\tag{A-5}
$$

For perfect thermal contact, the R^k terms in the equations above vanish. The terms given above correspond to the coefficients of the matrices ${}^{(k)}Z = {}^{(k)}D^{-1}(x_3^k)\left(J^k\right)^{-1}$, ${}^{(k)}N = \prod_{i=k}^{1}{}^{(i)}A$ and ${}^{(i)}A = \left(J^i\right){}^{(i)}D(x_3^i)\,{}^{(i)}D^{-1}(x_3^{i-1})$. Application of the boundary conditions at the top and bottom surfaces of the plate and using Eq. (A-1) for $k = n$, result in the following explicit expressions for the unknown constants of the first layer:

$$
\begin{aligned}
{}^{(1)}c_1 &= \frac{T_u - T_l e^{\,{}^{(1)}s x_3^0}\,{}^{(n)}\left(F_{12}e^{sx_3^n}+F_{22}e^{-sx_3^n}\right)}{{}^{(n)}\left(F_{11}e^{sx_3^n}+F_{21}e^{-sx_3^n}\right)-e^{2\,{}^{(1)}s x_3^0}\,{}^{(n)}\left(F_{12}e^{sx_3^n}+F_{22}e^{-sx_3^n}\right)} \\
{}^{(1)}c_2 &= \frac{T_l - {}^{(1)}c_1 e^{\,{}^{(1)}s x_3^0}}{e^{-\,{}^{(1)}s x_3^0}}
\end{aligned}
\tag{A-6}
$$

APPENDIX B

UNKNOWN CONSTANTS OF THE PARTICULAR SOLUTION OF LAYER *K* IN CHAPTER 3

The constants in the particular solution of layer k in Eq. (3-27) are derived as:

$$
\begin{aligned}
{}^{(k)}B_1 &= -\Big\{ pc_1\Big[(C_{33}s^2 - C_{55}p^2)(C_{12}\alpha_1 + C_{22}\alpha_2) - s^2(C_{23}+C_{55})(C_{13}\alpha_1 + C_{23}\alpha_2) - \\
&\quad - C_{55}\alpha_3(C_{23}p^2 + C_{33}s^2)\Big] \Big/ \Big[C_{22}p^2(C_{33}s^2 - C_{55}p^2) - C_{23}p^2s^2(C_{23}+2C_{55}) - C_{33}C_{55}s^4\Big]\Big\} \\
{}^{(k)}B_2 &= {}^{(k)}\left(\frac{c_2}{c_1}\right){}^{(k)}B_1 \\
{}^{(k)}D_1 &= -\Big\{ sc_1\Big[(C_{55}s^2 - C_{22}p^2)(C_{13}\alpha_1 + C_{33}\alpha_3) + p^2(C_{23}+C_{55})(C_{12}\alpha_1 + C_{23}\alpha_3) + \\
&\quad + C_{55}\alpha_2(C_{22}p^2 + C_{23}s^2)\Big] \Big/ \Big[C_{22}p^2(C_{33}s^2 - C_{55}p^2) - C_{23}p^2s^2(C_{23}+2C_{55}) - C_{33}C_{55}s^4\Big]\Big\} \\
{}^{(k)}D_2 &= -{}^{(k)}\left(\frac{c_2}{c_1}\right){}^{(k)}D_1
\end{aligned}
\tag{B-1}
$$

APPENDIX C

MATRIX ${}^{(k)}E$ IN CHAPTER 3

Positive discriminant:

$$
\begin{aligned}
&{}^{(k)}E_{11}(x_3) = {}^{(k)}X_1(x_3),\ {}^{(k)}E_{12}(x_3) = {}^{(k)}Y_1(x_3)\ ,{}^{(k)}E_{13}(x_3) = {}^{(k)}X_2(x_3)\\
&{}^{(k)}E_{14}(x_3) = {}^{(k)}Y_2(x_3),\ {}^{(k)}E_{21}(x_3) = {}^{(k)}\beta_1\,{}^{(k)}Y_1(x_3),\\
&{}^{(k)}E_{22}(x_3) = {}^{(k)}\lambda\,{}^{(k)}\beta_1\,{}^{(k)}X_1(x_3),\ {}^{(k)}E_{23}(x_3) = {}^{(k)}\beta_2\,{}^{(k)}Y_2(x_3)\\
&{}^{(k)}E_{24}(x_3) = {}^{(k)}\lambda\,{}^{(k)}\beta_2\,{}^{(k)}X_2(x_3),\\
&{}^{(k)}E_{31}(x_3) = {}^{(k)}\left(C_{33}\beta_1 m_1 - C_{23}p\right){}^{(k)}X_1(x_3)\\
&{}^{(k)}E_{32}(x_3) = {}^{(k)}\left(C_{33}\beta_1 m_1 - C_{23}p\right){}^{(k)}Y_1(x_3)\\
&{}^{(k)}E_{33}(x_3) = {}^{(k)}\left(C_{33}\beta_2 m_2 - C_{23}p\right){}^{(k)}X_2(x_3)\\
&{}^{(k)}E_{34}(x_3) = {}^{(k)}\left(C_{33}\beta_2 m_2 - C_{23}p\right){}^{(k)}Y_2(x_3)\\
&{}^{(k)}E_{41}(x_3) = {}^{(k)}C_{55}\,{}^{(k)}\left(\beta_1 p + \lambda m_1\right){}^{(k)}Y_1(x_3)\\
&{}^{(k)}E_{42}(x_3) = {}^{(k)}C_{55}\,{}^{(k)}\left(\lambda\beta_1 p + m_1\right){}^{(k)}X_1(x_3)\\
&{}^{(k)}E_{43}(x_3) = {}^{(k)}C_{55}\,{}^{(k)}\left(\beta_2 p + \lambda m_2\right){}^{(k)}Y_2(x_3)\\
&{}^{(k)}E_{44}(x_3) = {}^{(k)}C_{55}\,{}^{(k)}\left(\lambda\beta_2 p + m_2\right){}^{(k)}X_2(x_3)
\end{aligned}
\tag{C-1}
$$

Zero discriminant:

This case occurs when the layer is isotropic:

$$
\begin{aligned}
&{}^{(k)}E_{11}(x_3) = e^{px_3},\ {}^{(k)}E_{12}(x_3) = x_3 e^{px_3},\ {}^{(k)}E_{13}(x_3) = e^{-px_3},\ {}^{(k)}E_{14}(x_3) = x_3 e^{-px_3}\\
&{}^{(k)}E_{21}(x_3) = e^{px_3}\ ,\ {}^{(k)}E_{22}(x_3) = \left(\frac{4\,{}^{(k)}\nu - 3}{p} + x_3\right)e^{px_3},\ {}^{(k)}E_{23}(x_3) = -e^{-px_3}\\
&{}^{(k)}E_{24}(x_3) = \left(\frac{4\,{}^{(k)}\nu - 3}{p} - x_3\right)e^{-px_3},\ {}^{(k)}E_{31}(x_3) = \frac{p\,{}^{(k)}E}{1+{}^{(k)}\nu}e^{px_3}\\
&{}^{(k)}E_{32}(x_3) = \frac{px_3 + 2({}^{(k)}\nu - 1)}{1+{}^{(k)}\nu}\,{}^{(k)}E e^{px_3},\ {}^{(k)}E_{33}(x_3) = \frac{p\,{}^{(k)}E}{1+{}^{(k)}\nu}e^{-px_3}\\
&{}^{(k)}E_{34}(x_3) = \frac{px_3 + 2(1-{}^{(k)}\nu)}{1+{}^{(k)}\nu}\,{}^{(k)}E e^{-px_3},\ {}^{(k)}E_{41}(x_3) = \frac{p\,{}^{(k)}E}{1+{}^{(k)}\nu}e^{px_3}\\
&{}^{(k)}E_{42}(x_3) = \frac{px_3 + 2\,{}^{(k)}\nu - 1}{1+{}^{(k)}\nu}\,{}^{(k)}E e^{px_3},\ {}^{(k)}E_{43}(x_3) = -\frac{p\,{}^{(k)}E}{1+{}^{(k)}\nu}e^{-px_3}\\
&{}^{(k)}E_{44}(x_3) = -\frac{px_3 - 2\,{}^{(k)}\nu + 1}{1+{}^{(k)}\nu}\,{}^{(k)}E e^{-px_3}
\end{aligned}
\tag{C-2}
$$

where ${}^{(k)}\nu$ and ${}^{(k)}E$ are Poisson ratio and Young's modulus of the layer *k* and $p = m\pi/L$ with $m \in \mathbb{N}$. For plane-stress problems, ${}^{(k)}\nu$ and ${}^{(k)}E$ should be replaced by ${}^{(k)}\nu/\left(1+{}^{(k)}\nu\right)$ and ${}^{(k)}E\left(1+2\,{}^{(k)}\nu\right)/\left(1+{}^{(k)}\nu\right)^2$, respectively.

Negative discriminant:

This case occurs when the transverse stiffness of the layer is much higher than the in-plane stiffnesses

$$
\begin{aligned}
&{}^{(k)}E_{11}(x_3) = e^{{}^{(k)}\rho_1 x_3}\cos({}^{(k)}\rho_2 x_3);\ {}^{(k)}E_{12}(x_3) = e^{{}^{(k)}\rho_1 x_3}\sin({}^{(k)}\rho_2 x_3)\\
&{}^{(k)}E_{13}(x_3) = e^{-{}^{(k)}\rho_1 x_3}\cos({}^{(k)}\rho_2 x_3);\ {}^{(k)}E_{14}(x_3) = e^{-{}^{(k)}\rho_1 x_3}\sin({}^{(k)}\rho_2 x_3)\\
&{}^{(k)}E_{21}(x_3) = e^{{}^{(k)}\rho_1 x_3}\,{}^{(k)}\left[r_1\cos(\rho_2 x_3) + r_2\sin(\rho_2 x_3)\right]\\
&{}^{(k)}E_{22}(x_3) = e^{{}^{(k)}\rho_1 x_3}\,{}^{(k)}\left[r_1\sin(\rho_2 x_3) - r_2\cos(\rho_2 x_3)\right]\\
&{}^{(k)}E_{23}(x_3) = e^{-{}^{(k)}\rho_1 x_3}\,{}^{(k)}\left[r_2\sin(\rho_2 x_3) - r_1\cos(\rho_2 x_3)\right]\\
&{}^{(k)}E_{24}(x_3) = -e^{-{}^{(k)}\rho_1 x_3}\,{}^{(k)}\left[r_2\cos(\rho_2 x_3) + r_1\sin(\rho_2 x_3)\right]\\
&{}^{(k)}E_{31}(x_3) = e^{{}^{(k)}\rho_1 x_3}\,{}^{(k)}\left[-pC_{23}\cos(\rho_2 x_3) + C_{33}\left(\rho_1 r_1\cos(\rho_2 x_3) - \rho_2 r_1\sin(\rho_2 x_3)\right.\right.\\
&\left.\left.+\rho_1 r_2\sin(\rho_2 x_3) + \rho_2 r_2\cos(\rho_2 x_3)\right)\right]\\
&{}^{(k)}E_{32}(x_3) = e^{{}^{(k)}\rho_1 x_3}\,{}^{(k)}\left[-pC_{23}\sin(\rho_2 x_3) + C_{33}\left(-\rho_1 r_2\cos(\rho_2 x_3) + \rho_2 r_2\sin(\rho_2 x_3)\right.\right.\\
&\left.\left.+\rho_1 r_1\sin(\rho_2 x_3) + \rho_2 r_1\cos(\rho_2 x_3)\right)\right]\\
&{}^{(k)}E_{33}(x_3) = e^{-{}^{(k)}\rho_1 x_3}\,{}^{(k)}\left[-pC_{23}\cos(\rho_2 x_3) + C_{33}\left(\rho_1 r_1\cos(\rho_2 x_3) + \rho_2 r_1\sin(\rho_2 x_3)\right.\right.\\
&\left.\left.-\rho_1 r_2\sin(\rho_2 x_3) + \rho_2 r_2\cos(\rho_2 x_3)\right)\right]\\
&{}^{(k)}E_{34}(x_3) = e^{-{}^{(k)}\rho_1 x_3}\,{}^{(k)}\left[-pC_{23}\sin(\rho_2 x_3) + C_{33}\left(\rho_1 r_2\cos(\rho_2 x_3) + \rho_2 r_2\sin(\rho_2 x_3)\right.\right.\\
&\left.\left.+\rho_1 r_1\sin(\rho_2 x_3) - \rho_2 r_1\cos(\rho_2 x_3)\right)\right]\\
&{}^{(k)}E_{41}(x_3) = e^{{}^{(k)}\rho_1 x_3}\,{}^{(k)}C_{55}\,{}^{(k)}\left[\rho_1\cos(\rho_2 x_3) - \rho_2\sin(\rho_2 x_3) + p\left(r_1\cos(\rho_2 x_3) + r_2\sin(\rho_2 x_3)\right)\right]\\
&{}^{(k)}E_{42}(x_3) = e^{{}^{(k)}\rho_1 x_3}\,{}^{(k)}C_{55}\,{}^{(k)}\left[\rho_1\sin(\rho_2 x_3) + \rho_2\cos(\rho_2 x_3) + p\left(r_1\sin(\rho_2 x_3) - r_2\cos(\rho_2 x_3)\right)\right]\\
&{}^{(k)}E_{43}(x_3) = e^{-{}^{(k)}\rho_1 x_3}\,{}^{(k)}C_{55}\,{}^{(k)}\left[-\rho_1\cos(\rho_2 x_3) - \rho_2\sin(\rho_2 x_3) + p\left(-r_1\cos(\rho_2 x_3) + r_2\sin(\rho_2 x_3)\right)\right]\\
&{}^{(k)}E_{44}(x_3) = e^{-{}^{(k)}\rho_1 x_3}\,{}^{(k)}C_{55}\,{}^{(k)}\left[-\rho_1\sin(\rho_2 x_3) + \rho_2\cos(\rho_2 x_3) - p\left(r_1\sin(\rho_2 x_3) + r_2\cos(\rho_2 x_3)\right)\right]
\end{aligned}
\tag{C-3}
$$

with:

$$
\begin{aligned}
{}^{(k)}\rho_1 &= {}^{(k)}\left[\sqrt{\frac{\sqrt{A_1^2+|\Delta|}}{2A_0}}\cos\left(\frac{\arctan\left(-\sqrt{|\Delta|}/A_1\right)}{2}\right)\right] \\
{}^{(k)}\rho_2 &= {}^{(k)}\left[\sqrt{\frac{\sqrt{A_1^2+|\Delta|}}{2A_0}}\sin\left(\frac{\arctan\left(-\sqrt{|\Delta|}/A_1\right)}{2}\right)\right] \\
{}^{(k)}r_1 &= {}^{(k)}\left(\frac{\rho_1\left[C_{22}p^2-C_{55}\left(\rho_1^2+\rho_2^2\right)\right]}{p\left(C_{23}+C_{55}\right)\left(\rho_1^2+\rho_2^2\right)}\right) \\
{}^{(k)}r_2 &= {}^{(k)}\left(\frac{\rho_2\left[C_{22}p^2+C_{55}\left(\rho_1^2+\rho_2^2\right)\right]}{p\left(C_{23}+C_{55}\right)\left(\rho_1^2+\rho_2^2\right)}\right)
\end{aligned}
\tag{C-4}
$$

where ${}^{(k)}\Delta = {}^{(k)}(A_1^2 - 4A_0A_2)$ and ${}^{(k)}A_0$, ${}^{(k)}A_1$ and ${}^{(k)}A_2$ are defined in Eq. (3-32).

APPENDIX D

DERIVATION OF DISPLACEMENTS AND STRESSES IN CHAPTER 3

Expressions relating the four unknown constants, ${}^{(k)}a_{11}$, ${}^{(k)}a_{21}$, ${}^{(k)}a_{12}$ and ${}^{(k)}a_{22}$, to ${}^{(1)}M_l(x_3^0)$ are derived by substituting ${}^{(k)}M(x_3^k)$ on the left hand side of (3-44) with Eq. (3-39) and multiplying both sides by ${}^{(k)}E^{-1}(x_3^k)$:

$$\begin{aligned}
&{}^{(k)}\begin{bmatrix} a_{11} \\ a_{21} \\ a_{12} \\ a_{22} \end{bmatrix} = {}^{(k)}E^{-1}(x_3^k)\left(B^k\right)^{-1}\left\{\prod_{i=k}^{1}\left\{\left(B^i\right){}^{(i)}E(x_3^i){}^{(i)}E^{-1}(x_3^{i-1})\right\}\right\}\left\{{}^{(1)}M(x_3^0)-{}^{(1)}Q(x_3^0)\right\} \\
&+\sum_{i=2}^{k}\left(\prod_{j=k}^{i}\left\{\left(B^j\right){}^{(j)}E(x_3^j){}^{(j)}E^{-1}(x_3^{j-1})\right\}\left\{\left(B^{i-1}\right){}^{(i-1)}Q(x_3^{i-1})-{}^{(i)}Q(x_3^{i-1})\right\}\right)
\end{aligned} \tag{D-1}$$

for $k = 2, \ldots, n$. Inserting the expressions of the unknown in (D-1) into (3-39) yields:

$$\begin{aligned}
&{}^{(k)}M(x_3) = {}^{(k)}Q(x_3) + {}^{(k)}E(x_3){}^{(k)}E^{-1}(x_3^k)\left(B^k\right)^{-1} \\
&\times\left\{\prod_{i=k}^{1}\left\{\left(B^i\right){}^{(i)}E(x_3^i){}^{(i)}E^{-1}(x_3^{i-1})\right\}\right\}\left\{{}^{(1)}M(x_3^0)-{}^{(1)}Q(x_3^0)\right\} \\
&+\sum_{i=2}^{k}\left(\prod_{j=k}^{i}\left\{\left(B^j\right){}^{(j)}E(x_3^j){}^{(j)}E^{-1}(x_3^{j-1})\right\}\right. \\
&\left.\times\left\{\left(B^{i-1}\right){}^{(i-1)}Q(x_3^{i-1})-{}^{(i)}Q(x_3^{i-1})\right\}\right)
\end{aligned} \tag{D-2}$$

Equations (D-2) and (3-37) define displacements and transverse stresses in the layer k in terms of ${}^{(1)}M(x_3^0)$. The third and fourth elements of the vector ${}^{(1)}M(x_3^0)$ are obtained using Eq. (3-37) for $x_3 = x_3^0$ and $k = 1$ and the boundary conditions (3-12); the first and second elements are obtained using equations (3-44) for $k = n$ and the boundary conditions (3-12):

$$\begin{aligned}
{}^{(1)}M_1(x_3^0) &= {}^{(n)}\left(\frac{\Omega_{42}}{\Omega_{42}\Omega_{31}-\Omega_{41}\Omega_{32}}\right)\left[f_u+\mu_3-\frac{{}^{(n)}\Omega_{32}}{{}^{(n)}\Omega_{42}}\mu_4\right] \\
{}^{(1)}M_2(x_3^0) &= \frac{1}{{}^{(n)}\Omega_{42}}\left[-{}^{(n)}\Omega_{41}\,{}^{(1)}M_1(x_3^0)+\mu_4\right] \\
{}^{(1)}M_3(x_3^0) &= -f_l \\
{}^{(1)}M_4(x_3^0) &= 0
\end{aligned} \tag{D-3}$$

where μ_i for $i = 3, 4$ are:

$$\mu_i = \sum_{g=1}^{4} {}^{(n)}\Omega_{ig}\, {}^{(1)}Q_g(x_3^0) + {}^{(n)}\Omega_{i3} f_l - {}^{(n)}S_i - {}^{(n)}Q_i(x_3^n) \tag{D-4}$$

and ${}^{(k)}\Omega_{ig}$ and ${}^{(k)}S_i$ are defined by the recursive formulas:

$$\begin{aligned}
{}^{(k)}\Omega_{ig} &= \sum_{m=1}^{4} {}^{(k)}U_{im}\, {}^{(k-1)}\Omega_{mg} \quad \text{for } k = 2, ..., n\,; \; {}^{(1)}\Omega_{ig} = {}^{(1)}U_{ig} \\
{}^{(k)}U_{im} &= \sum_{n=1}^{4} \left\{ \sum_{p=1}^{4} B_{ip}^{k}\, {}^{(k)}E_{pn}(x_3^k) \right\} {}^{(k)}E^{-1}{}_{nm}(x_3^{k-1}) \\
{}^{(k)}S_i &= \sum_{q=1}^{4} {}^{(k)}U_{iq} \left[{}^{(k-1)}S_q - {}^{(k)}Q_q(x_3^{k-1}) + \sum_{b=1}^{4} \left(B^{k-1} \right)_{qb} {}^{(k-1)}Q_b(x_3^{k-1}) \right] \\
&\qquad \text{for } k = 2, ..., n\,; {}^{(1)}S_i = 0
\end{aligned} \tag{D-5}$$

where the elements of ${}^{(k)}Q$ and B^k are given in Eqs. (3-40) and (3-43) and those of ${}^{(k)}E$ in Appendix C. For fully bonded layers Eq. (D-5) simplifies as:

$$\begin{aligned}
{}^{(k)}\Omega_{ig} &= \sum_{m=1}^{4} {}^{(k)}U_{im}\, {}^{(k-1)}\Omega_{mg} \quad \text{for } k = 2, ..., n\,; \; {}^{(1)}\Omega_{ig} = {}^{(1)}U_{ig} \\
{}^{(k)}U_{im} &= \sum_{n=1}^{4} {}^{(k)}E_{in}(x_3^k)\, {}^{(k)}E^{-1}{}_{nm}(x_3^{k-1}) \\
{}^{(k)}S_i &= \sum_{q=1}^{4} {}^{(k)}U_{iq} \left[{}^{(k-1)}S_q - {}^{(k)}Q_q(x_3^{k-1}) + {}^{(k-1)}Q_q(x_3^{k-1}) \right] \\
&\qquad \text{for } k = 2, ..., n\,; {}^{(1)}S_i = 0
\end{aligned} \tag{D-6}$$

Explicit expressions for displacements and transverse shear and normal stresses in the generic layer k are obtained by inserting ${}^{(1)}M(x_3^0)$ from Eq. (D-3) into Eq. (D-2). The expressions are given in Eq. (3-46) in Chapter 3. The bending stress is derived using the displacements and constitutive and compatibility equations, and is given in Eq. (3-46).

APPENDIX E

MATRIX ${}^{(k)}\boldsymbol{E}(x_3)$ IN CHAPTER 3

Negative discriminant:

$$
\begin{aligned}
&{}^{(k)}E_{11} = {}^{(k)}C_1(x_3),\ {}^{(k)}E_{12} = {}^{(k)}S_1(x_3),\ {}^{(k)}E_{13} = {}^{(k)}C_2(x_3),\\
&{}^{(k)}E_{14} = {}^{(k)}S_2(x_3),\ {}^{(k)}E_{15} = {}^{(k)}C_3(x_3),\ {}^{(k)}E_{16} = {}^{(k)}S_3(x_3),\\
&{}^{(k)}E_{21} = {}^{(k)}L_1\,{}^{(k)}C_1(x_3),\ {}^{(k)}E_{22} = {}^{(k)}L_1\,{}^{(k)}S_1(x_3),\ {}^{(k)}E_{23} = {}^{(k)}L_2\,{}^{(k)}C_2(x_3),\\
&{}^{(k)}E_{24} = {}^{(k)}L_2\,{}^{(k)}S_2(x_3),\ {}^{(k)}E_{25} = {}^{(k)}L_3\,{}^{(k)}C_3(x_3),\ {}^{(k)}E_{26} = {}^{(k)}L_3\,{}^{(k)}S_3(x_3),\\
&{}^{(k)}E_{31} = {}^{(k)}\eta\,{}^{(k)}R_1\,{}^{(k)}S_1(x_3),\ {}^{(k)}E_{32} = {}^{(k)}R_1\,{}^{(k)}C_1(x_3),\ {}^{(k)}E_{33} = {}^{(k)}\eta\,{}^{(k)}R_2\,{}^{(k)}S_2(x_3),\\
&{}^{(k)}E_{34} = {}^{(k)}R_2\,{}^{(k)}C_2(x_3),\ {}^{(k)}E_{35} = {}^{(k)}\eta\,{}^{(k)}R_3\,{}^{(k)}S_3(x_3),\ {}^{(k)}E_{36} = {}^{(k)}R_3\,{}^{(k)}C_3(x_3),\\
&{}^{(k)}E_{41} = {}^{(k)}Y_{31}\,{}^{(k)}C_1(x_3),\ {}^{(k)}E_{42} = {}^{(k)}Y_{31}\,{}^{(k)}S_1(x_3),\ {}^{(k)}E_{43} = {}^{(k)}Y_{32}\,{}^{(k)}C_2(x_3),\\
&{}^{(k)}E_{44} = {}^{(k)}Y_{32}\,{}^{(k)}S_2(x_3),\ {}^{(k)}E_{45} = {}^{(k)}Y_{33}\,{}^{(k)}C_3(x_3),\ {}^{(k)}E_{46} = {}^{(k)}Y_{33}\,{}^{(k)}S_3(x_3),\\
&{}^{(k)}E_{51} = {}^{(k)}C_{55}\,{}^{(k)}\eta\,{}^{(k)}\left(m_1 + p_2R_1\right){}^{(k)}S_1(x_3),\ {}^{(k)}E_{52} = {}^{(k)}C_{55}\,{}^{(k)}\left(m_1 + p_2R_1\right){}^{(k)}C_1(x_3),\\
&{}^{(k)}E_{53} = {}^{(k)}C_{55}\,{}^{(k)}\eta\,{}^{(k)}\left(m_2 + p_2R_2\right){}^{(k)}S_2(x_3),\ {}^{(k)}E_{54} = {}^{(k)}C_{55}\,{}^{(k)}\left(m_2 + p_2R_2\right){}^{(k)}C_2(x_3),\\
&{}^{(k)}E_{55} = {}^{(k)}C_{55}\,{}^{(k)}\eta\,{}^{(k)}\left(m_3 + p_2R_3\right){}^{(k)}S_3(x_3),\ {}^{(k)}E_{56} = {}^{(k)}C_{55}\,{}^{(k)}\left(m_3 + p_2R_3\right){}^{(k)}C_3(x_3),\\
&{}^{(k)}E_{61} = {}^{(k)}C_{44}\,{}^{(k)}\eta\,{}^{(k)}\left(m_1L_1 + p_1R_1\right){}^{(k)}S_1(x_3),\ {}^{(k)}E_{62} = {}^{(k)}C_{44}\,{}^{(k)}\left(m_1L_1 + p_1R_1\right){}^{(k)}C_1(x_3),\\
&{}^{(k)}E_{63} = {}^{(k)}C_{44}\,{}^{(k)}\eta\,{}^{(k)}\left(m_2L_2 + p_1R_2\right){}^{(k)}S_2(x_3),\ {}^{(k)}E_{64} = {}^{(k)}C_{44}\,{}^{(k)}\left(m_2L_2 + p_1R_2\right){}^{(k)}C_2(x_3),\\
&{}^{(k)}E_{65} = {}^{(k)}C_{44}\,{}^{(k)}\eta\,{}^{(k)}\left(m_3L_3 + p_1R_3\right){}^{(k)}S_3(x_3),\ {}^{(k)}E_{66} = {}^{(k)}C_{44}\,{}^{(k)}\left(m_3L_3 + p_1R_3\right){}^{(k)}C_3(x_3),
\end{aligned}
\tag{E-1}
$$

where, for i = 1, 2 and 3:

$${}^{(k)}Y_{3i} = {}^{(k)}\left[-p_2C_{23} - p_1C_{13}L_i + \eta m_iR_iC_{33}\right]$$

Zero discriminant:

This case occurs when the layer is isotropic:

$$
\begin{aligned}
&{}^{(k)}E_{11}(x_3) = e^{cx_3},\ {}^{(k)}E_{12}(x_3) = e^{-cx_3},\ {}^{(k)}E_{13}(x_3) = x_3e^{cx_3},\ {}^{(k)}E_{14}(x_3) = x_3e^{-cx_3}\\
&{}^{(k)}E_{15}(x_3) = {}^{(k)}E_{16}(x_3) = 0,\ {}^{(k)}E_{21}(x_3) = 0\ ,\ {}^{(k)}E_{22}(x_3) = 0,\ {}^{(k)}E_{23}(x_3) = \frac{p_1}{p_2}x_3e^{cx_3}\\
&{}^{(k)}E_{24}(x_3) = \frac{p_1}{p_2}x_3e^{-cx_3},\ {}^{(k)}E_{25}(x_3) = e^{cx_3},\ {}^{(k)}E_{26}(x_3) = e^{-cx_3},\ {}^{(k)}E_{31}(x_3) = \frac{p_2}{c}e^{cx_3}\\
&{}^{(k)}E_{32}(x_3) = -\frac{p_2}{c}e^{-cx_3}\ ,\ {}^{(k)}E_{33}(x_3) = \frac{4\,{}^{(k)}\nu - 3 + cx_3}{p_2}e^{cx_3}
\end{aligned}
$$

$$
\begin{aligned}
&{}^{(k)}E_{34}(x_3)=\frac{4\,{}^{(k)}\nu-3-cx_3}{p_2}e^{-cx_3},\ {}^{(k)}E_{35}(x_3)=\frac{p_1}{c}e^{cx_3},\ {}^{(k)}E_{36}(x_3)=-\frac{p_1}{c}e^{-cx_3}\\
&{}^{(k)}E_{41}(x_3)=2\,{}^{(k)}\mu p_2 e^{cx_3},\ {}^{(k)}E_{42}(x_3)=2\,{}^{(k)}\mu p_2 e^{-cx_3}\\
&{}^{(k)}E_{43}(x_3)=\frac{2c}{p_2}\,{}^{(k)}\left[(\lambda+2\mu)\left(2\,{}^{(k)}\nu-1\right)+\mu cx_3\right]e^{cx_3}\\
&{}^{(k)}E_{44}(x_3)=\frac{2c}{p_2}\,{}^{(k)}\left[(\lambda+2\mu)\left(1-2\,{}^{(k)}\nu\right)+\mu cx_3\right]e^{-cx_3}\\
&{}^{(k)}E_{45}(x_3)=2\,{}^{(k)}\mu p_1 e^{cx_3},\ {}^{(k)}E_{46}(x_3)=2\,{}^{(k)}\mu p_1 e^{-cx_3}\\
&{}^{(k)}E_{51}(x_3)={}^{(k)}\mu\left(c+\frac{(p_2)^2}{c}\right)e^{cx_3},\ {}^{(k)}E_{52}(x_3)=-{}^{(k)}\mu\left(c+\frac{(p_2)^2}{c}\right)e^{-cx_3}\\
&{}^{(k)}E_{53}(x_3)=2\,{}^{(k)}\mu\left(2\,{}^{(k)}\nu-1+cx_3\right)e^{cx_3},\ {}^{(k)}E_{54}(x_3)=2\,{}^{(k)}\mu\left(2\,{}^{(k)}\nu-1-cx_3\right)e^{-cx_3}\\
&{}^{(k)}E_{55}(x_3)={}^{(k)}\mu\frac{p_2p_1}{c}e^{cx_3},\ {}^{(k)}E_{56}(x_3)=-{}^{(k)}\mu\frac{p_2p_1}{c}e^{-cx_3},\ {}^{(k)}E_{61}(x_3)={}^{(k)}\mu\frac{p_2p_1}{c}e^{cx_3}\\
&{}^{(k)}E_{62}(x_3)=-{}^{(k)}\mu\frac{p_2p_1}{c}e^{-cx_3},\ {}^{(k)}E_{63}(x_3)=\frac{2\,{}^{(k)}\mu p_1}{p_2}\left(2\,{}^{(k)}\nu-1+cx_3\right)e^{cx_3}\\
&{}^{(k)}E_{64}(x_3)=\frac{2\,{}^{(k)}\mu p_1}{p_2}\left(2\,{}^{(k)}\nu-1-cx_3\right)e^{-cx_3},\ {}^{(k)}E_{65}(x_3)={}^{(k)}\mu\left(c+\frac{(p_1)^2}{c}\right)e^{cx_3}\\
&{}^{(k)}E_{66}(x_3)=-{}^{(k)}\mu\left(c+\frac{(p_1)^2}{c}\right)e^{-cx_3}
\end{aligned}
\tag{E-2}
$$

with:

$$
c=\sqrt{(p_1)^2+(p_2)^2},\ {}^{(k)}\mu={}^{(k)}G,\ {}^{(k)}\lambda={}^{(k)}\left(\frac{E\nu}{(1+\nu)(1-2\nu)}\right)
$$

where ${}^{(k)}\nu$, ${}^{(k)}E$ and ${}^{(k)}G$ are Poisson ratio, Young and shear modulus of the layer *k* and $p_1=m_1\pi/b$, $p_2=m_2\pi/a$, and $m_1,m_2\in\mathbb{N}$.

Positive discriminant:

When the discriminant of the characteristic equation (3-75), ${}^{(k)}H={}^{(k)}(\frac{f^2}{4}+\frac{d^3}{27})$, is positive, the equation has two complex conjugate roots, and one real root. This case happens when the transverse stiffness of the layer is much higher than the in-plane stiffnesses, for instance in honeycomb cores of sandwich structures, and the elements of matrix ${}^{(k)}E(x_3)$ are:

$$^{(k)}E_{11}(x_3)=e^{^{(k)}\gamma_1 x_3}\cos(^{(k)}\gamma_2 x_3),\ ^{(k)}E_{12}(x_3)=e^{^{(k)}\gamma_1 x_3}\sin(^{(k)}\gamma_2 x_3)$$

$$^{(k)}E_{13}(x_3)=e^{-^{(k)}\gamma_1 x_3}\cos(^{(k)}\gamma_2 x_3),\ ^{(k)}E_{14}(x_3)=e^{-^{(k)}\gamma_1 x_3}\sin(^{(k)}\gamma_2 x_3)$$

$$^{(k)}E_{15}(x_3)=\ ^{(k)}C_1(x_3),\ ^{(k)}E_{16}(x_3)=\ ^{(k)}S_1(x_3)$$

$$^{(k)}E_{21}(x_3)=e^{^{(k)}\gamma_1 x_3}\ ^{(k)}\left(\xi_{11}\cos(\gamma_2 x_3)+\xi_{21}\sin(\gamma_2 x_3)\right)$$

$$^{(k)}E_{22}(x_3)=e^{^{(k)}\gamma_1 x_3}\ ^{(k)}\left(\xi_{12}\cos(\gamma_2 x_3)+\xi_{22}\sin(\gamma_2 x_3)\right)$$

$$^{(k)}E_{23}(x_3)=e^{-^{(k)}\gamma_1 x_3}\ ^{(k)}\left(\xi_{33}\cos(\gamma_2 x_3)+\xi_{43}\sin(\gamma_2 x_3)\right)$$

$$^{(k)}E_{24}(x_3)=e^{-^{(k)}\gamma_1 x_3}\ ^{(k)}\left(\xi_{34}\cos(\gamma_2 x_3)+\xi_{44}\sin(\gamma_2 x_3)\right)$$

$$^{(k)}E_{25}(x_3)=\ ^{(k)}L_1\ ^{(k)}C_1(x_3),\ ^{(k)}E_{26}(x_3)=\ ^{(k)}L_1\ ^{(k)}S_1(x_3)$$

$$^{(k)}E_{31}(x_3)=e^{^{(k)}\gamma_1 x_3}\ ^{(k)}\left(f_{11}\cos(\gamma_2 x_3)+f_{21}\sin(\gamma_2 x_3)\right)$$

$$^{(k)}E_{32}(x_3)=e^{^{(k)}\gamma_1 x_3}\ ^{(k)}\left(f_{12}\cos(\gamma_2 x_3)+f_{22}\sin(\gamma_2 x_3)\right)$$

$$^{(k)}E_{33}(x_3)=e^{-^{(k)}\gamma_1 x_3}\ ^{(k)}\left(f_{33}\cos(\gamma_2 x_3)+f_{43}\sin(\gamma_2 x_3)\right)$$

$$^{(k)}E_{34}(x_3)=e^{-^{(k)}\gamma_1 x_3}\ ^{(k)}\left(f_{34}\cos(\gamma_2 x_3)+f_{44}\sin(\gamma_2 x_3)\right)$$

$$^{(k)}E_{35}=\ ^{(k)}\eta\ ^{(k)}R_1\ ^{(k)}S_1(x_3),\ ^{(k)}E_{36}=\ ^{(k)}R_1\ ^{(k)}C_1(x_3)$$

$$^{(k)}E_{41}=e^{^{(k)}\gamma_1 x_3}\ ^{(k)}\left\{C_{33}\left[\cos(\gamma_2 x_3)\left(f_{11}\gamma_1+f_{21}\gamma_2\right)+\sin(\gamma_2 x_3)\left(f_{21}\gamma_1-f_{11}\gamma_2\right)\right]-\right.$$

$$\left.-C_{13}\left[\cos(\gamma_2 x_3)p_1\xi_{11}+\sin(\gamma_2 x_3)p_1\xi_{21}\right]-C_{23}\cos(\gamma_2 x_3)p_2\right\}$$

$$^{(k)}E_{42}=e^{^{(k)}\gamma_1 x_3}\ ^{(k)}\left\{C_{33}\left[\cos(\gamma_2 x_3)\left(f_{12}\gamma_1+f_{22}\gamma_2\right)+\sin(\gamma_2 x_3)\left(f_{22}\gamma_1-f_{12}\gamma_2\right)\right]-\right.$$

$$\left.-C_{13}\left[\cos(\gamma_2 x_3)p_1\xi_{12}+\sin(\gamma_2 x_3)p_1\xi_{22}\right]-C_{23}\sin(\gamma_2 x_3)p_2\right\}$$

$$^{(k)}E_{43}=-e^{-^{(k)}\gamma_1 x_3}\ ^{(k)}\left\{C_{33}\left[\cos(\gamma_2 x_3)\left(f_{33}\gamma_1-f_{43}\gamma_2\right)+\sin(\gamma_2 x_3)\left(f_{33}\gamma_2+f_{43}\gamma_1\right)\right]+\right.$$

$$\left.+C_{13}\left[\cos(\gamma_2 x_3)p_1\xi_{33}+\sin(\gamma_2 x_3)p_1\xi_{43}\right]+C_{23}\cos(\gamma_2 x_3)p_2\right\}$$

$$^{(k)}E_{44}=-e^{-^{(k)}\gamma_1 x_3}\ ^{(k)}\left\{C_{33}\left[\cos(\gamma_2 x_3)\left(f_{34}\gamma_1-f_{44}\gamma_2\right)+\sin(\gamma_2 x_3)\left(f_{34}\gamma_2+f_{44}\gamma_1\right)\right]+\right.$$

$$\left.+C_{13}\left[\cos(\gamma_2 x_3)p_1\xi_{34}+\sin(\gamma_2 x_3)p_1\xi_{44}\right]+C_{23}\sin(\gamma_2 x_3)p_2\right\}$$

$$
\begin{aligned}
{}^{(k)}E_{45} &= {}^{(k)}\left[-p_2C_{23} - p_1C_{13}L_1 + \eta m_1R_1C_{33}\right]{}^{(k)}C_1(x_3)\\
{}^{(k)}E_{46} &= {}^{(k)}\left[-p_2C_{23} - p_1C_{13}L_1 + \eta m_1R_1C_{33}\right]{}^{(k)}S_1(x_3)\\
{}^{(k)}E_{51} &= {}^{(k)}\left\{C_{55}e^{\gamma_1 x_3}\left[\cos(\gamma_2 x_3)\left(f_{11}p_2 + \gamma_1\right) + \sin(\gamma_2 x_3)\left(f_{21}p_2 - \gamma_2\right)\right]\right\}\\
{}^{(k)}E_{52} &= {}^{(k)}\left\{C_{55}e^{\gamma_1 x_3}\left[\cos(\gamma_2 x_3)\left(f_{12}p_2 + \gamma_2\right) + \sin(\gamma_2 x_3)\left(f_{22}p_2 + \gamma_1\right)\right]\right\}\\
{}^{(k)}E_{53} &= {}^{(k)}\left\{C_{55}e^{-\gamma_1 x_3}\left[\cos(\gamma_2 x_3)\left(f_{33}p_2 - \gamma_1\right) + \sin(\gamma_2 x_3)\left(f_{43}p_2 - \gamma_2\right)\right]\right\}\\
{}^{(k)}E_{54} &= {}^{(k)}\left\{C_{55}e^{-\gamma_1 x_3}\left[\cos(\gamma_2 x_3)\left(f_{34}p_2 + \gamma_2\right) + \sin(\gamma_2 x_3)\left(f_{44}p_2 - \gamma_1\right)\right]\right\}\\
{}^{(k)}E_{55} &= {}^{(k)}C_{55}\,{}^{(k)}\eta\,{}^{(k)}\left(m_1 + p_2R_1\right){}^{(k)}S_1(x_3),\ {}^{(k)}E_{56} = {}^{(k)}C_{55}\,{}^{(k)}\left(m_1 + p_2R_1\right){}^{(k)}C_1(x_3),\\
{}^{(k)}E_{61} &= {}^{(k)}\left\{C_{44}e^{\gamma_1 x_3}\left[\cos(\gamma_2 x_3)\left(f_{11}p_1 + \gamma_1\xi_{11} + \gamma_2\xi_{21}\right) + \sin(\gamma_2 x_3)\left(f_{21}p_1 + \gamma_1\xi_{21} - \gamma_2\xi_{11}\right)\right]\right\}\\
{}^{(k)}E_{62} &= {}^{(k)}\left\{C_{44}e^{\gamma_1 x_3}\left[\cos(\gamma_2 x_3)\left(f_{12}p_1 + \gamma_1\xi_{12} + \gamma_2\xi_{22}\right) + \sin(\gamma_2 x_3)\left(f_{22}p_1 + \gamma_1\xi_{22} - \gamma_2\xi_{12}\right)\right]\right\}\\
{}^{(k)}E_{63} &= {}^{(k)}\left\{C_{44}e^{-\gamma_1 x_3}\left[\cos(\gamma_2 x_3)\left(f_{33}p_1 - \gamma_1\xi_{33} + \gamma_2\xi_{43}\right) + \sin(\gamma_2 x_3)\left(f_{43}p_1 - \gamma_1\xi_{43} - \gamma_2\xi_{33}\right)\right]\right\}\\
{}^{(k)}E_{64} &= {}^{(k)}\left\{C_{44}e^{-\gamma_1 x_3}\left[\cos(\gamma_2 x_3)\left(f_{34}p_1 - \gamma_1\xi_{34} + \gamma_2\xi_{44}\right) + \sin(\gamma_2 x_3)\left(f_{44}p_1 - \gamma_1\xi_{44} - \gamma_2\xi_{34}\right)\right]\right\}\\
{}^{(k)}E_{65} &= {}^{(k)}C_{44}\,{}^{(k)}\eta\,{}^{(k)}\left(m_1L_1 + p_1R_1\right){}^{(k)}S_1(x_3),\ {}^{(k)}E_{66} = {}^{(k)}C_{44}\,{}^{(k)}\left(m_1L_1 + p_1R_1\right){}^{(k)}C_1(x_3)
\end{aligned}
\tag{E-3}
$$

where ${}^{(k)}\eta$, ${}^{(k)}m_1$, ${}^{(k)}L_1$, ${}^{(k)}R_1$, ${}^{(k)}C_1(x_3)$ and ${}^{(k)}S_1(x_3)$ are defined in Eqs. (3-78) and (3-79) and:

$$
{}^{(k)}\xi_{11} = {}^{(k)}\xi_{22} = {}^{(k)}\xi_{33} = {}^{(k)}\xi_{44} = {}^{(k)}\left(\frac{p_1\left[e_1e_3\left(\gamma_2\right)^2 + e_2e_4\left(\gamma_1\right)^2\right]}{p_2\left[\left(e_1\gamma_2\right)^2 + \left(e_2\gamma_1\right)^2\right]}\right)
$$

$$
{}^{(k)}\xi_{12} = -{}^{(k)}\xi_{21} = -{}^{(k)}\xi_{34} = {}^{(k)}\xi_{43} = {}^{(k)}\left(\frac{p_1\gamma_2\gamma_1\left[e_2e_3 - e_1e_4\right]}{p_2\left[\left(e_1\gamma_2\right)^2 + \left(e_2\gamma_1\right)^2\right]}\right)
$$

$$
{}^{(k)}f_{11} = {}^{(k)}f_{22} = -{}^{(k)}f_{33} = -{}^{(k)}f_{44} = {}^{(k)}\left(\frac{\left(C_{12} + C_{66}\right)p_1p_2\gamma_1 - r_2\gamma_1\xi_{11} - r_1\gamma_2\xi_{21}}{p_1\left(C_{13} + C_{44}\right)\left[\left(\gamma_1\right)^2 + \left(\gamma_2\right)^2\right]}\right)
$$

$$
{}^{(k)}f_{12} = -{}^{(k)}f_{21} = {}^{(k)}f_{34} = -{}^{(k)}f_{43} = -{}^{(k)}\left(\frac{\left(C_{12} + C_{66}\right)p_1p_2\gamma_2 + r_2\gamma_1\xi_{12} + r_1\gamma_2\xi_{22}}{p_1\left(C_{13} + C_{44}\right)\left[\left(\gamma_1\right)^2 + \left(\gamma_2\right)^2\right]}\right)
$$

$$
\begin{aligned}
{}^{(k)}r_1 &= {}^{(k)}\left(C_{44}\left[(\gamma_1)^2+(\gamma_2)^2\right]+C_{66}(p_2)^2+C_{11}(p_1)^2\right)\\
{}^{(k)}r_2 &= {}^{(k)}\left(C_{44}\left[(\gamma_1)^2+(\gamma_2)^2\right]-C_{66}(p_2)^2-C_{11}(p_1)^2\right)\\
{}^{(k)}r_3 &= {}^{(k)}\left(C_{55}\left[(\gamma_1)^2+(\gamma_2)^2\right]+C_{22}(p_2)^2+C_{66}(p_1)^2\right)\\
{}^{(k)}r_4 &= {}^{(k)}\left(C_{55}\left[(\gamma_1)^2+(\gamma_2)^2\right]-C_{22}(p_2)^2-C_{66}(p_1)^2\right)\\
{}^{(k)}e_1 &= {}^{(k)}\left[r_1(C_{23}+C_{55})-(p_1)^2(C_{12}+C_{66})(C_{13}+C_{44})\right]\\
{}^{(k)}e_2 &= {}^{(k)}\left[r_2(C_{23}+C_{55})+(p_1)^2(C_{12}+C_{66})(C_{13}+C_{44})\right]\\
{}^{(k)}e_3 &= {}^{(k)}\left[r_3(C_{13}+C_{44})-(p_2)^2(C_{12}+C_{66})(C_{23}+C_{55})\right]\\
{}^{(k)}e_4 &= {}^{(k)}\left[r_4(C_{13}+C_{44})+(p_2)^2(C_{12}+C_{66})(C_{23}+C_{55})\right]\\
{}^{(k)}\gamma_1 &= {}^{(k)}\left\{\left[(\mu_R)^2+(\mu_I)^2\right]^{\frac{1}{4}}\cos\left(\frac{\arctan\left(\frac{\mu_I}{\mu_R}\right)}{2}\right)\right\}\\
{}^{(k)}\gamma_2 &= {}^{(k)}\left\{\left[(\mu_R)^2+(\mu_I)^2\right]^{\frac{1}{4}}\sin\left(\frac{\arctan\left(\frac{\mu_I}{\mu_R}\right)}{2}\right)\right\}\\
{}^{(k)}\mu_R &= -\frac{1}{2}{}^{(k)}\left(\sqrt[3]{R+\sqrt{D}}+\sqrt[3]{R-\sqrt{D}}\right)-\frac{{}^{(k)}a_1}{3}\\
{}^{(k)}\mu_I &= \frac{1}{2}\sqrt{3}\,{}^{(k)}\left(\sqrt[3]{R+\sqrt{D}}-\sqrt[3]{R-\sqrt{D}}\right)\\
{}^{(k)}R &= {}^{(k)}\left(\frac{9a_1a_2-27a_3-2(a_1)^3}{54}\right),\ {}^{(k)}D = {}^{(k)}\left(\frac{3a_2-(a_1)^2}{9}\right)^3+{}^{(k)}R^2\\
{}^{(k)}a_1 &= -{}^{(k)}\left(\frac{B}{A}\right),\ {}^{(k)}a_2 = -{}^{(k)}\left(\frac{C}{A}\right),\ {}^{(k)}a_3 = -{}^{(k)}\left(\frac{D}{A}\right)
\end{aligned}
\tag{E-4}
$$

where ${}^{(k)}A$, ${}^{(k)}B$, ${}^{(k)}C$, and ${}^{(k)}D$ are defined in Eq. (3-74).

APPENDIX F

CONSTANTS ${}^{(1)}M_l(x_3^0)$, ${}^{(k)}\Omega_{rl}$ AND ${}^{(k)}S_t$ IN CHAPTER 3

$$
\begin{aligned}
&{}^{(1)}M_1(x_3^0) = \\
&{}^{(n)}\left[\frac{\left(\Omega_{62}\Omega_{53}-\Omega_{63}\Omega_{52}\right)\left(f_u+\mu_4\right)+\left(\Omega_{42}\Omega_{63}-\Omega_{43}\Omega_{62}\right)\mu_5+\left(\Omega_{43}\Omega_{52}-\Omega_{42}\Omega_{53}\right)\mu_6}{\Omega_{41}\left(\Omega_{62}\Omega_{53}-\Omega_{63}\Omega_{52}\right)+\Omega_{42}\left(\Omega_{63}\Omega_{51}-\Omega_{61}\Omega_{53}\right)+\Omega_{43}\left(\Omega_{61}\Omega_{52}-\Omega_{62}\Omega_{51}\right)}\right] \\
&{}^{(1)}M_2(x_3^0) = \\
&\frac{1}{{}^{(n)}\left(\Omega_{62}\Omega_{53}-\Omega_{63}\Omega_{52}\right)}\,{}^{(n)}\left\{\left(\Omega_{63}\Omega_{51}-\Omega_{61}\Omega_{53}\right){}^{(1)}M_1(x_3^0)-\Omega_{63}\mu_5+\Omega_{53}\mu_6\right\} \\
&{}^{(1)}M_3(x_3^0) = \\
&\frac{1}{{}^{(n)}\left(\Omega_{62}\Omega_{53}-\Omega_{63}\Omega_{52}\right)}\,{}^{(n)}\left\{\left(\Omega_{61}\Omega_{52}-\Omega_{62}\Omega_{51}\right){}^{(1)}M_1(x_3^0)+\Omega_{62}\mu_5-\Omega_{52}\mu_6\right\} \\
&{}^{(1)}M_4(x_3^0) = -f_l \\
&{}^{(1)}M_5(x_3^0) = 0 \\
&{}^{(1)}M_6(x_3^0) = 0
\end{aligned}
\qquad \text{(F-1)}
$$

where μ_i for $i = 4, 5, 6$ are $\mu_i = \sum_{g=1}^{6} {}^{(n)}\Omega_{ig}\,{}^{(1)}Q_g(x_3^0) + {}^{(n)}\Omega_{i4}f_l - {}^{(n)}S_i - {}^{(n)}Q_i(x_3^n)$ and ${}^{(k)}\Omega_{ig}$ and ${}^{(k)}S_i$ are defined by the recursive formulas:

$$
\begin{aligned}
&{}^{(k)}\Omega_{ig} = \sum_{m=1}^{6} {}^{(k)}U_{im}\,{}^{(k-1)}\Omega_{mg} \text{ for } k = 2, ..., n\,;\ {}^{(1)}\Omega_{ig} = {}^{(1)}U_{ig} \\
&{}^{(k)}U_{im} = \sum_{n=1}^{6}\left\{\sum_{p=1}^{6} B_{ip}^{k}\,{}^{(k)}E_{pn}(x_3^k)\right\}{}^{(k)}E^{-1}{}_{nm}(x_3^{k-1}) \\
&{}^{(k)}S_i = \sum_{q=1}^{6} {}^{(k)}U_{iq}\left[{}^{(k-1)}S_q - {}^{(k)}Q_q(x_3^{k-1}) + \sum_{b=1}^{6}\left(B^{k-1}\right)_{qb}\,{}^{(k-1)}Q_b(x_3^{k-1})\right] \text{ for } k = 2, ..., n\,;\ {}^{(1)}S_i = 0
\end{aligned}
\qquad \text{(F-2)}
$$

APPENDIX G

COEFFICIENTS AND TERMS IN THE EQUILIBRIUM EQUATIONS AND BOUNDARY CONDITIONS IN CHAPTER 4

The prescribed values of forces and couples at the plate edges:

$$\begin{aligned}
\tilde{N}_i &= \sum_{k=1}^{2} \int_{x_3^{k-1}}^{x_3^k} {}^{(k)}F_i^B \, dx_3 \\
\tilde{M}_2^b &= \sum_{k=1}^{2} \int_{x_3^{k-1}}^{x_3^k} {}^{(k)}F_2^B \, x_3 \, dx_3 \\
\tilde{M}_2^{zS} &= \sum_{k=1}^{2} \int_{x_3^{k-1}}^{x_3^k} {}^{(k)}F_2^B \, R_{S22}^k \, dx_3
\end{aligned} \tag{G-1}$$

where F_i^B for $i = 2$ and 3 are the components of the surface forces acting along the plate edges.

Constant coefficients in the equilibrium equations:

$$\begin{aligned}
C_{22}^r &= \sum_{k=1}^{2} {}^{(k)}\bar{C}_{22} \int_{x_3^{k-1}}^{x_3^k} (x_3)^r \, dx_3 \qquad C_{22}^{rS} = \sum_{k=1}^{2} {}^{(k)}\bar{C}_{22} \int_{x_3^{k-1}}^{x_3^k} (x_3)^r \, R_{S22}^k \, dx_3 \\
C_{22}^{S2} &= \sum_{k=1}^{2} {}^{(k)}\bar{C}_{22} \int_{x_3^{k-1}}^{x_3^k} (R_{S22}^k)^2 \, dx_3 \qquad C_{44}^P = \sum_{k=1}^{2} {}^{(k)}C_{44} \int_{x_3^{k-1}}^{x_3^k} \left(1 + R_{S22,3}^k\right)^2 dx_3 \\
C_{22}^S &= K_S \left(\Psi_{22}\right)^2
\end{aligned} \tag{G-2}$$

The homogenized boundary conditions in terms of the global kinematic variables:

$$\begin{aligned}
&\left(C_{22}^0 v_{02,2} + C_{22}^1 \varphi_{2,2} + C_{22}^{0S}\left[\varphi_{2,2} + w_{0,22}\right]\right) n_2 = \tilde{N}_2 \quad \text{or} \quad v_{02} = \tilde{v}_{02} \\
&\left(C_{22}^1 v_{02,2} + C_{22}^2 \varphi_{2,2} + C_{22}^{1S}\left[\varphi_{2,2} + w_{0,22}\right]\right) n_2 = \tilde{M}_2^b \quad \text{or} \quad \varphi_2 = \tilde{\varphi}_2 \\
&\left(\left[k_{44} C_{44}^P + C_{22}^S\right]\left(\varphi_2 + w_{0,2}\right) - C_{22}^{0S} v_{02,22} - C_{22}^{1S} \varphi_{2,22} - C_{22}^{S2}\left[\varphi_{2,22} + w_{0,222}\right]\right) n_2 = \tilde{N}_3 \\
&\text{or} \quad w_0 = \tilde{w}_0 \\
&\left(C_{22}^{0S} v_{02,2} + C_{22}^{1S} \varphi_{2,2} + C_{22}^{S2}\left[\varphi_{2,2} + w_{0,22}\right]\right) n_2 = \tilde{M}_2^{zS} \quad \text{or} \quad w_{0,2} = \tilde{w}_{0,2}
\end{aligned} \tag{G-3}$$

APPENDIX H

PERTURBATION ANALYSIS IN CHAPTER 4

Perturbation analysis is applied here to derived the asymptotic limits of the solution of the global variables of the homogenized model presented in Sect. 4.2 and given in Eq. (4-26). The relevant asymptotic limits correspond to the fully bonded limit (intact region with $1/K_S \to 0$) and fully debonded limit (delaminated region with $K_S \to 0$). The perturbation analysis investigates the solution given in Eq. (4-26) for small values of a perturbation parameter, δ, which is chosen as $\delta = 1/K_S \to 0$ to investigate the fully bonded limit, and $\delta = \overline{B} \to 0$, where $\overline{B}$ defined in Eq. (4-25) goes to zero with the same order as K_S, is used for convenience.

The global variables of the homogenized model, v_{02}, φ_2, and w_0, and $\gamma = \varphi_2 + w_{0,2}$, which is needed to calculate the interfacial relative displacements, Eq. (4-7), are expanded into power series of δ up to the first-order:

$$\begin{aligned}
\gamma &= \overset{0}{\gamma} + \delta \overset{1}{\gamma} + O\left(\delta^2\right) \\
w_0 &= \overset{0}{w}_0 + \delta \overset{1}{w}_0 + O\left(\delta^2\right) \\
\varphi_2 &= \overset{0}{\varphi}_2 + \delta \overset{1}{\varphi}_2 + O\left(\delta^2\right) \\
v_{02} &= \overset{0}{v}_{02} + \delta \overset{1}{v}_{02} + O\left(\delta^2\right)
\end{aligned} \tag{H-1}$$

where the superscript $\overset{i}{(.)}$ on the top of a variable indicates the order of the expansion term.

The integration constants c_i for i =1, 2, 3, in Eq. (4-26), which depend on the interfacial stiffness, have finite values, since γ in Eq. (4-26) cannot be unbounded; similar to Eq. (H-1), c_i for i =1, 2, 3 are also expanded into power series of δ up to the first-order, $c_i = \overset{0}{c}_i + \delta \overset{1}{c}_i + O\left(\delta^2\right)$. Substitution of the expansions of the global variables in Eq. (H-1) and $c_i = \overset{0}{c}_i + \delta \overset{1}{c}_i + O\left(\delta^2\right)$ into Eq. (4-26), and taking the limit as $\delta \to 0$ define the zero-order solutions of the global variables in Eq. (4-26).

Fully bonded limit

The fully bonded limit describes the intact portions of the plate. In this limit, $\delta = 1/K_S \to 0$, and Ψ_{22} in Eq. (4-8), $\hat{v}_2$ in Eq. (4-7) and C_{22}^S in Appendix G Eq. (G-2) vanish and R_{S22}^2 in Eq. (4-10) modifies in $R_{S22}^2 = \Lambda_{22}\left(x_3 - x_3^1\right)$. The constants C_{22}^{rS} and C_{22}^{S2} in Appendix G Eq. (G-2), and $\overline{A}$, $\overline{B}$, $\overline{C}$, $\overline{D}$ and $\overline{E}$ in

Eq. (4-25) simplify by substituting $R^2_{S22} = \Lambda_{22}\left(x_3 - x^1_3\right)$.The zero-order solution of the model are then obtained by substituting the simplified coefficients into Eq. (4-26). The zero-order solution coincides with the solution of the original first-order zigzag theory developed in [62] for fully bonded plates.

Fully debonded limit

The fully debonded limit describes the delaminated portion of the plate, $\delta = \overline{B} \to 0$. The order of the coefficients and parameters of the homogenized structural theory are given in Table H-1.

Table H-1: Orders of the coefficients when $\delta = \overline{B} \to 0$

Vanishing coefficients	Finite value coefficients	Unbounded coefficients
$O(\delta): K_S, \overline{B}$	$O(1): C^0_{22}, C^1_{22}, C^2_{22}, C^P_{44}, \overline{A}$	$O(1/\delta): \Psi_{22}, R^2_{S22}, C^{0S}_{22}$
	$\overline{E}, \Lambda_{22}, c_1, c_2, c_3, \frac{c_1 - c_2}{\sqrt{\overline{B}}}$	$C^{1S}_{22}, C^S_{22}, \overline{D}$
	$\frac{\overset{1}{c_1} - \overset{1}{c_2}}{\sqrt{\overline{B}}}, c_4, c_5 + \frac{1}{\overline{B}}, c_6 + \frac{1}{\overline{B}}, c_7$	$O(1/\delta^2): C^{S2}_{22}$
	$c_8 - C^{0S}_{22}, \overline{D}\overline{B}, C^{0S}_{22}\overline{B}, R^2_{S22,3}$	

When $C^1_{22} = 0$, i.e. when the reference surface $x_3 = 0$ coincides with the neutral axis of the intact portion of the plate in Figure 4-1(b), substitution of Eq. (H-1) and $c_i = \overset{0}{c}_i + \delta \overset{1}{c}_i + O\left(\delta^2\right)$ for i =1, 2, 3, into Eq. (4-26) and using the first four terms of the Maclaurin expansion of $e^{\sqrt{\overline{B}}x_2}$ and $e^{-\sqrt{\overline{B}}x_2}$ yield:

$$\overset{0}{\gamma} = \overset{0}{c_1} + \overset{0}{c_2} + \overset{0}{c_3} = const.$$

$$\overset{1}{\gamma} = \left(\frac{\overset{0}{c_1} + \overset{0}{c_2}}{2} \right) (x_2)^2 + \left(\frac{\overset{0}{c_1} - \overset{0}{c_2}}{\sqrt{\bar{B}}} \right) x_2 + \left(\overset{1}{c_1} + \overset{1}{c_2} + \overset{1}{c_3} \right)$$

$$\overset{0}{w_0} = \left(\frac{\bar{E}\overset{0}{c_3} + \left(D\bar{B} + \bar{E} \right) \left(\overset{0}{c_1} + \overset{0}{c_2} \right)}{6} \right) (x_2)^3 + \left(c_4 + \frac{\left(D\bar{B} + \bar{E} \right) \left(\overset{0}{c_1} - \overset{0}{c_2} \right)}{2\sqrt{\bar{B}}} \right) (x_2)^2 +$$

$$+ \left(c_5 + \left(D\bar{B} + \bar{E} \right) \left(\overset{1}{c_1} + \overset{1}{c_2} \right) + \frac{\left(D\bar{B} + \bar{E} \right) \left(\overset{0}{c_1} + \overset{0}{c_2} \right)}{\bar{B}} \right) x_2 + \tag{H-2}$$

$$+ \left(c_6 + \frac{\left(D\bar{B} + \bar{E} \right) \left(\overset{0}{c_1} - \overset{0}{c_2} \right)}{\bar{B}\sqrt{\bar{B}}} + \frac{\left(D\bar{B} + \bar{E} \right) \left(\overset{1}{c_1} - \overset{1}{c_2} \right)}{\sqrt{\bar{B}}} \right)$$

$$\overset{0}{\varphi_2} = -\overset{0}{w_{0,2}} + \left(\overset{0}{c_1} + \overset{0}{c_2} + \overset{0}{c_3} \right)$$

$$\overset{0}{v_{02}} = \left(\frac{-C_{22}^{0S} \bar{B} \left(\overset{0}{c_1} + \overset{0}{c_2} \right)}{2C_{22}^{0}} \right) (x_2)^2 + \left(c_7 + \frac{-C_{22}^{0S} \sqrt{\bar{B}} \left(\overset{0}{c_1} - \overset{0}{c_2} \right)}{C_{22}^{0}} \right) x_2 + \left(c_8 + \frac{-C_{22}^{0S} \left(\overset{0}{c_1} + \overset{0}{c_2} \right)}{C_{22}^{0}} \right)$$

The zero-order solution of the global variables $\overset{0}{\gamma}$, $\overset{0}{w_0}$, $\overset{0}{\varphi_2}$ and $\overset{0}{v_{02}}$, and $\overset{1}{\gamma}$ depend also on the first-order terms in the expansions of the integration constants, $\overset{1}{c_i}$ for i =1, 2, 3. Accounting for the fact that the terms in Eq. (H-2), and the interfacial relative displacements, Eq. (4-7), must be finite, allows to draw some conclusions on the orders of the integration constants $\overset{1}{c_1} - \overset{1}{c_2}$, and c_i for i =4, …, 8.

Substitution of $\gamma = \overset{0}{\gamma} + \delta \overset{1}{\gamma} + O\left(\delta^2\right)$ from Eqs. (H-1) and $\Psi_{22} = \left[\overset{-1}{\Psi_{22}} \right] (1/\delta) + O(1)$ into the interfacial relative displacements given in Eq. (4-7) yield:

$$\hat{v}_2 = \left(\overset{0}{\gamma} + \delta \overset{1}{\gamma} \right) \left[\overset{-1}{\Psi_{22}} \right] \frac{1}{\delta} + O(\delta) \tag{H-3}$$

Since the interfacial relative displacements must be finite, $\overset{0}{\gamma} = 0$, which results in $\overset{0}{c}_1 + \overset{0}{c}_2 + \overset{0}{c}_3 = 0$ and $\overset{0}{\varphi}_2 = -\overset{0}{w}_{0,2}$ in Eq. (H-2); substitution of $\overset{1}{\gamma}$ from Eq. (H-2) and Ψ_{22} from Eq. (4-8) into Eq. (H-3) yield:

$$\overset{0}{\hat{v}}_2 = \left[\left(\frac{\overset{0}{c}_1 + \overset{0}{c}_2}{2} \right) (x_2)^2 + \left(\frac{\overset{0}{c}_1 - \overset{0}{c}_2}{\sqrt{\overline{B}}} \right) x_2 + \left(\overset{1}{c}_1 + \overset{1}{c}_2 + \overset{1}{c}_3 \right) \right] {}^{(2)}C_{44} \left(1 + \Lambda_{22} \right) \tag{H-4}$$

Since $\overset{0}{\hat{v}}_2$ cannot be unbounded, $\left(\overset{0}{c}_1 - \overset{0}{c}_2 \right) \Big/ \sqrt{\overline{B}}$ should be finite, which means that $\left(c_1 - c_2 \right) \Big/ \sqrt{\overline{B}}$ is also finite. The orders of the coefficients given in Table H-1, are determined similarly by imposing the terms in Eq. (H-2) to be finite.

In the examples considered in Sect. 4.5, the calculated constant $\left(\overset{1}{c}_1 + \overset{1}{c}_2 + \overset{1}{c}_3 \right)$ does not yield a zero relative sliding displacement at the delamination tip. This is due to the imposition of the continuity conditions on the global variables only. A non-zero delamination tip relative displacement uniformly shifts the predicted relative sliding displacements of the layers in the delaminated portion of the plate, and has no other effect on the solutions of the homogenized model.

The interfacial shear tractions in Eq. (4-14) and the small-scale variable, Ω_2, in Eq. (4-7) are zero at the zero-order in the delaminated portion of the plate, since $\overset{0}{\gamma} = \overset{0}{\varphi}_2 + \overset{0}{w}_{0,2} = 0$. This leads the multiscale model to predict the same rotations for the upper and lower layers in the delaminated portion of the plate (see Eq. (4-27)); the rotations are then equal to the global bending rotation variable, φ_2. On the other hand, imposing the continuity conditions on φ_2 and $w_{0,2}$, makes the term $\overset{0}{\gamma} = \overset{0}{\varphi}_2 + \overset{0}{w}_{0,2}$ to be zero also in the intact portion of the plat at the traction-free delamination tip cross section. Therefore, the model also predicts the same rotations for the upper and lower layers in the intact region at the traction-free delamination tip cross section. As a consequence, the rotations of the layers at the delamination tip cross section are all equal, and the multiscale model neglects the root-rotations.

REFERENCES

[1] I.M. Daniel, O. Ishai, I.M. Daniel, I. Daniel, Engineering mechanics of composite materials, Oxford university press New York, 1994.

[2] Y. Jiao, J. Fish, On the equivalence between the s -method, the XFEM and the ply-by-ply discretization for delamination analyses of laminated composites, *International Journal of Fracture*, **191** (2015) 107-129.

[3] A.S. Herrmann, P.C. Zahlen, I. Zuardy, Sandwich Structures Technology in Commercial Aviation, in, Springer Netherlands, Dordrecht, 2005, pp. 13-26.

[4] M.K. Buragohain, Composite Structures: Design, Mechanics, Analysis, Manufacturing, and Testing, Taylor & Francis, a CRC title, part of the Taylor & Francis imprint, a member of the Taylor & Francis Group, the academic division of T&F Informa, plc, 2017.

[5] J. Zhang, K. Chaisombat, S. He, C.H. Wang, Glass/Carbon Fibre Hybrid Composite Laminates for Structural Applications in Automotive Vehicles, in, Springer Berlin Heidelberg, Berlin, Heidelberg, 2012, pp. 69-74.

[6] V.B. Tungikar, K.M. Rao, Three dimensional exact solution of thermal stresses in rectangular composite laminate, *Composite Structures*, **27** (1994) 419-430.

[7] M. Pelassa, R. Massabò, Explicit solutions for multi-layered wide plates and beams with perfect and imperfect bonding and delaminations under thermo-mechanical loading, *Meccanica*, **50** (2015) 2497-2524.

[8] N.J. Pagano, Exact Solutions for Rectangular Bidirectional Composites and Sandwich Plates, *Journal of Composite Materials*, **4** (1970) 20-34.

[9] S. Kapuria, P. Kumari, Multiterm Extended Kantorovich Method for Three-Dimensional Elasticity Solution of Laminated Plates, *Journal of Applied Mechanics*, **79** (2012) 061018-061018-061019.

[10] K. Bhaskar, T.K. Varadan, J.S.M. Ali, Thermoelastic solutions for orthotropic and anisotropic composite laminates, *Composites Part B: Engineering*, **27** (1996) 415-420.

[11] R. Massabò, F. Campi, Assessment and correction of theories for multilayered plates with imperfect interfaces, *Meccanica*, **50** (2015) 1045-1071.

[12] W.Q. Chen, J.B. Cai, G.R. Ye, Exact Solutions of Cross-Ply Laminates with Bonding Imperfections, *AIAA Journal*, **41** (2003) 2244-2250.

[13] F. Jiarang, Y. Jianqiao, An exact solution for the statics and dynamics of laminated thick plates with orthotropic layers, *International Journal of Solids and Structures*, **26** (1990) 655-662.

[14] F. Jiarang, Y. Jianqiao, Exact solutions of buckling for simply supported thick laminates, *Composite Structures*, **24** (1993) 23-28.

[15] G.W. Kim, K.Y. Lee, Influence of weak interfaces on buckling of orthotropic rectangular laminates, *Composite Structures*, **81** (2007) 427-431.

[16] H. Qian, D. Zhou, W. Liu, H. Fang, 3-D elasticity solutions of simply supported laminated rectangular plates in uniform temperature field, *Journal of Thermal Stresses*, **37** (2014) 661-677.

[17] H. Qian, D. Zhou, W. Liu, H. Fang, W. Lu, 3-D Elasticity Solutions of Layered Rectangular Plates Subjected to Thermo-Loads, *Journal of Thermal Stresses*, **38** (2015) 377-398.

[18] H. Qian, D. Zhou, W. Liu, H. Fang, W. Lu, Elasticity solutions of simply supported laminated cylindrical arches subjected to thermo-loads, *Composite Structures*, **131** (2015) 273-281.

[19] T.O. Williams, F.L. Addessio, A general theory for laminated plates with delaminations, *International Journal of Solids and Structures*, **34** (1997) 2003-2024.

[20] M.G. Andrews, R. Massabò, A. Cavicchi, B.N. Cox, Dynamic interaction effects of multiple delaminations in plates subject to cylindrical bending, *International Journal of Solids and Structures*, **46** (2009) 1815-1833.

[21] D. Bruno, F. Greco, Mixed mode delamination in plates: a refined approach, *International Journal of Solids and Structures*, **38** (2001) 9149-9177.

[22] G. Alfano, M.A. Crisfield, Finite element interface models for the delamination analysis of laminated composites: mechanical and computational issues, *International Journal for Numerical Methods in Engineering*, **50** (2001) 1701-1736.

[23] O. Allix, P. Ladevéze, A. Corigliano, Damage analysis of interlaminar fracture specimens, *Composite Structures*, **31** (1995) 61-74.

[24] Y. Mi, M.A. Crisfield, G.A.O. Davies, H.B. Hellweg, Progressive Delamination Using Interface Elements, *Journal of Composite Materials*, **32** (1998) 1246-1272.

[25] R. Massabò, F. Campi, An efficient approach for multilayered beams and wide plates with imperfect interfaces and delaminations, *Composite Structures*, **116** (2014) 311-324.

[26] R. Massabò, Influence of boundary conditions on the response of multilayered plates with cohesive interfaces and delaminations using a homogenized approach, *2014*, (2014) 11.

[27] A. Tessler, M. Di Sciuva , M. Gherlone, A Refined Zigzag Beam Theory for Composite and Sandwich Beams, *Journal of Composite Materials*, **43** (2009) 1051-1081.

[28] M. Di Sciuva, First-order displacement-based zigzag theories for composite laminates and sandwich structures: a review, *VII European Congress on Computational Methods in Applied Sciences and Engineering,Crete Island, Greece, 5-10 June 2016*, 4528-4552.

[29] N.J. Pagano, Exact Solutions for Composite Laminates in Cylindrical Bending, *Journal of Composite Materials*, **3** (1969) 398-411.

[30] N.J. Pagano, H.J. Hatfield, Elastic Behavior of Multilayered Bidirectional Composites, *AIAA Journal*, **10** (1972) 931-933.

[31] N.J. Pagano, A.S.D. Wang, Further Study of Composite Laminates Under Cylindrical Bending, *Journal of Composite Materials*, **5** (1971) 521-528.

[32] M. Savoia, J.N. Reddy, Three-dimensional thermal analysis of laminated composite plates, *International Journal of Solids and Structures*, **32** (1995) 593-608.

[33] S. Srinivas, A.K. Rao, Bending, vibration and buckling of simply supported thick orthotropic rectangular plates and laminates, *International Journal of Solids and Structures*, **6** (1970) 1463-1481.

[34] T.R. Tauchert, Thermoelastic analysis of laminated orthotropic slabs, *Journal of Thermal Stresses*, **3** (1980) 117-132.

[35] S.S. Vel, R.C. Batra, Exact Solution for Thermoelastic Deformations of Functionally Graded Thick Rectangular Plates, *AIAA Journal*, **40** (2002) 1421-1433.

[36] H. Murakami, Assessment of plate theories for treating the thermomechanical response of layered plates, *Composites Engineering*, **3** (1993) 137-149.

[37] G.A. Kardomateas, C.N. Phan, Three-dimensional elasticity solution for sandwich beams/wide plates with orthotropic phases: The negative discriminant case, *Journal of Sandwich Structures & Materials*, **13** (2011) 641-661.

[38] G.A. Kardomateas, Three-Dimensional Elasticity Solution for Sandwich Plates With Orthotropic Phases: The Positive Discriminant Case, *Journal of Applied Mechanics*, **76** (2008) 014505-014505-014504.

[39] S. Srinivas, A.K. Rao, C.V.J. Rao, Flexure of Simply Supported Thick Homogeneous and Laminated Rectangular Plates, *ZAMM - Journal of Applied Mathematics and Mechanics / Zeitschrift für Angewandte Mathematik und Mechanik*, **49** (1969) 449-458.

[40] S. Srinivas, A.K. Rao, Flexure of Thick Rectangular Plates, *Journal of Applied Mechanics*, **40** (1973) 298-299.

[41] S.S. Vel, R.C. Batra, The generalized plane strain deformations of thick anisotropic composite laminated plates, *International Journal of Solids and Structures*, **37** (2000) 715-733.

[42] J.G. Ren, Exact solutions for laminated cylindrical shells in cylindrical bending, *Composites Science and Technology*, **29** (1987) 169-187.

[43] J.G. Ren, Analysis of simply-supported laminated circular cylindrical shell roofs, *Composite Structures*, **11** (1989) 277-292.

[44] S. Abrate, Impact on Laminated Composite Materials, *Applied Mechanics Reviews*, **44** (1991) 155-190.

[45] W.Q. Chen, Y.F. Wang, J.B. Cai, G.R. Ye, Three-dimensional analysis of cross-ply laminated cylindrical panels with weak interfaces, *International Journal of Solids and Structures*, **41** (2004) 2429-2446.

[46] S. Kapuria, N. Dhanesh, Three-Dimensional Extended Kantorovich Solution for Accurate Prediction of Interlaminar Stresses in Composite Laminated Panels with Interfacial Imperfections, *Journal of Engineering Mechanics*, **141** (2015).

[47] B.A. Boley, J.H. Weiner, Theory of thermal stresses, John Wiley & Sons Inc, New York, 1960.

[48] A. Levy, D. Heider, J. Tierney, J.W. Gillespie, Inter-layer thermal contact resistance evolution with the degree of intimate contact in the processing of thermoplastic composite laminates, *Journal of Composite Materials*, **48** (2014) 491-503.

[49] G.E. Blandford, T.R. Tauchert, Thermoelastic analysis of layered structures with imperfect layer contact, *Computers & Structures*, **21** (1985) 1283-1291.

[50] T.C. Chen, H.I. Jang, Thermal Stresses in a Multilayered Anisotropic Medium With Interface Thermal Resistance, *Journal of Applied Mechanics*, **62** (1995) 810-811.

[51] W.T. Thomson, Transmission of Elastic Waves through a Stratified Solid Medium, *Journal of Applied Physics*, **21** (1950) 89-93.

[52] N.A. Haskell, The dispersion of surface waves on multilayered media, *Bulletin of the seismological Society of America*, **43** (1953) 17-34.

[53] M.J.S. Lowe, Matrix techniques for modeling ultrasonic waves in multilayered media, *IEEE Transactions on Ultrasonics, Ferroelectrics, and Frequency Control*, **42** (1995) 525-542.

[54] J.N. Reddy, A Simple Higher-Order Theory for Laminated Composite Plates, *Journal of Applied Mechanics*, **51** (1984) 745-752.

[55] J.M. Whitney, N.J. Pagano, Shear Deformation in Heterogeneous Anisotropic Plates, *Journal of Applied Mechanics*, **37** (1970) 1031-1036.

[56] S. Abrate, M. Di Sciuva, Equivalent single layer theories for composite and sandwich structures: A review, *Composite Structures*, **179** (2017) 482-494.

[57] S. Abrate, M. Di Sciuva, 1.16 Multilayer Models for Composite and Sandwich Structures, in: Comprehensive Composite Materials II, Elsevier, Oxford, 2018, pp. 399-425.

[58] J.M. Whitney, C.T. Sun, A higher order theory for extensional motion of laminated composites, *Journal of Sound and Vibration*, **30** (1973) 85-97.

[59] E. Reissner, On a certain mixed variational theorem and a proposed application, *International Journal for Numerical Methods in Engineering*, **20** (1984) 1366-1368.

[60] H. Murakami, Laminated composite plate theory with improved in-plane responses, *Journal of Applied Mechanics*, **53** (1986) 661-666.

[61] M. Gherlone, On the Use of Zigzag Functions in Equivalent Single Layer Theories for Laminated Composite and Sandwich Beams: A Comparative Study and Some Observations on External Weak Layers, *Journal of Applied Mechanics*, **80** (2013) 061004-061004-061019.

[62] M. di Sciuva, Bending, vibration and buckling of simply supported thick multilayered orthotropic plates: An evaluation of a new displacement model, *Journal of Sound and Vibration*, **105** (1986) 425-442.

[63] M. Di Sciuva, An Improved Shear-Deformation Theory for Moderately Thick Multilayered Anisotropic Shells and Plates, *Journal of Applied Mechanics*, **54** (1987) 589-596.

[64] M. Cho, R. Parmerter, Efficient higher order composite plate theory for general lamination configurations, *AIAA Journal*, **31** (1993) 1299-1306.

[65] M.D. Sciuva, Multilayered anisotropic plate models with continuous interlaminar stresses, *Composite Structures*, **22** (1992) 149-167.

[66] U. Icardi, Higher-order zig-zag model for analysis of thick composite beams with inclusion of transverse normal stress and sublaminates approximations, *Composites Part B: Engineering*, **32** (2001) 343-354.

[67] U. Icardi, Applications of Zig-Zag Theories to Sandwich Beams, *Mechanics of Advanced Materials and Structures*, **10** (2003) 77-97.

[68] S. Kapuria, G.G.S. Achary, An efficient higher order zigzag theory for laminated plates subjected to thermal loading, *International Journal of Solids and Structures*, **41** (2004) 4661-4684.

[69] S. Kapuria, S.D. Kulkarni, An improved discrete Kirchhoff quadrilateral element based on third-order zigzag theory for static analysis of composite and sandwich plates, *International Journal for Numerical Methods in Engineering*, **69** (2007) 1948-1981.

[70] S.D. Kulkarni, S. Kapuria, Free vibration analysis of composite and sandwich plates using an improved discrete Kirchhoff quadrilateral element based on third-order zigzag theory, *Computational Mechanics*, **42** (2008) 803-824.

[71] P. Kumari, S. Kapuria, Boundary layer effects in rectangular cross-ply Levy-type plates using zigzag theory, *ZAMM - Journal of Applied Mathematics and Mechanics / Zeitschrift für Angewandte Mathematik und Mechanik*, **91** (2011) 565-580.

[72] M. Yaqoob Yasin, S. Kapuria, An efficient layerwise finite element for shallow composite and sandwich shells, *Composite Structures*, **98** (2013) 202-214.

[73] P.C. Dumir, J.K. Nath, P. Kumari, S. Kapuria, Improved Efficient Zigzag and Third Order Theories for Circular Cylindrical Shells Under Thermal Loading, *Journal of Thermal Stresses*, **31** (2008) 343-367.

[74] R.C. Averill, Static and dynamic response of moderately thick laminated beams with damage, *Composites Engineering*, **4** (1994) 381-395.

[75] R.C. Averill, Y.C. Yip, Development of simple, robust finite elements based on refined theories for thick laminated beams, *Computers & Structures*, **59** (1996) 529-546.

[76] A. Tessler, M. Di Sciuva, M. Gherlone, A consistent refinement of first-order shear deformation theory for laminated composite and sandwich plates using improved zigzag kinematics, *Journal of Mechanics of Materials and Structures*, **5** (2010) 341-367.

[77] D. Versino, M. Gherlone, M. Di Sciuva, Four-node shell element for doubly curved multilayered composites based on the Refined Zigzag Theory, *Composite Structures*, **118** (2014) 392-402.

[78] A. Tessler, Refined zigzag theory for homogeneous, laminated composite, and sandwich beams derived from Reissner's mixed variational principle, *Meccanica*, **50** (2015) 2621-2648.

[79] M. Di Sciuva, M. Gherlone, L. Librescu, Implications of damaged interfaces and of other non-classical effects on the load carrying capacity of multilayered composite shallow shells, *International Journal of Non-Linear Mechanics*, **37** (2002) 851-867.

[80] Z.-q. Cheng, A.K. Jemah, F.W. Williams, Theory for Multilayered Anisotropic Plates With Weakened Interfaces, *Journal of Applied Mechanics*, **63** (1996) 1019-1026.

[81] R. Schmidt, L. Librescu, Geometric nonlinear theory of laminated anisotropic composite plates featuring interlayer slips, *Nova Journal of Mathematics, Game Theory and Algebra*, **5** (1996) 131-147.

[82] M. Di Sciuva, Geometrically nonlinear theory of multilayered plates with interlayer slips, *AIAA Journal*, **35** (1997) 1753-1759.

[83] J. Oh, M. Cho, J.-S. Kim, Dynamic analysis of composite plate with multiple delaminations based on higher-order zigzag theory, *International Journal of Solids and Structures*, **42** (2005) 6122-6140.

[84] M. Cho, J.S. Kim, Higher-Order Zig-Zag Theory for Laminated Composites With Multiple Delaminations, *Journal of Applied Mechanics*, **68** (2000) 869-877.

[85] J. Oh, M. Cho, J.-S. Kim, Buckling analysis of a composite shell with multiple delaminations based on a higher order zig-zag theory, *Finite Elements in Analysis and Design*, **44** (2008) 675-685.

[86] R.M.J. Groh, A. Tessler, Computationally efficient beam elements for accurate stresses in sandwich laminates and laminated composites with delaminations, *Computer Methods in Applied Mechanics and Engineering*, **320** (2017) 369-395.

[87] R.M.J. Groh, P.M. Weaver, A. Tessler, Application of the Refined Zigzag Theory to the Modeling of Delaminations in Laminated Composites, *Technical Memorandum NASA/TM-2015-218808, NASA*, (2015).

[88] A. Eijo, E. Oñate, S. Oller, A numerical model of delamination in composite laminated beams using the LRZ beam element based on the refined zigzag theory, *Composite Structures*, **104** (2013) 270-280.

[89] A. Eijo, E. Oñate, S. Oller, Delamination in laminated plates using the 4-noded quadrilateral QLRZ plate element based on the refined zigzag theory, *Composite Structures*, **108** (2014) 456-471.

[90] L. Librescu, R. Schmidt, A general linear theory of laminated composite shells featuring interlaminar bonding imperfections, *International Journal of Solids and Structures*, **38** (2001) 3355-3375.

[91] R. Massabò, Propagation of Rayleigh-Lamb waves in multilayered plates through a multiscale structural model, *International Journal of Solids and Structures*, **124** (2017) 108-124.

[92] E. Buckingham, On Physically Similar Systems; Illustrations of the Use of Dimensional Equations, *Physical Review*, **4** (1914) 345-376.

[93] Z. Suo, J.W. Hutchinson, Interface crack between two elastic layers, *International Journal of Fracture*, **43** (1990) 1-18.

[94] S. Li, J. Wang, M.D. Thouless, The effects of shear on delamination in layered materials, *Journal of the Mechanics and Physics of Solids*, **52** (2004) 193-214.

[95] M.G. Andrews, R. Massabò, The effects of shear and near tip deformations on energy release rate and mode mixity of edge-cracked orthotropic layers, *Engineering Fracture Mechanics*, **74** (2007) 2700-2720.

[96] Z. Suo, Delamination Specimens for Orthotropic Materials, *Journal of Applied Mechanics*, **57** (1990) 627-634.

[97] J.W. Hutchinson, Z. Suo, Mixed Mode Cracking in Layered Materials, in: J.W. Hutchinson, T.Y. Wu (Eds.) Advances in Applied Mechanics, Elsevier, 1991, pp. 63-191.

[98] P.C. Yang, C.H. Norris, Y. Stavsky, Elastic wave propagation in heterogeneous plates, *International Journal of Solids and Structures*, **2** (1966) 665-684.

[99] R.C. Østergaard, B.F. Sørensen, Interface crack in sandwich specimen, *International Journal of Fracture*, **143** (2007) 301-316.

[100] R. Massabo, B.N. Cox, Concepts for bridged Mode ii delamination cracks, *Journal of the Mechanics and Physics of Solids*, **47** (1999) 1265-1300.

[101] R. Massabò, D.R. Mumm, B. Cox, Characterizing Mode II Delamination Cracks in Stitched Composites, *International Journal of Fracture*, **92** (1998) 1-38.

[102] M.G. Andrews, R. Massabò, B.N. Cox, Elastic interaction of multiple delaminations in plates subject to cylindrical bending, *International Journal of Solids and Structures*, **43** (2006) 855-886.

[103] M.D. Thouless, The effects of transverse shear on the delamination of edge-notch flexure and 3-point bend geometries, *Composites Part B: Engineering*, **40** (2009) 305-312.

[104] J. Xie, A.M. Waas, M. Rassaian, Estimating the process zone length of fracture tests used in characterizing composites, *International Journal of Solids and Structures*, **100-101** (2016) 111-126.

[105] J. Xie, A.M. Waas, M. Rassaian, Closed-form solutions for cohesive zone modeling of delamination toughness tests, *International Journal of Solids and Structures*, **88-89** (2016) 379-400.

[106] A. Tessler, M. DiSciuva, M. Gherlone, Refinement of Timoshenko beam theory for composite and sandwich beams using zigzag kinematics, *NASA-TP-2007-215086, National Aeronautics and Space Administrations, Washington, D.C*, (2007).